



**MÓNIA ANDREIA  
RODRIGUES MARTINS ESTUDOS PARA O DESENVOLVIMENTO DE NOVOS  
PROCESSOS DE SEPARAÇÃO COM TERPENOS E  
SUA DISTRIBUIÇÃO AMBIENTAL**

**STUDIES FOR THE DEVELOPMENT OF NEW  
SEPARATION PROCESSES WITH TERPENES AND  
THEIR ENVIRONMENTAL DISTRIBUTION**





**MÓNIA ANDREIA  
RODRIGUES MARTINS**

**ESTUDOS PARA O DESENVOLVIMENTO DE NOVOS  
PROCESSOS DE SEPARAÇÃO COM TERPENOS E  
SUA DISTRIBUIÇÃO AMBIENTAL**

**STUDIES FOR THE DEVELOPMENT OF NEW  
SEPARATION PROCESSES WITH TERPENES AND  
THEIR ENVIRONMENTAL DISTRIBUTION**

Tese apresentada à Universidade de Aveiro para cumprimento dos requisitos necessários à obtenção do grau de Doutor em Engenharia Química, realizada sob a orientação científica do Professor Doutor João Manuel da Costa e Araújo Pereira Coutinho, Professor Catedrático do Departamento de Química da Universidade de Aveiro, e do Professor Doutor Simão Pedro de Almeida Pinho, Professor Coordenador da Escola Superior de Tecnologia e Gestão do Instituto Politécnico de Bragança.

Apoio financeiro da FCT e do FSE no âmbito do III Quadro Comunitário de Apoio (SFRH/BD/87084/2012).



**FCT**  
Fundação para a Ciência e a Tecnologia  
INSTITUTO DE INOVAÇÃO E CIÊNCIA



Aos meus pais.

## **o júri**

presidente

**Prof. Doutor Joaquim Manuel Vieira**

professor catedrático no Departamento de Engenharia Cerâmica e do Vidro da Universidade de Aveiro

**Prof. Doutora Isabel Maria Almeida Fonseca**

professora associada com agregação da Faculdade de Ciências e Tecnologia da Universidade de Coimbra

**Prof. Doutor Héctor Rodríguez Martínez**

professor associado do Departamento de Engenharia Química da Universidade de Santiago de Compostela

**Prof. Doutor Luís Manuel das Neves Belchior Faia dos Santos**

professor associado da Faculdade de Ciências da Universidade do Porto

**Prof. Doutor Simão Pedro de Almeida Pinho**

professor coordenador na Escola Superior de Tecnologia e Gestão do Instituto Politécnico de Bragança

**Prof. Doutora Maria Olga de Amorim e Sá Ferreira**

professora adjunta na Escola Superior de Tecnologia e Gestão do Instituto Politécnico de Bragança

## agradecimentos

Prof. João Coutinho pela oportunidade, conhecimentos e muita paciência  
Prof. Simão Pinho pelo desafio, confiança, ideias e palavras amigas  
Prof. Urszula Domańska for the opportunity and friendship  
Prof. Guilherme Máximo pela enorme paciência e grande amizade  
Prof.<sup>a</sup> Mariana Costa por toda a ajuda e disponibilidade  
Bernd Schröder, danke für deine Ratschläge, offenes Ohr und Freundschaft

Catarina pela amizade, por estar sempre lá e pelas imensas gargalhadas  
Pedro Manuel por bromas, asesoramiento y ayuda preciosa  
Tany pela amizade, disponibilidade e enorme companheirismo  
Kiki for being special, unique, and super friend  
Ranyere por todos os momentos de pura felicidade  
Marta pela amizade, preocupação e afeto  
Sarita pela amizade e pelos passeios de descapotável  
Lipa pela amizade e confiança (mesmo sem me conhecer)  
Carlitos pelas imensas gargalhadas e momentos únicos  
Flávia pelos conselhos, conversas e amizade  
Andreia pelas loucuras e confidências  
Chica Maria pelas muitas saídas, alegrias e companheirismo  
Ana Maria, Helena e Manu pelos bons momentos e conversas  
Vanessa Vieira pelas alegrias e boa disposição  
Lilis pela amizade, confiança e ótimo trabalho  
Emanuel pelas piadas nerds e companheirismo  
André pelo companheirismo e cumplicidade  
Rita Costa pela amizade, conselhos e motivação  
Ferrão pelos copos e bons momentos  
Jonathan pela confiança, amizade e 'aqueles' abraços  
Rita Teles pela paciência do 'preciso mesmo' e pela disponibilidade  
Pathfamily pela união, ajudas e alegrias

Vanessa Oliveira pela companhia, conversas e amizade  
Ana Caloto por los viajes, la compañía, la conversación y la amistad  
Estela pelas aventuras, viagens e conversas  
Paulinha pela amizade, ajuda e constante preocupação  
Martin, danke, dass Du mich zum Lachen bringst

Dear por seres especial e verdadeira, pela tua amizade infinita  
Marta pelo ombro amigo e afinidade  
Amigos de sempre pela presença, apoio e amizade

Pai, Irmão, Avô por acreditarem, pelo grande amor e muito afeto  
Aos que já partiram, por terem ajudado a ser quem sou  
Mãe pela vida, amor, confiança e toda a paciência nas longas ausências

**palavras-chave**

Terpenos, terpenoides, óleos essenciais, líquidos iônicos, solventes eutéticos profundos, coeficientes de atividade a diluição infinita, equilíbrio líquido-líquido, equilíbrio sólido-líquido, propriedades críticas.

**resumo**

Os terpenos pertencem ao que é provavelmente a maior e mais diversificada classe de produtos naturais com aplicações em vários setores devido aos seus sabores e fragrâncias. O seu elevado número, variedade de estruturas e complexidade química, fazem deles uma classe de compostos onde há ainda muitos estudos a serem realizados e questões a serem respondidas tanto sobre as suas propriedades termofísicas e equilíbrio de fases como sobre o seu impacto nos processos de extração e purificação e no ambiente. Ambos são relevantes para o desenvolvimento de biorrefinarias, onde estes compostos podem desempenhar um papel importante dada a sua ubiquidade, valor económico e variedade de aplicações.

Esta tese está relacionada com a extração de terpenos de fontes naturais e a sua posterior separação e purificação. Além do desenvolvimento de novos métodos experimentais para medir propriedades termodinâmicas e equilíbrios de fases, algumas abordagens teóricas foram também consideradas para o mesmo fim.

Inicialmente, de forma a criar novas aplicações para estes compostos e tirando vantagem da sua baixa solubilidade em água, tal como demonstrado por novas e precisas determinações experimentais, os terpenos são utilizados para preparar solventes hidrofóbicos sustentáveis e de baixo custo, no âmbito dos solventes eutéticos profundos. Depois, com base nos coeficientes de atividade a diluição infinita e previsões do COSMO-RS, foi feita uma seleção de líquidos iônicos com potencial para o fracionamento de terpenos. Mais ainda, visando o desenvolvimento de novos processos de separação de terpenos, foram também formulados e caracterizados solventes eutéticos profundos compostos por sais de amónio e ácidos monocarboxílicos. Finalmente, e com o objetivo de desenvolver modelos precisos para o destino dos terpenos no ambiente, uma série de propriedades físico-químicas essenciais foi medida e modelada.

**keywords**

Terpenes, terpenoids, essential oils, ionic liquids, deep eutectic solvents, activity coefficients at infinite dilution, liquid-liquid equilibria, solid-liquid equilibria, critical properties.

**abstract**

Terpenes belong to what is probably the largest and most diverse class of natural products with applications in several industries due to their flavor, and fragrance. Their high number, variety of structures and chemical complexity, make of them a class of compounds for which there are still many studies to be carried out and questions to be answered both concerning their thermophysical properties and phase equilibria and their impact in their extraction and purification processes and on their environmental impact. Both are relevant for the development of the biorefinery where these compounds may play an important role given their ubiquity, economic value and variety of applications. This thesis is related to terpenes extraction from natural sources and their subsequent separation and purification. Besides to the development of new experimental procedures for thermodynamic properties and equilibrium measurements, some theoretical approaches were also applied to this end. First, to create new applications for this compounds, and taking advantage of their very low solubility in water as shown by new and accurate experimental determinations, terpenes are used to prepare sustainable and cheap hydrophobic solvents within the deep eutectic solvents framework. After, based on the activity coefficients at infinite dilution measurements and COSMO-RS predictions a selection of ILs was made with potential for terpenes fractionation. Yet, and aiming at the development of new separation processes of terpenes, deep eutectic solvents composed of ammonium salts and monocarboxylic acids were also formulated and characterized. Finally, and targeting the development of accurate models for the fate of terpenes in the environment, a range of essential physicochemical properties of terpenes were measured and modelled.

## Contents

List of Figures .....	vi
List of Tables.....	xii
Nomenclature .....	xv
Chapter 1 – General Introduction .....	1
<b>1.1. General context</b> .....	<b>3</b>
<b>1.1.1. Terpenes</b> .....	<b>3</b>
<b>Properties and applications</b> .....	<b>7</b>
<b>Production and deterpenation</b> .....	<b>12</b>
<b>Environmental impact</b> .....	<b>16</b>
<b>1.1.2. Designer solvents</b> .....	<b>18</b>
<b>Ionic liquids</b> .....	<b>18</b>
<b>Deep eutectic solvents</b> .....	<b>21</b>
<b>1.2. Scope and objectives</b> .....	<b>25</b>
Chapter 2 – Terpenes Applications .....	29
<b>2.1. Introduction</b> .....	<b>31</b>
<b>2.2. Experimental</b> .....	<b>32</b>
<b>2.2.1. Materials</b> .....	<b>32</b>
<b>2.2.2. Methods</b> .....	<b>34</b>
<b>2.3. Theoretical approach</b> .....	<b>34</b>
<b>2.4. Tunable hydrophobic deep eutectic solvents and eutectic mixtures based on terpenes</b> .....	<b>36</b>
<b>2.4.1. Abstract</b> .....	<b>36</b>
<b>2.4.2. Results and discussion</b> .....	<b>37</b>
<b>2.5. Conclusions</b> .....	<b>46</b>
Chapter 3 – Extraction, Production and Deterpenation .....	47
<b>3.1. Ionic liquids as separation agents</b> .....	<b>49</b>
<b>3.1.1. Introduction</b> .....	<b>49</b>
<b>3.1.2. Experimental methods</b> .....	<b>50</b>



3.1.3.	Theoretical approach.....	52
3.1.4.	Activity coefficients at infinite dilution of organic solutes and water on polar imidazolium-based ionic liquids.....	56
3.1.4.1.	Abstract.....	56
3.1.4.2.	Chemicals.....	57
3.1.4.3.	Results and discussion.....	58
3.1.5.	Selection of ionic liquids to be used as separation agents for terpenes and terpenoids.....	73
3.1.5.1.	Abstract.....	73
3.1.5.2.	Chemicals.....	73
3.1.5.3.	Results and discussion.....	76
3.1.6.	Conclusions.....	86
3.2.	Measurement and PC-SAFT modeling of solid-liquid equilibrium of deep eutectic solvents of quaternary ammonium chlorides and carboxylic acids.....	87
3.2.1.	Abstract.....	88
3.2.2.	Introduction.....	88
3.2.3.	Experimental.....	90
3.2.3.1.	Materials.....	90
3.2.3.2.	Methods.....	90
3.2.4.	Theoretical approach.....	92
3.2.5.	Results and discussion.....	100
3.2.6.	Conclusion.....	109
3.3.	Indirect assessment of the fusion properties of choline chloride from solid-liquid equilibria data.....	110
3.3.1.	Abstract.....	110
3.3.2.	Introduction.....	111
3.3.3.	Experimental.....	112
3.3.3.1.	Materials.....	112
3.3.3.2.	Methods.....	112
3.3.4.	Theoretical approach.....	114

3.3.5.	Results and discussion .....	116
3.3.6.	Conclusion .....	120
<b>3.4.</b>	<b>Solid-liquid phase diagrams of eutectic solvents based on choline chloride and fatty acids or alcohols .....</b>	<b>120</b>
3.4.1.	Abstract .....	120
3.4.2.	Introduction .....	121
3.4.3.	Experimental .....	121
3.4.3.1.	Materials .....	121
3.4.3.2.	Methods .....	122
3.4.4.	Theoretical approach .....	122
3.4.5.	Results and discussion .....	123
3.4.6.	Conclusion .....	128
Chapter 4 –	Environmental Impact .....	129
<b>4.1.</b>	<b>Critical properties of terpenes and terpenoids .....</b>	<b>131</b>
4.1.1.	Abstract .....	131
4.1.2.	Introduction .....	131
4.1.3.	Experimental .....	134
4.1.3.1.	Material .....	134
4.1.3.2.	Methods .....	134
4.1.4.	Theoretical approach .....	136
4.1.5.	Results and discussion .....	140
4.1.6.	Conclusions .....	150
<b>4.2.</b>	<b>Mutual solubilities, densities and viscosities of ionic liquids and water .....</b>	<b>151</b>
4.2.1.	Introduction .....	151
4.2.2.	Experimental methods .....	153
4.2.3.	Theoretical approach .....	155
4.2.4.	Impact of the cation symmetry on the mutual solubilities between water and imidazolium-based ionic liquids .....	159
4.2.4.1.	Abstract .....	159

4.2.4.2.	Chemicals .....	160
4.2.4.3.	Results and discussion .....	161
4.2.5.	Analysis of the isomerism effect on the mutual solubilities of bis(trifluoromethylsulfonyl)imide-based ionic liquids with water .....	169
4.2.5.1.	Abstract .....	169
4.2.5.2.	Chemicals .....	170
4.2.5.3.	Results and discussion .....	171
4.2.6.	Densities, viscosities and derived thermodynamic properties of water-saturated imidazolium-based ionic liquids .....	180
4.2.6.1.	Abstract .....	180
4.2.6.2.	Chemicals .....	181
4.2.6.3.	Results and discussion .....	182
4.2.7.	Conclusions .....	193
4.3.	Aqueous solubilities of five <i>N</i> -(diethylaminothiocarbonyl)benzimidazole derivatives at $T = 298.15$ K .....	195
4.3.1.	Abstract .....	195
4.3.2.	Introduction .....	195
4.3.3.	Experimental .....	197
4.3.3.1.	Material .....	197
4.3.3.2.	Methods .....	198
4.3.4.	Theoretical approach .....	200
4.3.5.	Results and discussion .....	203
4.3.6.	Conclusions .....	213
4.4.	Terpene solubility in water and their environmental distribution .....	213
4.4.1.	Abstract .....	213
4.4.2.	Introduction .....	214
4.4.3.	Experimental .....	216
4.4.3.1.	Material .....	216
4.4.3.2.	Methods .....	217
4.4.4.	Results and discussion .....	217

<b>4.4.5. Conclusions</b> .....	226
Chapter 5 – Final Remarks and Future Work .....	229
List of Publications .....	235
References.....	239

## List of Figures

<b>Figure 1.1.</b> Record count of works on terpenes and/or terpenoids. Values extracted from ISI Web of Knowledge in January, 2017. ....	4
<b>Figure 1.2.</b> A visual introduction to some common terpenes and terpenoids and their structures (i.u. isoprene units). ....	6
<b>Figure 1.3.</b> Simplified scheme of terpenes biosynthesis.....	7
<b>Figure 1.4.</b> Mass percent composition ranges of components of different citrus essential oils (adapted from Arce and Soto, 2008). <sup>54</sup> .....	14
<b>Figure 1.5.</b> Common structures of ILs cations and anions.....	19
<b>Figure 1.6.</b> a) A simple eutectic phase diagram; b) Interaction mechanism of [Ch]Cl with a generic HBD.....	22
<b>Figure 1.7.</b> Structures of HBD and HBA commonly used in the deep eutectic solvents formulation (adapted from Francisco et al. <sup>135</sup> ). ....	23
<b>Figure 1.8.</b> Schematic illustration of the work developed on this thesis.....	28
<b>Figure 2.1.</b> Structures of the compounds investigated in this work.....	33
<b>Figure 2.2.</b> Solid-liquid phase diagrams of mixtures composed of monocarboxylic acids and terpenes. Symbols represent the experimental data measured in this work while the solid lines represent the ideal solubility curves.....	40
<b>Figure 2.3.</b> System L(-)-menthol + Thymol after cooling down to 193.15 K. ....	41
<b>Figure 2.4.</b> Density of mixtures involving monocarboxylic acids and L(-)-menthol or thymol. ....	42
<b>Figure 2.5.</b> Thermal expansion coefficient representation of mixtures of L(-)-menthol or thymol and monocarboxylic acids.....	43
<b>Figure 2.6.</b> Viscosity of mixtures involving monocarboxylic acids and L(-)-menthol or thymol. ....	44
<b>Figure 2.7.</b> Energy barrier of the mixtures investigated at 338.15 K as a function of the monocarboxylic acid used.....	45
<b>Figure 3.1.</b> Activity coefficients at infinite dilution of several solutes in ILs, at 398.15 K for alcohols and water, and 358.15 K for the other organic compounds. ○, [C <sub>4</sub> mim]Cl; ◇, [C <sub>4</sub> mim][CH <sub>3</sub> SO <sub>3</sub> ]; Δ, [C <sub>4</sub> mim][(CH <sub>3</sub> ) <sub>2</sub> PO <sub>4</sub> ]. The dotted line represents the number of carbons in the solutes structure, N. Symbols with the same color correspond to solutes of the same chemical family.....	58
<b>Figure 3.2.</b> Comparison of the experimental activity coefficients at infinite dilution with values from literature for two ionic liquids: (a) [C <sub>4</sub> mim]Cl, ◆ THF, ● ethanol, ▲ water (empty symbols correspond to literature data <sup>230</sup> ); (b) [C <sub>4</sub> mim][CH <sub>3</sub> SO <sub>3</sub> ], ◆ decane, ● dec-1-ene, ▲ THF, ■ 1,4-dioxane, ▼ toluene, ◀ methanol, ▶ butan-1-ol (empty symbols correspond to literature data <sup>231</sup> ). ....	63

**Figure 3.3.** Activity coefficients at infinite dilution of selected solutes in ILs, at 398.15 K for propan-1-ol, and 358.15 K for the other organic compounds. .... 65

**Figure 3.4.** Partial molar excess energies as a function of the activity coefficients at infinite dilution of the organic solutes studied in the ILs [C<sub>4</sub>mim]Cl, [C<sub>4</sub>mim][CH<sub>3</sub>SO<sub>3</sub>] and [C<sub>4</sub>mim][(CH<sub>3</sub>)<sub>2</sub>PO<sub>4</sub>], at 358.15 and 398.15 K. The line represents  $\overline{G}_m^{E,\infty}$  and the symbols correspond to:  $\diamond$ ,  $\overline{H}_m^{E,\infty}$  and  $\Delta$ ,  $T_{ref}\overline{S}_m^{E,\infty}$  ..... 68

**Figure 3.5.** Comparison of density experimental values with literature data. Symbols:  $\blacktriangle$  [C<sub>4</sub>mim]Cl, this work;  $\blacktriangle$  [C<sub>4</sub>mim]Cl<sup>236</sup>;  $\blacktriangle$  [C<sub>4</sub>mim]Cl<sup>237</sup>;  $\blacktriangle$  [C<sub>4</sub>mim]Cl<sup>238</sup>;  $\blacktriangle$  [C<sub>4</sub>mim]Cl<sup>239</sup>;  $\blacktriangle$  [C<sub>4</sub>mim]Cl<sup>240</sup>;  $\blacklozenge$  [C<sub>4</sub>mim][CH<sub>3</sub>SO<sub>3</sub>], this work;  $\blacklozenge$  [C<sub>4</sub>mim][CH<sub>3</sub>SO<sub>3</sub>]<sup>223</sup>;  $\bullet$  [C<sub>4</sub>mim][(CH<sub>3</sub>)<sub>2</sub>PO<sub>4</sub>], this work;  $\bullet$  [C<sub>4</sub>mim][(CH<sub>3</sub>)<sub>2</sub>PO<sub>4</sub>]<sup>235</sup>. .... 70

**Figure 3.6.** Experimental gas–liquid partition coefficients,  $K_L$ , for organic solutes and water in the ILs studied.  $\circ$ , [C<sub>4</sub>mim]Cl;  $\diamond$ , [C<sub>4</sub>mim][CH<sub>3</sub>SO<sub>3</sub>];  $\Delta$ , [C<sub>4</sub>mim][(CH<sub>3</sub>)<sub>2</sub>PO<sub>4</sub>]. The dotted line represents the number of carbons in the solutes structure,  $N$ . Symbols with the same color correspond to solutes of the same chemical family. .... 70

**Figure 3.7.** Activity coefficients at infinite dilution of terpenes and terpenoids in the ILs studied, at 408.15 K.  $\square$ , [C<sub>4</sub>mim]Cl;  $\circ$ , [C<sub>4</sub>mim][CH<sub>3</sub>SO<sub>3</sub>];  $\Delta$ , [C<sub>4</sub>mim][(CH<sub>3</sub>)<sub>2</sub>PO<sub>4</sub>];  $\diamond$ , [C<sub>4</sub>mim][CF<sub>3</sub>SO<sub>3</sub>]. .... 76

**Figure 3.8.** Activity coefficients at infinite dilution as a function of the solubility parameters (calculated through reference <sup>248</sup>) of terpenes and terpenoids in the ILs studied, at 408.15 K. Empty symbols were not used in the fit. .... 78

**Figure 3.9.** Partial molar excess energies at infinite dilution as a function of the natural logarithm of the activity coefficients at infinite dilution of the terpenes and terpenoids in the ILs study, at 408.15 K. The full line represents  $\overline{G}_m^{E,\infty}$  and the symbols correspond to:  $\diamond$ ,  $\overline{H}_m^{E,\infty}$  and  $\Delta$ ,  $T_{ref}\overline{S}_m^{E,\infty}$ . .... 80

**Figure 3.10.** Experimental gas–liquid partition coefficients,  $K_L$ , for terpenes and terpenoids in the ILs studied, at 408.15 K.  $\square$ , [C<sub>4</sub>mim]Cl;  $\circ$ , [C<sub>4</sub>mim][CH<sub>3</sub>SO<sub>3</sub>];  $\Delta$ , [C<sub>4</sub>mim][(CH<sub>3</sub>)<sub>2</sub>PO<sub>4</sub>];  $\diamond$ , [C<sub>4</sub>mim][CF<sub>3</sub>SO<sub>3</sub>]. .... 81

**Figure 3.11.** Experimental and COSMO-RS predictions of  $S_{ij}^\infty$  and  $k_j^\infty$  of all solutes at 408.15 K in the different ionic liquids studied. Color code:  $\blacklozenge$  [1-2];  $\blacklozenge$  [2-4];  $\blacklozenge$  [4-10];  $\blacklozenge$  [10-20];  $\blacklozenge$  [20-30]; and  $\blacklozenge$  >30. Capacities,  $\blacklozenge$  <0.01;  $\blacklozenge$  [0.01-0.05];  $\blacklozenge$  [0.05-0.1];  $\blacklozenge$  [0.1-0.2];  $\blacklozenge$  [0.2-1];  $\blacklozenge$  [1-2];  $\blacklozenge$  [2-5]; and  $\blacklozenge$  > 5. .... 83

**Figure 3.12.**  $S_{ij}^\infty$  and  $k_j^\infty$  of all solutes at 408.15 K in selected ILs, computed by COSMO-RS. Color code: Selectivities,  $\blacklozenge$  [1-2];  $\blacklozenge$  [2-4];  $\blacklozenge$  [4-10];  $\blacklozenge$  [10-20];  $\blacklozenge$  [20-30]; and  $\blacklozenge$  >30; Capacities,  $\blacklozenge$  <0.01;  $\blacklozenge$  [0.01-0.05];  $\blacklozenge$  [0.05-0.1];  $\blacklozenge$  [0.1-0.2];  $\blacklozenge$  [0.2-1];  $\blacklozenge$  [1-2];  $\blacklozenge$  [2-5]; and  $\blacklozenge$  > 5. .... 85

**Figure 3.13.** a) Experimental densities of aqueous solutions of [N<sub>3333</sub>]Cl measured in this work at atmospheric pressure:  $\blacksquare$ ,  $x_{IL}=0.0931$ ;  $\bullet$ ,  $x_{IL}=0.1608$ . b) Water activity coefficients at 298.15 K:  $\blacklozenge$ , Lindenbaum et al.<sup>276</sup>;  $\blacktriangle$ , this work. Symbols represent experimental data while the solid lines depict the PC-SAFT results using  $k_{ij} = -0.1167$  between water and [N<sub>3333</sub>]Cl and the water parameters also used in reference<sup>274</sup>. .... 95

<b>Figure 3.14.</b> Densities and vapor pressures of pure monocarboxylic acids. The symbols represent experimental data from ref. <sup>279</sup> while the solid lines represent the PC-SAFT results for capric acid (●), palmitic acid (■) and stearic acid (▲), respectively.....	97
<b>Figure 3.15.</b> Solid-liquid phase diagrams of DES composed of monocarboxylic acids and symmetrical quaternary ammonium chlorides. Symbols represent the experimental data measured in this work while the solid lines depict the PC-SAFT modelling. ....	102
<b>Figure 3.16.</b> Solid-liquid equilibrium (left) and activity coefficients (right) for the DES [N <sub>2222</sub> ]Cl + lauric acid. Legend: ●, experimental; —, PC-SAFT; ---, ideal. ....	103
<b>Figure 3.17.</b> Deviations to the experimental data measured in this work: ■, ideal; ■, PC-SAFT for a) [N <sub>1111</sub> ]Cl + carboxylic acids b) [N <sub>2222</sub> ]Cl + carboxylic acids c) [N <sub>3333</sub> ]Cl + carboxylic acids. ....	106
<b>Figure 3.18.</b> a) Eutectic compositions b) eutectic temperatures c) melting-temperature depression of the various DES studied, estimated by PC-SAFT. ●, [N <sub>1111</sub> ]Cl; ■, [N <sub>2222</sub> ]Cl; ▲, [N <sub>3333</sub> ]Cl. ....	107
<b>Figure 3.19.</b> Solid-liquid phase diagrams for the [Ch]Cl+Ionic compounds systems studied. [Ch]Cl(1)+ (○) [Ch][Ac](2); (⊕)[Ch][Prop](2); (◇) [Ch][Buta](2); (□)[N <sub>4444</sub> ]Cl(2); (△)[P <sub>4444</sub> ]Cl(2); (▽) [BzCh]Cl(2); (✕)[C <sub>4</sub> mpyr]Cl(2); (✕)[Ch][NTf <sub>2</sub> ](2); (○)[C <sub>2</sub> mim]Cl(2); (⊕)[C <sub>2</sub> OHmim]Cl(2). ....	116
<b>Figure 3.20.</b> Plot of the regression by equation 3.29 of the experimental data for the solubility of [Ch]Cl in [Ch]Cl+Ionic compounds systems. [Ch]Cl(1)+ (○) [Ch][Ac](2); (⊕)[Ch][Prop](2); (◇) [Ch][Buta](2); (□)[N <sub>4444</sub> ]Cl(2); (△)[P <sub>4444</sub> ]Cl(2); (▽) [BzCh]Cl(2); (✕)[C <sub>4</sub> mpyr]Cl(2); (✕)[Ch][NTf <sub>2</sub> ](2); (○)[C <sub>2</sub> mim]Cl(2); (⊕)[C <sub>2</sub> OHmim]Cl(2). (—) ideal solution ( $T_{fus,[Ch]Cl} = 597$ K, $\Delta_{fus}H_{[Ch]Cl} = 4300$ J·mol <sup>-1</sup> ). ....	118
<b>Figure 3.21.</b> Solid-liquid phase diagrams of [Ch]Cl + fatty alcohols and fatty acids. (●) Experimental data, (- - -) Ideal solution. [Ch]Cl + (a) 1-tetradecanol; (b) 1-hexadecanol; (c) 1-octadecanol; (d) Decanoic acid; (e) Dodecanoic acid; (f) Tetradecanoic acid; (g) Hexadecanoic acid; (h) Octadecanoic acid.....	126
<b>Figure 4.1.</b> Schematic representation of the procedure followed in this work.....	134
<b>Figure 4.2.</b> Density, $\rho$ , of pure terpenes and terpenoids as a function of temperature and at 0.1 MPa. ....	141
<b>Figure 4.3.</b> Percentage relative deviations between density data determined here and those from literature (references on Table 4.2). ....	142
<b>Figure 4.4.</b> Temperature change ( $\Delta T / K$ ) and critical pressure and acentric factor ratio for the different contribution methods and compounds studied. ....	144
<b>Figure 4.5.</b> Global average relative deviation between the experimental and the predicted densities and vapor pressures, calculated using the PR and SRK EoS, with critical properties estimated by Joback, CG, and WJ methods ....	145
<b>Figure 4.6.</b> Temperature change ( $\Delta T / K$ ) and critical pressure and acentric factor ratio between Soave-Redlich-Kwong and Peng-Robinson EoS for the compounds studied.....	147
<b>Figure 4.7.</b> Average relative deviation between the experimental and the predicted densities and vapor pressures, calculated using the SRK and the PR, with critical properties estimated by the same EoS. ....	148

**Figure 4.8.** Scheme of the apparatus used for the mutual solubility measurements. (A), PID temperature controller; (B), Isolated air bath; (B1) Aluminum block; (B2), Pt100 (class 1/10) temperature sensor; (B3), Thermostatic fluid; (C), Refrigerated bath. .... 154

**Figure 4.9.** Chemical structures of the studied imidazolium-based ILs. .... 161

**Figure 4.10.** Liquid-liquid phase diagrams of water and ionic liquids: (a) ionic-liquid-rich phase; and (b) water-rich phase. Symbols (experimental data): (+), [C<sub>1</sub>C<sub>1</sub>im][NTf<sub>2</sub>]; (◆), [C<sub>2</sub>C<sub>2</sub>im][NTf<sub>2</sub>]; (◇), [C<sub>3</sub>C<sub>1</sub>im][NTf<sub>2</sub>]; (■), [C<sub>3</sub>C<sub>3</sub>im][NTf<sub>2</sub>]; (□), [C<sub>5</sub>C<sub>1</sub>im][NTf<sub>2</sub>]; (▲), [C<sub>4</sub>C<sub>4</sub>im][NTf<sub>2</sub>]; (△), [C<sub>7</sub>C<sub>1</sub>im][NTf<sub>2</sub>]; (●), [C<sub>5</sub>C<sub>5</sub>im][NTf<sub>2</sub>]; and (○), [C<sub>9</sub>C<sub>1</sub>im][NTf<sub>2</sub>]. The matching color full and dashed lines represent, respectively, the COSMO-RS predictions for the ILs containing asymmetric and symmetric cations. .... 163

**Figure 4.11.** Comparison with literature data: (a) ionic-liquid-rich phase; and (b) water-rich phase. Symbols: (●), [C<sub>1</sub>C<sub>1</sub>im][NTf<sub>2</sub>] this work; (○), [C<sub>1</sub>C<sub>1</sub>im][NTf<sub>2</sub>]<sup>405</sup>; (●), [C<sub>2</sub>C<sub>2</sub>im][NTf<sub>2</sub>] this work; and (○), [C<sub>2</sub>C<sub>2</sub>im][NTf<sub>2</sub>]<sup>406</sup>. .... 164

**Figure 4.12.** Solubility of [NTf<sub>2</sub>]-based ILs in water (expressed in mole fraction) as function of the IL molar volume:  $\ln(x_{IL}) = -0.0309 (V_m/\text{cm}^3 \cdot \text{mol}^{-1}) + 0.9357$ ;  $R^2 = 0.9947$ . All data are at 298.15 K. ... 165

**Figure 4.13.** Standard molar entropy of solution,  $\Delta_{sol}S_m^0$ , as function of total methylene groups in the alkyl side chains, N, of ILs. Symbols: (◆, solid line), [C<sub>n</sub>C<sub>1</sub>im][PF<sub>6</sub>],<sup>380</sup>  $\Delta_{sol}S_m^0 = -4.7 \cdot N + 10.3$ ,  $R^2 = 0.9931$ ; (■, dashed line), [C<sub>n</sub>C<sub>1</sub>im][NTf<sub>2</sub>],<sup>378</sup>  $\Delta_{sol}S_m^0 = -5.2 \cdot N + 19.4$ ,  $R^2 = 0.9832$ ; and (▲, dotted line), [C<sub>n</sub>C<sub>n</sub>im][NTf<sub>2</sub>],  $\Delta_{sol}S_m^0 = -4.5 \cdot N - 23.2$ ,  $R^2 = 0.9459$ . The symbols and line represents the estimated  $\Delta_{sol}S_m^0$  calculated using Equation 4.23 and dependency of  $\Delta_{sol}S_m^0$  as function of N, respectively. All data are at 298.15 K. .... 167

**Figure 4.14.** Schematic representation of chemical structure of the studied imidazolium-based ionic liquids. .... 170

**Figure 4.15.** Liquid-liquid phase diagram for water and ionic liquids: (a), ionic-liquid-rich phase; and (b) water-rich phase: (x), [C<sub>1</sub>im][NTf<sub>2</sub>]; (◆), [C<sub>2</sub>im][NTf<sub>2</sub>]; (◇), [C<sub>1</sub>C<sub>1</sub>im][NTf<sub>2</sub>]; (■), [C<sub>2</sub>C<sub>3</sub>im][NTf<sub>2</sub>]; (□), [C<sub>4</sub>C<sub>1</sub>im][NTf<sub>2</sub>]; (▲), [C<sub>4</sub>C<sub>1</sub>C<sub>1</sub>im][NTf<sub>2</sub>]; (△), [C<sub>3</sub>C<sub>3</sub>im][NTf<sub>2</sub>]; and (○), [C<sub>5</sub>C<sub>1</sub>im][NTf<sub>2</sub>]. The lines at the same colors represent the COSMO-RS predictions for the compounds measured in this work. .... 173

**Figure 4.16.** Schematic representation of the percent decrease in the mutual solubilities of ILs with water, when introducing a methyl group. .... 175

**Figure 4.17.** Calculated versus experimental solubility of bis(trifluoromethylsulfonyl)imide-based ionic liquids at 298.15 K in (a) IL-rich phase and (b) water-rich phase. .... 178

**Figure 4.18.** Solubility of bis(trifluoromethylsulfonyl)imide-based ionic liquids in water as a function of the ionic liquid molar volume:  $\ln(x_{IL}) = -0.0309 (V_m/\text{cm}^3 \cdot \text{mol}^{-1}) + 0.9357$ ;  $R^2 = 0.9947$ ,<sup>403</sup> at 298.15 K. (◆), data used in the correlation; and (●), new data. .... 179

**Figure 4.19.** Schematic representation of the chemical structure of the studied imidazolium-based ILs. .... 181

**Figure 4.20.** Density of the symmetric and asymmetric water-saturated ILs as function of temperature, (a, b), respectively; and density relative deviations between the pure<sup>182</sup> and the



symmetric and asymmetric water-saturated ILs, (c, d), respectively: (◆), [C<sub>1</sub>C<sub>1</sub>im][NTf<sub>2</sub>]; (●), [C<sub>2</sub>C<sub>2</sub>im][NTf<sub>2</sub>]; (▲), [C<sub>3</sub>C<sub>3</sub>im][NTf<sub>2</sub>]; (□), [C<sub>4</sub>C<sub>4</sub>im][NTf<sub>2</sub>]; (◇), [C<sub>5</sub>C<sub>5</sub>im][NTf<sub>2</sub>]; (▽), [C<sub>6</sub>C<sub>6</sub>im][NTf<sub>2</sub>]; (○), [C<sub>7</sub>C<sub>7</sub>im][NTf<sub>2</sub>]; (◆), [C<sub>8</sub>C<sub>8</sub>im][NTf<sub>2</sub>]; (▷), [C<sub>10</sub>C<sub>10</sub>im][NTf<sub>2</sub>]; (\*), [C<sub>2</sub>C<sub>1</sub>im][NTf<sub>2</sub>]; (o), [C<sub>3</sub>C<sub>1</sub>im][NTf<sub>2</sub>]; (x), [C<sub>4</sub>C<sub>1</sub>im][NTf<sub>2</sub>]; (Δ), [C<sub>5</sub>C<sub>1</sub>im][NTf<sub>2</sub>]; (□), [C<sub>7</sub>C<sub>1</sub>im][NTf<sub>2</sub>]; (◇), [C<sub>9</sub>C<sub>1</sub>im][NTf<sub>2</sub>]; and (▽), [C<sub>11</sub>C<sub>1</sub>im][NTf<sub>2</sub>]. ..... 183

**Figure 4.21.** Density of the studied pure<sup>182</sup> (empty symbols) and water-saturated (full symbols) [NTf<sub>2</sub>]-based ILs as a function of the cation structure (alkyl side chain length increase) at 298.15 K. Colorful symbols correspond to isomers, and black symbols correspond to ILs with no corresponding isomers. .... 186

**Figure 4.22.** Thermal expansion coefficient of pure<sup>182</sup> and water-saturated ILs at 323.15 K and 0.1 MPa as a function of the cation structure (alkyl side chain length increase). The full and empty symbols represent water-saturated and pure ILs, respectively. Colorful symbols correspond to isomers, and black symbols correspond to ILs with no corresponding isomers. .... 188

**Figure 4.23.** Viscosity of the of the symmetric and asymmetric water-saturated ILs as function of temperature, (a, b), respectively, and viscosity relative deviations between the pure<sup>182,421</sup> and the symmetric and asymmetric water-saturated ILs (c, d), respectively: (◆), [C<sub>1</sub>C<sub>1</sub>im][NTf<sub>2</sub>]; (\*), [C<sub>2</sub>C<sub>1</sub>im][NTf<sub>2</sub>]; (o), [C<sub>3</sub>C<sub>1</sub>im][NTf<sub>2</sub>]; (●), [C<sub>2</sub>C<sub>2</sub>im][NTf<sub>2</sub>]; (x), [C<sub>4</sub>C<sub>1</sub>im][NTf<sub>2</sub>]; (Δ), [C<sub>5</sub>C<sub>1</sub>im][NTf<sub>2</sub>]; (▲), [C<sub>3</sub>C<sub>3</sub>im][NTf<sub>2</sub>]; (□), [C<sub>7</sub>C<sub>1</sub>im][NTf<sub>2</sub>]; (□), [C<sub>4</sub>C<sub>4</sub>im][NTf<sub>2</sub>]; (◇), [C<sub>9</sub>C<sub>1</sub>im][NTf<sub>2</sub>]; (◇), [C<sub>5</sub>C<sub>5</sub>im][NTf<sub>2</sub>]; (▽), [C<sub>11</sub>C<sub>1</sub>im][NTf<sub>2</sub>]; (▽), [C<sub>6</sub>C<sub>6</sub>im][NTf<sub>2</sub>]; (○), [C<sub>7</sub>C<sub>7</sub>im][NTf<sub>2</sub>]; (◆), [C<sub>8</sub>C<sub>8</sub>im][NTf<sub>2</sub>]; and (▷), [C<sub>10</sub>C<sub>10</sub>im][NTf<sub>2</sub>]. ..... 189

**Figure 4.24.** Viscosity dependence of the pure<sup>182,421</sup> and water-saturated [NTf<sub>2</sub>]-based ILs studied, at 298.15 K, as a function of the cation structure (alkyl side chain length increase). The matching empty and colorful symbols represent, respectively, the pure and water-saturated ILs. Colorful symbols correspond to isomers, and black symbols correspond to ILs with no corresponding isomers. .... 190

**Figure 4.25.** Energy barrier of pure<sup>182,421</sup> and water-saturated ILs at 323.15 K and 0.1 MPa, as a function of the cation structure (alkyl side chain length increase). The matching empty and colorful symbols represent, respectively, the pure and water-saturated ILs. Colorful symbols correspond to isomers, and black symbols correspond to ILs with no corresponding isomers. .... 192

**Figure 4.26.** Deviation ( $E_{Dev}$ ) between the water-saturated and the pure ILs energy barriers at 323.15 K, as a function of: (a) the total number of carbons in the alkyl chain length,  $N$ ; and (b) the experimental mole fraction water solubility,  $x_w$  (at 298.15 K). .... 193

**Figure 4.27.** Chemical structures of the title compounds. .... 196

**Figure 4.28.** Experimental setup for the aqueous solubility measurements. A: Test tubes, B: dialysis tubing containing ultra-pure water, C: sampling glass tube, D: rubber cup, E: thermostated bath, F: stirrer. .... 198

**Figure 4.29.** Sigma profiles of most stable conformers of the respective *N*-(diethylaminothiocarbonyl)benzimidazole derivatives, BP-TZVP level of theory. The sigma profile of water is plotted as reference. The range beyond  $\sigma = \pm 0.01 \text{ e}\cdot\text{\AA}^{-2}$  is considered as being strongly polar and potentially hydrogen-bonding (with a hydrogen-bond threshold value at  $\sigma_{hb} = 0.0079 \text{ e}\cdot\text{\AA}^{-2}$ ).<sup>218</sup> ..... 205

**Figure 4.30.** Sigma potentials of most stable conformers of the respective *N*-(diethylaminothiocarbonyl)benzimidazole derivatives, at  $T = 298.15$  K, BP-TZVP level of theory, revealing the effect of successive substitution on the enamine side of the title compounds. The sigma potential of water is plotted as reference..... 205

**Figure 4.31.** Chemical space diagram of the title compounds and selected urea-based pesticides (6 – Diuron; 7 – Fenuron; 8 – Fluometuron; 9 – Linuron; 10 – Barban; 11 – Chlorpropham; 12 – Diphenamid; 13 – Propachlor; 14 – Propanil; 15 – Aldicarb; 16 – Methomyl; 17 – Carbaryl; 18 – Parafluron; 19 – Triflumuron; 20 – Flufenoxuron; 21 – Chlorfluazuron; 22 –Teflubenzuron; 23 – Noviflumuron; 24 – Cyflufenamid; 25 – Penthiopyrad; 26 – Flutolanil; 27 – Fluopicolide; 28 – Etoxazole; 29 – Bistrifluron; 30 – Hexaflumuron; 31 – Lufenuron; 32 – Novaluron; 33 – Diflubenzuron; 34 – Dichlorbenzuron)..... 210

**Figure 4.32.** Comparison of the experimental aqueous solubilities of toluene and *p*-xylene with data from literature. The colorful filled symbols represent experimental points measured in this work and the open symbols and lines represent experimental and calculated data compiled and selected by Góral et al.<sup>479</sup> The black filled triangles correspond to values measured by Neely et al.<sup>480</sup> ..... 218

**Figure 4.33.** Structures and mole fraction water solubilities of toluene, *p*-xylene and *p*-cymene at 298.15 K..... 220

**Figure 4.34.** Chemical space diagram of the terpenes investigated in this work and some other selected compounds, namely isoprene, toluene and *p*-xylene. .... 226

## List of Tables

<b>Table 1.1.</b> Generic properties/applications of terpenes in several industries. <sup>10,28-30</sup> .....	9
<b>Table 1.2.</b> Major commercial sources of terpenes (adapted from Schwab et al. <sup>30</sup> ). .....	12
<b>Table 1.3.</b> Terpenes extracted from natural sources using ILs or ILs solutions (adapted from Passos et al. <sup>115</sup> ). .....	21
<b>Table 1.4.</b> Terpenes extracted from natural sources using DES. ....	25
<b>Table 2.1.</b> Compounds description and their melting properties herewith values from literature. ....	33
<b>Table 3.1.</b> Studied ionic liquids: name, structure, abbreviation, source, molar mass (M), melting point (T <sub>M</sub> ) and purity. ....	57
<b>Table 3.2.</b> Activity coefficients at infinite dilution of organic compounds and water in ILs, at different temperatures. <sup>a</sup> .....	59
<b>Table 3.3.</b> Comparison between the activity coefficients at infinite dilution with values from literature at 358.15 K. ....	64
<b>Table 3.4.</b> Density of the pure ILs studied as a function of temperature at 0.1 MPa. ....	69
<b>Table 3.5.</b> Selectivities ( $S_{ij}^{\infty}$ ) and capacities ( $k_j^{\infty}$ ) at infinite dilution for different separation problems at 358.15 K. ....	72
<b>Table 3.6.</b> Name, structure, abbreviation, supplier, molar mass (M), melting point (T <sub>M</sub> ) and purity of the investigated ionic liquids. ....	74
<b>Table 3.7.</b> Names, structures, supplier, molar mass (M), boiling points (T <sub>BP</sub> ) and mass fraction purities of the terpenes and terpenoids used. ....	75
<b>Table 3.8.</b> Selectivities ( $S_{ij}^{\infty}$ ) / capacities ( $k_j^{\infty}$ ) at infinite dilution for $\alpha$ -pinene / $\beta$ -pinene at 408.15 K in different solvents. ....	86
<b>Table 3.9.</b> Sources and purities of the compounds used in this work. ....	90
<b>Table 3.10.</b> PC-SAFT molecular parameters for symmetrical quaternary ammonium chlorides (2B association scheme). ....	96
<b>Table 3.11.</b> PC-SAFT pure-component parameters for monocarboxylic acids (2B association scheme). ....	97
<b>Table 3.12.</b> Melting properties for pure compounds measured in this work and comparison with literature. ....	101
<b>Table 3.13.</b> Binary parameters applied within PC-SAFT model. ....	104
<b>Table 3.14.</b> Pure component properties. ....	113
<b>Table 3.15.</b> Pure component properties. ....	122

<b>Table 3.16.</b> Experimental ( $x_1$ , $T$ ) and calculated ( $\gamma_i$ ) data of the solid-liquid equilibria for the systems investigated in this work. ....	123
<b>Table 3.17.</b> Eutectic points, experimental and obtained by the ideal liquid phase model. ....	127
<b>Table 4.1.</b> Names, structures, sources, molar mass ( $M$ ), boiling points <sup>a</sup> ( $T_{BP}$ ) and mass fraction purities (declared by the supplier) of the terpenes and terpenoids used. ....	135
<b>Table 4.2.</b> Maximum relative deviations between the experimental values measured in this work and those reported in the literature. ....	142
<b>Table 4.3.</b> Critical properties of terpenes and terpenoids estimated with different contribution methods. ....	143
<b>Table 4.4.</b> Critical properties and acentric factor of terpenes estimated according with the approach II. ....	147
<b>Table 4.5.</b> Critical properties and acentric mean absolute error between those calculated by group contribution methods and those estimated by the SRK and PR EoS. ....	149
<b>Table 4.6.</b> Comparison between estimated and experimental critical temperatures. ....	150
<b>Table 4.7.</b> Investigated ionic liquids: name, abbreviation, source, molecular mass ( $M$ ), and purity. ....	160
<b>Table 4.8.</b> Experimental mole fraction solubility of water ( $x_w$ ) in ILs as a function of temperature and at 0.10 KPa. <sup>a</sup> ....	161
<b>Table 4.9.</b> Experimental mole fraction solubility of ionic liquid ( $x_{IL}$ ) in water as a function of temperature and at 0.10 KPa. <sup>a</sup> ....	162
<b>Table 4.10.</b> Estimated parameters for the mole fraction of water in the IL-rich phase and IL in the water-rich phase estimated using Equations 4.19 and 4.20, respectively. <sup>a</sup> ....	166
<b>Table 4.11.</b> Standard thermodynamic molar properties of solution of ionic liquids in water at 298.15 K. <sup>a</sup> ....	166
<b>Table 4.12.</b> Standard molar properties of solvation of ionic liquids in water at 298.15 K. <sup>a</sup> ....	168
<b>Table 4.13.</b> Investigated ionic liquids: name, abbreviation, source, molecular mass ( $M$ ), and purity. ....	170
<b>Table 4.14.</b> Experimental mole fraction solubility of water in ionic liquids, $x_w$ , at different temperatures and at 0.10 MPa. <sup>a</sup> ....	172
<b>Table 4.15.</b> Experimental mole fraction solubility of ionic liquids in water, $x_{IL}$ , at different temperatures and at 0.10 MPa. <sup>a</sup> ....	172
<b>Table 4.16.</b> Correlation parameters for the mole fraction solubility of water in the IL-rich phase and IL in the water-rich phase. <sup>a</sup> ....	176
<b>Table 4.17.</b> Standard molar properties of solution of ILs in water, at 298.15 K. <sup>a</sup> ....	176

<b>Table 4.18.</b> Investigated ionic liquids: chemical name, abbreviation, source, molecular weight ( $M_w$ ) and purity. ....	182
<b>Table 4.19.</b> Experimental and estimated mole fraction solubility of water ( $x_w$ ) in the investigated ILs, at 298.15 K and 0.10 MPa. ....	185
<b>Table 4.20.</b> Thermal expansion coefficients, $\alpha_p$ , of pure <sup>182</sup> and water-saturated ILs, estimated using Equation 4.28 at 323.15 K and 0.1 MPa. <sup>a</sup> .....	187
<b>Table 4.21.</b> Fitting coefficients of the VTF equation and derived energy barrier, $E$ , of pure <sup>182,421</sup> and water-saturated ILs at 323.15 K and 0.1 MPa. <sup>a</sup> .....	191
<b>Table 4.22.</b> Experimental aqueous solubilities at 298.15 K and expanded uncertainties ( $U$ ) for a 95% confidence interval.....	203
<b>Table 4.23.</b> Comparison of experimental data and COSMO-RS aqueous solubilities, both at the BP-TZVP and BP-TZVPD-FINE level of theory, referring to the crystalline state. ....	207
<b>Table 4.24.</b> Standard molar enthalpies of sublimation, $\Delta_{cr}^g H_m^0(298.15 \text{ K})$ , of <i>N</i> -(diethylaminothiocarbonyl)benzimidazole derivatives. Literature data and COSMO-RS results, both at the BP-TZVP and BP-TZVPD-FINE level of theory.....	208
<b>Table 4.25.</b> Name, structure, supplier, CAS, molar mass ( $M$ ), and purity (declared by the supplier) of the investigated compounds. ....	216
<b>Table 4.26.</b> Experimental mole fraction ( $x_{\text{terpene}}$ ) of terpenes in water as a function of temperature and at atmospheric pressure. <sup>a</sup> .....	219
<b>Table 4.27.</b> Experimental and calculated mole fraction ( $x_{\text{terpene}}$ ) of terpenes in water at 298.15 K. ....	221
<b>Table 4.28.</b> Estimated parameters for the mole fraction of terpenes in water estimated using Equation 4.38, along with the corresponding errors at the 95% confidence level.....	223
<b>Table 4.29.</b> Standard thermodynamic molar properties of solution of terpenes in water at $T_{hm} = 310.42 \text{ K}$ together with the errors at the 95% confidence level. ....	224

## Nomenclature

### Abbreviations

<sup>13</sup> C, Carbon 13	IGRs, Commercial Insect Growth Regulants
<sup>19</sup> F, Fluor 19	ILs, Ionic Liquids
<sup>1</sup> H, Hydrogen 1	KF, Karl Fischer
AAD, Absolute Average Deviation	Lit., Literature
ARD, Average Relative Deviation	LLE, Liquid-Liquid Equilibrium
BFC, Bioconcentration Factor	MEP, Methylerythritol Phosphate Pathway
BP_TZVP, Basis Parameterization_Triple-ζ Valence Polarized	MEV, Mevalonic Acid Pathway
BVOC, Biogenic Volatile Organic Compounds	Min, Minute
CG, Constantinou and Gani	n.a., not available
CO <sub>2</sub> , Carbone Dioxide	NMP, N-methyl-2-pyrrolidinone
COSMO-RS, CONductor-like Screening MOdel for Real Solvents	NMR, Nuclear Magnetic Resonance
CPA, Cubic-Plus-Association	NRTL, Non-Random Two-Liquid Model
DES, Deep Eutectic Solvents	PBT, Persistence, Bioaccumulation, Toxicity
DMADP, Dimethylallyl Diphosphate	PC-SAFT, Perturbed-Chain Statistical Associating Fluid Theory
DSC, Differential Scanning Calorimetry	PR, Peng-Robinson
EoS, Equations of State	QSPR, Quantitative Structure Property Relation
EPA, Environmental Protection Agency	RD, Relative Deviation
Eq., Equation	SAFT, Statistical Associating Fluid Theory
exp., Experimental	SLE, Solid-Liquid Equilibrium
FDP, Farnesyl Diphosphate	SRK, Soave-Redlich-Kwong
FTIR, Fourier Transform InfraRed	TCD, Thermal Conductivity Detector
GC-MS, Gas Chromatography – Mass Spectrometry	TGA, Thermogravimetric Analysis
GDP, Geranyl Diphosphate	THF, Tetrahydrofuran
GFDP, Geranylarnesyl Diphosphate	UCST, Upper Critical Solution Temperature
GGDP, Geranylgeranyl Diphosphate	UNIFAC, Universal Functional-group Activity Coefficients
GLC, Gas-Liquid Chromatography	US\$, United States Dollar
GRAS, Generally Recognized As Safe	USA, United States of America
H, Hydrogen	UV, Ultraviolet
H <sub>2</sub> O, Water	UV-Vis, Ultraviolet-Visible
HB, Hydrogen Bond	VLE, Vapor-Liquid Equilibrium
HBA, Hydrogen Bond Acceptor	VOC, Volatile Organic Compounds
HBD, Hydrogen Bond Donor	VTF, Vogel-Tammann-Fulcher
i.u., Isoprene Units	WJ, Wilson and Jasperson
IDP, Isopentenyl Diphosphate	

## Salts

[Ch]Cl, Choline Chloride

[N<sub>1111</sub>]Cl, Tetramethylammonium Chloride

[N<sub>2222</sub>]Cl, Tetraethylammonium Chloride

[N<sub>3333</sub>]Cl, Tetrapropylammonium Chloride

[N<sub>4444</sub>]Cl, Tetrabutylammonium Chloride

[P<sub>4444</sub>]Cl, Tetrabutylphosphonium Chloride

LiCl, Lithium Chloride

NaBr, Sodium Bromide

## Ionic Liquids Cations

[BzCh]<sup>+</sup>,

Benzylidimethyl(2-hydroxyethyl)-ammonium

[C<sub>10</sub>C<sub>10</sub>im]<sup>+</sup>, 1,3-didecylimidazolium

[C<sub>11</sub>C<sub>1</sub>im]<sup>+</sup>, 1-methyl-3-undecylimidazolium

[C<sub>1</sub>C<sub>1</sub>im]<sup>+</sup>, 1,3-dimethylimidazolium

[C<sub>1</sub>im]<sup>+</sup>, 1-methylimidazolium

[C<sub>2</sub>C<sub>1</sub>im]<sup>+</sup>, [C<sub>2</sub>mim]<sup>+</sup>,

1-ethyl-3-methylimidazolium

[C<sub>2</sub>C<sub>2</sub>im]<sup>+</sup>, 1,3-diethylimidazolium

[C<sub>2</sub>C<sub>3</sub>im]<sup>+</sup>, 1-ethyl-3-propylimidazolium

[C<sub>2</sub>im]<sup>+</sup>, 1-ethylimidazolium

[C<sub>2</sub>OHmim]<sup>+</sup>,

1-(2-hydroxyethyl)-3-methylimidazolium

[C<sub>3</sub>-3-C<sub>1</sub>py]<sup>+</sup>, 3-methyl-1-propylpyridinium

[C<sub>3</sub>C<sub>1</sub>im]<sup>+</sup>, 1-methyl-3-propylimidazolium

[C<sub>3</sub>C<sub>1</sub>pip]<sup>+</sup>, 1-methyl-1-propylpiperidinium

[C<sub>3</sub>C<sub>1</sub>pyr]<sup>+</sup>, 1-methyl-1-propylpyrrolidinium

[C<sub>3</sub>C<sub>3</sub>im]<sup>+</sup>, 1,3-dipropylimidazolium

[C<sub>4</sub>-3-C<sub>1</sub>py]<sup>+</sup>, 1-butyl-3-methylpyridinium

[C<sub>4</sub>-4-C<sub>1</sub>py]<sup>+</sup>, 1-butyl-4-methylpyridinium

[C<sub>4</sub>C<sub>1</sub>C<sub>1</sub>im]<sup>+</sup>, 1-butyl-2,3-dimethylimidazolium

[C<sub>4</sub>C<sub>1</sub>im]<sup>+</sup>, [C<sub>4</sub>mim]<sup>+</sup>,

1-butyl-3-methylimidazolium

[C<sub>4</sub>C<sub>1</sub>pyr]<sup>+</sup>, 1-butyl-1-methylpyrrolidinium

[C<sub>4</sub>C<sub>4</sub>im]<sup>+</sup>, 1,3-dibutylimidazolium

[C<sub>4</sub>mpyr]<sup>+</sup>, 1-butyl-1-methylpyrrolidinium

[C<sub>4</sub>py]<sup>+</sup>, 1-butylpyridinium

[C<sub>5</sub>C<sub>1</sub>im]<sup>+</sup>, 1-methyl-3-pentylimidazolium

[C<sub>5</sub>C<sub>5</sub>im]<sup>+</sup>, 1,3-dipentylimidazolium

[C<sub>6</sub>C<sub>1</sub>im]<sup>+</sup>, 1-hexyl-3-methylimidazolium

[C<sub>6</sub>C<sub>6</sub>im]<sup>+</sup>, 1,3-dihexylimidazolium

[C<sub>6</sub>py]<sup>+</sup>, 1-hexylpyridinium

[C<sub>7</sub>C<sub>1</sub>im]<sup>+</sup>, 1-heptyl-3-methylimidazolium

[C<sub>7</sub>C<sub>7</sub>im]<sup>+</sup>, 1,3-diheptylimidazolium

[C<sub>8</sub>C<sub>1</sub>im]<sup>+</sup>, 1-methyl-3-octylimidazolium

[C<sub>8</sub>C<sub>1</sub>im]<sup>+</sup>, 1-methyl-3-octylimidazolium

[C<sub>8</sub>C<sub>8</sub>im]<sup>+</sup>, 1,3-dioctylimidazolium

[C<sub>8</sub>py]<sup>+</sup>, 1-octylpyridinium

[C<sub>9</sub>C<sub>1</sub>im]<sup>+</sup>, 1-nonyl-3-methylimidazolium

[Ch]<sup>+</sup>, Cholinium-

[C<sub>n</sub>C<sub>m</sub>im]<sup>+</sup>, Imidazolium-

[C<sub>n</sub>C<sub>m</sub>pip]<sup>+</sup>, Piperidinium-

[C<sub>n</sub>C<sub>m</sub>py]<sup>+</sup>, Pyridinium-

[C<sub>n</sub>C<sub>m</sub>pyr]<sup>+</sup>, Pyrrolidinium-

[N<sub>11(2(0)1)0</sub>]<sup>+</sup>,

*N,N*-Dimethyl(2-methoxyethyl)ammonium

[N<sub>*nmp*</sub>]<sup>+</sup>, Ammonium-

[P<sub>66614</sub>]<sup>+</sup>, Trihexyltetradecylphosphonium

[P<sub>*nmp*</sub>]<sup>+</sup>, Phosphonium-

[S<sub>*nmp*</sub>]<sup>+</sup>, Sulphonium-

## Ionic Liquids Anions

[(C<sub>8</sub>H<sub>17</sub>)<sub>2</sub>PO<sub>2</sub>]<sup>-</sup>,

Bis(2,4,4-trimethylpentyl)phosphinate

[(CH<sub>3</sub>(CH<sub>2</sub>)<sub>3</sub>)<sub>2</sub>PO<sub>4</sub>]<sup>-</sup>, Dibutylphosphate

[(CH<sub>3</sub>)<sub>2</sub>PO<sub>4</sub>]<sup>-</sup>, Dimethylphosphate

[(CH<sub>3</sub>CH<sub>2</sub>)<sub>2</sub>PO<sub>4</sub>]<sup>-</sup>, Diethylphosphate

[Ac]<sup>-</sup>, [OAc]<sup>-</sup>, [CH<sub>3</sub>CO<sub>2</sub>]<sup>-</sup>, Acetate

[BCN<sub>4</sub>]<sup>-</sup>, Tetracyanoborate

[BF<sub>4</sub>]<sup>-</sup>, Tetrafluoroborate

[Buta]<sup>-</sup>, Butanoate

[C(CN)<sub>3</sub>]<sup>-</sup>, Tricyanomethane

[CF<sub>3</sub>SO<sub>3</sub>]<sup>-</sup>, Trifluoromethanesulfonate

[CH<sub>3</sub>SO<sub>3</sub>]<sup>-</sup>, Methanesulfonate

[CH<sub>3</sub>SO<sub>4</sub>]<sup>-</sup>, Methylsulfate

[C<sub>3</sub>CO<sub>2</sub>]<sup>-</sup>, Isobutyrate

[C<sub>n</sub>CO<sub>2</sub>]<sup>-</sup>, Alkylcarboxylate

[N(CN)<sub>2</sub>]<sup>-</sup>, Dicyanimide

[NO<sub>3</sub>]<sup>-</sup>, Nitrate

[NTf<sub>2</sub>]<sup>-</sup>, Bis(trifluoromethylsulfonyl)imide

[OH]<sup>-</sup>, Hydroxyde  
 [PF<sub>6</sub>]<sup>-</sup>, Hexafluorophosphate  
 [Prop]<sup>-</sup>, Propanoate  
 [SCN]<sup>-</sup>, Thiocyanate  
 [TFA]<sup>-</sup>, Trifluoroacetate

[TOS]<sup>-</sup>, Tosylate  
 Br<sup>-</sup>, Bromide  
 Cl<sup>-</sup>, Chloride  
 I<sup>-</sup>, Iodide

## Symbols

$U_0$	Column outlet volumetric flow rate	$a_w$	Water activity
$B_{12}$	Mixed second virial coefficient	$c$	Molar concentration
$V_1^*$	Molar volume of the solute	$C_p$	Heat capacity
$J_2^3$	Pressure correction term	$E$	Energy barrier
$t_R$	Retention time for the solute	$H$	Henry's law constant
$t_G$	Retention time for the unreturned	$k$	Capacity
gas		$K_{AW}$	Air-water partition coefficient
$P_1^*$	Saturated vapor pressure	$K_L$	Gas-liquid partition coefficients
$B_{11}$	Second virial coefficient	$K_{OA}$	Octanol-air partition coefficient
$T_f$	Temperature at the column outlet	$K_{OC}$	Soil-sorption partition coefficient
$P_W$	Water vapor pressure	$K_{OW}$	Octanol-water partition coefficient
$\gamma_i$	Activity coefficient	$m$	Mass
$\gamma_{13}^\infty$	Activity coefficient at infinite dilution	$M, M_w$	Molar mass
$k_{ij}$	Adjustable binary interaction parameter	$M_j$	Number of groups of type $j$ with second order group contributions
$\varepsilon^{AiBi}$	Association-energy parameter	$N$	Number of carbons
$\kappa^{AiBi}$	Association-volume parameter	$n$	Number of moles
$k_{ij\_eps}$	Binary interaction parameter for correction of the cross-association energy	$N_{atoms}$	Number of atoms in the compound
$\varphi$	Fugacity	$N_{exp}$	Number of experimental points
$V_1^\infty$	Partial molar volume at infinite dilution	$N_k$	Number of groups of type $k$ in the molecule
$\sigma_i$	Segment diameter	$N_r$	Number of rings
$m_i^{seg}$	Segment number	$p$	Vapor pressure
$u_i$	Van der Waals dispersion energy parameter	$P_0$	Outlet pressure
$\gamma^w$	Water activity coefficient	$P_c$	Critical pressure
$\Delta_{fus}H$	Enthalpy of fusion	$P_i$	Inlet pressure
$a$	Molar Helmholtz energy	$R$	Ideal gas constant
		$S$	Selectivity
		$S$	Solubility
		$T$	Temperature
		$T_b, T_{BP}$	Boiling temperature
		$T_c$	Critical temperature
		$tc1k, pc1k, vc1k$	CG contributions of first order



$tc2j, pc2j, vc2j$	CG contributions of second order	$\Delta G$	Gibbs free energy
$tck, pck, vck$	Joback contributions	$\Delta H$	Enthalpy
$T_M, T_{fus}$	Melting temperature	$\Delta S$	Entropy
$U$	volumetric flow rate at the outlet of the column	$\Delta tcj, \Delta pcj$	WJ second order group contributions
$u$	Standard uncertainty	$\Delta tck, \Delta pck$	WJ first order atomic contributions
$V$	Volume	$\eta$	Viscosity
$V_N$	Net retention volume	$\lambda$	Wavelength
$w$	Acentric factor	$M$	Chemical potential
wt%	Weight fraction percentage	$\rho$	Density
$x$	Mole fraction	$\rho_L$	Fluid liquid-density
$\alpha_p$	Isobaric thermal expansion coefficient		

### Subscripts

$A, B$	Ionic compound	$m$	Molar
$acid$	Carboxylic acids	$o$	Octanol
$dev$	Deviation	$P$	Isobaric condition
exp	Experimental	$p$	Pressure
$fus$	Fusion	Sol	Solution
$i$	Component i	Svt	Solvation
$i$	Non-associating component	$V$	Volume
IL	Ionic liquid	$w$	Water
$j$	Component j	$x$	Constant composition

### Superscripts

$\infty$	Infinite dilution	$assoc$	Associative interactions
$res$	Residual	$l$	Liquid phase
$id$	Ideal	$s$	Solid phase
exp	Experimental	$O$	Pure compound
calc	Calculated	$E$	Eutectic
$hc$	Hard-chain fluid interactions	$O$	Standard
$disp$	Dispersive interactions		

# Chapter 1 – General Introduction

*Journal of Chemical Ecology*, Vol. 19, No. 8, 1993

Best wishes,  
JDW

## JUST HOW INSOLUBLE ARE MONOTERPENES?

JEFFREY D. WEIDENHAMER,<sup>1,\*</sup> FRANCISCO A. MACIAS,<sup>1,3</sup>  
NIKOLAUS H. FISCHER,<sup>1</sup> and G. BRUCE WILLIAMSON<sup>2</sup>

<sup>1</sup>Department of Chemistry  
<sup>2</sup>Department of Botany  
Louisiana State University  
Baton Rouge, Louisiana 70803

**Abstract**—Prior generalizations about the ecological roles of monoterpenes may be misleading if based on the presumed insolubility of monoterpenes in water. We determined the aqueous solubility of 31 biologically active monoterpenes by gas chromatography. While hydrocarbons were of low solubility (< 35 ppm), oxygenated monoterpenes exhibited solubilities one or two orders of magnitude higher, with ranges of 155–6990 ppm for ketones and of 183–1360 ppm for alcohols. Many monoterpenes are phytotoxic in concentrations under 100 ppm, well below the saturated aqueous concentrations of oxygenated monoterpenes. Therefore, even dilute, unsaturated solutions of monoterpenes, occurring naturally in plant tissues and soil solutions, may act as potent biological inhibitors.

**Key Words**—Allicopathy, monoterpenes, *Calamintha ashei*, *Conradina coccinea*, unsolic acid, borneol, camphor, juglone, solubility.

### INTRODUCTION

Monoterpenes operate as chemical defenses against herbivores (Eisner, 1964) and disease (W. H. Muller, 1965), fragrances attractive to pollinators (Harborne, 1988), and phytotoxins inhibitory to other plants (Muller et al., 1964; Muller and Chou, 1972; Gant and Clebsch, 1975). Chemically, the molecular skeletons of monoterpenes possess 10 carbon atoms derived from two C<sub>5</sub> isoprene units. They exist as hydrocarbons or as oxygenated moieties with aldehyde, alcohol, ketone, ester, and other functionalities. Furthermore, they may be acyclic,

\*To whom correspondence should be addressed. Current address: Department of Chemistry, Ashland University, Ashland, Ohio 44805.  
†Current address: Departamento de Química Orgánica, Universidad de Cádiz, 11510 Puerto Real, Cádiz, Spain.



## 1.1. General context

At a time when new chemical products are increasingly sought after to address societal needs without neglecting the growing focus on a greener, more environmentally friendly and sustainable development, it seems appropriate to emphasize the topic of natural and renewable sources for these compounds. These trends are spurring the demand for research, development and innovation of natural products.<sup>1</sup> Essential oils are one of the most important classes of natural products with application in food, pharmaceutical, cosmetics, fine chemicals and perfumery industries due to their flavor, fragrances and spices. They are also used as precursors in syntheses of new drugs and as sources of complex aromatic derivatives. Per year circa 100,000 tons of volatile essential oils, with a value of about 1 billion US\$, are produced worldwide. In 2015, the total world fragrance and flavor market was estimated to be approximately US\$ 24 billion, a 33% growth from 2006.<sup>2,3</sup> Besides from the volatile oils, 250,000-300,000 tons of turpentine are also produced, from which about 100,000 tons are used for the production of terpenes such as camphor, camphene, limonene and *p*-cymene.<sup>4</sup> As far as essential oils are concerned, terpenes are the largest and most important class of natural products.

### 1.1.1. Terpenes

The word terpene was first used by Kekulé, in 1866, as a generic term of compounds with the general formula  $C_{10}H_{16}$ . It derives from the German “Terpentin”, from which compounds of this class were first isolated. The suffix “ene” indicates the presence of olefinic bonds. Between 1884 and 1887, Kekulé’s assistant Otto Wallach described the structural formula of many terpenes and proposed the “isoprene rule” that says that terpenes are constructed from isoprene units. Robinson later perfected this rule by suggesting that the isoprene units are connected head-to-tail, the isopropyl part of 2-methylbutane being defined as the *head*, and the ethyl moiety as the *tail*.<sup>5</sup> In 1950 Ruzicka proposed the “biogenetic isoprene rule” which states that all terpenes are obtained by specific precursors sharing a common biosynthetic pathway.<sup>6,7</sup> Wallach, Robinson and Ruzicka all were recipient of the Nobel Prize in Chemistry.<sup>8</sup>

Along the years, many other important scientists worked on this subject, to characterize, extract and purify these compounds (Figure 1.1). After the World War II, chromatographic methods emerged, along with an increase on the number of works on terpenes. The distillation processes were replaced by improved chromatographic methods that allowed a more effective and faster separation of essential oil into its hundreds of components, facilitating their characterization.

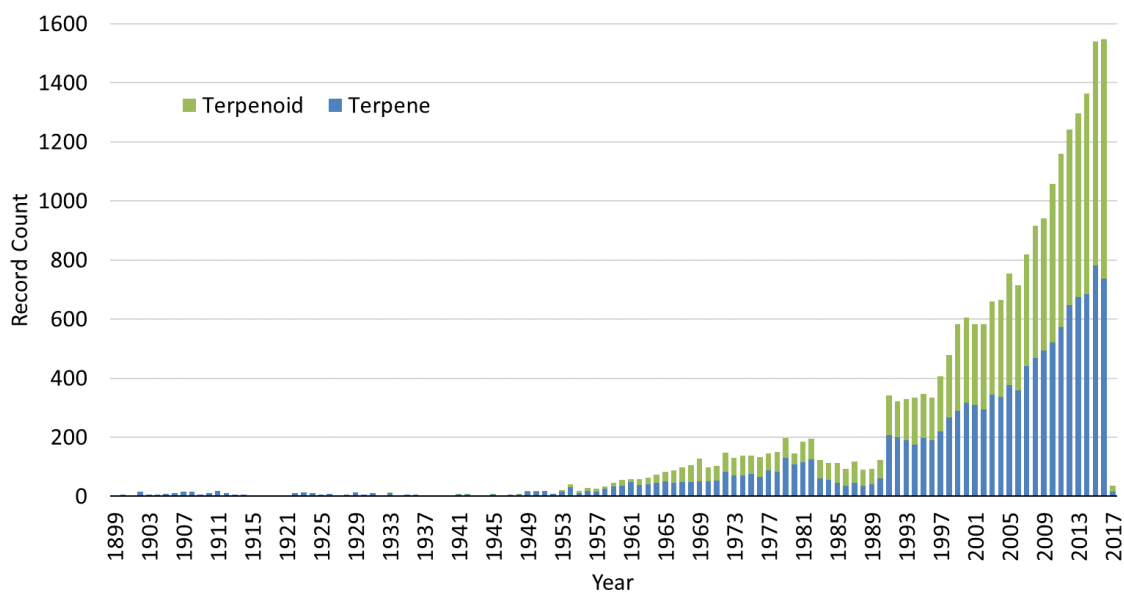


**Figure 1.1.** Record count of works on terpenes and/or terpenoids. Values extracted from ISI Web of Knowledge in January, 2017.

Terpenes have been used since the Egyptians<sup>9</sup> and their importance both in nature and for human related applications is huge. One of the reasons for their widespread use is the abundance and diversity of these compounds; they are found in all living organisms. Using a basic five carbon building block, the isoprene, nature creates an array of compounds with a wide range of structural variations and a vast number of purposes.<sup>10</sup> Structurally, terpenes are unsaturated acyclic, monocyclic, or polycyclic hydrocarbons. They can also occur as oxygenated derivatives, such as alcohols, ethers, aldehydes, ketones, and carboxylic acids, called terpenoids.<sup>11</sup> In this work the term terpene includes both, the terpene hydrocarbons and the terpene oxygenated derivatives – terpenoids. Figure 1.2 shows some terpenes and terpenoids structures and their classification based on the number of isoprene units.

Terpenes are divided into several groups and sub-groups according to the pathway by which they are synthesized by nature, or according to their structures, since these arise directly from their biosynthesis. As presented in Figure 1.2, the primary classification is related to the number of isoprene units. The fundamental family members are hemiterpenes or hemiterpenoids – compounds containing only one unit of isoprene that is widely produced and emitted in nature.<sup>10</sup> Monoterpenes and sesquiterpenes are present in nature as components of essential oils of herbs and spices, of flower scents, and of turpentine; and thus, widely used in perfumery and flavor industries.<sup>12</sup> Their mixtures can form up to 5% of a plant dry weight.<sup>13</sup> Monoterpenes are components of anticancer and antimicrobial drugs,<sup>14</sup> while sesquiterpenes present antibiotic activities.<sup>15,16</sup> Containing four units of isoprene, diterpenes arise from the metabolism of geranylgeranyl pyrophosphate<sup>17</sup> and occur in almost all plant families. Taxol is a diterpene drug used to treat cancer.<sup>18</sup> The least common group, sesterterpenes are primarily isolated from fungi and marine organisms and rarely found in higher plants.<sup>19</sup> The C<sub>30</sub> constituents derived from squalene – triterpenes – are largely found in nature, mainly in resins, and are important structural components of plant cell membranes.<sup>20,21</sup> Comprising eight units of isoprene, tetraterpenes are formed by the coupling of two geranylgeranyl pyrophosphate molecules. Important tetraterpenes are the yellow or orange-red carotenoid pigments.<sup>17</sup> Polyterpenes are composed of many isoprene units and to date have no biological function associated.<sup>12</sup> Examples are found in rubber and gutta-percha, macromolecules of molecular weight over 100 000. While in mono-, sesqui-, di- and sesterterpenes the isoprene units are linked to each other from *head-to-tail*, tri- and tetraterpenes contain one *tail-to-tail* connection in the center.<sup>12</sup>

Hemiterpenes <i>Hemiterpenoids</i> 1 i.u. (C <sub>5</sub> H <sub>8</sub> )	Monoterpenes <i>Monoterpenoids</i> 2 i.u. (C <sub>10</sub> H <sub>16</sub> )	Sesquiterpenes <i>Sesquiterpenoids</i> 3 i.u. (C <sub>15</sub> H <sub>24</sub> )	Diterpenes <i>Diterpenoids</i> 4 i.u. (C <sub>20</sub> H <sub>32</sub> )	Sesterterpenes <i>Sesterterpenoids</i> 5 i.u. (C <sub>25</sub> H <sub>40</sub> )	Triterpenes <i>Triterpenoids</i> 6 i.u. (C <sub>30</sub> H <sub>48</sub> )	Tetraterpenes <i>Tetraterpenoids</i> 8 i.u. (C <sub>40</sub> H <sub>64</sub> )	Polyterpenes <i>Polyterpenoids</i> (C <sub>5</sub> H <sub>8</sub> ) <sub>n</sub>	
		<b>Acyclic</b>						<b>Acyclic</b>
 Isoprene	 Citronellol	 $\alpha$ -farnesene	 Phytol		 Squalene	 Lycopene	 Natural Rubber	
 Isovaleric Acid	 Geraniol	 Farnesol				 Phytoene	 Gutta-percha	
 Prenol	 Linalool	 Nerolidol						
		<b>Monocyclic</b>			<b>Tetracyclic</b>		<b>Monocyclic</b>	
 Carvacrol	 S-Carvone	 Elemol	 Humulene	 Cembrene A	 Geranyl-farnesol	 Cucurbitane	 Torulene	
 Limonene	 Menthol	 Thymol	 Zingiberene	 Retinol		 Lanosterol	 $\gamma$ -Carotene	
		<b>Bicyclic</b>					<b>Bicyclic</b>	
 Borneol	 Camphor	 Eucalyptol	 Cardinene	 Caryophyllene	 Labdane		 $\alpha$ -Carotene	
 $\alpha$ -pinene	 $\beta$ -pinene	 Mutisianthol					 $\beta$ -Carotene	
		<b>Tricyclic</b>			<b>Pentacyclic</b>			
 Cyclosantene	 $\alpha$ -santalol	 Ferruginol	 Cafestol	 $\alpha$ -amyrin	 Betulinic Acid			

Figure 1.2. A visual introduction to some common terpenes and terpenoids and their structures (i.u. isoprene units).

Concerning the biosynthesis, all terpenes derive from the precursors isopentenyl diphosphate (IDP) and its allylic isomer dimethylallyl diphosphate (DMADP), called 'active isoprene'.<sup>22–24</sup> These are formed through two metabolic pathways: the mevalonic acid pathway (MEV) and the methylerythritol phosphate pathway (MEP). As can be seen in Figure 1.3, hemiterpenes can be formed directly through DMADP while the assembly of this with 1 – 4 units of IDP gives rise to the immediate precursors of terpenes, GDP, FDP, GGDP and GFDP, respectively.<sup>22</sup> The conformation adopted by the chain determines the terpene structure, being the most common the cyclic forms with a mono-, bi-, tri-, tetra- or pentacyclic structures.<sup>8</sup>

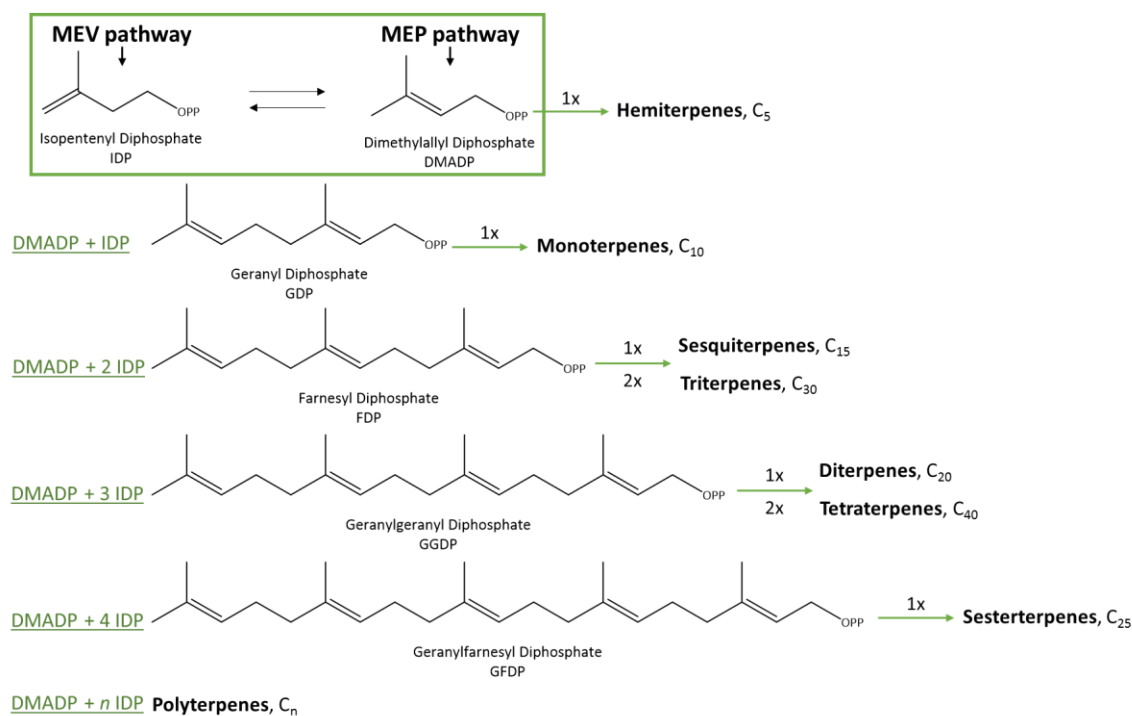


**Figure 1.3.** Simplified scheme of terpenes biosynthesis.

### Properties and applications

Many plants as balm trees, caraway, carnation, citrus fruits, conifer wood, coriander, eucalyptus, lavender, lemon grass, lilies, peppermint species, roses, rosemary, sage, thyme and violet, are known due to their aroma, taste and medicinal properties, being terpenes the main responsible for these properties. With more than 55.000 different structures,<sup>25,26</sup> the properties and applications of this class of natural compounds are



difficult to overstate. Many of them are considered as GRAS (Generally Recognized As Safe)<sup>27</sup> and their importance makes them attractive to be used in diverse industries. Table 1.1 shows some of the generic applications of terpenes in pharmaceutical,<sup>28</sup> food additives,<sup>29</sup> cosmetics,<sup>10</sup> perfumery,<sup>10</sup> fine chemicals<sup>30</sup> and agriculture<sup>30</sup> industries as well as some of their properties and examples of terpenes or their sources.

Due to their biological importance and particular properties, the study of these natural products led to the discovery of an enormous variety of useful drugs for the treatment of diverse diseases. In the pharmaceutical field terpenes are used as excipients to enhance skin penetration, active principles of drugs and components of non-prescription drugs.<sup>28</sup> In 2002, the market of terpene-based pharmaceuticals generated about US\$ 12 billion.<sup>28</sup> The anticancer taxol and the antimalarial artemisinin are two of the better-known terpene-based drugs.<sup>31</sup> Menthol and camphor are non-prescription drugs widely used in the pharmaceutical field. In 2015, the sales of Salonpas (5.7% menthol and 1.12% camphor),<sup>32</sup> a famous topical analgesic, in the United States reached US\$ 60.1 million.<sup>33</sup> In the food industry, terpenes are also very attractive due to their several appealing properties that allow them to be used as safer alternatives to chemical additives.<sup>34,35</sup> The culinary herbs basil, cinnamon, coriander, cumin, lavender, mint, oregano, and rosemary; and trees like eucalyptus, fir and myrtle are famous sources of terpenes.<sup>29</sup> When added to chocolate products, limonene was proposed as a reducer of the fat content and viscosity and therefore its addition can improve the final product quality.<sup>36,37</sup>

Fragrances make terpenes and essential oils the most important natural products used by the cosmetic and perfumery industries since ancient times. According to Euromonitor International<sup>38</sup> the beauty industry generated US\$ 465 billion in sales in 2014, with a 5 per cent yearly growth, being China and Brazil the most promising markets. This is an evidence that the global demand for cosmetics and perfumes, and consequently essential oils, is still an extremely important and profitable market. There are more than 3000 known essential oils and from these, around 300 are used commercially in the flavor and fragrances market.<sup>34</sup> Citrus peel and neroli oil are examples of widely applied essential oils in perfumes, colognes and other high-end fragrances. Neroli is a highly prized floral oil

produced from orange blossoms by steam distillation. To produce 1 kg of neroli oil, 850 kg of orange blossoms are necessary.<sup>39</sup>

**Table 1.1.** Generic properties/applications of terpenes in several industries.<sup>10,28–30</sup>

<b>Pharmaceutical Industries</b>	<b>Essential Oil or Compound</b>
Analgesic	Oils of oregano, myrtle, eucalyptus, lemon and orange
Antibiotic	$\alpha/\beta$ -pinene, illudinic acid, manoalide
Anticancer	Paclitaxel, halomon, mutisianthol, ferruginol, cafestol
Antifungal	Thymol, labdane
Antihyperglycemic	Pycnanthuquinones A and B
Anti-inflammatory	$\alpha/\beta$ -pinene, $\alpha$ -humulene, trans-caryophyllene, labdane
Antimicrobial	Zuccarinin, carvacrol, thymol
Antiparasitic	Artemisinin, betulinic acid
Antiviral	$\beta$ -caryophyllene, star anise oil
<b>Food Additives Industries</b>	
Color agents	Carotenoids
Antioxidants	Safranal, carnosol, eugenol, thymol, carvacrol
Natural preservative	Oregano, rosemary and thyme essential oils
Organoleptic agents (flavor, fragrances, spices)	Steviol (stevia), lactisole, sabinene, camphor, humulene
Natural food additives	Steviol (stevia)
<b>Cosmetics and Perfumery Industries</b>	
Organoleptic agents (flavor, fragrances)	$\alpha/\beta$ -ocimene, $\beta$ -myrcene, citral A, S-limonene, patchoulol
Repellent	Geraniol, citronellal, camphor, farnesene
Antibacterial	Carvacrol
Emulsifier	Lanosterol, saponins, ursolic acid
Conditioner and Lubricant	Lanosterol
<b>Fine Chemicals Industries</b>	
Synthetic precursors and intermediates	Menthol, menthone, terpineol, linalool, $\alpha/\beta$ -pinene
Chiral building blocks	$\alpha/\beta$ -pinene, limonene
<b>Agriculture</b>	
Pesticides	Pyrethrins, limonene
Plant protectors	Farnesene
Animal feed	Zeaxanthin
Phytohormones	Fusicoccanes, abscisic acid

Volatile mono-, sesqui- and diterpenes are the most important subclasses of terpenes economically important as perfumes and fragrances. Extracted from various eucalyptus species, eucalyptol is one monoterpenoid widely used in perfumery and as a nasal decongestant. Other examples are  $\alpha$ -ocimene,  $\beta$ -ocimene,  $\beta$ -myrcene, citral A, S-limonene, verbenone, zingiberene, bisabolane, bisabolene, caryophyllene, and patchoulol. Patchoulol is a sesquiterpene alcohol found in the essential oil Patchouli, an important material in perfumery that also gives name to a French perfume brand. Another important application of patchoulol is its use in the synthesis of the chemotherapy drug Taxol. Verbena, that has as main constituent verbenone, is the signature fragrance of *L'Occitane*, a well-known company located in Provence, France.

As one of the most abundant and diverse classes of compounds produced by animals and plants, terpenes can be converted into commercially important fine chemicals to be used in the industries and as synthetic intermediates and chiral building blocks.<sup>30</sup> A well-known engineering application for terpenoids is the norbornadiene-quadracyclane system, a photochemical conversion cycle for the storage of solar energy.<sup>40</sup> One example that demonstrates the use of monoterpenes as building block for the production of chiral fine chemicals is the synthesis of the herbicide cinmethylin developed by the Shell Oil Company.<sup>41</sup> In addition, there are evidences that plants, animals and microorganisms produce terpenes as defense mechanisms against predators, pathogens and competitors,<sup>42</sup> protection against abiotic stress,<sup>43</sup> and signalization.<sup>44</sup> Thus, terpenes have also been explored as pesticides.<sup>45</sup>

Due to the similar physico chemical properties between some other organic solvents and terpenes as  $\alpha$ -pinene, limonene and *p*-cymene, studies have been performed to explore the possibility of replacing them.<sup>46,47</sup> Limonene was studied for recycling and reduction of polystyrene volume as an alternative to hydrocarbon based solvents.<sup>48,49</sup> Tanzi et al.<sup>50</sup> have shown that terpenes could be an efficient alternative to benzene for the recovery of triglycerides from the algae *Chlorella vulgaris*.

In addition, it is also important to highlight the polyterpene rubber and the essential oil turpentine. Produced by the rubber tree as a defensive secretion, natural rubber is a

polymer of isoprene widely used due to its elastic properties.<sup>9</sup> In 2015, a total of around 26.8 million metric tons of natural and synthetic rubber were produced globally.<sup>51</sup> On the other hand, turpentine is, by far, the essential oil most produced in the world. Their main constituents are  $\alpha$ -pinene (30 000 tons / year) and  $\beta$ -pinene, and in small amounts some other monoterpenes. With an annual production of around 330 000 tons, this secondary product of paper pulp industry has been used for decades as an important source for applications requiring large-scale supplies. Examples are its use as a solvent, particularly for paints, and as feedstock for the synthesis of other materials of commercial interest, particularly the monoterpenes production, and fragrance ingredients.<sup>10</sup> During colonial times, turpentine was included in the term *naval stores* originally used to denote resin-based components of pine trees used in building and maintaining of wooden sailing ships as waterproof agents.

Concerning synthesis, the fact is that basic monoterpenes skeletons can interconvert to give rise to other monoterpenes or their derivatives.<sup>7,30</sup> Industrially, the abundant  $\alpha$ -pinene and  $\beta$ -pinene are thermal or acidic isomerized in order to produce molecular skeletons of other naturally occurring chemicals, especially when their natural sources are not abundant.<sup>7</sup>  $\alpha$ -terpineol is obtained when turpentine is distilled in an acidic medium, causing the opening of the ring of  $\alpha$ -pinene.<sup>10</sup> By thermal cycloreversion  $\beta$ -pinene leads to myrcene, that can subsequently be converted into (R)-(+)-citronellal.<sup>12</sup>

As can be seen in Table 1.2, the second major source of terpenes is citrus essential oil, a co-product of citrus juice that has as major constituent (>95%) the monoterpenes limonene (30 000 tons/year) and terpinene, followed by other essential oils produced in less quantity.

Although most terpenes present “good” characteristics that lead to important applications, there are also a set of compounds with negative features. The monoterpene thujone is the toxic agent present in *Artemisia absinthium* from which the liqueur absinthe is made. Isovaleric acid is a major component of the cause of foot odor, however it is widely applied in perfumery. Umbellulone is produced by Californian “headache

trees” and causes headaches; pulegone causes abortions, camphene is explosive and ascaridole is poisonous and explosive.

**Table 1.2.** Major commercial sources of terpenes (adapted from Schwab et al.<sup>30</sup>).

Essential Oil	Main terpenes	Tons oil/year
Turpentine	$\alpha$ -pinene, $\beta$ -pinene	330 000
Citrus	<i>R</i> -(+)-limonene	30 000
<i>Mentha arvensis</i>	(-)-menthol	4800
Peppermint	(-)-menthol, (-)-menthone	3200
Cedarwood	$\alpha$ -cedrene, $\beta$ -cedrene	2600
<i>Eucalyptus globulus</i>	Eucalyptol	2070
<i>Litsea cubeba</i>	Citral	2000
Clove leaf	$\beta$ -caryophyllene	2000
Spearmint	<i>R</i> -(-)-carvone	1300

Aiming at the development of new applications for this important class of compounds and taking advantage of their hydrophobic character, a part of this thesis is devoted to the attempt to prepare sustainable and cheap hydrophobic solvents from mixtures of terpenes combined with other terpenes or other organic solvents or chemicals – Chapter 2.

### Production and deterpenation

Essential oils are extracted from their natural sources through four basic processes: tapping, expression, distillation and solvents extraction. Tapping is the process of damage the trees bark to collect the exuded resin. Turpentine gum and natural rubber are collect using this process. Some other resins as olibanum and myrrh are also produced by this method, however they suffer further processing after collection. Many citrus oils and, in particular, bergamot oils are produced by physical pressure of the natural source, process called expression. The resulting oil is called an expressed oil.<sup>10</sup>

Due to their high volatility, essential oils and terpenes can also be isolated from plant by distillation, one of the most important methods. This comprises three types: dry distillation, steam distillation and hydrodiffusion. In dry distillation high temperatures or

direct flames are applied to the recipient containing the raw material. This technique is usually used for oils with high boiling points as those derived from wood, such as cade and birch tar oils. In steam distillation the oils are co-distilled by adding water or steam to the recipient. The water is then removed with, for example, a Florentine flask. In order to save energy, in hydrodiffusion steam is introduced at the top of the recipient and the water and oil collected at the bottom.<sup>10</sup>

The most important method to extract essential oils is solvent extraction, divided in ethanolic extraction, enfleurage and simple solvent extraction. The first is more applied to materials, as the ambergris produced through the triterpenoid ambreine that is excreted by the sperm whale. When subjected to ethanol extraction ambergris forms a tincture. Enfleurage was used since ancient Egyptians until the early twentieth century. The process consisted in mixing the raw material with purified fat that is then melted and the mixture filtered. After cooling the mixture formed a pomade where the essential oils are diffused. However, the concentration was low and the final product not very convenient. In more recent times, ethanol was used to extract the fat by dissolving the essential oils. Ethanol was then distilled. Nowadays the most important and most used technique is solvent extraction. Initially was made with benzene but due to concerns related to its possible toxic effects was replaced by petroleum ether, acetone, hexane, ethyl acetate, or their mixtures.<sup>10</sup>

When in high concentrations the monoterpene hydrocarbons can be undesirable and are removed from the essential oils, process known as deterpenation.<sup>52</sup> In this process, the essential oils are separated in two fractions, one rich in terpene hydrocarbons and another rich in oxygenated terpene derivatives.<sup>53</sup> The fraction rich in terpene hydrocarbons, mainly monoterpenes and sesquiterpenes, contributes little to the flavor and fragrance, is poor soluble in water and alcohols and may be easily oxidized, while the fraction rich in oxygenated compounds is the responsible for its organoleptic characteristics.<sup>54</sup> Whereas some applications involve the non-deterpenated oil, as aromatherapy, others require the concentration of the oxygenated compounds by the hydrocarbons removal in order to increase the stability and the solubility in water, and other organic solvents used in food technology.

Lemon oil is an example of one essential oil dominated by a volatile fraction composed by terpene hydrocarbons ( $\approx 90\%$ ), such as limonene, and some of their oxygenated derivatives – Figure 1.4. That fraction presents low boiling point and is prone to oxidation to produce molecules that cause strong off-flavors. Besides, they do not contribute significantly to the oil fragrance, in comparison to the other fraction that provides most of the flavor character.<sup>5</sup> To have acceptable flavor in lemonade drink, the level of lemon oil required would result in an excess of terpene hydrocarbons exceeding the solubility limit. On the other hand, the oxygenated chemicals are soluble, what makes the deterpenation of utmost importance in order to improve the quality of the final product and have a clear drink.<sup>10</sup> This fractionation increases the essential oils commercial value, since the fraction composed by oxygenated compounds is preferred by many industries.<sup>55</sup>

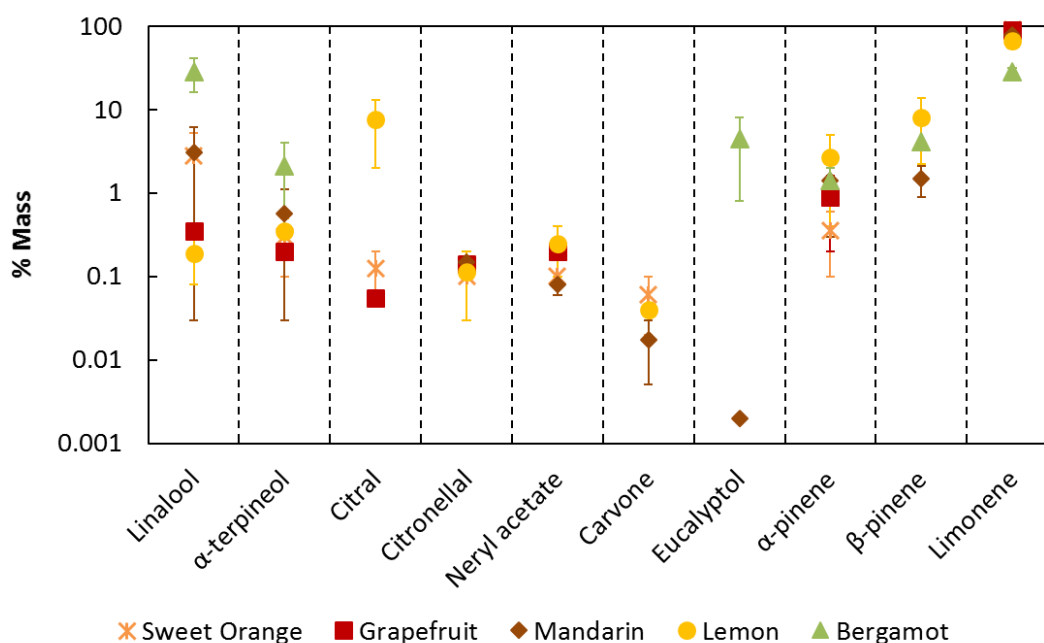


**Figure 1.4.** Mass percent composition ranges of components of different citrus essential oils (adapted from Arce and Soto, 2008).<sup>54</sup>

Vacuum and steam distillations,<sup>56</sup> membrane processes,<sup>57</sup> supercritical extraction,<sup>58–60</sup> solvent (or liquid-liquid) extraction<sup>52,61–63</sup> and chromatography<sup>64</sup> are the techniques most used to remove hydrocarbons from essential oils. The solvent extraction is preferred, since this method requires less energy, than processes such as distillation and

supercritical fluid extraction, while retaining the most volatile aliphatic chemicals,<sup>65</sup> and preserving the organoleptic properties of the original oil. Large-scale deterpenation is generally carried out by vacuum distillation or extraction into dilute alcohol or other solvents.<sup>54</sup> Nowadays, newer technologies are being tested and one of the most interesting approaches currently under development is the use of ionic liquids (ILs).<sup>54</sup>

To be applied in food,<sup>23</sup> perfumery,<sup>66</sup> medicines<sup>67,68</sup> and cosmetics,<sup>69</sup> or for research purposes, pure terpenes must be extracted from essential oils, usually by fractional distillation.<sup>12</sup> To the best of our knowledge, the first academic study published in the open literature on terpenes extraction dates back to 1959,<sup>70</sup> and since then a vast number of works were published in the field.<sup>10</sup> In a laboratorial scale, chromatographic methods of separation predominantly in the gas or liquid phase allow the isolation of small amounts with high purities.

In the isolation process, first the raw material is dried, chopped or ground and then extracted with inert solvents at low temperatures, to prevent artifacts formation. Water, ethanol, or methanol are used to extract polar compounds while petroleum ether is used for the less-polar ones. The extracts are then dried under vacuum or freeze-dried and fractionated by column chromatography. Liquid chromatography with medium- or high-pressure is used to the final purifications.<sup>12</sup>

However, and despite terpenes abundance, most are present in low concentrations (Figure 1.4), so they tend to be expensive or even uneconomic to exploit.<sup>10</sup> An example is the anticancer paclitaxel, found in *Taxus brevifolia*. The level of terpene in the bark is very low, being needed three trees with several hundred years old to produce paclitaxel to treat one patient. As the number of trees in the world is insufficient, researchers are focused on attempts to synthesize paclitaxel.<sup>10</sup> Moreover, since 1960's natural sources of terpenes can no longer meet their worldwide demand. Thus, although many terpenes are isolated from natural sources most are nowadays produced by synthetic methods. Two thirds of monoterpenes in the market are manufactured by synthetic or semi-synthetic processes. As main components of turpentine, the essential oil most produced in the world,  $\alpha$ -pinene and  $\beta$ -pinene arise as raw materials for the production of many of the



commercially important terpenes and their derivatives (i.e., terpineol, linalool, linalyl acetate, nerol, geraniol, and citral).<sup>71</sup>

For the production of pure terpenes from natural materials,<sup>72</sup> or for the deterpenation, the separation of terpenes is of the utmost importance, being an area regarding eagerly for new technological developments. Thus, to replace noxious organic solvents used in the terpenes production or essential oils deterpenation and to increase the process yield, Chapter 3 investigates the potential of ionic liquids for terpenes fractionation. Moreover, another classes of neoteric solvents, the deep eutectic solvents, are formulated and characterized aiming at the development of new separation processes.

### **Environmental impact**

With the advent of the biorefinery, and the increasing importance and volume of terpene production and applications, especially in the fragrance and flavor, pharmaceutical and chemical industries, their environmental impact needs to be considered. Over the last years, the role of terpenes as biogenic volatile organic compounds (BVOC) as well as in aerosol formation became an important topic of research on the chemistry of the atmosphere, with a new emphasis on the ongoing climate change debate.<sup>24,73,74</sup> It is thought that, on a global scale, volatile organic compounds of biogenic origin exceed by far the amount of anthropogenic emissions, while this is not necessarily true on a regional scale, regarding industrialized and heavily encumbered areas.

Forests present emission of large quantities of unsaturated hydrocarbons like isoprene, mono- and sesquiterpenes. They are subject to gas-phase oxidation reactions, and the reaction products contribute to particle formation.<sup>74,75</sup> Smaller degradation fragments will remain for long times in the atmosphere influencing its chemistry. Until recently, it was widely believed that VOC only contributed to secondary aerosol formation when composed of six or more carbon atoms, but recent studies suggest the involvement of smaller molecules on a considerable scale. About half of global BVOC-emissions originate in isoprene.<sup>76</sup>

In terms of quantities, biorefineries are on their way to become a new important anthropogenic source of terpenes and thus, envisioning the risk assessment of large scale operations, environmentally relevant physicochemical property data have to be known. However, data on water solubility and vapor pressure of terpenes – two of the most important properties – are scarce and often inconsistent, and their temperature dependency largely unknown.<sup>11,77–82</sup>

Perdue et al.<sup>83</sup> emphasized the importance of physicochemical properties of monoterpenes in another environmental context: their fate in the soil and the aquatic environment. Their interest was driven by possible environmental consequences due to emerging applications of terpenoids as, among others, replacement for chlorofluorocarbons, and therefore their increasing production.<sup>83</sup> Also here, there is a scarcity of available data for basic physicochemical property data, while several models are available for their estimation.<sup>83</sup> Physicochemical parameters such as water solubility, vapor pressures and octanol-water partition coefficients, allow an ample description of the behavior of a substance in the environmental compartments, from multi-compartment analysis to transport and distribution of substances over the compartment boundaries.

In order to contribute to the development of accurate models for the fate of terpenes in the environment, on this thesis a range of physicochemical properties such as densities, water solubilities and critical properties will be accurately measured and/or estimated – Chapter 4. Moreover, water solubilities, vapor pressure and octanol-water partition coefficients can describe a hypothetical chemical space that allows a first screening of compounds with respect to their probable distribution in the environment once released.

The natural emissions of terpenes cannot be targeted for intervention unlike the anthropogenic. Thus, the researchers goal must be the search of strategies and technologies to reduce the environmental impacts of terpenes from biorefineries. For this purpose, aiming at maximizing efficiency and minimizing waste new eco-friendly solvents will be here investigated.

### 1.1.2. Designer solvents

Within the framework of green chemistry, solvents occupy a strategic place. In this context, to be qualified as a green medium, solvents must be non-toxic, biodegradable, recyclable, non-flammable, and economic, among others. The point is to minimize the environmental and health impact of common noxious organic solvents used in industries. Up to now, the number of available solvents proposed as green include ethanol,<sup>84</sup> water,<sup>85</sup> supercritical CO<sub>2</sub>,<sup>86</sup> and recently ionic liquids<sup>87</sup> and deep eutectic solvents.<sup>88</sup>

Regarding the terpenes extraction and separation, water<sup>89,90</sup> and several organic solvents as alcohols,<sup>49,61,89,91–99</sup> acetonitrile, nitromethane and dimethylformamide,<sup>100</sup> glycols<sup>101,102</sup> and aminoethanol have been investigated.<sup>103</sup> Lately, ionic liquids have been also investigated as potential substituent for organic solvents.<sup>52,53,63,104–107</sup> Moreover, in this work the neoteric deep eutectic solvents are proposed to the extraction of terpenes.

#### **Ionic liquids**

Ionic liquids are a novel and remarkable class of compounds that have received enormous attention during the past decade.<sup>108</sup> Chemically, they are composed by bulky organic cations coupled with organic or inorganic anions that, unlike conventional salts, are liquid at or close to room temperature, as result of their low-charge density and low symmetry ions. This makes them attractive as alternative solvents for many chemical reactions and separation processes.<sup>109</sup> The combination of ions can lead to a large number of ILs, what provides considerable flexibility in the selection of the most suitable pairs for a specific chemical application and, consequently, to significant changes in their thermophysical properties such as density, viscosity, heat capacity, thermal conductivity, as well as their solvation ability. Therefore, they have been categorized as “designer solvents” owing to the very large number of possible cations and anions combinations that can be envisioned.<sup>110</sup>

The first ionic liquid, ethylammonium nitrate, was synthesized almost a century ago by Paul Walden<sup>111</sup> and in 1934 the first process concerning ILs industrial applications in the preparation of cellulose solutions was patented.<sup>112</sup> Thereafter the number of scientific

works reporting on ionic liquids increased progressively. However, the boom occurred in the past years with the discover of air- and water-stable ILs, as well as of task-specific compounds.<sup>108</sup> Nowadays a large number of ILs can be synthesized being the most widely studied the cations imidazolium-, pyridinium-, pyrrolidinium-, piperidinium-, and quaternary-ammonium and phosphonium, combined with the anions chloride, bromide, acetate, hexafluorophosphate and tetrafluoroborate – Figure 1.5. Moreover, the green chemistry framework led to eco-friendlier alternatives, as derivatives from carboxylic acids and amino-acid-based anions and cholinium- and amino-acid- based cations.<sup>113</sup>

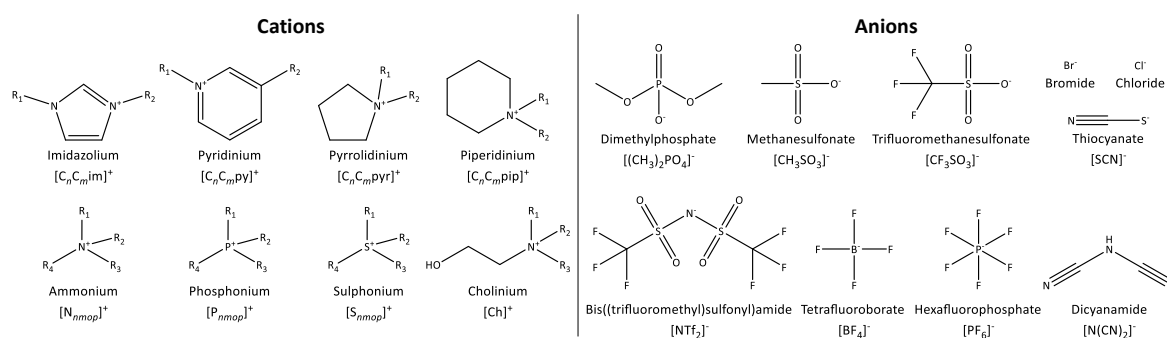


**Figure 1.5.** Common structures of ILs cations and anions.

Due to their ionic nature, most ILs are known to present interesting properties, such as a negligible vapor pressure, chemical and thermal stability, high ionic conductivity, large liquid temperature ranges and high solvating capacity for organic, inorganic, and organometallic compounds.<sup>87,109</sup> Due to these unique characteristics, ILs are often considered green solvents with a potential to replace conventional volatile organic solvents that are believed to contribute to the global warming.<sup>110,114</sup> Many recent reviews summarize the large range of applications of ionic liquids in organic synthesis, catalysis, biocatalysis, electrochemistry, and separation technology.<sup>108,115,116</sup>

Over the past years, the role of ionic liquids in fragrance and flavor chemistry has been explored. Main investigations include chemical synthesis of fragrance and flavor materials in ionic liquids, extraction of natural compounds from biomass, and determination of fluid-fluid equilibria for essential oil deterpenation using ILs.<sup>106,115,117,118</sup>

In 2005 Forsyth et al.<sup>119</sup> investigated the use of ionic liquid solvents to synthesize lily-of-the-valley Liliac fragrances and Petrat et al.<sup>120</sup> found that the evaporation of a perfume could be delayed using an ionic liquid as fixative. A similar discovery was patented by BASF, discovering that azeotropes can be broken using ILs in order to affect the compounds volatility.<sup>121</sup> Concerning cleaning products, Procter & Gamble has an extensive portfolio of patents involving ILs including the treatment or cleaning agents for surfaces, the protection or stabilization of benefit agents and the improvement of processability of active concentrates.<sup>117</sup>

Table 1.3 shows terpenes extracted from biomass using ILs or ILs solutions. The most used ILs are imidazolium-based cations combined with Br<sup>-</sup>, Cl<sup>-</sup> and [BF<sub>4</sub>]<sup>-</sup> anions – pure, or in mixtures of water or ethanol. Due to its utmost importance in malaria treatment, the extraction of the sesquiterpene lactone artemisinin from the plant *Artemisia annua* was evaluated by Bioniqs Ltd using ILs as solvents in the solid-liquid extraction process.<sup>122</sup> In this work, a specific ionic liquid, [N<sub>11(2(0)1)0</sub>][C<sub>2</sub>CO<sub>2</sub>], was designed for the extraction of artemisinin. As far as we know, this was the first patent concerning the application of ILs in the extraction of value-added compounds from biomass.

One year Later, Wu et al.<sup>123</sup> investigated the extraction of tanshinones from *Salvia miltiorrhiza Bunge* using surfactant ionic liquids suggesting that the extraction is micelle-mediated since the tanshinones are lipophilic compounds. The same terpenoids were also studied by Bi et al.<sup>124</sup> that suggested the application of IL-based ultrasound-assisted extraction for the extraction and pre-concentration of tanshinones. Later the same author applied the former technique using ethanol solutions to the extraction of astaxanthin, the most valuable carotenoid, from shrimp waste.<sup>125</sup> Another technique, IL-based microwave-assisted simultaneous extraction and distillation was usefully applied by Liu et al.<sup>126</sup> to extract carnolic acid, rosmarinic acid and essential oils from *Rosmarinus officinalis*.

Bica and co-workers<sup>106</sup> dissolved fresh fragrance biomass in ionic liquids in order to isolate essential oils. The liquid solutions were subjected to vacuum distillation and a distilled fraction composed of two layers, limonene and water, obtained allowing the isolation of high purity limonene. The IL was totally recovered. Additionally, the same

group explored the extraction of the pharmaceutically active betulin from birch bark using pure ILs.<sup>127</sup> This triterpene presents many interesting characteristics as the antitumor, antiviral and antimalarial properties, as well as their derivatives (betulinic acid and bevirimat) that have been studied as contributors to a new anti-HIV drug.

In 2013, aqueous ionic liquid based ultrasonic assisted extraction was applied to ginsenosides.<sup>128</sup> This approach showed the highest extraction yields of total ginsenosides ( $\approx 17 \text{ mg}\cdot\text{g}^{-1}$ ) when compared with water or ethanol. Finally, Onda et al.<sup>129</sup> extracted the terpene trilactone bilobalide from *Ginkgo biloba* leaves using the biomass-dissolving ionic liquid 1-butyl-3-methylimidazolium chloride. In combination with methanol, an efficient extraction was achieved.

**Table 1.3.** Terpenes extracted from natural sources using ILs or ILs solutions (adapted from Passos et al.<sup>115</sup>).

Terpene	Natural Source	ILs / ILs solutions
Artemisinin <sup>122</sup>	<i>Artemisia annua</i>	$[\text{N}_{nmop}]^+ + [\text{C}_n\text{CO}_2]^-$
Tanshinones <sup>123,124</sup>	<i>Salvia miltiorrhiza Bunge</i>	$[\text{C}_n\text{C}_m\text{im}]^+ + \text{Br}^-; \text{Cl}^- + \text{water}$
Astaxanthin <sup>125</sup>	Shrimp waste	$[\text{C}_n\text{C}_m\text{im}]^+ + \text{Br}^-; [\text{BF}_4]^-; [\text{CH}_3\text{SO}_4]^-; \text{Cl}^- + \text{ethanol}$
Limonene <sup>106</sup>	Orange peels	$[\text{C}_n\text{C}_m\text{im}]^+ + [\text{C}_n\text{CO}_2]^-; \text{Cl}^-$
Carnosic acid <sup>126</sup>	<i>Rosmarinus officinalis</i>	$[\text{C}_n\text{C}_m\text{im}]^+ + \text{Br}^-; [\text{BF}_4]^-; [\text{NO}_3]^-; \text{Cl}^- + \text{water}$
Betulin <sup>127</sup>	Birch bark	$[\text{C}_n\text{C}_m\text{im}]^+; [\text{C}_n\text{C}_m\text{pyr}]^+; [\text{C}_n\text{C}_m\text{py}]^+ + \text{Br}^-; \text{Cl}^-; [(\text{CH}_3)_2\text{PO}_4]^-; [\text{BF}_4]^-; [\text{C}_n\text{CO}_2]^-; [\text{C}_{13}\text{CO}_2]^-; [\text{N}(\text{CN})_2]^-; [\text{PF}_6]^-; [\text{NTf}_2]^-$
Ginsenosides <sup>128</sup>	Ginseng root	$[\text{C}_n\text{C}_m\text{im}]^+ + \text{Br}^-; [\text{BF}_4]^-; \text{I}^- + \text{water}$
Bilobalide <sup>129</sup>	<i>Ginkgo biloba</i> leaves	$[\text{C}_n\text{C}_m\text{im}]^+; [\text{P}_{nmop}]^+ + \text{Cl}^-; [\text{OH}]^-$

### Deep eutectic solvents

With the growing focus in green chemistry, researchers are increasingly seeking environmentally friendly solvents. Recently, a new class of eco-friendly solvents has been proposed by Abbott and co-workers,<sup>130</sup> the Deep Eutectic Solvents (DES). These are

mixtures of two, or more compounds, formed by hydrogen bond complexation, for which the eutectic point is far below the melting point of each individual component.<sup>131</sup> As represented in Figure 1.6a, the eutectic point corresponds to the minimum temperature and system composition at which the system is still in the liquid phase.

DES can be easily prepared by mixing the components at a moderate temperature, without chemical reactions and complex purification steps. Many are prepared using cheap and well-characterized biodegradable materials, making the “synthesis” green and safe.<sup>131,132</sup> They may also be classified as designer solvents since their structures can be adjusted by selecting the hydrogen-bond donor–acceptor combinations, tailoring their phase behavior and physical properties.<sup>133</sup> The most common components used in DES formulations are quaternary ammonium salts, particularly choline chloride ([Ch]Cl), due to its non-toxicity, biodegradability and economic synthesis. When combined with polyols, urea, carboxylic acids, sugars or other safe hydrogen bond donors, DES are formed. The interaction mechanism of choline chloride with a generic hydrogen bond donor (HBD) is represented in Figure 1.6b.

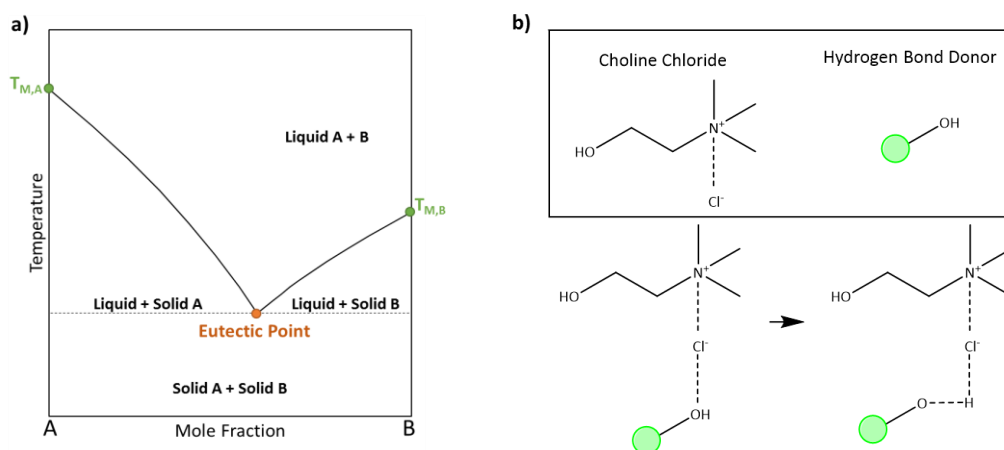


**Figure 1.6.** a) A simple eutectic phase diagram; b) Interaction mechanism of [Ch]Cl with a generic HBD.

DES exhibit a wide range of properties which make them an attractive family of solvents for different applications in catalysis, organic synthesis, dissolution and extraction processes, electrochemistry and material chemistry.<sup>131,134,135</sup> Their low toxicity, non-volatility, non-flammability and non-reactivity with water together with their

renewability, biodegradability and availability of precursors, are some of the favorable characteristics of these compounds.<sup>131,136</sup> The renewability of a DES depends mainly on its starting materials. For most DES described in literature, the precursors used in their preparation are abundant natural compounds (Figure 1.7).

Owing to their promising applications, efforts have been devoted to the physicochemical characterization of DES. It has been shown that usually they are denser than water and show different melting points depending on the starting materials, and also on the molar ratio of these precursors. Like ILs, the DES often present high viscosities at room temperature. Due to these high values of viscosity, they usually present low ionic conductivities.<sup>131</sup>

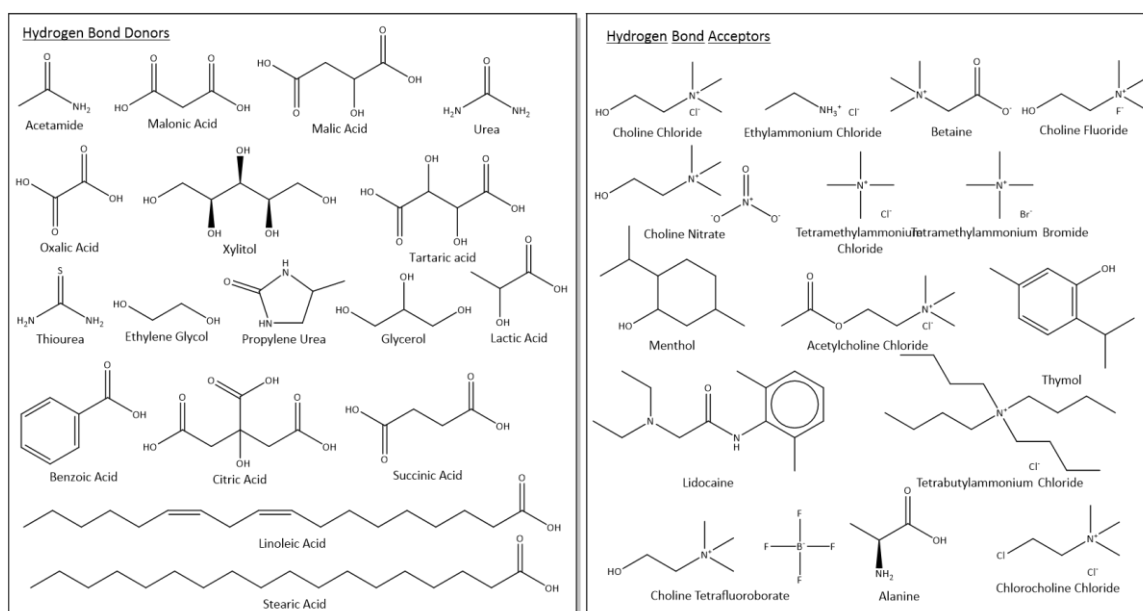


**Figure 1.7.** Structures of HBD and HBA commonly used in the deep eutectic solvents formulation (adapted from Francisco et al.<sup>135</sup>).

Since DES emergence, they have been applied to a wide range of biomass types to extract different compounds, including terpenes – Table 1.4. The first study was performed in 2014, where terpenes linalool,  $\alpha$ -terpineol, terpinyl acetate were extracted from *Chamaecyparis obtusa* leaves using mixtures of choline chloride and ethylene glycol by headspace-solvent microextraction.<sup>137</sup>



After, Zhang et al.<sup>138</sup> and Lee and Row<sup>139</sup> investigated the extraction of astaxanthin from shrimp byproducts and marine products, respectively. Zhang et al.<sup>138</sup> applied an ultrasonic-assisted method obtaining more astaxanthin ( $146 \mu\text{g}\cdot\text{g}^{-1}$ ) with [Ch]Cl+1,2-butanediol (1:5) than when using the traditional organic solvent ethanol ( $102 \mu\text{g}\cdot\text{g}^{-1}$ ). Later, Lee and Row<sup>139</sup> evaluated ILs and DES as additives for the extraction of astaxanthin by the same method. The optimal DES was synthesized from methyl triphenyl phosphonium bromide and 1,2-butanediol (1:4) while the optimal IL was 1-ethyl-3-methylimidazolium bromide. The amount of astaxanthin extracted from *Portunus trituberculatus* waste was  $73.49 \text{ mg}\cdot\text{g}^{-1}$  using the DES compared with  $47.30 \text{ mg}\cdot\text{g}^{-1}$  using the IL.

The extraction of ginsenosides from white ginseng was used as a way to demonstrate the tuneability as well as recyclability of DES by Jeong et al.<sup>140</sup> A mixture of glycerol, L-proline, and sucrose (9:4:1) was found to be the DES with high efficient extraction. Additionally, was confirmed that the DES is merely an extraction solvent with no influence on the bioactivity of the ginsenosides extracted. The addition of glycerol to a binary DES proved to increase extraction efficiencies while reducing viscosities. The ginsenosides were successfully recovered by solid-phase extraction and the DES recycled through simple freeze-drying of the washes from the solid-phase extraction procedure.

Last year, Wang et al.<sup>141</sup> applied a ball mill-assisted deep eutectic solvent-based extraction method to extract tanshinones from *Salvia miltiorrhiza Bunge*. The developed method was found to be greener, more efficient, and faster than conventional, environmentally harmful extraction methods such as methanol-based ultrasound-assisted extraction and heat reflux extraction.

Although no extraction was performed, Bruinhorst et al.<sup>142</sup> showed the disintegration of orange peel waste in deep eutectic solvents. Due to the viscosity decrease, the addition of water to DES lowered the amount of remaining solids and the disintegration times. This work offers new possibilities for the development of orange peel waste valorization routes and in the possible extraction of essential oils and pure terpenes, namely limonene, from these wastes using DES.

**Table 1.4.** Terpenes extracted from natural sources using DES.

Terpene	Natural Source	DES components
Linalool, $\alpha$ -terpineol, terpinyl acetate <sup>137</sup>	<i>Chamaecyparis obtusa</i> leaves	[Ch]Cl; ethylene glycol
Astaxanthin <sup>138,139</sup>	Shrimp byproducts / Marine products	[Ch]Cl; zinc chloride; tetramethyl ammonium chloride, methyl triphenyl phosphonium bromide; ethylene glycol; glycerol; urea; 1,2- butanediol; 2,3- butanediol; 1,3- butanediol; 1,4- butanediol; 1,6- hexanediol; methacrylic acid; phenol; oxalic acid; glycerin
Ginsenosides <sup>140</sup>	White ginseng	[Ch]Cl; glycerol; L-proline; xylitol; citric acid; adonitol; betaine; D-(+)-galactose; D-(-)-fructose; D-(+)-glucose; DL-malic acid; sucrose
Tanshinones <sup>141</sup>	<i>Salvia miltiorrhiza Bunge</i>	[Ch]Cl; ethyl glycol; glycerol; 1,2- butanediol; 1,3- butanediol; 1,4- butanediol; 2,3- butanediol

In another perspective, a hydrophobic DES composed of menthol and lauric acid was used to successfully extract indium from hydrochloric and oxalic acids aqueous solutions with low acidity (pH  $\approx$  3).<sup>143</sup> Results provide an opportunity for valuable metallic compounds extraction from aqueous phases by means of cheap and ecofriendly solvents.

In industry, there is an important application of DES involving natural compounds that must be mentioned: Eutectys™ by Naturex. This new set of botanical extracts based on the patented extraction process Eutectigenesis,<sup>144</sup> which consists of extracting active compounds of plants through the formation of natural DES. This breakthrough eco-extraction technology offers a natural alternative to conventional solvents and makes it possible to capture the plant most precious metabolites.<sup>145</sup> Due to the nature of the compounds used, the extracts main remain contaminated with DES after extraction.

## 1.2. Scope and objectives

With more than 55000 structures and a large range of applications in several industries, terpenes are nowadays a very important research topic. However, due to the high number of structures and their complexity, there are still a lot of knowledge to be gathered and questions to be answered. This thesis aims at contributing to deepen the understanding of terpenes concerning their applications; their extraction, production or

deterpenation; and the environmental problems associated with natural and anthropogenic emissions. To a better understanding of this work, a schematic representation is presented in Figure 1.8.

Taking advantage of their very low solubility in water, terpenes arise as suitable candidates to prepare sustainable hydrophobic solvents to be used in novel processes and products. To the best of our knowledge, so far, only a few works reported hydrophobic eutectic mixtures and, among them, those that are liquid at room temperature are very limited. Moreover, the absence of phase diagrams is common, despite the important information they can provide on the range of compositions and temperatures for operating these systems. **Chapter 2** deals with eutectic solvents and deep eutectic solvents composed by terpenes and monocarboxylic acids, and mixtures of terpenes (section 2.4). Phase diagrams are characterized and analyzed in the whole composition range, and the physicochemical properties densities and viscosities of the eutectic point explored.

To be used in industrial applications, terpenes must first be extracted from their natural sources, most often as essential oils. In the fractionation of these essential oils for the production of pure terpenes or their deterpenation, noxious organic solvents are commonly used. In order to replace them and to develop more efficient processes, this work investigates the use of neoteric solvents: ionic liquids and deep eutectic solvents. **Chapter 3** addresses the ability of the ILs to act as entrainers in separation processes (3.1.4) and the selection of ILs as separation agents of terpenes and terpenoids (3.1.5) – both using measurements of activity coefficients at infinite dilution and, for terpenes, the design of better ionic liquids based on COSMO-RS predictions. Based on the results of this work, the design of novel DES, composed of ammonium salts and monocarboxylic acids, are carried out and the DES solid-liquid phase diagrams characterized and modeled with PC-SAFT (3.2). Moreover, being choline chloride the most used salt used to prepare DES and since the compound decomposes upon melting, its melting properties are indirectly estimated from solid-liquid equilibria data (3.3). New eutectic systems formed by choline chloride and a fatty alcohol, or a fatty acid are then prepared and characterized (3.4).

As stated above, many plants release scented vapors formed mainly by monoterpenes. Labeled recently as volatile organic compounds, these turn into aerosols once in the atmosphere. Moreover, the emerging applications of terpenes are leading to the increase of their anthropogenic production and thus, their fate in the air, soil and aquatic compartments is concerning the environmentalists. Thus, in **Chapter 4**, a range of essential physicochemical properties of terpenes are accurately measured and modelled or calculated, contributing for the development of accurate models for the fate of terpenes in the environment, and to develop predictive theoretical models for these properties. When deriving the activity coefficients at infinite dilution, the lack of physical properties was noted, namely the critical properties – essential to many thermodynamic models. Accordingly, the first work presented in this chapter (4.1) responds to this using group-contribution methods and equations of state for the estimation of critical properties of terpenes, and the best set is recommended. In another context, since ILs have been studied to extract and fractionate terpenes, their environmental fate, especially in water, is also important. Thus, the mutual solubilities, densities and viscosities for a range of ILs and water are measured and discussed (4.2.4, 4.2.5, 4.2.6) and the same experimental method is then applied to measure the solubility of terpenes in water. However, it proved to be inappropriate due to the formation of emulsions after stirring which cause sampling problems. A new technique is then developed and firstly applied to sparingly soluble *N*-(diethylaminothiocarbonyl)benzimidazole derivatives (4.3) providing accurate results and thus applied to determining the solubility of terpenes in water (4.4). Moreover, the measured properties, along with some others from literature, are used to draw a two-dimensional plot describing a hypothetical chemical space that allows a first screening of compounds with respect to their probable distribution in the environment once released.

Finally, a conclusion is addressed and future work envisioned (Chapter 5).

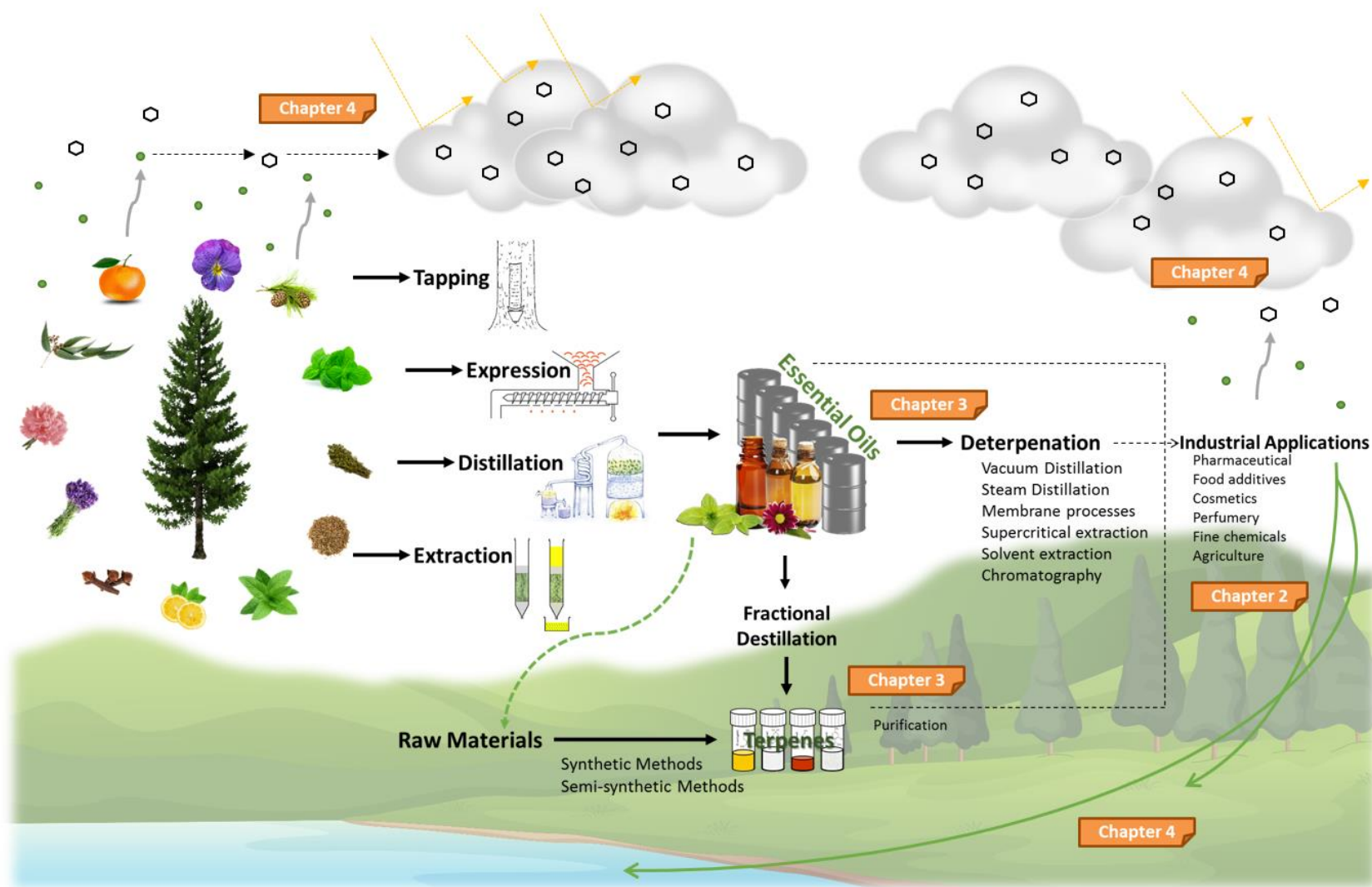


Figure 1.8. Schematic illustration of the work developed on this thesis.

# Chapter 2 – Terpenes Applications





## 2.1. Introduction

Nowadays the modern chemistry is strongly influenced by the concepts of *green chemistry* and *sustainability*. On this framework, there is a demand for new eco-friendly solvents able to dissolve a large spectrum of solutes. Currently, two of the most important focus of researchers are ionic liquids and, more recently, deep eutectic solvents (DES).<sup>88,146</sup>

Most of the DES proposed so far were prepared through the combination of a salt or an ionic liquid, with nontoxic and biodegradable compounds such as carboxylic acids,<sup>147</sup> polyols, and sugars;<sup>148,149</sup> being the vast majority hydrophilic. To the best of our knowledge, only a few works reported hydrophobic deep eutectic mixtures<sup>143,150–152</sup> and, among them, the absence of phase diagrams is common, despite the important information that they can provide on the range of compositions and temperatures for operating these systems. Moreover, a thermodynamic evaluation of the physical properties of these systems is rarely presented.

Due to their very low solubility in water and low price, terpenes mixtures arise as candidates to prepare sustainable and cheap hydrophobic solvents. Limonene is a promising candidate due to the similar physico chemical properties with organic solvents and has already been studied as an alternative to hydrocarbon based solvents in the recycling and reduction of polystyrene volume.<sup>48,49</sup> Menthol, borneol, camphor and thymol are monoterpenoids used in different industries and their eutectic mixtures have been investigated for different applications. In the pharmaceutical field, mixtures of borneol/menthol,<sup>153–155</sup> camphor/menthol<sup>156,157</sup> and camphor/borneol<sup>158</sup> were used as vehicles for transdermal delivery.<sup>159,160</sup> Moreover mixtures of thymol with ibuprofen<sup>161</sup> and meloxicam;<sup>160</sup> camphor with ibuprofen<sup>162</sup> and lidocaine;<sup>163</sup> and of menthol with ibuprofen,<sup>161,164,165</sup> testosterone,<sup>166</sup> lidocaine,<sup>167</sup> and ubiquinone<sup>168</sup> have been investigated as analgesic, antimicrobial and anti-inflammatory compounds.<sup>152</sup> Recently, mixtures of menthol and ibuprofen, benzoic acid, acetylsalicylic acid or phenylacetic acid were proposed as therapeutic deep eutectic solvent used to design a controlled drug



delivery system using supercritical fluid technology,<sup>169</sup> and as dissolution enhancers of active pharmaceutical ingredients.<sup>170</sup>

In the extraction field, menthol-lauric acid mixture was proposed as a hydrophobic DES able to extract indium from aqueous solutions;<sup>143</sup> and hydrophobic mixtures of menthol and naturally occurring acids, namely pyruvic acid, acetic acid, L-lactic acid, and lauric acid were applied as solvents in the extraction of caffeine, tryptophan, isophthalic acid, and vanillin.<sup>152</sup>

The main goal of this work is to prepare eutectic solvents and DES composed by the terpenes menthol and thymol, and the monocarboxylic caprylic, capric, lauric, myristic, palmitic, stearic and oleic acids, and mixtures of terpenes (menthol+thymol, menthol+camphor, menthol+borneol, borneol+camphor, thymol+camphor, thymol+borneol). Phase diagrams of these mixtures are characterized and analyzed in the whole composition range, through differential scanning calorimetry (DSC). Moreover, the eutectic composition, and the physicochemical properties density and viscosity are measured in order to characterize these systems.

## **2.2. Experimental**

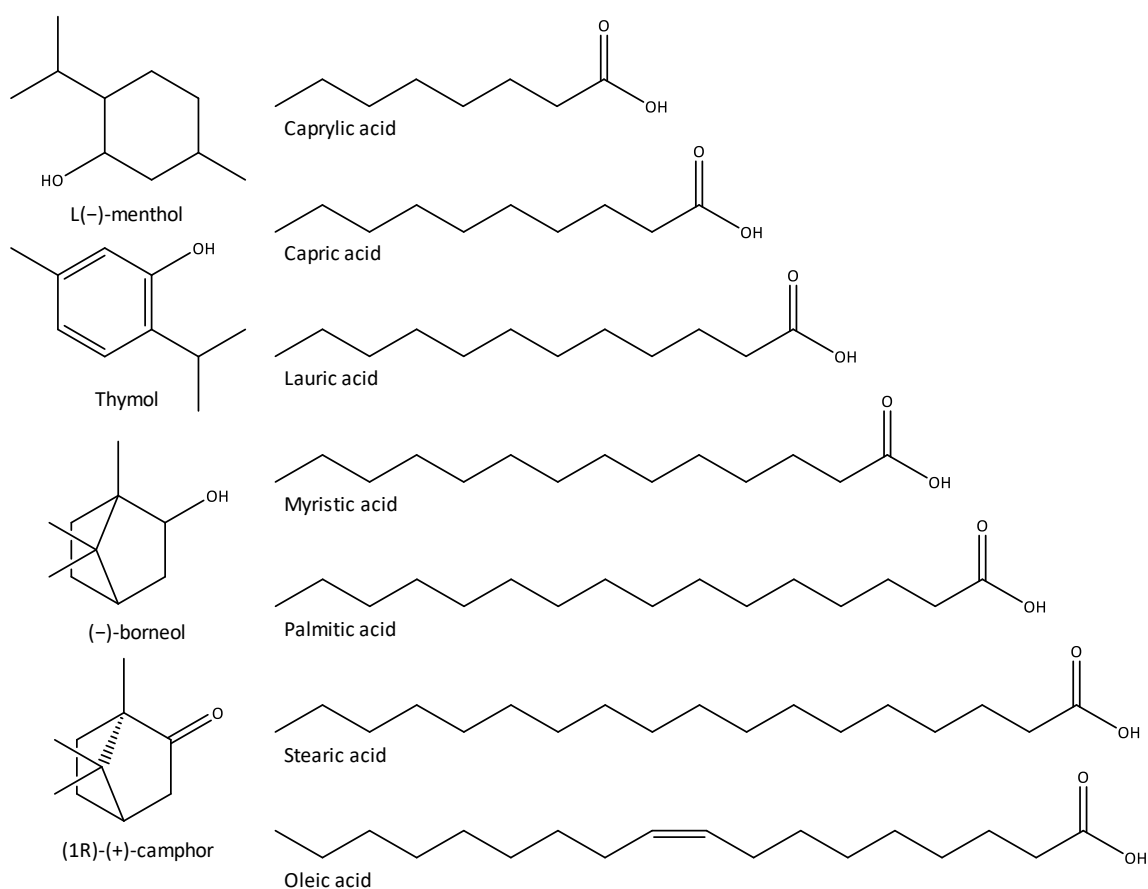
### **2.2.1. Materials**

Information on the investigated compounds is summarized in Table 2.1 and Figure 2.1. The samples were used as received without further purification. The terpenes purity was evaluated by <sup>1</sup>H, and <sup>13</sup>C NMR spectra and GC-MS.

**Table 2.1.** Compounds description and their melting properties herewith values from literature.

Compound	Supplier	CAS	wt % <sup>a</sup>	$T_{fus} / K$		$\Delta_{fus}H / kJ \cdot mol^{-1}$	
				exp.	lit.	exp.	lit.
L(-)-menthol	Acros	2216-51-5	99.7	315.68 ± 0.22	315.9 <sup>171</sup> 316.7 <sup>171</sup>	12.89 ± 0.77	12.83 <sup>171</sup>
Thymol	Sigma	89-83-8	≥99.5	323.50 ± 0.34	323.1 <sup>171</sup> 322.8 <sup>171</sup>	19.65 ± 0.42	17.54 <sup>171</sup>
(-)-borneol	Fluka	464-45-9	≥99	480.57 ± 0.06	480.3 <sup>172</sup>	7.60 ± 0.13	7.3 <sup>172</sup>
(1R)-(+)-camphor	Aldrich	464-49-3	98	450.42 ± 0.41	451.8 <sup>173</sup>	5.28 ± 0.18	6.2 <sup>173</sup>
Caprylic acid	Sigma	124-07-2	≥99	288.20 ± 0.09	289.50 <sup>174</sup>	19.80 ± 0.54	21.38 <sup>174</sup>
Capric acid	Sigma	334-48-5	99-100	304.75 ± 0.05	305.48 <sup>175</sup>	27.50 ± 1.29	27.23 <sup>175</sup>
Lauric acid	Sigma	143-07-7	≥99	317.48 ± 0.14	318.48 <sup>175</sup>	37.83 ± 0.20	34.62 <sup>175</sup>
Myristic acid	Sigma	544-63-8	≈95	327.03 ± 0.04	328.93 <sup>175</sup>	41.29 ± 0.38	43.95 <sup>175</sup>
Palmitic acid	Aldrich	57-10-3	≥98	336.84 ± 0.10	336.36 <sup>176</sup>	51.02 ± 0.22	53.02 <sup>176</sup>
Stearic acid	Merck	<i>n.a.</i>	≥97	343.67 ± 0.07	344.04 <sup>176</sup>	61.36 ± 0.42	61.1 <sup>176</sup>
Oleic acid	Aldrich	112-80-1	90	284.45 ± 0.11	286.45 <sup>174</sup>	32.45 ± 2.01	39.6 <sup>174</sup>

<sup>a</sup>Declared by the supplier. *n.a.*: not available.

**Figure 2.1.** Structures of the compounds investigated in this work.

### 2.2.2. Methods

#### Differential scanning calorimetry

Binary mixtures were prepared by adding the compounds into glass vessels at different molar ratios, on the full composition range, using an analytic balance XP205 (Mettler Toledo, precision =  $2 \times 10^{-4}$  g). The mixtures were melted under stirring on a heating plate until a homogeneous liquid mixture was obtained and then cooled at room temperature. Samples (2 – 5 mg) were hermetically sealed in aluminum pans and weighed in a micro analytical balance AD6 (PerkinElmer, USA, precision =  $2 \times 10^{-6}$  g).

The melting points of pure components and their mixtures were determined using a DSC 2920 calorimeter from TA Instruments working at atmospheric pressure and coupled to a cooling system. The equipment was previously calibrated with indium. The analytical procedure was based on a cooling ramp down to 208.15 K at  $5 \text{ K} \cdot \text{min}^{-1}$ , followed by a heating ramp up to 10 K above melting, at a  $1 \text{ K} \cdot \text{min}^{-1}$ . A constant nitrogen flow (purity  $\geq 0.99999$  mass fraction) was used as purge gas in order to avoid condensation of water at low temperatures. Data were analyzed through the TA Universal Analysis software (TA Instruments) and the melting temperatures taken as the peak temperature. At least three cycles of cooling and heating were performed for pure compounds.

#### Density and viscosity

Densities and viscosities were measured at atmospheric pressure and in the temperature range from 278.15 to 373.15 K using an automated SVM 3000 Anton Paar rotational Stabinger viscometer–densimeter (temperature uncertainty:  $\pm 0.02$  K; absolute density uncertainty:  $\pm 5 \times 10^{-4} \text{ g} \cdot \text{cm}^{-3}$ ; dynamic viscosity relative uncertainty:  $\pm 0.35\%$ ).

### 2.3. Theoretical approach

#### Solid-liquid equilibria

The solid-liquid equilibria of the mixtures investigated in this work was described using the thermodynamic expression:<sup>177</sup>

$$\ln(x_i \gamma_i) = \frac{\Delta_{\text{fus}} H}{R} \left( \frac{1}{T_{\text{fus}}} - \frac{1}{T} \right) + \frac{\Delta_{\text{fus}} C_p}{R} \left( \frac{T_{\text{fus}}}{T} - \ln \frac{T_{\text{fus}}}{T} - 1 \right) \quad (2.1)$$

where  $\gamma_i$  is activity coefficient at a certain liquid mole fraction composition  $x_i$ ,  $T$  is the absolute temperature,  $T_{\text{fus}}$  and  $\Delta_{\text{fus}} H$  are the melting temperature and enthalpy of fusion of the pure compound, respectively,  $R$  is the universal gas constant, and  $\Delta_{\text{fus}} C_p$  is the difference between the heat capacity of compound  $i$  in the liquid and solid phases. The last term of the equation has a negligible value when compared to the second,<sup>178,179</sup> and was not taken into account.

### Density

From the linear dependency of the density with temperature, Equation 2.2, the isobaric thermal expansion coefficient,  $\alpha_p$ , which considers the volumetric changes with temperature, can be calculated according to Equation 2.3,

$$\ln \rho = A_0 + A_1 T \quad (2.2)$$

$$\alpha_p = -\frac{1}{\rho} \left( \frac{\partial \rho}{\partial T} \right)_p = -\left( \frac{\partial \ln \rho}{\partial T} \right)_p = -A_1 \quad (2.3)$$

where  $\rho$  is the density, and  $A_0$  and  $A_1$  are fitting parameters.

### Viscosity

The viscosity, that describes the internal resistance of a fluid to a shear stress, can be correlated through the Vogel–Tammann–Fulcher (VTF) model,<sup>180</sup> expressed by,

$$\eta(T) = A_\eta \exp \left[ \frac{B_\eta}{T - C_\eta} \right] \quad (2.4)$$

where  $A_\eta$ ,  $B_\eta$ , and  $C_\eta$  are adjustable parameters estimated from experimental data.

Hereafter, the energy barrier ( $E$ ) – that is the energy value that must be overcome in order for the fluids to move past each other<sup>181</sup> – can be determined based on the viscosity dependence with temperature using the following equation,<sup>182</sup>

$$E = R \frac{\partial(\ln[\eta(T)])}{\partial(1/T)} \quad (2.5)$$

where  $\eta$  is viscosity, and  $R$  is the ideal gas constant.

## **2.4. Tunable hydrophobic deep eutectic solvents and eutectic mixtures based on terpenes**

Mónia A. R. Martins, Paula V. A. Pontes, Liliana P. Silva, Guilherme J. Máximo, Eduardo A. C. Batista, Simão P. Pinho & João A. P. Coutinho, in preparation.

### **2.4.1. Abstract**

Inspired by the lack of well-characterized hydrophobic deep eutectic mixtures, in this work we aim at the preparation and characterization of eutectic solvents and deep eutectic solvents composed by terpenes and monocarboxylic acids, and mixtures of terpenes. Their phase diagrams were analyzed in the whole composition range, through differential scanning calorimetry. Additionally, densities and viscosities at the eutectic compositions for mixtures of L(-)-menthol, or thymol, and monocarboxylic acids were measured. Results show that mixtures between thymol or menthol, and monocarboxylic acids, form normal eutectic solvents. The eutectic temperatures of these mixtures increase with the alkyl chain of the monocarboxylic acid. Moreover, the eutectic composition also varies depending on the monocarboxylic acid used. On the other hand, mixtures of terpenes L(-)-menthol, thymol, (R)-(+)-camphor and (-)-borneol form deep eutectic solvents. Mixtures of terpenes containing thymol were impossible to crystallize at very low temperatures (208.15 K), however visual results indicate the existence of glass transitions at lower temperatures. The new eutectic solvents composed by terpenes and monocarboxylic acids present densities lower than water and low viscosities (1.3 – 100.6 mPa·s). Viscosity decreases with temperature increase, and with the decrease of the alkyl chain length of the monocarboxylic acids. In general mixtures involving thymol are less viscous and denser.

## 2.4.2. Results and discussion

### Solid-liquid phase diagrams

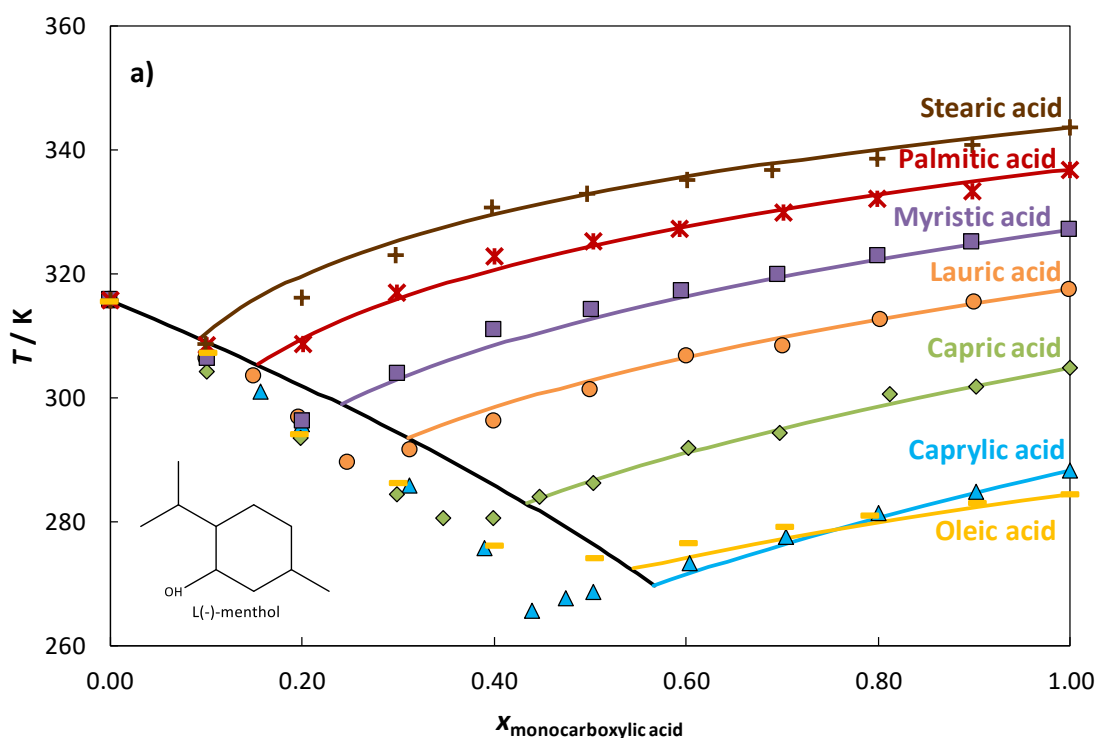
The measured melting properties of the pure compounds used in this work are presented in Table 2.1, along with values from literature. Both sets are in good agreement, validating the measurements of the melting points presented in this work. Concerning melting enthalpies, only for oleic acid a significant difference to the values from literature was found, probably due to the low mass fraction purity of the compound used in this work.

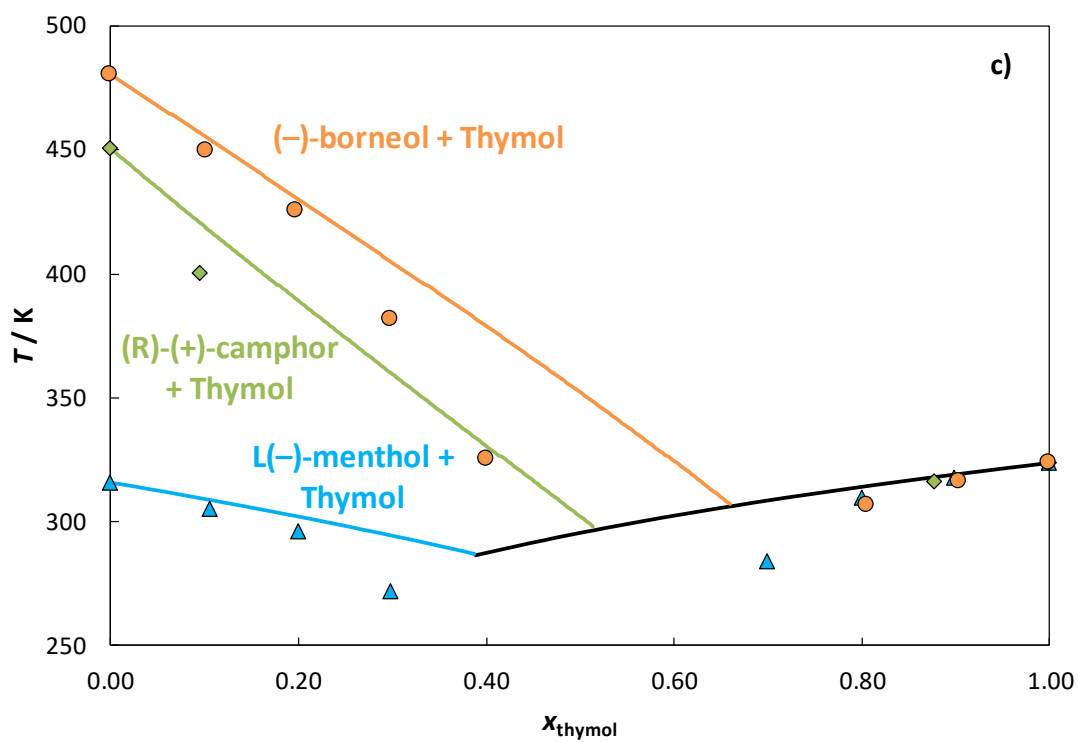
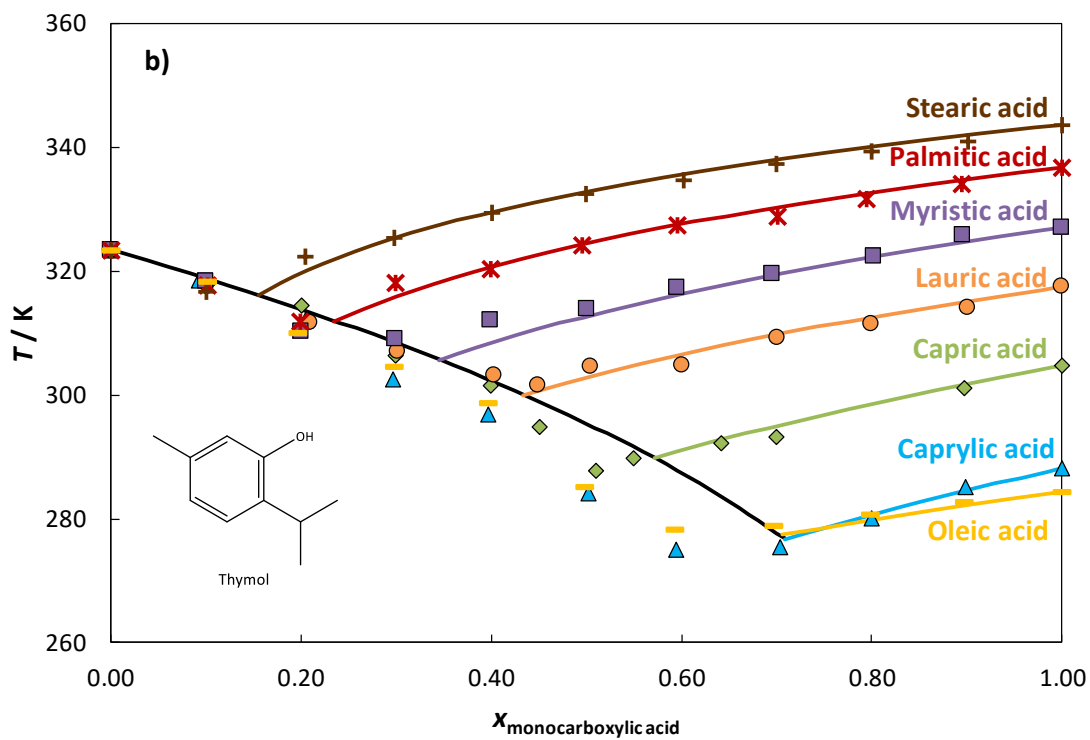
The solid-liquid experimental data for the 20 mixtures investigated are plotted in Figure 2.2 together with the ideal solubility curves (eq. 2.1), and listed in Table S2.1 of Appendix 2, along with the activity coefficients estimated from equation 2.1. As can be seen, mixtures of terpenes thymol or L(-)-menthol with monocarboxylic acids form normal eutectic mixtures, while mixtures of (R)-(+)-camphor + L(-)-menthol and (-)-borneol + L(-)-menthol form deep eutectic solvents (Figure 2.2d). Due to limitations in the experimental device used, the phase diagrams of mixtures involving thymol were not completed; however, the measured data points indicate that these mixtures do not crystallize, forming glasses instead.<sup>135,183</sup> The mixtures were placed in an ultra-freezer at 193.15 K during approximately 2 hours, Figure 2.3, and their aspect was found to be glass-like, corroborating the later statement. All mixtures with complete phase diagrams exhibited a phase behavior characterized by a single eutectic point, with the exception of (-)-borneol + (R)-(+)-camphor (Figure 2.2e), whose phase diagram indicates the existence of a solid solution in this organic system.

Unlike the DES composed of mixtures of terpenes, the melting point depressions (and the deviations to the ideal behavior) of mixtures of thymol or L(-)-menthol with monocarboxylic acids are relatively small. Thus, less complex hydrogen-bonding networks are established in these systems, and only HB interactions between the hydroxyl group of the terpene and the hydroxyl group of the monocarboxylic acid are expected to occur (in opposition with DES where different types of HB interactions are formed). As shown in Figure 2.2a and b, these systems have only slight deviations to the ideal behavior mainly

in the terpene solubility curve, while the solubility curve of the acid presents an almost ideal behavior. In both groups (thymol or L(-)-menthol + monocarboxylic acids) a higher eutectic temperature was observed for the systems involving acids with higher melting temperatures. Additionally, the eutectic compositions are found to be richer in acid for the lower chain length acids due to their lower melting points. Ribeiro et al.<sup>152</sup> reported 286.99 K as the melting point of the mixture DL-menthol and lauric acid at 0.66:0.33 (mole fraction ratio), where in this work the value measured was 291.54 K at the composition ratio 0.69:0.31.

All mixtures of terpenes present large deviations to ideal behavior, especially those involving thymol, and the mixture of camphor+borneol that seems to form a solid solution. Thus, to better analyze these systems modeling work will be carried out in future, and additional experimental measurements on the mixtures involving thymol must also be performed. Taking this into account, mixture of terpenes will not be considered in the second part of this work.







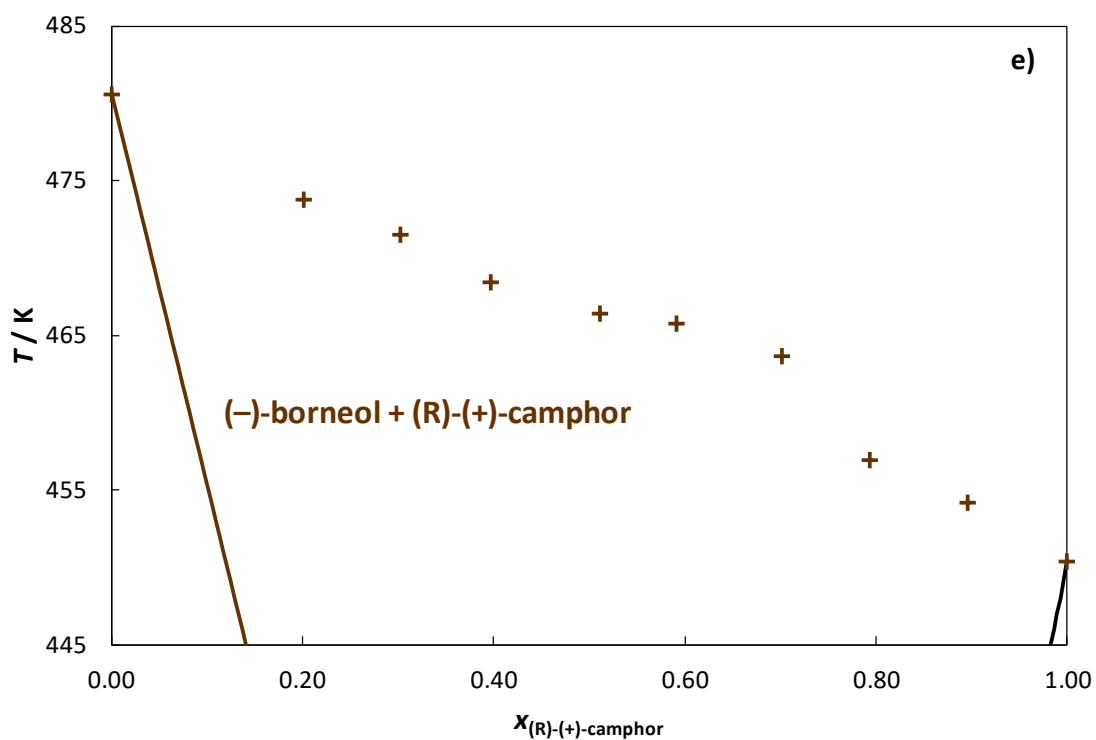
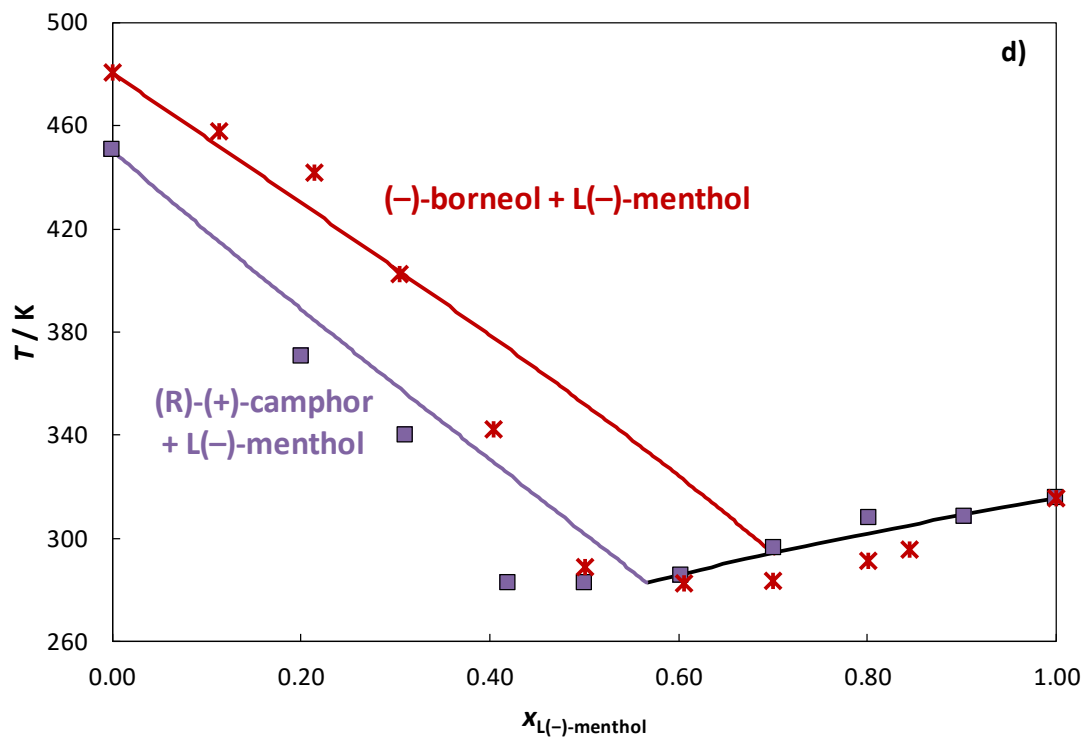


**Figure 2.2.** Solid-liquid phase diagrams of mixtures composed of monocarboxylic acids and terpenes. Symbols represent the experimental data measured in this work while the solid lines represent the ideal solubility curves.



**Figure 2.3.** System L(–)-menthol + Thymol after cooling down to 193.15 K.

In order to evaluate thymol or L(–)-menthol + monocarboxylic acids mixtures as potential solvents, their mixtures at the experimental eutectic composition are characterized in the next sections. Density and viscosity are relevant solvent properties once they have an important impact on the mass transport phenomena, affecting solvents suitability for specific applications.

### Density

Densities of the mixtures were determined at atmospheric pressure, in the temperature range from 278.15 to 373.15 K, and are reported in Figure 2.4 and Tables S2.2 and S2.3 of Appendix 2, together with the mole fraction of the monocarboxylic acid at the eutectic point. The densities of pure thymol and L(–)-menthol (see Chapter 4.1) are also displayed in Figure 2.4 for comparative purposes.

In all mixtures studied the density decrease with the temperature increase. Mixtures involving thymol present higher densities than the ones involving L(–)-menthol and the range in which they vary is also broader. The density of pure thymol is higher than the densities involving mixtures with monocarboxylic acids, while the density of pure L(–)-menthol is in between of those.

Mixtures of monocarboxylic acids with L(–)-menthol follow a well-defined trend in which the density decrease with the increase of the chain of the fatty acid. Oleic acid, the only unsaturated fatty acid studied, is an exception and the density values of the mixture oleic acid + L(–)-menthol crosses the other mixtures studied. Concerning the mixtures with

thymol, the opposite trend is observed, i.e., the densities decrease with the decrease of the chain of the fatty acid with the exception of lauric and oleic acid.

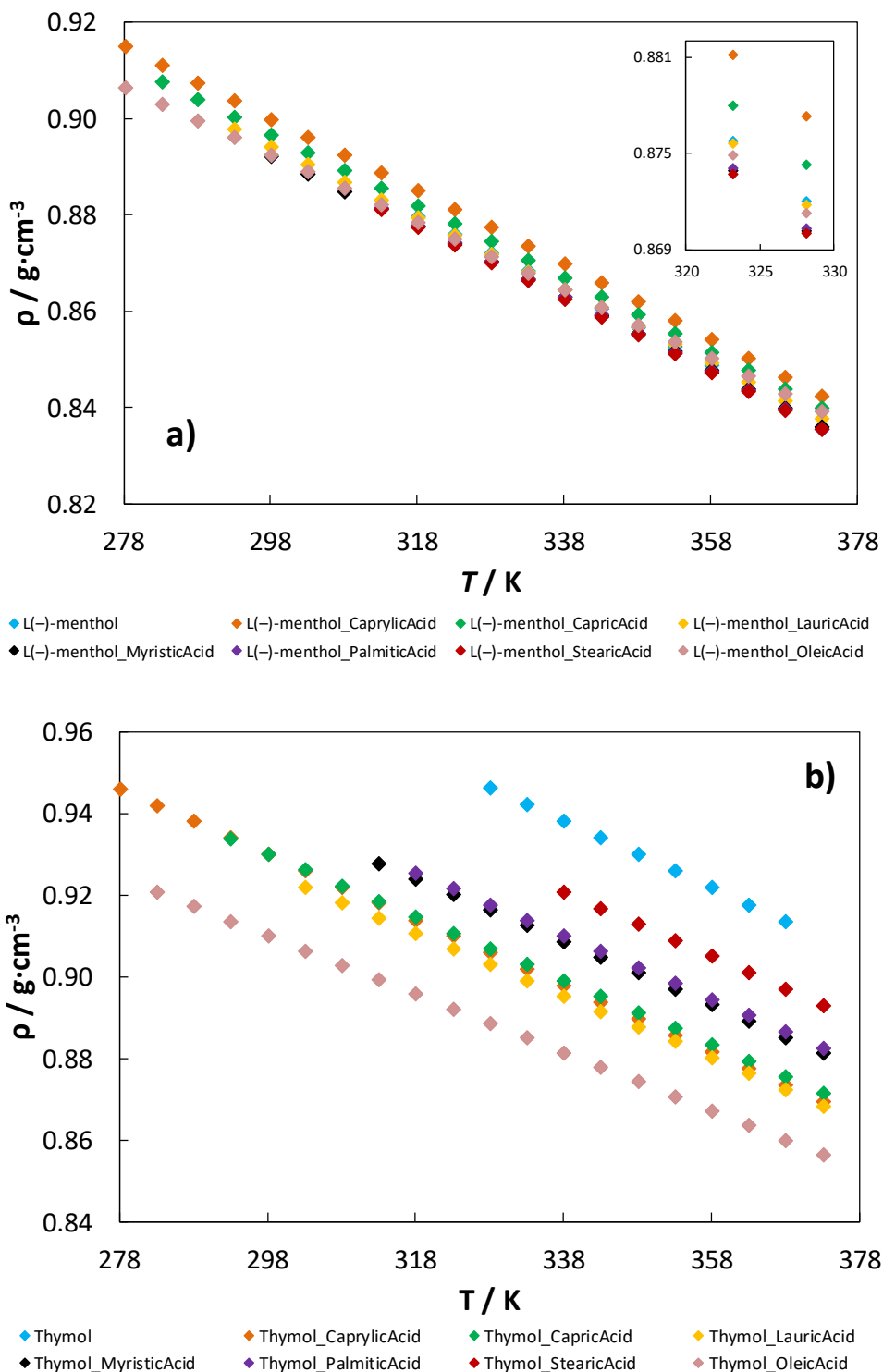


**Figure 2.4.** Density of mixtures involving monocarboxylic acids and L(-)-menthol or thymol.

The experimental density data was further correlated according with the linear equation 2.2 (parameters available in Table S2.4) and the isobaric thermal expansion coefficient,  $\alpha_p$ , derived from equation 2.3. No temperature dependence was assigned to this value. Figure 2.5 illustrates the results obtained as a function of the monocarboxylic acid.  $\alpha_p$  values are in general very similar, varying between  $-8.0 \times 10^{-4}$  and  $-8.9 \times 10^{-4}$ . No well-defined dependence of  $\alpha_p$  with the chain length of the monocarboxylic acid was observed. Oleic acid presents considerable superior values of  $\alpha_p$  in mixture with both terpenes studied. Moreover, caprylic and palmitic acids shows significant differences in mixture with the two terpenes. The isobaric thermal expansion coefficient is higher in thymol than in L(-)-menthol with the exception of caprylic acid.

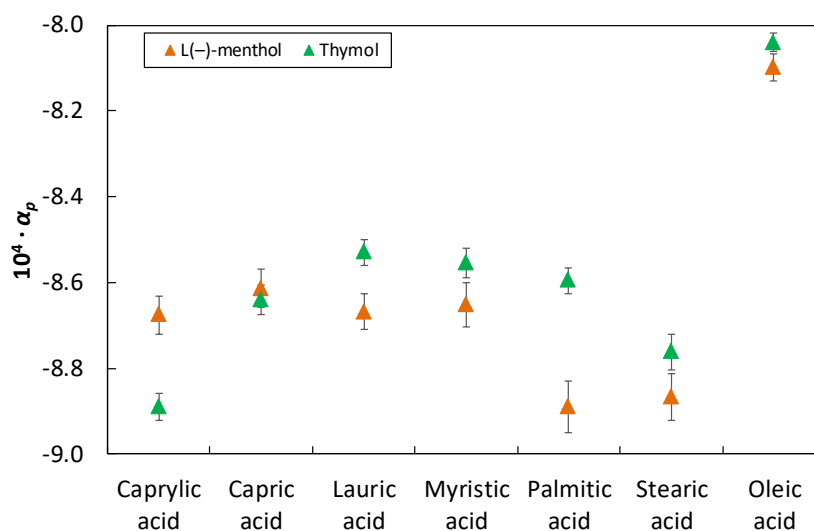


**Figure 2.5.** Thermal expansion coefficient representation of mixtures of L(-)-menthol or thymol and monocarboxylic acids.

Ribeiro et al.<sup>152</sup> also reported the densities of the mixture DL-menthol and lauric acid, however not at the eutectic composition and thus no comparison can be addressed.

### Viscosity

The new experimental viscosity data for the mixtures under study were also determined at atmospheric pressure, in the temperature range from 278.15 to 373.15 K and are depicted in Figure 2.6 and presented in Tables S2.5 and S2.6.

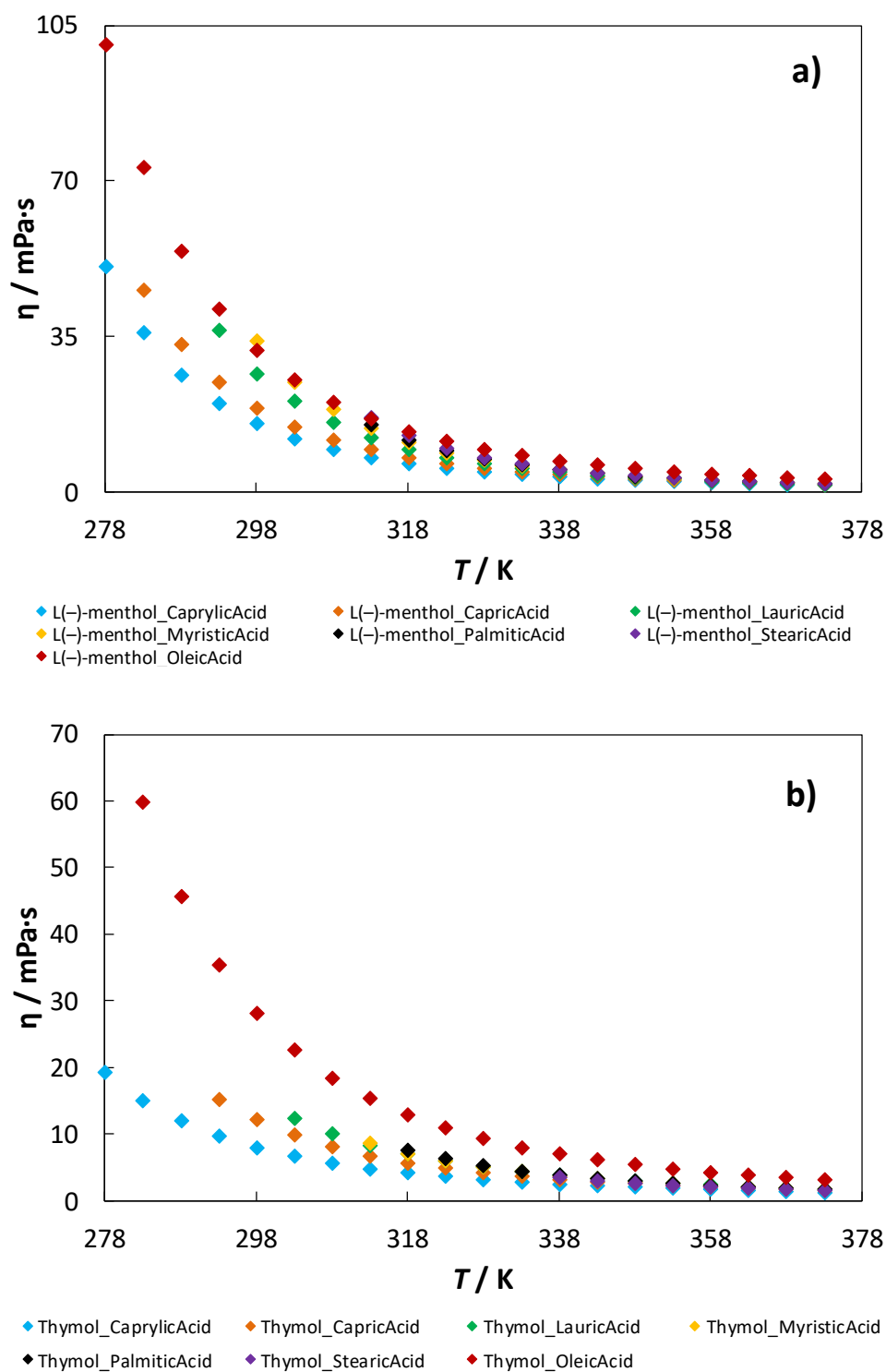


**Figure 2.6.** Viscosity of mixtures involving monocarboxylic acids and L(-)-menthol or thymol.

Viscosity values decrease with increasing temperature and with the decrease of the monocarboxylic chain length. Mixtures with oleic acid present the higher viscosities for

both evaluated mixtures with terpenes. Contrary to what happen in density, the range of viscosities of mixtures of L(-)-menthol is broader than the range of viscosities of mixtures involving thymol, and these show lower viscosities.

Experimental viscosity values were fitted using the VTF equation (eq. 2.4) and the estimated parameters are listed in Table S2.7 together with the energy barrier,  $E$ , calculated through equation 2.5 at 338.15 K. This temperature was chosen because is the lowest temperature at which all mixtures are liquid. The energy barrier as a function of the monocarboxylic acid used in the mixture is represented in Figure 2.7.

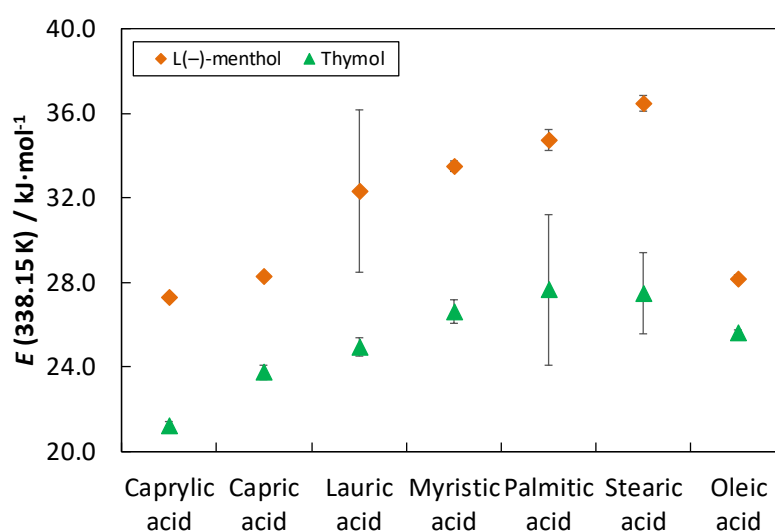


**Figure 2.7.** Energy barrier of the mixtures investigated at 338.15 K as a function of the monocarboxylic acid used.

The energy barrier increases with the increase of the chain length of the fatty acid used in the mixture, and for mixtures with the same monocarboxylic acid, the ones with thymol present lower energy barrier values. Being  $E$  the energy barrier of a fluid to shear stress, the higher this value the more difficult it is for the molecules to move past each other. Thus, as caprylic acid is the smaller monocarboxylic acid used, it presents the smaller value of  $E$ . Oleic acid is an exception presenting smaller values than most of the other acids in both series. Due to the presence of a double bond, this compound has a superior ability of entanglement decreasing the energy barrier.

## **2.5. Conclusions**

Novel eutectic and deep eutectic mixtures were prepared from natural materials as monocarboxylic acids and terpenes. Mixtures involving monocarboxylic acids and terpenes were found to be normal eutectic mixture, while some mixtures of terpenes were considered deep eutectic solvents. Mixtures of terpenes containing thymol indicate the formation of glasses instead of crystallizing. Almost all systems presented a eutectic point below room temperature. The new eutectic solvents composed by terpenes and monocarboxylic acids present densities lower than water and low viscosities (1.3 – 100.6 mPa·s) and in general mixtures involving thymol are less viscous and denser.

# Chapter 3 – Extraction, Production and Deterpenation







### 3.1. Ionic liquids as separation agents

#### 3.1.1. Introduction

To fully exploit the ionic liquids potential as solvents in separation processes involving terpenes or other organic solutes, and to avoid a large number of experimental liquid-liquid extractions, the ILs-solutes interactions must be known. The understanding of such interactions can be derived from physico-chemical measurements such as solubilities,<sup>184,185</sup> solute activity coefficients at infinite dilution ( $\gamma_{13}^{\infty}$ ),<sup>186–189</sup> molecular simulation,<sup>190,191</sup> spectroscopic techniques,<sup>192–194</sup> vapor-liquid equilibrium (VLE) data<sup>195,196</sup> and liquid-liquid equilibrium (LLE) data,<sup>197,198</sup> as well as from thermodynamic models such as equations of state<sup>199</sup> or from prediction tools such like COSMO-RS.<sup>196,197</sup> COSMO-RS (CONductor-like Screening MOdel for Real Solvents) is a quantum chemical approach, developed by Klamt and Eckert<sup>200</sup> and used by several authors,<sup>201,202</sup> for the *a priori* prediction of activity coefficients at infinite dilution and other thermophysical data using only structural information of the molecules.

Moreover, to replace a conventional separation process by another that uses ILs, this must be more performant and cost-effective, what is, in general, difficult. Due to their cost, higher than for commodity solvents, the main challenges in applying ionic liquids are related to their recovery and reutilization. Therefore, a good knowledge of ILs physical-chemical properties, and phase equilibria, is a fundamental step for the design and optimization of industrial processes.<sup>87</sup>

Very useful for screening purposes, the activity coefficient of solutes at infinite dilution are related to the relative strength of intermolecular interaction with the ionic liquid, being the lowest values usually observed for polar substances such as alcohols, ketones and ethers; a result from the hydrogen bonding, the  $\pi$ - $\pi$ ,  $\sigma$ - $\pi$ , or other strong interactions.<sup>203</sup>  $\gamma_{13}^{\infty}$  can be determined from retention times using gas-liquid chromatography (GLC)<sup>204–206</sup> or through the diluter technique.<sup>207,208</sup> In the GLC method, the chromatographic column is coated with the ionic liquid and the solutes introduced with a carrier gas. This technique works for solutes that are retained by the IL more

strongly than by the carrier gas (usually helium).<sup>109</sup> The solutes retention times are a measure of the strength of interaction, i.e., the activity coefficients at infinite dilution, of the solute in the ionic liquids. Solute-solvent interactions, selectivities and capacities can be derived from activity coefficients at infinite dilution.<sup>187,189</sup>

Based on the concepts expressed above, the work reported on this section was carried out to investigate the application of activity coefficients at infinite dilution data to select ionic liquids able to promote the separation and purification of common organic solutes and terpenes. Ionic liquids with same cation and different anions were chosen to rationalize the effect of changes in the structures, evaluating polarity, as these anions present solvatochromic parameters reflecting very high hydrogen-bond acceptor ability.

Experimental activity coefficients at infinite dilution values were determined by gas-liquid chromatography. The ILs density as a function of temperature was measured to calculate the gas-liquid partition coefficients,  $K_L$ . Additionally, excess thermodynamic properties at infinite dilution were discussed and comparisons with literature addressed. Concerning terpenes, the new data here gathered were used to evaluate the ability of COSMO-RS in the description of the selectivities and capacities for these compounds, and the model was then applied to screen different IL cations and anions for terpenes and terpenoids separation.

### **3.1.2. Experimental methods**

#### **Activity coefficients at infinite dilution**

The activity coefficients at infinite dilution were determined using the GLC method.<sup>209–211</sup> Experiments were carried out using a PerkinElmer Clarus 500 gas chromatograph equipped with a heated on-column injector and a thermal conductivity detector (TCD). The injector and detector temperatures were kept at 473.15 K during the experiments, value above the boiling point of the solutes. Helium was used as the carrier gas and the exit gas flow rates were measured with one Agilent Precision Gas Flow Meter placed on the outside, after the detector, with an uncertainty of  $\pm 0.1 \text{ cm}^3 \cdot \text{min}^{-1}$ . The inlet pressure,  $P_i$ , was measured by a pressure gauge installed on the gas chromatograph with an

uncertainty of  $\pm 0.1$  kPa and the outlet pressure,  $P_0$ , was measured using the same Agilent Precision Gas Flow Meter with an uncertainty of  $\pm 0.07$  kPa. The settled inlet pressure was 10 kPa for alkanes, cycloalkanes, alkenes, cycloalkenes, alkynes and ethers; 60 kPa for aromatic hydrocarbons, ketones, cyclic ethers, esters, butyraldehyde, acetonitrile, pyridine, 1-nitropropane and thiophene; and 80 kPa for alcohols, water and terpenes. The outlet pressure ranged between [97.84 – 101.08] kPa. Data were collected and processed using the TotalChrom Workstation software.

Column packing containing between 45% to 55% IL stationary phase coated onto a 100–120 mesh Chromosorb W/AW – DMCS solid support material (supplied by Sigma-Aldrich), were prepared by the rotary evaporation technique.<sup>212,213</sup> High amounts of ILs were used to avoid possible residual adsorption effects of the solutes on the solid support. Each IL was dissolved in methanol and dispersed in Chromosorb. After coating, the mixture was shaken, and vacuum-assisted rotary evaporation was used to remove the methanol. Masses of the stationary phase and of the solid support were weighed with a precision of  $\pm 1 \times 10^{-4}$  g. Glass columns of 1 m length and 4 mm internal diameter were filled with the dry packing and placed in the chromatograph to equilibrate during 6 h, at 388 K and 60 kPa. The stream of helium gas was passed through the stationary phase for the final drying. A large amount of column packing is used also to prevent the residual adsorption of solute onto the column packing, a very important feature, especially for alkanes. For each IL, at least two columns were prepared, with different IL packing's percentage. The deviations between the  $\gamma_{13}^{\infty}$  in the different columns, for a given set of solutes, was always less than 3%. In general, the major contributions to the errors were from solutes with smaller retention times, as alkanes, cycloalkanes, ketones and some ethers. The repeatability of  $\gamma_{13}^{\infty}$  values from two columns were within  $\pm 1.5\%$  for the vast majority of the solutes.

In order to measure the retention times, solutes were injected in the column in volumes of (0.01 to 0.3)  $\mu\text{L}$ , to be at infinite dilution conditions. In each measurement, together with the organic solutes, air was also injected, as a non-retained component. Absolute values of retention times varied between 0.04 to 249.72 min corresponding to  $\alpha$ -pinene

and carvacrol, respectively. Each experiment was repeated at least twice to establish repeatability. The temperature of the column was maintained constant to within  $\pm 0.02$  K. Measured retention times were generally reproducible within 0.01 – 0.03 min depending upon the temperature and the individual solute. Values of the dead time,  $t_G$ , equivalent to the retention time of a completely non-retained component, in this case air, were also measured. Considering the solute retention times accuracy (0.001 min), and the standard deviations (in parentheses) related with: solute vapor pressures ( $< 5\%$ ), mass of the stationary phase ( $< 1 \times 10^{-4}$  g), flow rate of helium ( $0.1 \text{ cm}^3 \cdot \text{min}^{-1}$ ), inlet (0.1 kPa) and outlet (0.07 kPa) pressures, and oven temperature (0.02 K); the uncertainties in  $\gamma_{13}^\infty$  were estimated by error propagation to be less than 3%.

### Densities

Densities measurements of the pure ILs were carried out at atmospheric pressure and in the (293.15 to 373.15) K temperature range using an automated SVM3000 Anton Paar rotational Stabinger viscometer-densimeter. The equipment uses Peltier elements for fast and efficient thermostatzation. The uncertainty of temperature is  $\pm 0.02$  K and the absolute uncertainty in density is  $\pm 5 \cdot 10^{-4} \text{ g} \cdot \text{cm}^{-3}$ . Additional details related with the equipment can be found elsewhere.<sup>214</sup>

#### 3.1.3. Theoretical approach

##### Activity coefficients at infinite dilution

When an infinitesimal amount of solute sample is introduced into a GLC column with a non-volatile stationary phase it is possible to calculate the activity coefficient at infinite dilution for the solute (1) partitioning between the carrier gas (2) and the non-volatile liquid solvent (3) through the solute retention,<sup>205</sup> according to the equation developed by Everett<sup>215</sup> and Cruickshank et al.<sup>216</sup>:

$$\ln \gamma_{13}^\infty = \ln \left( \frac{n_3 RT}{V_N P_1^*} \right) - \frac{P_1^* (B_{11} - V_1^*)}{RT} + \frac{P_0 J_2^3 (2B_{12} - V_1^\infty)}{RT} \quad (3.1)$$

where  $n_3$  is the number of moles of solvent on the column packing,  $T$  is the GC oven

temperature where the column is placed,  $V_N$  is the net retention volume of the solute,  $P_1^*$  is the saturated vapor pressure of the solute,  $B_{11}$  is the second virial coefficient of the pure solute,  $V_1^*$  is the molar volume of the solute,  $P_0$  is the outlet pressure,  $J_2^3$  is a pressure correction term,  $B_{12}$  is the mixed second virial coefficient of the solute and the carrier gas (helium), and  $V_1^\infty$  is the partial molar volume of the solute at infinite dilution in the solvent. The standard state for the solute is pure liquid at system temperature and zero pressure, and all temperature dependent properties are calculated at  $T$ .

The pressure correction term  $J_2^3$ ,<sup>217</sup> and the net retention volume of the solute,  $V_N$ , are given by the following equations:

$$J_2^3 = \frac{2 (P_i / P_0)^3 - 1}{3 (P_i / P_0)^2 - 1} \quad (3.2)$$

$$V_N = (J_2^3)^{-1} U_0 (t_R - t_G) \quad (3.3)$$

where  $t_R$  and  $t_G$  are the retention times for the solute and an unreturned gas (air), respectively, and  $U_0$  is the column outlet volumetric flow rate, corrected for the vapor pressure of water by,

$$U_0 = U \left( 1 - \frac{P_w}{P_0} \right) \frac{T}{T_f} \quad (3.4)$$

where  $T_f$  is the temperature at the column outlet,  $P_w$  is the vapor pressure of water at  $T_f$ , and  $U$  is the volumetric flow rate measured at the outlet of the column.

### COSMO-RS

COSMO-RS is a well-established *a priori* method to predict thermophysical properties of fluids and liquid mixtures based on unimolecular quantum calculations. Theoretical details about this method can be found elsewhere.<sup>200,218,219</sup> To predict the  $\gamma_{13}^\infty$  with COSMO-RS first it is necessary to generate distinct input files, for solutes and IL cations

and anions, using BP functional B88-p86 with a triple- $\xi$  valence polarized basis set (TZVP) and the resolution of identity standard (RI) approximation using TURBOMOLE 6.1 program package.<sup>220</sup> The following calculation consists mainly of statistical thermodynamics and were performed using COSMOtherm, which provides an efficient and flexible implementation of the COSMO-RS method. The parameterization adopted was BP\_TZVP\_C30\_1401 (COSMOconfX v3.0, COSMOlogic GmbH & Co KG, Leverkusen, Germany). It contains intrinsic parameters of COSMOtherm and element specific parameters, required for the calculation of physiochemical data. In all calculation, ILs have been described by an equimolar mixture of the cation and the anion, that contribute  $\sigma$ -profile as two different compounds, allowing the study of specific contribution of each counter ion. As consequence, it is necessary to scale the calculated values with the factor 0.5.<sup>219</sup> Moreover, the lowest energy conformations of all the species involved were used in the COSMO-RS calculations.

### Thermodynamic functions at infinite dilution

The activity coefficients at infinite dilution were determined as a function of temperature, allowing the determination of some important partial molar excess thermodynamic functions, namely the Gibbs free energy ( $\overline{G}_m^{E,\infty}$ ), enthalpy ( $\overline{H}_m^{E,\infty}$ ) and entropy ( $\overline{S}_m^{E,\infty}$ ) that will help to explore and rationalize the collected experimental information. Since the experimental activity coefficients were measured at infinite dilution, the partial molar excess properties were estimated using the following equations,

$$\overline{G}_m^{E,\infty} = RT \ln(\gamma_{13}^\infty) \quad (3.5)$$

$$\overline{H}_m^{E,\infty} = R \left( \frac{\partial \ln \gamma_{13}^\infty}{\partial \ln(1/T)} \right)_{p,\bar{x}} \quad (3.6)$$

$$\overline{S}_m^{E,\infty} = \frac{\overline{H}_m^{E,\infty} - \overline{G}_m^{E,\infty}}{T} \quad (3.7)$$

where subscripts  $p$  and  $x$  indicate isobaric condition and constant composition, respectively.

### Gas-liquid partition coefficients

To use volatile solvents for technical purposes, their characterization is required. The partition coefficients are many times used for this purpose, since the solubility of selected substances can be predicted from them. These coefficients are also highly important in chemical engineering and environmental modelling, where the distribution of individual compounds between different organic phases and water or air, is of importance.

Aiming at the determination of the order of elution from columns, partition coefficients are extracted from the retention data and many numbers have been published as a by-product of chromatographic separations, where their determination usually constitutes part of the procedure. In this work, the gas–liquid partition coefficient  $K_L = (c_1^L / c_1^G)$  for a solute partitioning between the carrier gas and the ILs was calculated from the solute retention according to the following equation,<sup>221</sup>

$$\ln(K_L) = \ln\left(\frac{V_N \rho_3}{m_3}\right) - \frac{P_0 J_2^3 (2B_{12} - V_1^\infty)}{RT} \quad (3.8)$$

in which  $\rho_3$  is the density of the IL and  $m_3$  is the mass of the IL.

### Selectivity and capacity

The selectivity between the solutes  $i$  and  $j$ ,  $S_{ij}^\infty$  and the capacity  $k_j^\infty$  of the separation process are defined as follow:<sup>207</sup>

$$S_{ij}^\infty = \gamma_i^\infty / \gamma_j^\infty \quad (3.9)$$

$$k_j^\infty = 1 / \gamma_j^\infty \quad (3.10)$$

where  $j$  is the solute that presents the smaller activity coefficients at infinite dilution in the solvent (in this work, the ILs).



### 3.1.4. Activity coefficients at infinite dilution of organic solutes and water on polar imidazolium-based ionic liquids

Mónia A. R. Martins, João A. P. Coutinho, Simão P. Pinho & Urszula Domańska, *Journal of Chemical Thermodynamics* 91, 194–203 (2015), DOI: 10.1016/j.jct.2015.07.042

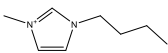
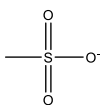
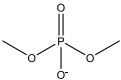
#### 3.1.4.1. Abstract

The separation of aromatic hydrocarbons from C4–C10 aliphatic hydrocarbon mixtures is challenging since these hydrocarbons have boiling points in a close range, and several combinations form azeotropes. The discussion on the desulphurization, or denitrogenation of fuels is also important nowadays. Thus, the activity coefficients at infinite dilution,  $\gamma_{13}^{\infty}$ , of 55 organic solutes and water in three ionic liquids with the common cation 1-butyl-3-methylimidazolium and the polar anions  $\text{Cl}^-$ ,  $[\text{CH}_3\text{SO}_3]^-$  and  $[(\text{CH}_3)_2\text{PO}_4]^-$ , were determined by gas-liquid chromatography at four temperatures in the range (358.15 to 388.15) K for alcohols and water, and (398.15 to 428.15) K for the other organic solutes including alkanes, cycloalkanes, alkenes, cycloalkenes, alkynes, ketones, ethers, cyclic ethers, aromatic hydrocarbons, esters, butyraldehyde, acetonitrile, pyridine, 1-nitropropane and thiophene. From the experimental  $\gamma_{13}^{\infty}$  values, the partial molar excess Gibbs free energy,  $\overline{G}_m^{E,\infty}$ , enthalpy  $\overline{H}_m^{E,\infty}$ , and entropy  $\overline{S}_m^{E,\infty}$ , at infinite dilution, were estimated to provide more information about the interactions between the solutes and the ILs. Moreover, densities were measured and gas-liquid partition coefficients ( $K_L$ ) calculated. Selectivities at infinite dilution for some separation problems such as octane/benzene, cyclohexane/benzene and cyclohexane/thiophene were calculated using the measured  $\gamma_{13}^{\infty}$ , and compared with literature values for *N*-methyl-2-pyrrolidinone (NMP), sulfolane, and other ionic liquids with a common cation or anion of the ILs here studied. From the obtained infinite dilution selectivities and capacities, it can be concluded that the ILs studied may replace conventional entrainers applied for the separation processes of aliphatic/aromatic hydrocarbons.

### 3.1.4.2. Chemicals

The chemical structure and some of the properties of the studied ILs are presented in Table 3.1. Organic solutes source and purity can be found in Table S3.1 of Appendix 3. To reduce the water and volatile compounds individual samples of ILs were dried under vacuum at 0.1 Pa and constant stirring at 353 K, for a minimum of 48 h. After, the purity of each ionic liquid was further checked by  $^1\text{H}$ , and  $^{13}\text{C}$ , NMR spectra. Additional drying was applied keeping the ILs during 72 hours at 300 K under reduced pressure to remove volatile impurities and traces of water. The water content of the dried ILs was determined using the Karl Fischer titration technique (method TitroLine KF). Samples were dissolved in dry methanol and titrated with a step of 2.5  $\mu\text{L}$ . The analysis showed that the water content was found to be below 300 ppm for all samples. The organic solutes were used without further purification once GLC technique separates impurities in the column. The water used in the measurements was distilled and filtered, presenting a final mass fraction purity higher than 0.999, being the analysis performed through density measurement.

**Table 3.1.** Studied ionic liquids: name, structure, abbreviation, source, molar mass ( $M$ ), melting point ( $T_M$ ) and purity.

Chemical Formula		Chemical Name	Supplier	$M$ ( $\text{g}\cdot\text{mol}^{-1}$ )	$T_M$ (K)	Purity (mass %)
Cation	Anion					
	$\text{Cl}^-$	1-butyl-3-methylimidazolium chloride, [C <sub>4</sub> mim]Cl	IoLiTec	174.67	341.95 <sup>a</sup>	99
		1-butyl-3-methylimidazolium methanesulfonate, [C <sub>4</sub> mim][CH <sub>3</sub> SO <sub>3</sub> ]	IoLiTec	234.32	$\approx$ 353.15 <sup>b</sup>	99
		1-butyl-3-methylimidazolium dimethyl phosphate, [C <sub>4</sub> mim][(CH <sub>3</sub> ) <sub>2</sub> PO <sub>4</sub> ]	IoLiTec	264.26	n.a. <sup>c</sup>	98

<sup>a</sup>Ref.<sup>222</sup>; <sup>b</sup>Ref.<sup>223</sup>; <sup>c</sup>Not available.

### 3.1.4.3. Results and discussion

The average values of the activity coefficients at infinite dilution for several organic solutes, and water, in the studied ILs are presented in Table 3.2. The temperature dependent properties required for the  $\gamma_{13}^{\infty}$  calculations were obtained using equations and constants taken from the literature.<sup>224</sup> The values of  $B_{12}$  were calculated using the Tsonopolous<sup>225</sup> correlation, applying the information also found in Poling and Prausnitz.<sup>224</sup> The measurements were carried out in the temperature range between (358.15 and 388.15) K, with intervals of 10 K. The lower temperature value was chosen regarding the ILs melting points, namely of [C<sub>4</sub>mim]Cl and [C<sub>4</sub>mim][CH<sub>3</sub>SO<sub>3</sub>], to avoid their solidification inside the column. Alcohols and water were measured between (398.15 and 428.15) K due to their usual longer retention times. In order to explore the data, a comparison at a fixed temperature, 358.15 K, is presented in Figure 3.1 (for alcohols and water the values are presented at 398.15 K).

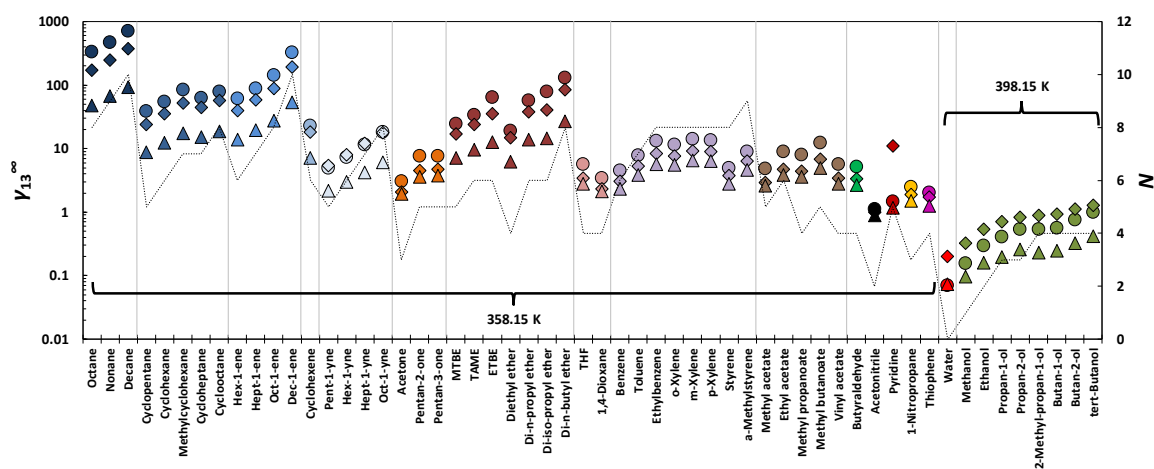


**Figure 3.1.** Activity coefficients at infinite dilution of several solutes in ILs, at 398.15 K for alcohols and water, and 358.15 K for the other organic compounds. ○, [C<sub>4</sub>mim]Cl; ◇, [C<sub>4</sub>mim][CH<sub>3</sub>SO<sub>3</sub>]; Δ, [C<sub>4</sub>mim]((CH<sub>3</sub>)<sub>2</sub>PO<sub>4</sub>). The dotted line represents the number of carbons in the solutes structure, *N*. Symbols with the same color correspond to solutes of the same chemical family.

**Table 3.2.** Activity coefficients at infinite dilution of organic compounds and water in ILs, at different temperatures.<sup>a</sup>

Organic Solutes	[C <sub>4</sub> mim]Cl <sup>b</sup>				[C <sub>4</sub> mim][CH <sub>3</sub> SO <sub>3</sub> ] <sup>c</sup>				[C <sub>4</sub> mim][[(CH <sub>3</sub> ) <sub>2</sub> PO <sub>4</sub> ] <sup>d</sup>				
	T / K	358.15	368.15	378.15	388.15	358.15	368.15	378.15	388.15	358.15	368.15	378.15	388.15
Octane		330.66	302.07	268.50	258.36	170.84	164.58	159.96	155.32	47.90	46.22	44.57	43.35
Nonane		475.82	432.95	393.64	375.50	250.53	239.46	229.20	223.29	67.86	63.95	61.45	59.15
Decane		704.04	637.87	579.72	560.12	371.49	351.76	340.15	324.31	93.39	88.52	84.67	81.58
Cyclopentane		38.69	36.24	33.50	31.83	23.85	23.70	23.50	23.26	8.76	8.59	8.41	8.33
Cyclohexane		54.69	50.90	47.36	44.92	35.18	34.49	33.90	33.81	12.29	11.88	11.64	11.45
Methylcyclohexane		84.25	79.00	73.02	69.85	52.79	51.70	50.88	50.40	17.38	16.78	16.40	16.07
Cycloheptane		62.67	58.82	55.41	53.57	44.21	43.33	42.59	42.25	15.14	14.64	14.26	14.00
Cyclooctane		79.55	75.40	71.10	68.62	57.11	55.66	54.42	53.60	18.77	18.24	17.72	17.33
Hex-1-ene		61.71	57.87	53.94	51.97	39.66	39.99	40.01	40.26	13.89	13.71	13.40	13.20
Hept-1-ene		88.90	83.76	79.33	77.17	59.23	58.91	58.68	58.03	19.61	19.38	19.15	18.91
Oct-1-ene		141.84	134.44	125.75	122.50	88.06	86.76	86.48	85.64	27.49	26.95	26.46	26.22
Dec-1-ene		322.82	305.86	284.63	277.46	192.88	187.08	181.89	179.06	53.50	52.23	50.44	49.24
Cyclohexene		22.84	22.30	21.48	21.31	18.44	18.59	18.73	19.00	7.15	7.13	7.11	7.11
Pent-1-yne		4.89	5.25	5.51	5.78	5.46	5.84	6.26	6.67	2.18	2.32	2.46	2.60
Hex-1-yne		7.33	7.85	8.19	8.61	8.02	8.52	9.06	9.64	3.01	3.22	3.39	3.57
Hept-1-yne		11.63	12.30	12.74	13.33	11.97	12.64	13.34	14.11	4.21	4.48	4.70	4.93
Oct-1-yne		18.32	19.20	19.73	20.45	17.77	18.58	19.47	20.39	6.04	6.22	6.48	6.74
Acetone		3.05	3.12	3.17	3.27	2.06	2.12	2.22	2.30	1.92	1.96	2.02	2.10
Pentan-2-one		7.59	7.71	7.78	8.01	4.50	4.59	4.76	4.91	3.63	3.70	3.78	3.94
Pentan-3-one		7.60	7.72	7.78	7.97	4.68	4.79	4.88	5.09	3.73	3.81	3.89	4.04
MTBE		24.61	23.80	23.02	22.85	16.97	17.39	17.90	18.55	7.17	7.35	7.48	7.66
TAME		33.96	33.14	32.18	32.06	23.82	24.18	24.67	25.26	9.50	9.61	9.66	9.75
ETBE		64.78	59.34	55.67	53.32	35.29	35.59	36.10	36.62	12.75	12.78	12.89	12.95
Diethyl ether		19.27	18.93	18.36	18.39	14.69	14.91	14.98	15.32	6.21	6.30	6.39	6.48

Chapter 3 – Extraction, Production and Deterpenation

Di- <i>n</i> -propyl ether	57.40	55.26	52.78	51.93	38.11	38.73	38.94	39.41	13.95	13.73	13.55	13.42
Di- <i>iso</i> -propyl ether	78.53	71.67	63.98	59.12	40.59	-	40.79	41.19	14.39	14.27	14.22	14.12
Di- <i>n</i> -butyl ether	130.04	124.82	118.31	116.17	83.87	82.13	81.55	80.53	26.78	26.23	25.90	25.52
THF	5.66	5.67	5.67	5.70	3.41	3.48	3.59	3.72	2.79	2.84	2.89	3.02
1,4-Dioxane	3.47	3.55	3.65	3.74	2.33	2.41	2.49	2.62	2.13	2.19	2.25	2.37
Benzene	4.51	4.59	4.72	4.82	3.08	3.19	3.29	3.46	2.33	2.41	2.49	2.63
Toluene	7.78	7.91	8.09	8.36	5.32	5.45	5.68	5.84	3.86	3.99	4.09	4.29
Ethylbenzene	13.15	13.25	13.51	13.73	8.45	8.61	8.76	9.05	5.73	5.87	5.97	6.26
<i>o</i> -Xylene	11.55	11.72	11.93	12.28	7.64	7.79	7.99	8.21	5.54	5.70	5.79	6.03
<i>m</i> -Xylene	14.31	14.50	14.69	15.02	9.27	9.43	9.57	9.92	6.49	6.60	6.73	7.00
<i>p</i> -Xylene	13.63	13.72	14.00	14.29	9.03	9.20	9.37	9.71	6.31	6.44	6.59	6.86
Styrene	4.96	5.18	5.42	5.73	3.79	3.96	4.20	4.40	2.79	2.93	3.06	3.26
<i>α</i> -Methylstyrene	9.01	9.33	9.83	10.34	6.43	6.71	6.96	7.41	4.57	4.77	4.98	5.29
Methyl acetate	4.82	4.89	5.01	5.09	2.94	3.03	3.14	3.33	2.58	2.65	2.73	2.85
Ethyl acetate	9.02	9.06	9.10	9.16	4.76	4.88	5.00	5.28	3.81	3.91	4.01	4.18
Methyl propanoate	8.00	8.09	8.20	8.31	4.43	4.56	4.68	4.90	3.56	3.65	3.76	3.93
Methyl butanoate	12.30	12.43	12.57	12.69	6.79	7.21	7.39	7.84	4.93	5.04	5.17	5.39
Vinyl acetate	5.66	5.74	5.86	6.05	3.47	3.58	3.76	3.92	2.79	2.88	2.99	3.13
Butyraldehyde	5.24	5.31	5.43	5.54	3.33	3.44	3.58	3.74	2.66	2.74	2.82	2.97
Acetonitrile	1.12	1.16	1.21	1.28	0.99	1.03	1.08	1.12	0.88	0.92	0.95	1.00
Pyridine	1.47	1.55	1.64	1.78	10.93	10.80	10.61	10.47	1.18	1.23	1.28	1.35
1-Nitropropane	2.51	2.61	2.69	2.80	1.89	1.96	2.02	2.13	1.50	1.56	1.62	1.72
Thiophene	2.04	2.16	2.27	2.41	1.72	1.81	1.94	2.05	1.24	1.35	1.43	1.53
<b><i>T</i> / K</b>	<b>398.15</b>	<b>408.15</b>	<b>418.15</b>	<b>428.15</b>	<b>398.15</b>	<b>408.15</b>	<b>418.15</b>	<b>428.15</b>	<b>398.15</b>	<b>408.15</b>	<b>418.15</b>	<b>428.15</b>
Methanol	0.156	0.166	0.176	0.191	0.325	0.340	0.357	0.373	0.097	0.105	0.115	0.125
Ethanol	0.297	0.313	0.332	0.353	0.533	0.553	0.576	0.599	0.160	0.173	0.189	0.205
Propan-1-ol	0.408	0.434	0.464	0.501	0.711	0.744	0.783	0.823	0.197	0.218	0.239	0.264

Chapter 3 – Extraction, Production and Deterpenation

Propan-2-ol	0.542	0.577	0.619	0.668	0.835	0.878	0.928	0.976	0.256	0.282	0.311	0.344
2-Methyl-propan-1-ol	0.540	0.576	0.615	0.665	0.893	0.938	0.991	1.042	0.230	0.254	0.281	0.313
Butan-1-ol	0.558	0.594	0.635	0.680	0.937	0.984	1.024	1.071	0.247	0.271	0.299	0.324
Butan-2-ol	0.749	0.804	0.865	0.931	1.114	1.181	1.255	1.333	0.327	0.365	0.406	0.451
<i>tert</i> -Butanol	0.987	1.067	1.159	1.269	1.285	1.385	1.483	1.594	0.419	0.471	0.527	0.592
Water	0.070	0.077	0.085	0.094	0.200	0.214	0.228	0.239	0.073	0.081	0.092	0.101

<sup>a</sup>Standard uncertainties are:  $u(\gamma_{13}^{\infty}) = 3\%$  and  $u(T) = 0.02\text{ K}$ . <sup>b</sup>Packing: 52.1 %,  $n_3 = 17.02\text{ mmol}$ . <sup>c</sup>Packing: 49.8 %,  $n_3 = 11.48\text{ mmol}$ . <sup>d</sup>Packing: 47.3 %,  $n_3 = 9.39\text{ mmol}$ .

The higher the interactions between the solutes and the ionic liquids, the higher the retention times measured, and the lower the activity coefficients at infinite dilution.<sup>226,227</sup>

A global analysis of Figure 3.1 shows that water presents the lower  $\gamma_{13}^{\infty}$  values indicating the highest interaction with the ionic liquids, what is expected since the ionic liquids were chosen with highly polar anions. Other polar solutes such as alcohols, thiophene, 1-nitropropane, pyridine and acetonitrile present also low  $\gamma_{13}^{\infty}$  values. On the opposite, alkanes and alkenes, the less polar solvents, present the weakest interactions with the ILs studied. Moreover, analyzing Figure 3.1 it is possible to observe that the  $\gamma_{13}^{\infty}$  increases with the chain length for the alkanes, cycloalkanes, alkenes, alkynes, ketones, ethers, aromatic hydrocarbons (increasing radicals) and alcohols. The experimental values obtained in this work for aliphatic and aromatic hydrocarbons are much larger than those observed in other ILs with the same cation.<sup>204,228</sup> However, if compared with ILs with the same anion the  $\gamma_{13}^{\infty}$  are similar,<sup>211</sup> indicating a dominant role of the anion on these interactions. The  $\gamma_{13}^{\infty}$  value for acetonitrile at  $T = 358.15$  K is considerably low in all ILs studied suggesting the high potential for the extraction of acetonitrile from aliphatic hydrocarbons. In  $[\text{C}_4\text{mim}][(\text{CH}_3)_2\text{PO}_4]$ , also pyridine (1.18), 1-nitropropane (1.50) and thiophene (1.24) have low  $\gamma_{13}^{\infty}$  values at  $T = 358.15$  K, suggesting a high selectivity for the extraction of nitrogen and sulfur-containing compounds from alkanes.

The temperature dependence of  $\gamma_{13}^{\infty}$  is presented in the Appendix 3 (Figure S3.1). Increasing the temperature, a decrease in the natural logarithm of  $\gamma_{13}^{\infty}$  with the reciprocal temperature is observed for alkanes, cycloalkanes, alkenes, cycloalkenes, and few ethers. The inverse dependence is observed for all the other solutes, what will be hereafter taken into consideration.

According to Cláudio et al.,<sup>229</sup> the polarity of the ILs studied follow the trend:  $[(\text{CH}_3)_2\text{PO}_4]^- > \text{Cl}^- > [\text{CH}_3\text{SO}_3]^-$ , in conformity with the relative values of  $\gamma_{13}^{\infty}$  observed for water and alcohols, the most polar solutes studied. Pyridine that is an aromatic ring with one methine group (=CH-) replaced by a nitrogen atom, also show the same behavior because

of its high hydrogen bonding ability. The other organic solutes studied follow the trend:  $[(\text{CH}_3)_2\text{PO}_4]^- > [\text{CH}_3\text{SO}_3]^- > \text{Cl}^-$ .

### Comparison with literature data

Similar studies have been published on solute activity coefficients at infinite dilution in ILs. Figure 3.2 shows the experimental  $\gamma_{13}^\infty$  of several solutes in the ILs  $[\text{C}_4\text{mim}]\text{Cl}$  and  $[\text{C}_4\text{mim}][\text{CH}_3\text{SO}_3]$ , and the respective literature values. To the best of our knowledge, no data are available for the IL  $[\text{C}_4\text{mim}][(\text{CH}_3)_2\text{PO}_4]$ . Analyzing Figure 3.2 in general, results are very consistent. The solutes THF and 1,4-dioxane are clear exception; THF in both ILs and 1,4-dioxane in  $[\text{C}_4\text{mim}][\text{CH}_3\text{SO}_3]$ , with more significant deviation to the literature values.<sup>230,231</sup> Additionally, our experimental data shows an increase in  $\gamma_{13}^\infty$  of toluene in  $[\text{C}_4\text{mim}][\text{CH}_3\text{SO}_3]$ , with increasing temperature, while the data reported by Stark et al.<sup>231</sup> shows the opposite trend. All the others aromatic hydrocarbons studied in this work, such as benzene, ethylbenzene, *p*-, *m*-, *o*-xylene, present the same slope observed for toluene. Moreover, for further comparison purposes data from literature involving ILs presenting the same cation, or one of the anions, were selected. Some standard organic solutes and the temperature of 358.15 K were chosen and are presented in Table 3.3.

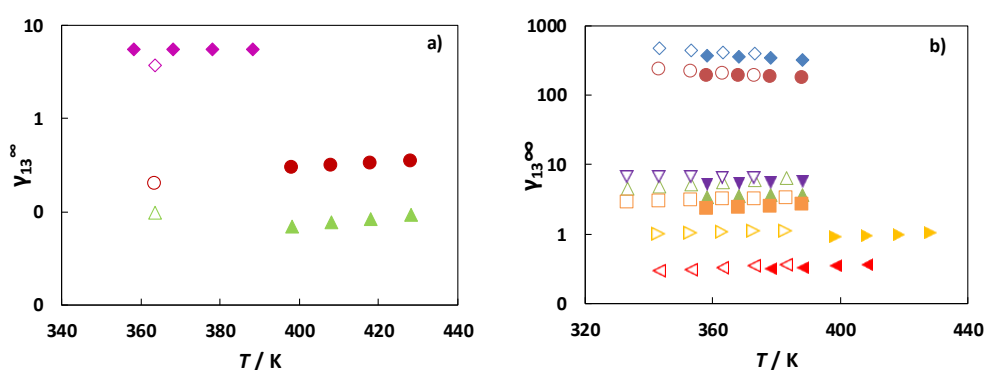


**Figure 3.2.** Comparison of the experimental activity coefficients at infinite dilution with values from literature for two ionic liquids: (a)  $[\text{C}_4\text{mim}]\text{Cl}$ ,  $\blacklozenge$  THF,  $\bullet$  ethanol,  $\blacktriangle$  water (empty symbols correspond to literature data<sup>230</sup>); (b)  $[\text{C}_4\text{mim}][\text{CH}_3\text{SO}_3]$ ,  $\blacklozenge$  decane,  $\bullet$  dec-1-ene,  $\blacktriangle$  THF,  $\blacksquare$  1,4-dioxane,  $\blacktriangledown$  toluene,  $\blacktriangleleft$  methanol,  $\blacktriangleright$  butan-1-ol (empty symbols correspond to literature data<sup>231</sup>).



**Table 3.3.** Comparison between the activity coefficients at infinite dilution with values from literature at 358.15 K.

Ionic Liquids	Octane	Cyclohexane	Benzene	Ethanol	Water	Reference
[C <sub>4</sub> mim]Cl	330.7	54.7	4.5	0.22 <sup>a</sup>	0.04 <sup>a</sup>	This Work
[C <sub>8</sub> mim]Cl	17.1 <sup>a</sup>	7.8 <sup>a</sup>	1.3 <sup>a</sup>	-	-	206
[C <sub>2</sub> mim][CH <sub>3</sub> SO <sub>3</sub> ]	275.3 <sup>a</sup>	45.5 <sup>a</sup>	4.3	0.47	0.09	211
[C <sub>2</sub> mim][CH <sub>3</sub> SO <sub>3</sub> ]	356.7 <sup>a</sup>	50.5 <sup>a</sup>	4.1 <sup>a</sup>	0.36 <sup>a</sup>	-	232
[C <sub>4</sub> mim][CH <sub>3</sub> SO <sub>3</sub> ]	170.8	35.2	3.1	0.44 <sup>a</sup>	0.15 <sup>a</sup>	This Work
[C <sub>1</sub> mim][(CH <sub>3</sub> ) <sub>2</sub> PO <sub>4</sub> ]	246.1 <sup>a</sup>	39.6 <sup>a</sup>	3.8 <sup>a</sup>	0.13 <sup>a</sup>	0.05 <sup>a</sup>	207
[C <sub>4</sub> mim][(CH <sub>3</sub> ) <sub>2</sub> PO <sub>4</sub> ]	47.9	12.3	2.3	0.10 <sup>a</sup>	0.04 <sup>a</sup>	This Work
[C <sub>2</sub> mim][(CH <sub>3</sub> CH <sub>2</sub> ) <sub>2</sub> PO <sub>4</sub> ]	83.4 <sup>a</sup>	24.6 <sup>a</sup>	2.3 <sup>a</sup>	-	-	233
[C <sub>4</sub> mim][(CH <sub>3</sub> (CH <sub>2</sub> ) <sub>3</sub> ) <sub>2</sub> PO <sub>4</sub> ]	6.2 <sup>b</sup>	2.6 <sup>b</sup>	0.9 <sup>b</sup>	-	-	234

<sup>a</sup>Extrapolated value; <sup>b</sup>Interpolated value.

Regarding the anion chloride, increasing the alkyl chain length on the cation decreases considerably the  $\gamma_{13}^{\infty}$  with non-polar solvents. The same is observed for the non-polar solvents on the other anions studied suggesting that the increase on the cation alkyl chain enhances the dispersive interactions with the non-polar solvents. In comparison the effect on the polar compounds such as ethanol and water seems to be negligible, within the experimental uncertainty of the data, suggesting that for these compounds the dominant interactions are related to the anions and no longer with the cation.

### Effect of the anion

As mentioned before, the anion has a large influence on the activity coefficients at infinite dilution. To better understand this effect, some organic solutes with different characteristics were investigated. The ion–dipole interactions were studied using acetonitrile, to clarify the IL ability to solvate dipolar molecules. Octane and toluene allowed the investigation of  $\sigma$ -electron and  $\pi$ -electron dispersion forces, respectively. The hydrogen bond acceptor and donor properties of the ILs were investigated with propan-1-ol (a hydrogen bond donor) and 1,4-dioxane (a hydrogen bond acceptor), respectively. The influence of the anion on the solvation properties of ILs was investigated with the

three ILs studied in this work,  $[\text{C}_4\text{mim}]\text{Cl}$ ,  $[\text{C}_4\text{mim}][\text{CH}_3\text{SO}_3]$  and  $[\text{C}_4\text{mim}][(\text{CH}_3)_2\text{PO}_4]$ . The effect of the nature of the anion on  $\gamma_{13}^\infty$  of the organic solutes chosen is displayed in Figure 3.3.

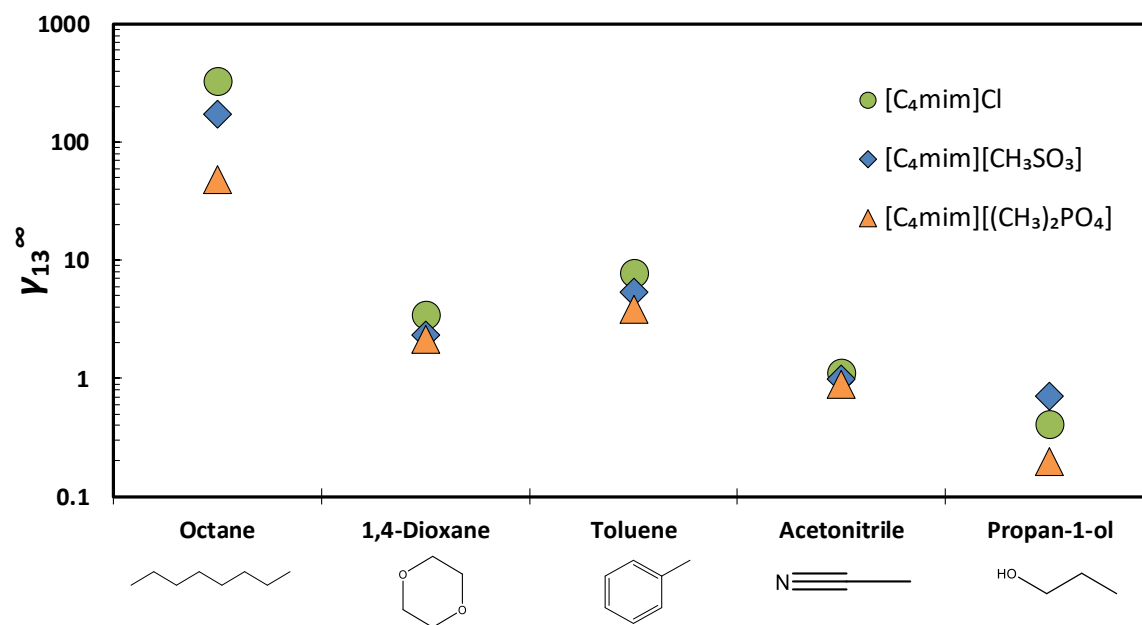


**Figure 3.3.** Activity coefficients at infinite dilution of selected solutes in ILs, at 398.15 K for propan-1-ol, and 358.15 K for the other organic compounds.

As can be seen, for acetonitrile, all  $\gamma_{13}^\infty$  are very close, however chloride gives the larger value, followed by the anions methanesulfonate and dimethyl phosphate, where the dipole is better accommodated. Concerning 1,4-dioxane and propan-1-ol, the hydrogen bond acceptor and donor, it is possible to see that the choice of the anion has an important effect in the  $\gamma_{13}^\infty$  values. The  $\gamma_{13}^\infty$  of propan-1-ol decreases in the order of  $[\text{CH}_3\text{SO}_3]^- > \text{Cl}^- > [(\text{CH}_3)_2\text{PO}_4]^-$  by a factor close to 2. This sequence is in complete agreement to the rank based on the solvatochromic  $\beta$  parameter<sup>235</sup> for the description of the hydrogen bonding accepting ability of each anion. The  $\gamma_{13}^\infty$  of 1,4-dioxane decreases according to  $\text{Cl}^- > [\text{CH}_3\text{SO}_3]^- > [(\text{CH}_3)_2\text{PO}_4]^-$ . This happens because this solute can only interact with the cation ring's hydrogen atoms if they are not engaged in strong interactions with basic anions, and hence the activity coefficients are higher in the

chloride-based IL. When comparing between the five solutes, the lower values of  $\gamma_{13}^{\infty}$  in propan-1-ol attest the hydrogen-bond acceptor character of the anions chosen.

For the  $\pi$  and  $\sigma$ -electron dispersion forces the choice of the anion also plays a significant role. The lowest  $\gamma_{13}^{\infty}$  of toluene, and hence the highest degree of interaction, is found for the  $[(\text{CH}_3)_2\text{PO}_4]^-$ , followed by  $[\text{CH}_3\text{SO}_3]^-$  and  $\text{Cl}^-$ . For octane the same trend was observed however, this solute shows higher  $\gamma_{13}^{\infty}$  values and a higher variation between the different ionic liquids.

### Thermodynamic functions at infinite dilution

The partial excess molar properties such as Gibbs energy, enthalpy, and entropy, all at infinite dilution, for the organic solutes and water in the studied ILs at the reference temperatures  $T = 358.15$  K and  $T = 398.15$  (alcohols and water), were evaluated to provide more information about the interactions between the solutes and the ILs. The thermodynamic functions at infinite dilution, calculated through the  $\gamma_{13}^{\infty}$  values are listed in Appendix 3 (Table S3.2) at the reference temperatures.

The  $\overline{H}_m^{E,\infty}$ , calculated through the temperature dependence of  $\gamma_{13}^{\infty}$  (equation 3.6), exhibit negative values for almost all solutes, expressing the favorable interactions between the solute and the solvent, except for alkanes, cycloalkanes, alkenes, cycloalkenes and a few ethers, all apolar compounds, and the ILs. The  $\overline{G}_m^{E,\infty}$  is positive for most of the solutes, apart from alcohols, water, and acetonitrile (for  $[(\text{CH}_3)_2\text{PO}_4]^-$  and  $[\text{CH}_3\text{SO}_3]^-$ ), indicating strong interactions solute-IL for these polar solutes. The largest positive values of  $\overline{G}_m^{E,\infty}$  are exhibited by aliphatic hydrocarbons, showing again the weak aliphatic hydrocarbon-IL interactions. Lastly,  $\overline{S}_m^{E,\infty}$  are  $< 0$  for all solutes studied, indicating their reorganization inside the ionic liquid phase, and often representing the dominance of entropic effect over the enthalpic one.

To further understand the molecular level interactions in these systems, Figure 3.4 relates  $\gamma_{13}^{\infty}$  and partial molar excess properties, where three different areas can be distinguished.

The region (II) corresponds to the ILs–organic solutes systems with positive deviations to Raoult’s law,  $\gamma_{13}^{\infty} > 1$  and, to some organic solutes also  $\overline{G}_m^{E,\infty}$  and  $\overline{H}_m^{E,\infty}$  are positive. In this region, mainly constituted by non-polar solutes such as alkanes, cycloalkenes, alkenes and a few ethers, no particular affinity between ILs and organic solutes molecules is expected. This low interaction between organic solutes and ILs can lead to the formation of immiscible solutions and consequently, phase separation. Thus, they may find themselves as potential solvents in liquid–liquid extraction, as will be shown below.

The region (III) corresponds to the ILs–organic solutes systems with negative deviations from Raoult’s law ( $\gamma_{13}^{\infty} < 1$ ) that is related to a spontaneous dissolution of organic solutes in the ILs. From all the solutes studied, only alcohols and water lie in this region, due to their strong polarity. All the partial excess molar properties studied are negative, revealing that the hydrogen bonding between organic solutes and the IL anions is much stronger than hydrogen bonding between solute–solute or IL–IL molecules, leading to an exothermic mixing behavior of these systems. As expected, systems with IL composed by the anion with stronger hydrogen basicity,  $[(\text{CH}_3)_2\text{PO}_4]^-$ , exhibits lower values of  $\overline{H}_m^{E,\infty}$ .

Region (IV) presents  $\gamma_{13}^{\infty} > 1$ ,  $\overline{S}_m^{E,\infty}$  and  $\overline{H}_m^{E,\infty} < 0 \text{ kJ}\cdot\text{mol}^{-1}$ . This is the region where most organic solutes fall. For some solutes  $\overline{G}_m^{E,\infty}$  is close to 0, while the enthalpic and entropic contributions are both negative, meaning that they cancel each other. As can be observed in Figure 3.4, when region (IV) is compared to region (II) the dominance of the entropic term over the enthalpic is evident. It is also relevant to notice that that when the interaction between the solute and IL are strong (regions I or III), the enthalpic effect is always dominant.

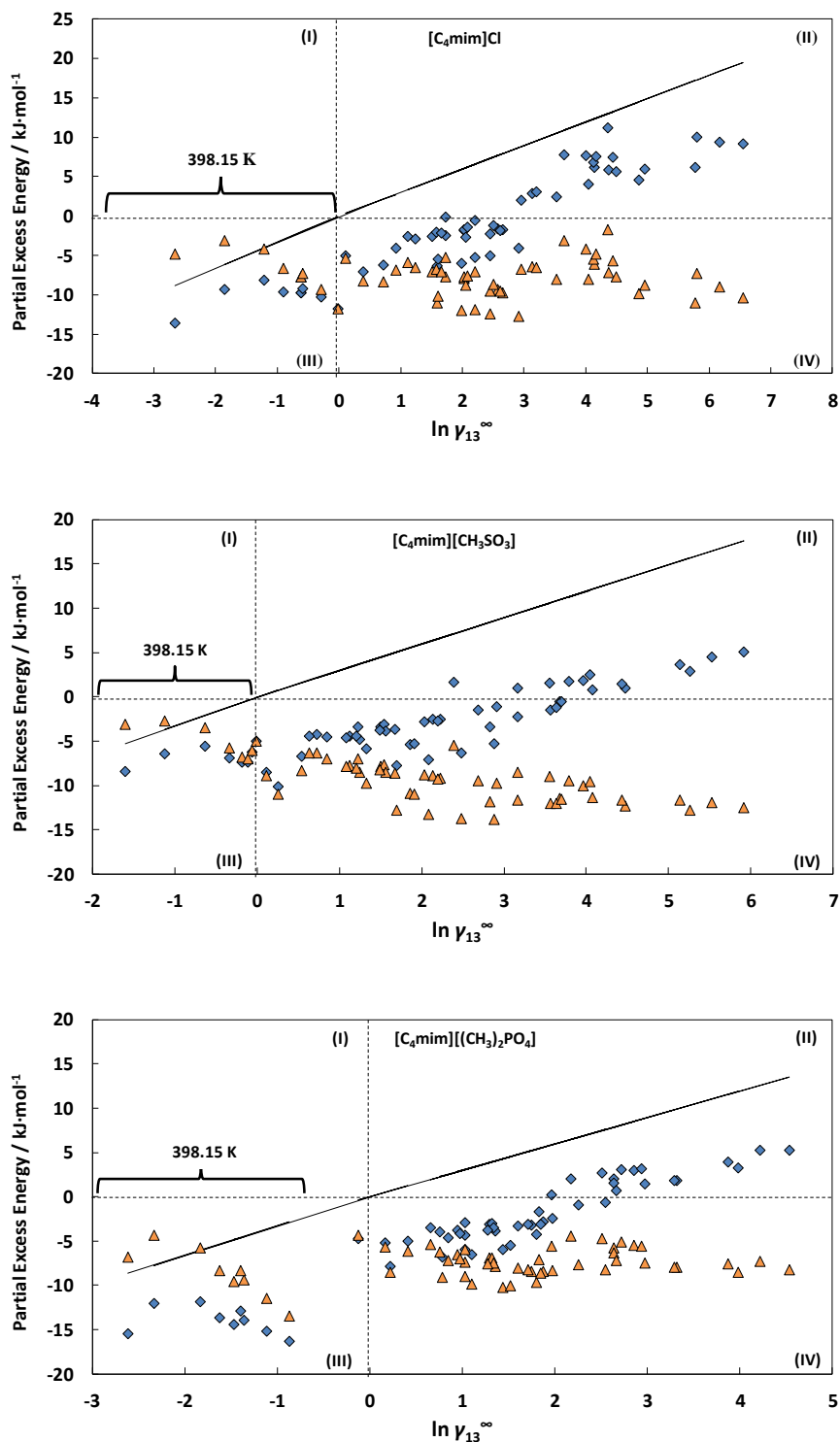


**Figure 3.4.** Partial molar excess energies as a function of the activity coefficients at infinite dilution of the organic solutes studied in the ILs  $[\text{C}_4\text{mim}]\text{Cl}$ ,  $[\text{C}_4\text{mim}][\text{CH}_3\text{SO}_3]$  and  $[\text{C}_4\text{mim}][(\text{CH}_3)_2\text{PO}_4]$ , at 358.15 and 398.15 K. The line represents  $\overline{G}_m^{E,\infty}$  and the symbols correspond to:  $\diamond$ ,  $\overline{H}_m^{E,\infty}$  and  $\Delta$ ,  $T_{\text{ref}}\overline{S}_m^{E,\infty}$ .

### Gas-liquid partition coefficients

To calculate the gas–liquid partition coefficients,  $K_L$ , the ILs densities were measured over the temperature range from (293.15 to 373.15) K and the results are listed in Table 3.4. Density data were previously reported and are represented in Figure 3.5, along with the experimental values from this work. As can be seen for the ILs [C<sub>4</sub>mim][(CH<sub>3</sub>)<sub>2</sub>PO<sub>4</sub>] and [C<sub>4</sub>mim][CH<sub>3</sub>SO<sub>3</sub>] the experimental values are in good agreement with literature, with a maximum relative deviation of 0.11 and 0.08%, respectively. Concerning [C<sub>4</sub>mim]Cl more data sets are available, which show some inconsistencies within each other. Our data show very good agreement to those published by Machida et al.<sup>236</sup> and He et al.,<sup>237</sup> presenting larger deviations to others.<sup>238–240</sup> However, taking in account the IL purity and water content, which sometimes are not given, discrepancies are not that significant, being the maximum relative deviation of 1.26% concerning the data of Kavitha et al.,<sup>239</sup> for the IL [C<sub>4</sub>mim]Cl at 313.15 K.

**Table 3.4.** Density of the pure ILs studied as a function of temperature at 0.1 MPa.

<i>T</i> / K	$\rho$ / g·cm <sup>-3</sup> <sup>a</sup>		
	[C <sub>4</sub> mim]Cl	[C <sub>4</sub> mim][CH <sub>3</sub> SO <sub>3</sub> ]	[C <sub>4</sub> mim][(CH <sub>3</sub> ) <sub>2</sub> PO <sub>4</sub> ]
293.15			1.1665
298.15			1.1632
303.15			1.1594
308.15	1.0794		1.1562
313.15	1.0766		1.1527
318.15	1.0737		1.1495
323.15	1.0709		1.1461
328.15	1.0681		1.1430
333.15	1.0652	1.1506	1.1397
338.15	1.0624	1.1474	1.1365
343.15	1.0596	1.1443	1.1333
348.15	1.0569	1.1412	1.1301
353.15	1.0543	1.1379	1.1269
358.15	1.0517	1.1349	1.1237
363.15	1.0490	1.1319	1.1206
368.15	1.0464	1.1288	1.1174
373.15	1.0439	1.1258	

<sup>a</sup>Standard uncertainties, *u*, are  $u(\rho) = \pm 5 \cdot 10^{-4}$  g·cm<sup>-3</sup>,  $u(T) = 0.02$  K and  $u_r(p) = 0.05$ .

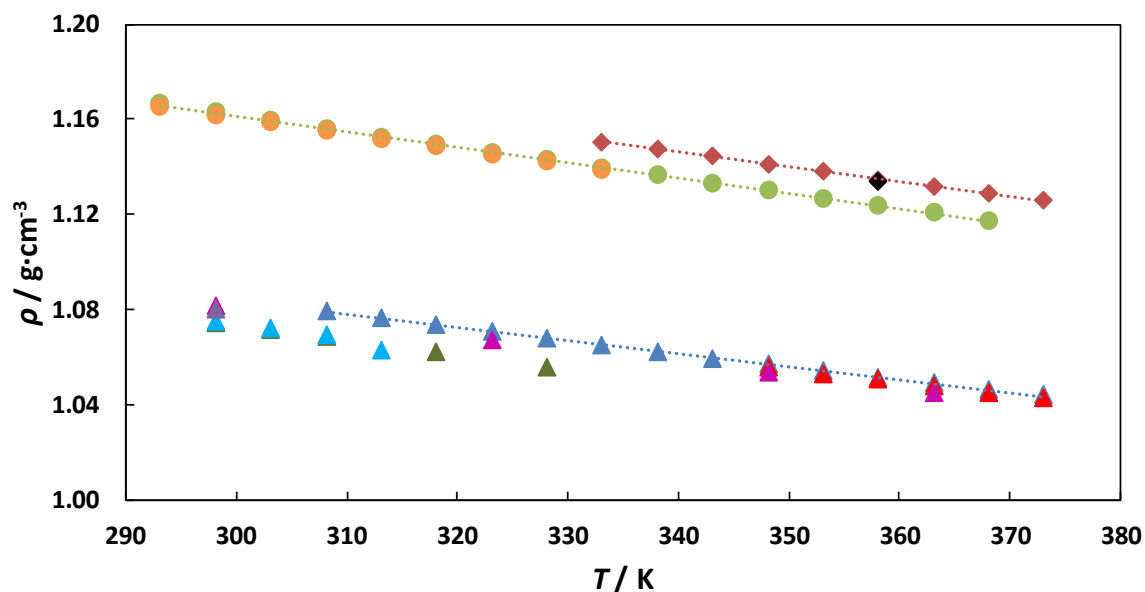


**Figure 3.5.** Comparison of density experimental values with literature data. Symbols: ▲ [C<sub>4</sub>mim]Cl, this work; ▲ [C<sub>4</sub>mim]Cl<sup>236</sup>; ▲ [C<sub>4</sub>mim]Cl<sup>237</sup>; ▲ [C<sub>4</sub>mim]Cl<sup>238</sup>; ▲ [C<sub>4</sub>mim]Cl<sup>239</sup>; ▲ [C<sub>4</sub>mim]Cl<sup>240</sup>; ◆ [C<sub>4</sub>mim][CH<sub>3</sub>SO<sub>3</sub>], this work; ◆ [C<sub>4</sub>mim][CH<sub>3</sub>SO<sub>3</sub>]<sup>223</sup>; ● [C<sub>4</sub>mim][(CH<sub>3</sub>)<sub>2</sub>PO<sub>4</sub>], this work; ● [C<sub>4</sub>mim][(CH<sub>3</sub>)<sub>2</sub>PO<sub>4</sub>]<sup>235</sup>.

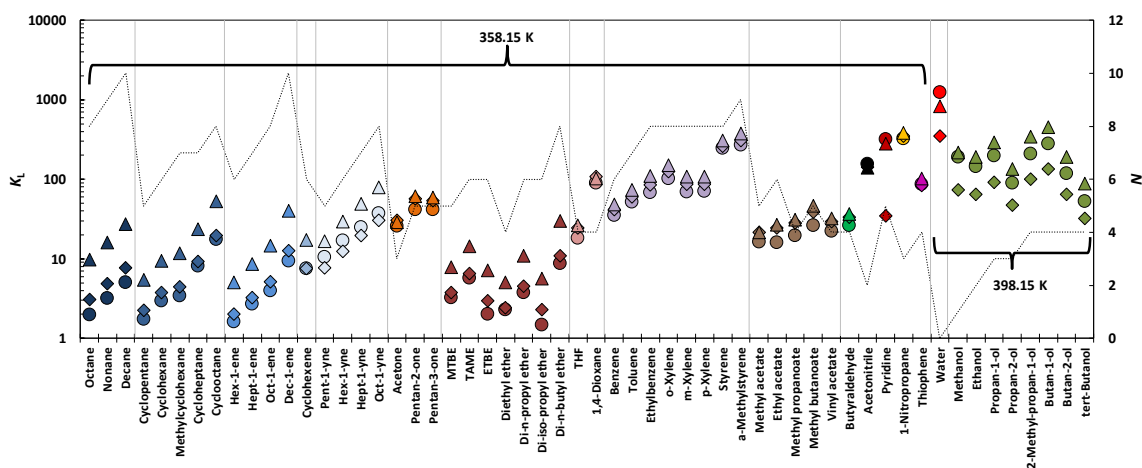


**Figure 3.6.** Experimental gas–liquid partition coefficients,  $K_L$ , for organic solutes and water in the ILs studied. ○, [C<sub>4</sub>mim]Cl; ◇, [C<sub>4</sub>mim][CH<sub>3</sub>SO<sub>3</sub>]; △, [C<sub>4</sub>mim][(CH<sub>3</sub>)<sub>2</sub>PO<sub>4</sub>]. The dotted line represents the number of carbons in the solutes structure,  $N$ . Symbols with the same color correspond to solutes of the same chemical family.

The gas–liquid partition compares the affinity of the solute to both phases. Results are listed in Appendix 3 (Table S3.3) and presented in Figure 3.6. As can be seen, for all solutes  $K_L$  decreases with increasing temperature, and increases with the alkyl chain in aliphatic and aromatic hydrocarbons, and ketones. The highest value is observed for water  $K_L = 1233.27$  in [C<sub>4</sub>mim]Cl at  $T = 358.15$  K, whereas the lowest value is observed for di-*iso*-propyl ether (0.99) in the same IL at 388.15 K. This is consistent with previous analyses, since higher  $K_L$  value corresponds to larger affinities of the solute to the liquid phase.

### Selectivities and capacities

The measurements of the activity coefficients at infinite dilution can be used to evaluate the performance of ILs as solvents for several practical chemical separation problems.<sup>230,241,242</sup> This is achieved by the calculation of selectivities and capacities. A suitable solvent should possess both a high selectivity and a high capacity for the components to be separated. The results obtained for  $S_{ij}^{\infty}$  and  $k_j^{\infty}$ , were calculated using equations 3.9 and 3.10, and the results are presented in Table 3.5, along with values from literature for ILs presenting the same anion or cation as those studied here. Some other important industrial solvents such as *N*-methyl-2-pyrrolidinone (NMP) and sulfolane are presented as well for comparison purposes.

Analyzing Table 3.5 it is possible to see that the separation of octane/benzene is the easiest, especially with [C<sub>4</sub>mim]Cl and the methanesulfonate-based anions. The lowest values of selectivity are found for [C<sub>8</sub>mim]Cl and [C<sub>4</sub>mim][[(CH<sub>3</sub>(CH<sub>2</sub>)<sub>3</sub>)<sub>2</sub>PO<sub>4</sub>], both present a cation and a anion, respectively, with a longer alkyl chain. The cyclohexane/benzene separation problem is, according with the calculated values, the most difficult separation. As can be seen, selectivities are similar, but much lower than for the previous system. Despite the low capacity value the IL [C<sub>4</sub>mim]Cl is, once again, the one that makes the separation easier. Regarding the separation of sulfur compounds from aliphatic hydrocarbons, cyclohexane/thiophene, the values are similar among the studied ILs, but [C<sub>4</sub>mim]Cl is again the solvent presenting better selectivities. Common solvents, NMP and



sulfolane, have lower values of selectivities in both aliphatic/aromatic separations than the ILs here studied.

**Table 3.5.** Selectivities ( $S_{ij}^{\infty}$ ) and capacities ( $k_j^{\infty}$ ) at infinite dilution for different separation problems at 358.15 K.

<b>Ionic Liquids</b>		$S_{ij}^{\infty} / k_j^{\infty}$			<b>Reference</b>
<b>Cation</b>	<b>Anion</b>	<b>Octane / Benzene</b>	<b>Cyclohexane / Benzene</b>	<b>Cyclohexane / Thiophene</b>	
[C <sub>4</sub> mim] <sup>+</sup>	Cl <sup>-</sup>	73.32 / 0.22	12.13 / 0.22	26.75 / 0.49	This work
	[CH <sub>3</sub> SO <sub>3</sub> ] <sup>-</sup>	55.50 / 0.32	11.43 / 0.32	20.41 / 0.58	This work
	[(CH <sub>3</sub> ) <sub>2</sub> PO <sub>4</sub> ] <sup>-</sup>	20.58 / 0.43	5.28 / 0.43	9.88 / 0.80	This work
	[(CH <sub>3</sub> (CH <sub>2</sub> ) <sub>3</sub> ) <sub>2</sub> PO <sub>4</sub> ] <sup>-</sup>	7.20 / 1.17	3.06 / 1.17	-	234, <i>a</i>
	[CF <sub>3</sub> SO <sub>3</sub> ] <sup>-</sup>	30.61 / 0.61	8.16 / 0.61	11.27 / 0.85	204
[C <sub>8</sub> mim] <sup>+</sup>	Cl <sup>-</sup>	13.67 / 0.80	6.04 / 0.80	-	206, <i>b</i>
[C <sub>2</sub> mim] <sup>+</sup>	[CH <sub>3</sub> SO <sub>3</sub> ] <sup>-</sup>	64.02 / 0.23 <sup>b</sup>	10.57 <sup>b</sup> / 0.23 <sup>b</sup>	21.75 / 0.48	211
		86.08 / 0.24	12.18 / 0.24	24.59 / 0.49	232, <i>b</i>
[C <sub>1</sub> mim] <sup>+</sup>	[(CH <sub>3</sub> ) <sub>2</sub> PO <sub>4</sub> ] <sup>-</sup>	65.71 / 0.27	10.58 / 0.27	-	207, <i>b</i>
[C <sub>2</sub> mim] <sup>+</sup>	[(CH <sub>3</sub> CH <sub>2</sub> ) <sub>2</sub> PO <sub>4</sub> ] <sup>-</sup>	36.24 / 0.43	10.70 / 0.43	-	233, <i>b</i>
<b>Other solvents</b>					
Sulfolane		26.03 / 0.44	-	-	243, <i>a</i>
NMP		-	4.49 / -	- / 0.93	244, <i>b</i>

<sup>a</sup>Interpolated value; <sup>b</sup>Extrapolated value.

Another very important problem is the de-nitrogenation of fuels. The values of selectivity for the separation of nitrogen compounds from aliphatic hydrocarbons as for example octane/pyridine or octane/1-nitropropane are (224.57, 15.63 and 40.57) and (131.54, 90.23 and 31.86) for Cl<sup>-</sup>, [CH<sub>3</sub>SO<sub>3</sub>]<sup>-</sup> and [(CH<sub>3</sub>)<sub>2</sub>PO<sub>4</sub>]<sup>-</sup>, respectively, at 358.15 K. The values presented for the IL [C<sub>4</sub>mim]Cl are very promising.

### 3.1.5. Selection of ionic liquids to be used as separation agents for terpenes and terpenoids

Mónia A. R. Martins, Urszula Domańska, Bernd Schröder, João A. P. Coutinho & Simão P. Pinho, *ACS Sustainable Chemistry & Engineering* 4, 548–556 (2016), DOI: 10.1021/acssuschemeng.5b01357

#### 3.1.5.1. Abstract

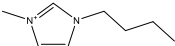
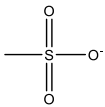
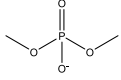
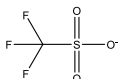
In this work ionic liquids are evaluated for the first time as solvents for extraction and entrainers in separation processes involving terpenes and terpenoids. For that purpose activity coefficients at infinite dilution,  $\gamma_{13}^{\infty}$ , of terpenes and terpenoids, in the ionic liquids [C<sub>4</sub>mim]Cl, [C<sub>4</sub>mim][CH<sub>3</sub>SO<sub>3</sub>], [C<sub>4</sub>mim][(CH<sub>3</sub>)<sub>2</sub>PO<sub>4</sub>], and [C<sub>4</sub>mim][CF<sub>3</sub>SO<sub>3</sub>] were determined by gas-liquid chromatography at six temperatures in the range (398.15 to 448.15) K. Based on the experimental values, a correlation of  $\gamma_{13}^{\infty}$  with an increase of the solubility parameters is proposed. The infinite dilution thermodynamic functions were calculated showing the entropic effect is dominant over the enthalpic. Gas-liquid partition coefficients give indications about the recovery and purification of terpenes and terpenoids from ionic liquid solutions. Presenting a strong innovative character, COSMO-RS was evaluated for the description of the selectivities and capacities, showing to be a useful tool for the screening of ionic liquids to find suitable candidates for terpenes and terpenoids extraction, and separation. COSMO-RS predictions show that in order to achieve the maximum separation efficiency, polar anions should be used such as bis(2,4,4-trimethylpentyl)phosphinate or acetate, while high capacities require nonpolar cations such as phosphonium.

#### 3.1.5.2. Chemicals

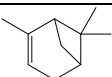
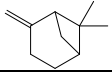
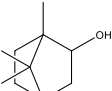
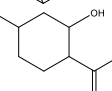
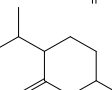
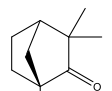
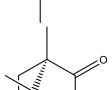
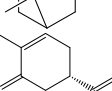
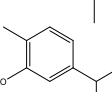
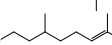
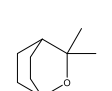
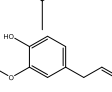
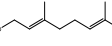
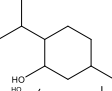
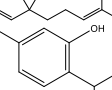
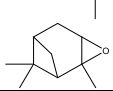
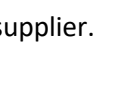
The properties of the ionic liquids used in this work are presented in Table 3.6, while the terpenes and terpenoids description is available in Table 3.7 and Table S3.4. The individual samples of the ILs used were purified under vacuum (0.1 Pa and 353 K) and constant stirring, for at least 48 h. The purity was then analyzed using <sup>1</sup>H, <sup>13</sup>C, and <sup>19</sup>F NMR spectra. To further reduce the water traces and the volatile impurities, ILs individual

samples were additionally dried during 72 hours at 300 K under reduced pressure. Karl-Fischer titration was used to determine the water content of the dry ILs. For that, samples were dissolved in dry methanol and titrated with a step of 2.5  $\mu\text{L}$ . The water content was found to be below 300 ppm for all samples. Terpenes and terpenoids were used without any further purification since the GLC technique operates at elevated temperatures ( $> 398.15 \text{ K}$ ) and thus, impurities can be removed from the column.

**Table 3.6.** Name, structure, abbreviation, supplier, molar mass ( $M$ ), melting point ( $T_M$ ) and purity of the investigated ionic liquids.

Chemical Formula		Chemical Name	Supplier	$M$ ( $\text{g}\cdot\text{mol}^{-1}$ )	$T_M$ (K)	Purity (mass %)
Cation	Anion					
	$\text{Cl}^-$	1-butyl-3-methylimidazolium chloride, [C <sub>4</sub> mim]Cl	IoLiTec	174.67	341.95 <sup>222</sup>	99
		1-butyl-3-methylimidazolium methanesulfonate, [C <sub>4</sub> mim][CH <sub>3</sub> SO <sub>3</sub> ]	IoLiTec	234.32	$\approx$ 353.15 <sup>223</sup>	99
		1-butyl-3-methylimidazolium dimethyl phosphate, [C <sub>4</sub> mim][[(CH <sub>3</sub> ) <sub>2</sub> PO <sub>4</sub> ]	IoLiTec	264.26	< 253.15	98
		1-butyl-3-methylimidazolium trifluoromethanesulfonate, [C <sub>4</sub> mim][CF <sub>3</sub> SO <sub>3</sub> ]	IoLiTec	288.29	289.15 <sup>245</sup>	99

**Table 3.7.** Names, structures, supplier, molar mass ( $M$ ), boiling points ( $T_{BP}$ ) and mass fraction purities of the terpenes and terpenoids used.

Chemicals	Supplier	CAS	$M$ (g·mol <sup>-1</sup> )	$T_{BP}$ (K) <sup>246</sup>	Mass fraction purity <sup>a</sup>	
Terpenes						
$\alpha$ -pinene		Sigma-Aldrich	80-56-8	136.237	429.29	98%
$\beta$ -pinene		Sigma-Aldrich	18172-67-3	136.237	439.19	99%
Terpenoids						
(-)-borneol		Fluka	464-45-9	154.252	485.80	≥99%
(-)-Isopulegol		SAFC	89-79-2	154.252	480.98	≥98%
(-)-menthone		Fluka	14073-97-3	154.252	483.15	≥99%
(1R)-(-)-fenchone		Aldrich	7787-20-4	152.236	466.15	≥98%
(1R)-(+)-camphor		Aldrich	464-49-3	152.236	480.55	98%
(S)-(+)-carvone		Merck	2244-16-8	150.221	504.15	96%
Carvacrol		SAFC	499-75-2	150.221	510.15	99%
DL-citronellol		Sigma	106-22-9	156.268	496.40	≈95%
Eucalyptol		Aldrich	470-82-6	154.252	449.55	99%
Eugenol		Aldrich	97-53-0	164.204	526.35	99%
Geraniol		Sigma-Aldrich	106-24-1	154.252	503.15	98%
L(-)-menthol		Acros	2216-51-5	156.268	487.40	99.7%
Linalool		Aldrich	78-70-6	154.252	470.15	97%
Thymol		Sigma	89-83-8	150.221	505.65	≥99.5%
$\alpha$ -pinene oxide		Aldrich	1686-14-2	152.236	489.51	97%

<sup>a</sup>Declared by the supplier.

### 3.1.5.3. Results and discussion

#### Activity coefficients at infinite dilution

The experimental measurements of the activity coefficients at infinite dilution of terpenes and terpenoids in ILs were carried out between (398.15 and 448.15) K, with intervals of 10 K, and the average values at each temperature are presented in Table S3.5 of Appendix 3. The properties required for the  $\gamma_{13}^{\infty}$  calculations are presented in Table S3.4, as well as literature sources and methods applied in their estimation. The virial coefficients were calculated using the correlation proposed by Tsonopolous,<sup>225</sup> available in Poling and Prausnitz.<sup>224</sup> High temperatures were adopted to avoid long retention times of solutes, and to prevent the solidification of the ionic liquids used inside the column. To better understand and explore the data, a comparison at a fixed temperature, 408.15 K, is presented in Figure 3.7. This temperature was chosen since it is the lowest temperature at which data are available for all the solutes studied in, at least, one ionic liquid.

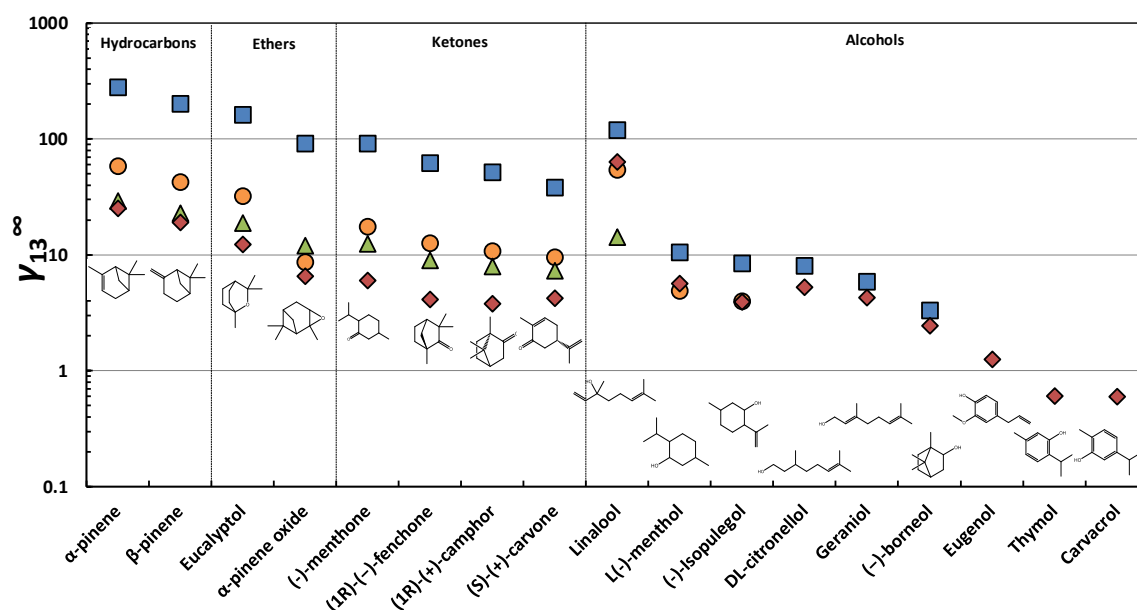


**Figure 3.7.** Activity coefficients at infinite dilution of terpenes and terpenoids in the ILs studied, at 408.15 K. □, [C<sub>4</sub>mim]Cl; ○, [C<sub>4</sub>mim][CH<sub>3</sub>SO<sub>3</sub>]; △, [C<sub>4</sub>mim][(CH<sub>3</sub>)<sub>2</sub>PO<sub>4</sub>]; ◇, [C<sub>4</sub>mim][CF<sub>3</sub>SO<sub>3</sub>].

As shown in Figure 3.7,  $\alpha$ -pinene and  $\beta$ -pinene show the weakest interactions with the ILs studied. This was expected since all the ionic liquids used present polar anions and thus, interact better with polar solutes as terpenoid alcohols, while the interactions with hydrocarbons (terpenes), and terpenoid ethers and ketones are weaker presenting higher values of activity coefficients at infinite dilution.

The terpenoid linalool is a clear exception, presenting an increase in the activity coefficients at infinite dilution and, additionally, a change in the ILs trend, when compared with the other alcohols. Trying to rationalize this apparent outlier, the sigma profiles of all ILs and solutes in their most stable form were computed by COSMO-RS and are presented in Figure S3.2 of Appendix 3. The alcohols sigma profiles show that linalool is the only one that does not present an H-bond donor character. Since the ILs anions have an H-bond acceptor character, the interactions are weaker and, consequently, the  $\gamma_{13}^{\infty}$  increase. Moreover, the change in the ILs trend suggests that in this case the anion-cation interaction is dominant face to the solute-anion interaction.

Due to the long retention times, and to the TCD detector sensitivity limit, the activity coefficients at infinite dilution of a few alcohols, in some ionic liquids, were not possible to measure. However, in  $[\text{C}_4\text{mim}][\text{CF}_3\text{SO}_3]$ , the least polar IL,<sup>229</sup> all solutes were measured. No significant differences were observed between the aromatic and the aliphatic terpenoids suggesting that the cyclical structure does not have a relevant impact in the activity coefficients at infinite dilution in the aromatic imidazolium ILs here investigated.

In our previous work,<sup>247</sup> measurements of  $\gamma_{13}^{\infty}$  for organic solutes with the same ILs were carried out. Considering the functional groups, the same trend of  $\gamma_{13}^{\infty}$  was found: hydrocarbons > ethers > ketones > alcohols. Moreover, the ILs trend observed for the activity coefficients at infinite dilution magnitude was  $[\text{CF}_3\text{SO}_3]^- < [(\text{CH}_3)_2\text{PO}_4]^- < [\text{CH}_3\text{SO}_3]^- < \text{Cl}^-$ , which is in good agreement with the polarity trend described by Cláudio et al.<sup>229</sup>

The dependency with the temperature is presented in Figure S3.3 of Appendix 3. For most solutes there is a linear increase or decrease in the natural logarithm of  $\gamma_{13}^{\infty}$  with the reciprocal temperature. The compounds (-)-menthone, (S)-(+)-carvone and (1R)-(+)-

camphor in  $[C_4mim]Cl$ ; (–)-menthone, geraniol and (1R)-(+)-camphor in  $[C_4mim][CH_3SO_3]$ ; and (1R)-(–)-fenchone and eucalyptol in  $[C_4mim][(CH_3)_2PO_4]$  and  $[C_4mim][CF_3SO_3]$  present almost an independent behavior of the logarithm of  $\gamma_{13}^\infty$  with the reciprocal temperature, and thus their enthalpy of solution is close to zero.

Despite the large number of studies published on the measurement of activity coefficients at infinite dilution of solvents in ionic liquids, to the best of our knowledge no data for activity coefficients at infinite dilution of terpenes and terpenoids was previously reported using ILs as a stationary phase, and no comparison is possible.

On an attempt to systematize the data collected here, correlations of the activity coefficients at infinite dilution of the terpenes and terpenoids measured with some of their properties (e.g. dipolar moment, solubility parameter, molar volume) were evaluated. The most promising results are reported on Figure 3.8 for the correlation with the solubility parameters calculated through the relation presented by Goharshadi and Hesabi.<sup>248</sup> Results show a decrease of the activity coefficient at infinite dilution with the increase of the solubility parameter. Additionally, the different ILs presents almost parallel trend lines, suggesting a predictive character to be explored as soon as more data are available.

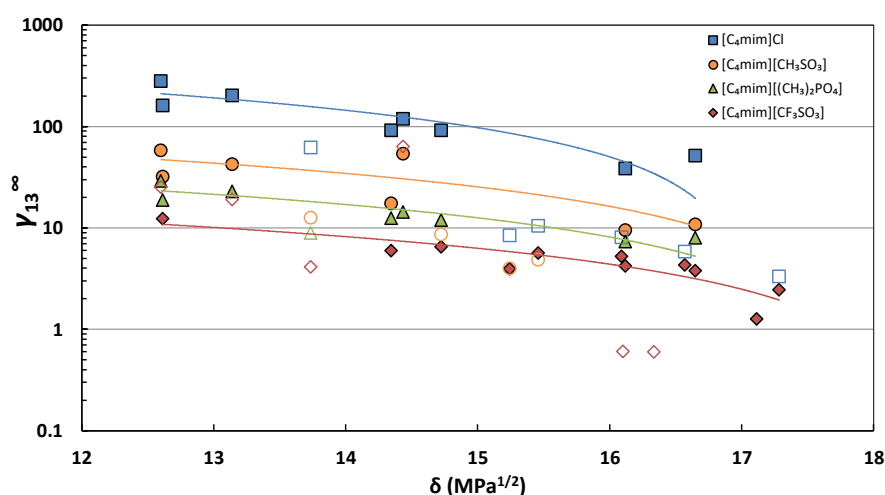


**Figure 3.8.** Activity coefficients at infinite dilution as a function of the solubility parameters (calculated through reference <sup>248</sup>) of terpenes and terpenoids in the ILs studied, at 408.15 K. Empty symbols were not used in the fit.

### Thermodynamic functions at infinite dilution

To obtain additional information concerning the interactions between the solutes and the ionic liquids, the partial excess molar properties at infinite dilution were analyzed. The Gibbs energy, enthalpy, and entropy, for terpenes and terpenoids in the investigated ILs at  $T = 408.15$  K, were calculated through the  $\gamma_{13}^{\infty}$  values and are listed in Table S3.6 of Appendix 3. As mentioned before, there are some solutes in some ILs that present a small variation with the temperature and hence, in those cases, the partial molar excess enthalpy at infinite dilution is close to zero.

The partial molar excess properties as a function of  $\gamma_{13}^{\infty}$  are presented in Figure 3.9. As can be seen, two different areas can be distinguished for ILs composed by the more polar anions ( $\text{Cl}^-$ ,  $[\text{CH}_3\text{SO}_3]^-$ ,  $[(\text{CH}_3)_2\text{PO}_4]^-$ ), and three areas for the IL  $[\text{C}_4\text{mim}][\text{CF}_3\text{SO}_3]$ . Region (I) and (II), common to all ILs studied, represents the ILs–organic solutes systems with positive deviations to Raoult’s law,  $\gamma_{13}^{\infty} (\overline{G}_m^{E,\infty}) > 1$ . When  $\overline{H}_m^{E,\infty}$  is also positive, region (I), no particular affinity between ILs and solutes molecules is expected, as for hydrocarbons, ketones and ethers. Due to the weak interaction, these mixtures have potential to the formation of two immiscible phases. In region (II) both enthalpy and entropy are negative, clearly indicating the dominance of the entropic over the enthalpic effect. Indeed, in both regions, the partial excess enthalpy is close to zero, and the entropic effect is always dominant.

$[\text{C}_4\text{mim}][\text{CF}_3\text{SO}_3]$  presents also region IV, with negative deviations from Raoult’s law ( $\gamma_{13}^{\infty} < 1$ ). This region is characterized by favorable interactions between the solutes and the ILs, related with spontaneous dissolution, and consequently the enthalpic effect is dominant. The only solutes belonging to that region are carvacrol and thymol, both presenting strong polarity, where all the partial excess molar properties investigated are negative, showing that the HB between carvacrol and thymol, and the anion  $[\text{CF}_3\text{SO}_3]^-$  is favorable. The terpenoid linalool, highlighted before due to the absence of an H-bond donor region character, shows an extremely low value of the excess molar enthalpy at infinite dilution,



when compared with all the other solutes. The interaction of this compound with the ILs is highly influenced by the temperature.

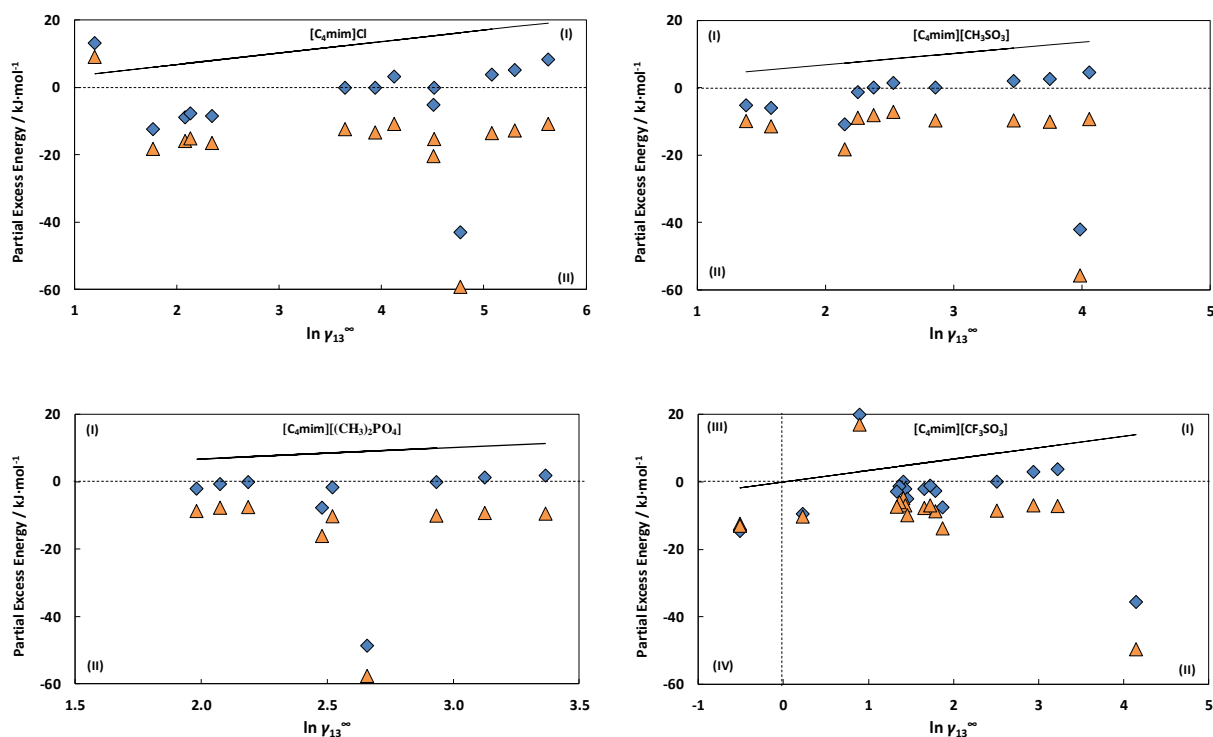


**Figure 3.9.** Partial molar excess energies at infinite dilution as a function of the natural logarithm of the activity coefficients at infinite dilution of the terpenes and terpenoids in the ILs study, at 408.15 K. The full line represents  $\overline{G}_m^{E,\infty}$  and the symbols correspond to:  $\diamond$ ,  $\overline{H}_m^{E,\infty}$  and  $\Delta$ ,  $T_{ref}\overline{S}_m^{E,\infty}$ .

### Gas-liquid partition coefficients

Gas-liquid partition coefficients,  $K_L$ , were calculated from retention times using the densities of the pure ILs previously reported.<sup>247,249,250</sup> Assuming an ideal gas phase, the gas-liquid partition coefficients can be used to understand the terpenes and terpenoids extraction using ILs, and their subsequently evaporation in order to recover the ILs, at low pressures. Moreover, these parameters are also useful to understand the role of ILs on the fractionation of a complex mixture of terpenes and terpenoids. Results at a fixed temperature are presented in Figure 3.10. In general, the highest values are observed for more polar solutes like alcohols, with the less polar IL, [C<sub>4</sub>mim][CF<sub>3</sub>SO<sub>3</sub>]. As expected,  $\alpha$ -

and  $\beta$ -pinene present the lowest values of the gas liquid partition coefficients, especially with the IL  $[\text{C}_4\text{mim}]\text{Cl}$ . These coefficients indicate the possibility to separate terpenes from the terpenoid alcohol or ketone fractions. The  $K_L$  always decreases with increasing temperature as can be seen in Table S3.7 of Appendix 3.

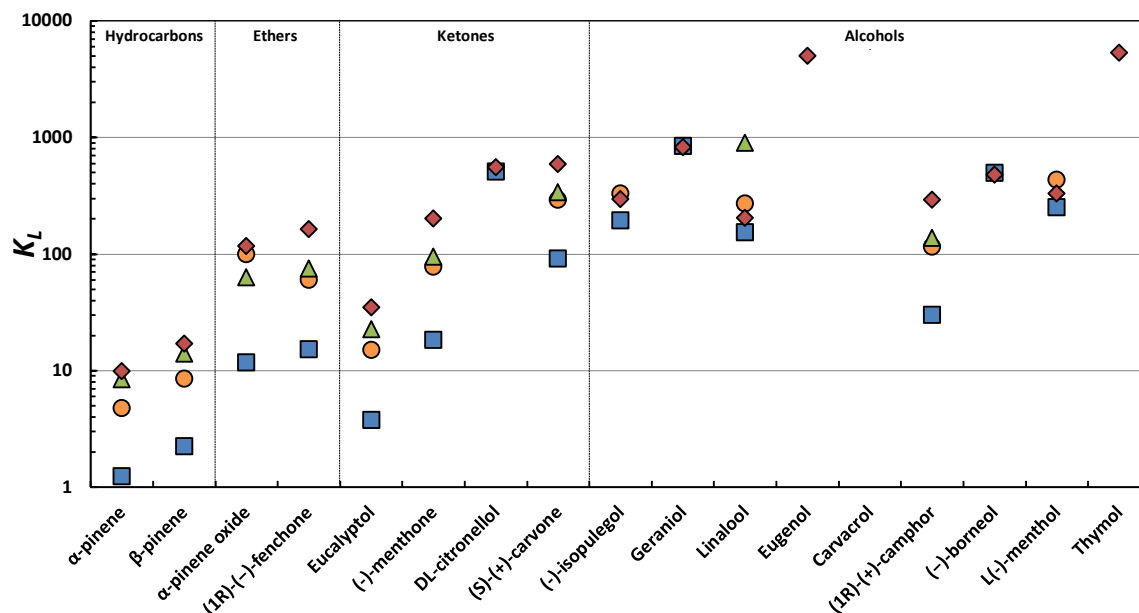
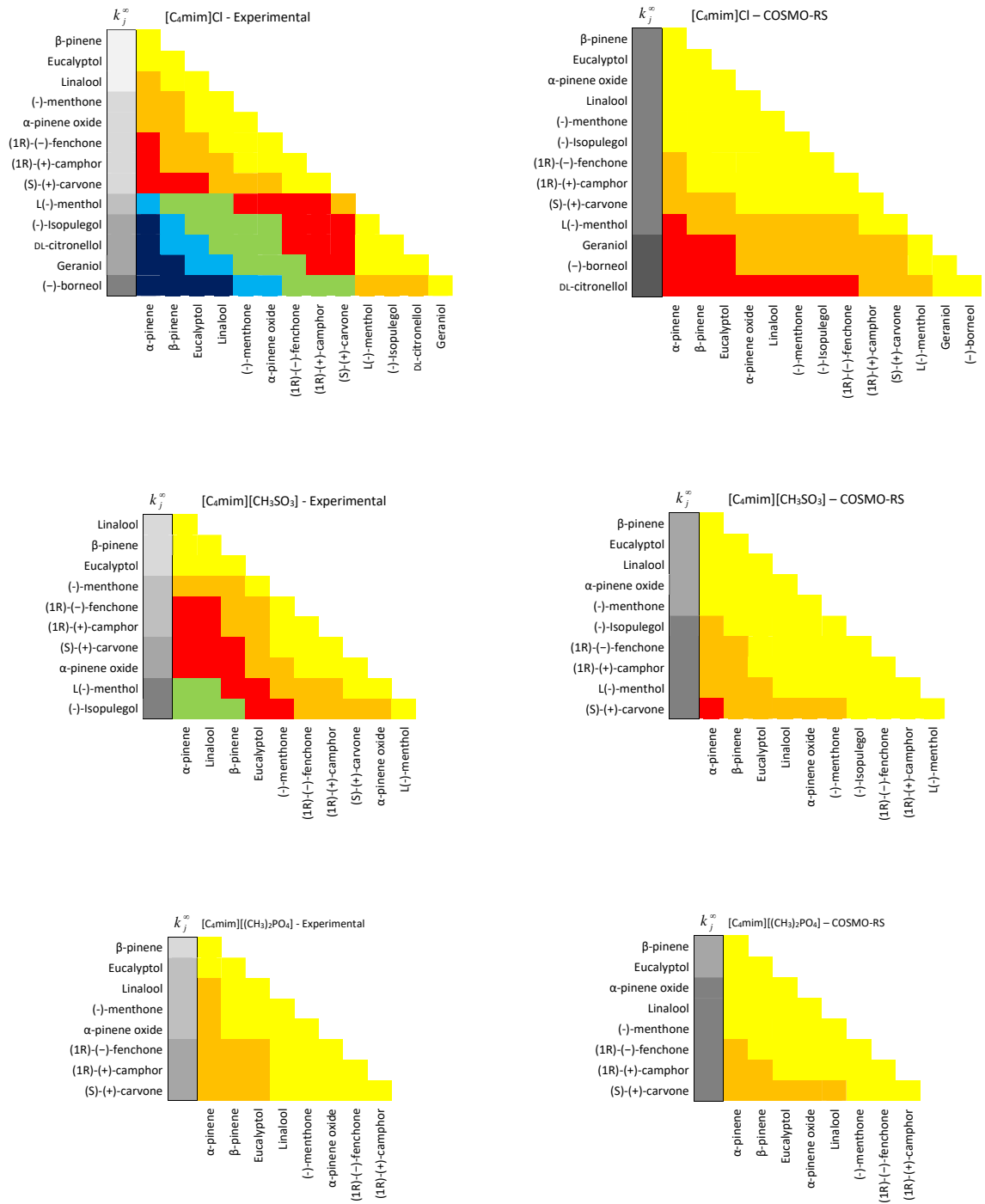


**Figure 3.10.** Experimental gas–liquid partition coefficients,  $K_L$ , for terpenes and terpenoids in the ILs studied, at 408.15 K. □,  $[\text{C}_4\text{mim}]\text{Cl}$ ; ○,  $[\text{C}_4\text{mim}][\text{CH}_3\text{SO}_3]$ ; △,  $[\text{C}_4\text{mim}][(\text{CH}_3)_2\text{PO}_4]$ ; ◇,  $[\text{C}_4\text{mim}][\text{CF}_3\text{SO}_3]$ .

### Selectivities and capacities

Selectivities,  $S_{ij}^\infty$ , and capacities,  $k_j^\infty$ , can be used to evaluate the ILs performance as solvents for separation processes.<sup>230,241,242</sup> Considering the similarities in molecular structures and physical properties of terpenes and terpenoids, and therefore, the problems involved in their extraction from essential oils and subsequent fractionation, these two parameters must be known. According to the definition, a suitable solvent should present both a high selectivity and capacity for the components to be separated.<sup>251</sup> Experimental results along with the selectivities and capacities predicted using COSMO-RS are schematically presented in Figure 3.11.

### Chapter 3 – Extraction, Production and Deterpenation



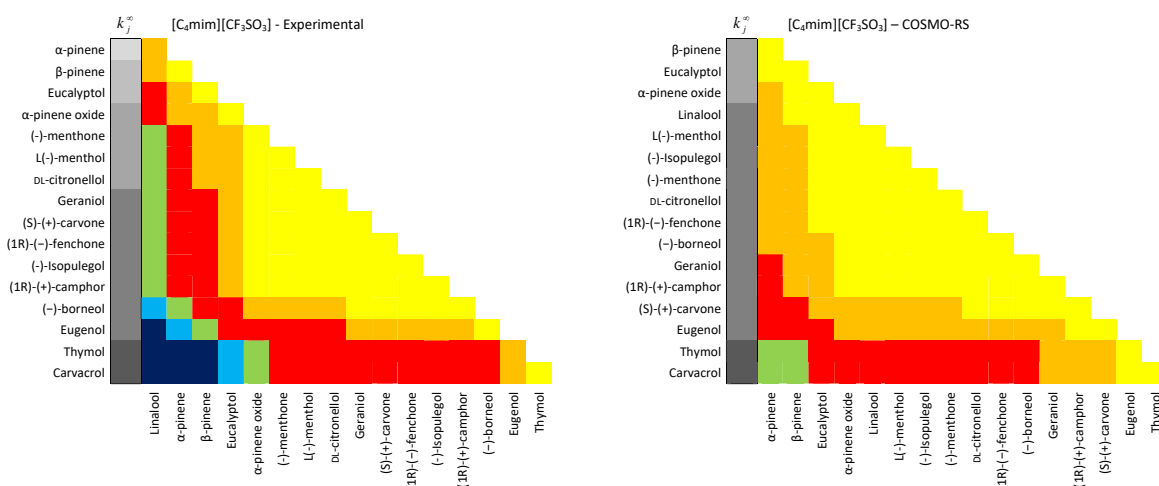


**Figure 3.11.** Experimental and COSMO-RS predictions of  $S_{ij}^{\infty}$  and  $k_j^{\infty}$  of all solutes at 408.15 K in the different ionic liquids studied. Color code:  $\color{yellow}\blacktriangle$  [1-2];  $\color{orange}\blacktriangle$  [2-4];  $\color{red}\blacktriangle$  [4-10];  $\color{green}\blacktriangle$  [10-20];  $\color{blue}\blacktriangle$  [20-30]; and  $\color{darkblue}\blacktriangle$  >30. Capacities,  $\color{lightgrey}\blacktriangle$  <0.01;  $\color{mediumgrey}\blacktriangle$  [0.01-0.05];  $\color{darkgrey}\blacktriangle$  [0.05-0.1];  $\color{black}\blacktriangle$  [0.1-0.2];  $\color{darkblue}\blacktriangle$  [0.2-1];  $\color{lightblue}\blacktriangle$  [1-2];  $\color{darkblue}\blacktriangle$  [2-5]; and  $\color{black}\blacktriangle$  > 5.

The experimental capacity takes the highest values for the pairs containing thymol or carvacrol, when the anion of the IL is  $[\text{CF}_3\text{SO}_3]^-$  (1.661 and 1.671, respectively), and the lowest values for the pairs containing  $\beta$ -pinene or eucalyptol in  $[\text{C}_4\text{mim}]\text{Cl}$  (0.005 and 0.006, respectively). From the experimental selectivities it is possible to identify the most complicated separation problems: (-)-menthone/ $\alpha$ -pinene oxide and thymol/carvacrol, with a  $S_{ij}^{\infty}$  value close to 1 in the ILs  $[\text{C}_4\text{mim}]\text{Cl}$  and  $[\text{C}_4\text{mim}][\text{CF}_3\text{SO}_3]$ , respectively. Inversely, the pairs linalool/thymol and linalool/carvacrol present high selectivity and capacity values with the IL  $[\text{C}_4\text{mim}][\text{CF}_3\text{SO}_3]$ , showing that this ionic liquid may be used in their separation. In general, experimental capacities are considerably lower than 1 and most of the selectivities fall in the range [1-2] and [2-4]. Selectivities ranges were chosen based on the numerical results obtained. Among the studied ILs,  $[\text{C}_4\text{mim}][\text{CF}_3\text{SO}_3]$  is the one that seems to present high selectivities and capacities, indicating that ILs with low polarity should be used in the terpenes and terpenoids separation. However, the major limitation that the ionic liquids studied in this work present are the low capacities that would prevent their application into a separation process.

To improve the separation efficiency, new ILs must be evaluated. For that purpose, an ILs screening, computed using COSMO-RS, was attempted. To validate COSMO-RS predictions, the ILs studied in this work were used. Figure 3.11 shows that the selectivities obtained with COSMO-RS are generally lower than the experimental ones, which may be attributed to an over estimation of the hydrogen bonding interactions between ILs and solutes. Accordingly, COSMO-RS capacities are in general superior to the experimental ones. In spite of the quantitative deviations obtained with COSMO-RS from experimental data, in general the model is able to correctly estimate the order of the selectivities and capacities for the terpenes and terpenoids studied. A better agreement with the experimental data is obtained for the less polar ILs, such as [C<sub>4</sub>mim][(CH<sub>3</sub>)<sub>2</sub>PO<sub>4</sub>] and [C<sub>4</sub>mim][CF<sub>3</sub>SO<sub>3</sub>].

According with the experimental results obtained in this work, better selectivities and capacities are achieved with the less-polar ILs. As the COSMO-RS predictions seem to be more precise also for these compounds, a set of selectivities and capacities of terpenes and terpenoids with selected ILs was computed using COSMO-RS: cations, 1-butyl-3-methyl-imidazolium, [C<sub>4</sub>mim]<sup>+</sup>; and trihexyltetradecylphosphonium, [P<sub>66614</sub>]<sup>+</sup>; were combined with the anions tetracyanoborate, [BCN<sub>4</sub>]<sup>-</sup>; bis(trifluoromethylsulfonyl)imide, [NTf<sub>2</sub>]<sup>-</sup>; bis(2,4,4-trimethylpentyl)phosphinate, [(C<sub>8</sub>H<sub>17</sub>)<sub>2</sub>PO<sub>2</sub>]<sup>-</sup>; tosylate, [TOS]<sup>-</sup>; methylsulfate, [CH<sub>3</sub>SO<sub>4</sub>]<sup>-</sup>; trifluoroacetate, [TFA]<sup>-</sup>; and acetate, [OAc]<sup>-</sup>. The ionic liquids were chosen based on the polarity of the cations and anions to cover a wide range of differentiated polarities between the ion pair. The most relevant cases unveiled by this search are presented in Figure 3.12, while the other compounds studied are presented in Figure S3.4 of Appendix 3. COSMO-RS predictions show that the higher selectivities are obtained using polar anions such as bis(2,4,4-trimethylpentyl)phosphinate or acetate; while to obtain high capacities nonpolar cations such as phosphonium based must be preferred. This indicates that terpenes and terpenoids extraction must be made using cations and anions presenting distinct characteristics to fulfill simultaneously the requirements of high selectivities and capacities. The experimental validation of these predictions and the use of these ionic liquids for terpene and terpenoids separation are currently under development in our laboratory.

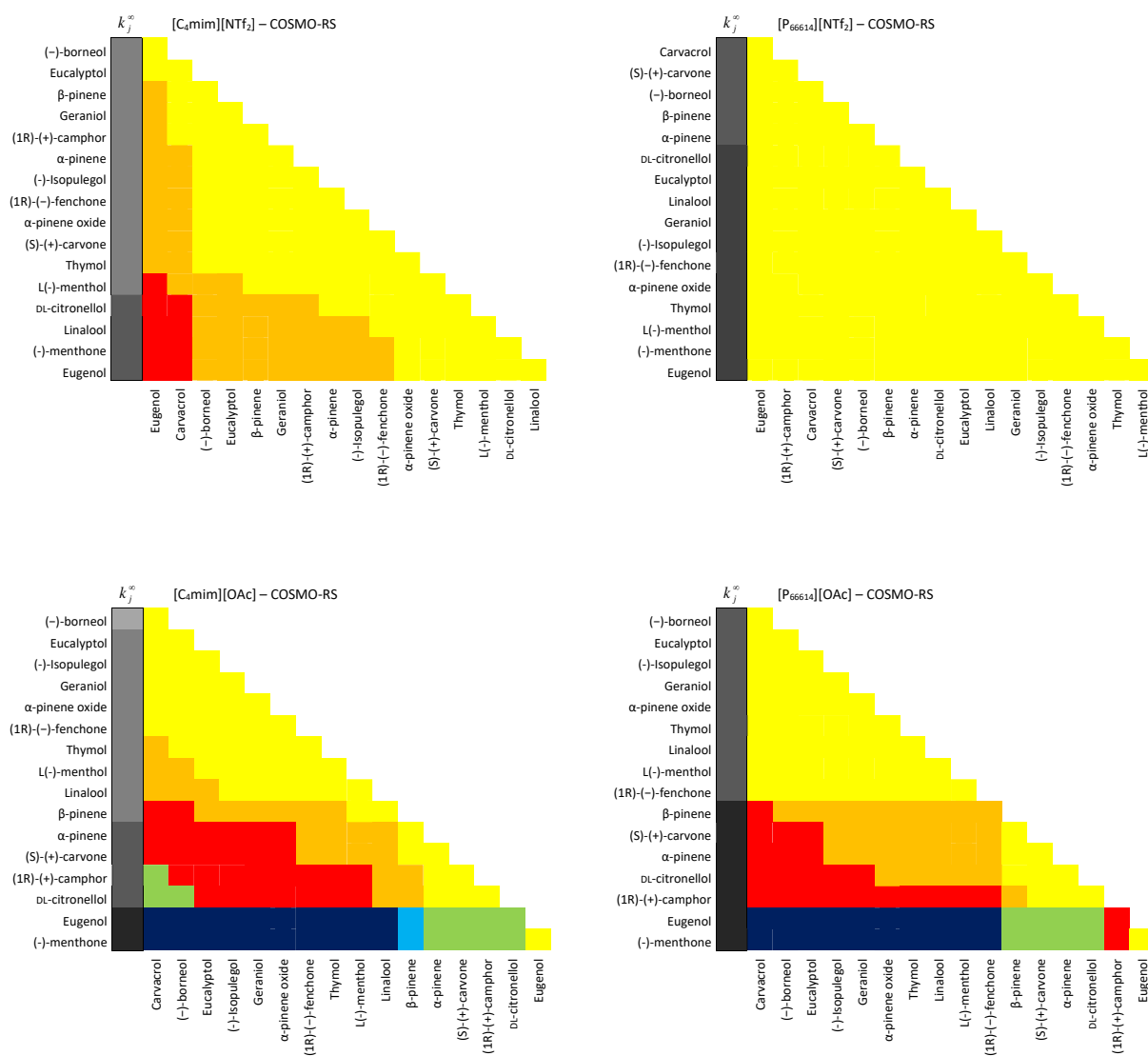


**Figure 3.12.**  $S_{ij}^{\infty}$  and  $k_j^{\infty}$  of all solutes at 408.15 K in selected ILs, computed by COSMO-RS. Color code: Selectivities,  $\color{yellow}\blacklozenge$  [1-2];  $\color{orange}\blacklozenge$  [2-4];  $\color{red}\blacklozenge$  [4-10];  $\color{green}\blacklozenge$  [10-20];  $\color{blue}\blacklozenge$  [20-30]; and  $\color{darkblue}\blacklozenge$  >30; Capacities,  $\color{lightgrey}\blacklozenge$  <0.01;  $\color{grey}\blacklozenge$  [0.01-0.05];  $\color{darkgrey}\blacklozenge$  [0.05-0.1];  $\color{black}\blacklozenge$  [0.1-0.2];  $\color{black}\blacklozenge$  [0.2-1];  $\color{black}\blacklozenge$  [1-2];  $\color{black}\blacklozenge$  [2-5]; and  $\color{black}\blacklozenge$  > 5.

Among the compounds studied, a literature survey showed that an important separation problem is  $\alpha$ -pinene/ $\beta$ -pinene, a mixture extracted from turpentine,<sup>10,30</sup> usually by steam-distillation.<sup>252,253</sup> The experimental results obtained for  $S_{ij}^{\infty}$  and  $k_j^{\infty}$  are presented in Table 3.8, along with selected COSMO-RS results and values from literature for some other important solvents.

According to Table 3.8, it is possible to see that the experimental ILs studied present similar selectivities to the solvents studied by Díaz et al.<sup>254</sup> However, the capacities are much lower. As discussed before, to increase the capacity, ionic liquids with low polarity must be used. [C<sub>4</sub>mim][CF<sub>3</sub>SO<sub>3</sub>] is the most promising solvent with respect to separation amongst the ILs experimentally evaluated in this work. Based on the COSMO-RS result for that IL, this agrees with the experimental information. Moreover, according to COSMO-RS the ILs [P<sub>66614</sub>][(C<sub>8</sub>H<sub>17</sub>)<sub>2</sub>PO<sub>2</sub>] and [P<sub>66614</sub>][OAc] show good potential to be applied as agent for the  $\alpha$ -pinene/ $\beta$ -pinene separation

**Table 3.8.** Selectivities ( $S_{ij}^{\infty}$ ) / capacities ( $k_j^{\infty}$ ) at infinite dilution for  $\alpha$ -pinene /  $\beta$ -pinene at 408.15 K in different solvents.

Solvent	Selectivities ( $S_{ij}^{\infty}$ ) / capacities ( $k_j^{\infty}$ )	Reference
[C <sub>4</sub> mim]Cl	1.386 / 0.005	
[C <sub>4</sub> mim][CH <sub>3</sub> SO <sub>3</sub> ]	1.364 / 0.024	
[C <sub>4</sub> mim][(CH <sub>3</sub> ) <sub>2</sub> PO <sub>4</sub> ]	1.271 / 0.044	
[C <sub>4</sub> mim][CF <sub>3</sub> SO <sub>3</sub> ]	1.327 / 0.053	
[C <sub>4</sub> mim][CF <sub>3</sub> SO <sub>3</sub> ] – COSMO-RS	1.313 / 0.105	This work
[C <sub>4</sub> mim][(C <sub>8</sub> H <sub>17</sub> ) <sub>2</sub> PO <sub>2</sub> ] – COSMO-RS	1.315 / 2.467	
[P <sub>66614</sub> ][(C <sub>8</sub> H <sub>17</sub> ) <sub>2</sub> PO <sub>2</sub> ] – COSMO-RS	1.205 / 6.237	
[C <sub>4</sub> mim][OAc] – COSMO-RS	1.590 / 1.137	
[P <sub>66614</sub> ][OAc] – COSMO-RS	1.260 / 5.940	
Dinonyl phthalate	1.260 / 1.156 <sup>a</sup>	
Amine 220	1.304 / 0.849 <sup>a</sup>	
Tricresyl phosphate	1.113 / 0.643 <sup>a</sup>	254
Carbowax 6000	1.346 / 6.601 <sup>a</sup>	
Ethylene glycol phthalate	1.375 / 0.292 <sup>a</sup>	
Carbowax 1500	1.424 / 1.300 <sup>a</sup>	

<sup>a</sup>Extrapolated value.

### 3.1.6. Conclusions

New data of activity coefficients at infinite dilution of ILs composed by the cation 1-butyl-3-methylimidazolium and the anions chloride, methanesulfonate, dimethylphosphate and trifluoromethanesulfonate were measured by gas–liquid chromatography techniques for organic solutes, water, and terpenes at different temperatures. When possible comparisons with literature were carried out, showing consistent trends among the different ILs analyzed. The infinite dilution thermodynamic function and the gas-liquid

partition coefficients were calculated and analyzed. It was concluded that the hydrogen bonding between organic solutes and the ILs anion plays a significant role on the interaction of the ILs with organic solutes, and determines the enthalpic behavior of the binary mixtures. On the other hand, in the vast majority of the binary mixtures of terpenes and ILs the entropic effect was dominant over the enthalpic one.

The ability of the ILs to act as entrainers in important separations problems such as octane/benzene, cyclohexane/benzene and cyclohexane/thiophene was evaluated. In spite of the lower capacities obtained, the selectivities achieved were quite high and, thus, these ILs could be used as an alternative separating agent for the separation processes of aliphatic/aromatic hydrocarbons.

COSMO-RS was evaluated for the description of the selectivities and capacities for the systems involving terpenes studied, and showed to be a useful tool for the screening of ionic liquids to find suitable candidates for terpenes and terpenoids extraction and separation before extensive experimental measurements. COSMO-RS predictions on capacities and selectivities show that in order to achieve the maximum separation efficiency polar anions such as bis(2,4,4-trimethylpentyl)phosphinate or acetate should be used and combined with nonpolar cations such as phosphonium that would maximize the capacities of the solvents. For the specific  $\alpha$ -pinene/ $\beta$ -pinene separation, the ionic liquids studied in this work present satisfactory selectivity values, but very low capacities, and a set of ILs were identified to have good potential for this difficult separation problem.

### **3.2. Measurement and PC-SAFT modeling of solid-liquid equilibrium of deep eutectic solvents of quaternary ammonium chlorides and carboxylic acids**

Paula V. A. Pontes, Emanuel A. Crespo, Mônia A. R. Martins, Liliana P. Silva, Catarina M. S. S. Neves, Guilherme J. Máximo, Miriam Dupas Hubinger, Eduardo A. C. Batista, Simão P. Pinho, João A. P. Coutinho, & Christoph Held, *Fluid Phase Equilibria*, in press (2017), DOI: 10.1016/j.fluid.2017.04.007.



### 3.2.1. Abstract

In this study the solid-liquid equilibria (SLE) of 15 binary mixtures composed of one of three different symmetrical quaternary ammonium chlorides and one of five different fatty acids were measured. The experimental data obtained showed extreme negative deviations to ideality causing large melting-temperature depressions (up to 300K) that are characteristic for deep eutectic systems. The experimental data revealed the strengthening of the HBA-HBD complex with increase of the alkyl chain length of the quaternary ammonium chloride and with increase of the chain length of the carboxylic acid. The pronounced decrease of melting temperatures in these deep eutectic systems is mainly caused by strong hydrogen-bonding interactions, and thermodynamic modeling required an approach that takes hydrogen bonding into account. Thus, the measured phase diagrams were modelled with perturbed-chain statistical associating theory based on the classical molecular homonuclear approach. The model showed very good agreement with the experimental data using a semi-predictive modeling approach, in which binary interaction parameters between quaternary ammonium chloride and carboxylic acid correlated with chain length of the components. This supports the findings into the phase behavior and interactions present in these systems and allows estimating eutectic points of such highly non-ideal mixtures.

### 3.2.2. Introduction

Aiming at sustainable process design and considering the growing focus on green chemistry, there has been an effort towards the development of novel and environmentally friendly solvents with equivalent or better performance than classical organic solvents, such as the neoteric deep eutectic solvents (DES).

While much work has been reported using these novel solvents, the number of DES which are liquid at room temperature is still very limited. Moreover, data on their solid-liquid equilibria (SLE) is surprisingly scarce despite the important information it provides on the operation window (range of compositions and temperatures) as well as on donor-acceptor interactions in these systems. Likewise, modeling the SLE by suitable equations of state (EoS) and/or activity coefficient models is a poorly explored research field due to

both, lack of enough comprehensive and reliable experimental data and the strong and highly complex interactions between the DES constituents that are not easily captured by most models.

In the past few years, Statistical Associating Fluid Theory (SAFT), a molecular-based model that accounts for the repulsive and attractive interactions of fluids,<sup>255,256</sup> has been used to successfully describe a wide variety of systems.<sup>257,258</sup> Additionally, Perturbed-Chain SAFT (PC-SAFT),<sup>259</sup> the most prominent modification of original SAFT, was already successfully applied to systems containing DES. Verevkin et al.<sup>260</sup> used PC-SAFT to model infinite dilution activity coefficients of 23 different solutes in [Ch]Cl:glycerol and Zubeir et al.<sup>261</sup> used PC-SAFT to model the CO<sub>2</sub> solubility in quaternary ammonium salts + lactic acid mixtures.

The renewability of a DES depends mainly on its starting materials being most of the DES described in literature prepared using abundant natural compounds. The most common precursors are quaternary ammonium salts, particularly choline chloride, due to its non-toxicity, biodegradability and economic synthesis, combined with polyols, urea, carboxylic acids, sugars or other safe hydrogen bond donors. Monocarboxylic acids with long aliphatic chains, known as fatty acids, are the major co-products of the vegetable oils refining. Their use in DES would have a positive impact on the processes sustainability since, besides their vast natural sources, they allow purification of the extracts when used as solvents for extraction operations.<sup>262</sup>

In this context, the purpose of this work is to measure the solid-liquid phase diagrams of fifteen new DES composed of one quaternary ammonium salt [tetramethylammonium chloride ([N<sub>1111</sub>]Cl), tetraethylammonium chloride ([N<sub>2222</sub>]Cl) and tetrapropylammonium chloride ([N<sub>3333</sub>]Cl)] and of one fatty acid (capric acid, lauric acid, myristic acid, palmitic acid or stearic acid) that are commonly found in vegetable oils. PC-SAFT is here applied for the first time to describe the DES solid-liquid phase diagrams by fitting energy related binary interaction parameters to the measured experimental data allowing to obtain information about the non-ideality of the compounds in the liquid phase and new insights regarding the hydrogen-bonding interactions between the DES constituents.

### 3.2.3. Experimental

#### 3.2.3.1. Materials

The quaternary ammonium salts (hydrogen-bond acceptor, HBA) and the fatty acids (hydrogen-bond donor, HBD) used to prepare the DES are described in Table 3.9. The quaternary ammonium salts were dried under vacuum at room temperature during at least three days while fatty acids were used as received from the supplier. Indium, used for the DSC calibration, was supplied by PerkinElmer with a purity higher than 0.999 (molar fraction).

**Table 3.9.** Sources and purities of the compounds used in this work.

Component	Molecular Formula	CAS number	Supplier	Purity (mass %) <sup>a</sup>
HBA (Quaternary Ammonium Salts)				
[N <sub>1111</sub> ]Cl	C <sub>4</sub> H <sub>12</sub> ClN	75-57-0	Sigma-Aldrich	97.0
[N <sub>2222</sub> ]Cl	C <sub>8</sub> H <sub>20</sub> ClN	56-34-8	Sigma-Aldrich	98.0
[N <sub>3333</sub> ]Cl	C <sub>12</sub> H <sub>28</sub> ClN	5810-42-4	Sigma-Aldrich	98.0
HBD (Fatty Acids)				
Capric acid	C <sub>10</sub> H <sub>20</sub> O <sub>2</sub>	334-48-5	Sigma	≥ 99.0
Lauric acid	C <sub>12</sub> H <sub>24</sub> O <sub>2</sub>	143-07-7	Sigma	≥ 99.0
Myristic acid	C <sub>14</sub> H <sub>28</sub> O <sub>2</sub>	544-63-8	Sigma	≈ 95.0
Palmitic acid	C <sub>16</sub> H <sub>32</sub> O <sub>2</sub>	57-10-3	Aldrich	≥ 98.0
Stearic acid	C <sub>18</sub> H <sub>36</sub> O <sub>2</sub>	57-11-4	Merck	≥ 97.0

<sup>a</sup>According to the supplier

#### 3.2.3.2. Methods

##### Solid-liquid equilibria

Mixtures of the HBA-HBD were prepared in the whole composition range, allowing the measurement of the solid-liquid phase diagrams. Three different experimental methodologies were used: the visual method, the melting points measurement method, and differential scanning calorimetry. These are explained in the following.

For the visual method binary mixtures were weighted at room temperature using an analytical balance model ALS 220-4N from Kern with an accuracy of  $\pm 0.002$  g, inside a dry-argon glove-box. Vials with the mixtures were heated in an oil bath under stirring using a heating plate until complete melting prior to recrystallization. After the first cycle the melting temperatures corresponding to the last crystal disappearance were recorded. The temperature was measured with a Pt100 probe with a precision of  $\pm 0.1$  K. This procedure was repeated at least two times.

For measurements of the melting points samples were prepared as described in the visual method procedure. After recrystallization solid mixtures were ground in the glove-box and the powder was filled into a capillary. Melting temperatures were then determined with an automatic glass capillary device model M-565 from Büchi (100-240 V, 50-60 Hz, 150 W, temperature resolution: 0.1 K). A temperature gradient of  $0.5 \text{ K}\cdot\text{min}^{-1}$  was used and the melting points measurements were repeated at least two times.

Differential Scanning Calorimetry (DSC) was applied in specific cases indicated in Tables S3.8, S3.9, and S3.10. Mixtures were prepared into a glass vessel on an analytic balance XP205 (Mettler Toledo, precision =  $2 \times 10^{-4}$  g) in a glove box under inert nitrogen atmosphere (purity  $\geq 0.99996$  mass fraction). The mixtures were melted under stirring on a heating plate until a homogeneous liquid mixture was obtained, and the mixture then cooled at room temperature. Samples (2 - 5 mg) were hermetically sealed in aluminum pans inside the glovebox and then weighed in a micro analytical balance AD6 (PerkinElmer, USA, precision =  $2 \times 10^{-6}$  g). A DSC 2920 calorimeter (TA Instruments) working at atmospheric pressure and coupled to a cooling system was used for the sample analysis. The method was based on a cooling run at  $5 \text{ K}\cdot\text{min}^{-1}$  until 208.15 K followed by a heating run with a rate of  $1 \text{ K}\cdot\text{min}^{-1}$  until 10 K above melting. Nitrogen (purity  $\geq 0.99999$  mass fraction) was used as purge gas. The melting temperatures of the samples were assumed to be the maximum temperatures of the melting peak, taking into account the appearance of broad thermo events in the melting of the eutectic mixtures (see Figure S3.5). Data were analyzed through the TA Universal Analysis software (TA Instruments). For pure compounds, the uncertainty of the equilibrium data was

calculated by the average of the standard deviations of triplicates. The equipment was previously calibrated with indium.

### **Water activities**

Water activities ( $a_w$ ) measurements were carried out using a Novasina hygrometer LabMaster-  $a_w$  (Lucerne, Switzerland) with an accuracy of  $0.001a_w$  and  $\pm 0.20$  K in the controlled temperature chamber. The instrument principle is based on resistive-electrolytic method. The equipment was initially calibrated with six saturated pure salt standard solutions (water activity ranging from 0.113 to 0.973), provided by the supplier. Moreover, in order to achieve the given accuracy, a calibration curve was built using at least six aqueous solutions of LiCl or NaBr at different salt molalities and results were compared to those recommended in literature.<sup>263,264</sup> Quaternary ammonium solutions were prepared at room temperature by mixing salts and water at the desired composition. The water content is presented in Table S3.11. Samples of approximately 2–3 cm<sup>3</sup> were then filled into proper cells and placed in the air-tight equilibrium chamber. When a constant value was reached, the water activity was recorded. Usually, solutions reached equilibrium in less than 1 h.

### **Density of mixtures**

The density measurements were performed at atmospheric pressure and in the temperature range from 298.15 to 358.15 K using an automated SVM 3000 Anton Paar rotational Stabinger viscometer–densimeter (temperature uncertainty:  $\pm 0.02$  K; absolute density uncertainty:  $\pm 5 \times 10^{-4}$  g·cm<sup>-3</sup>). The solutions prepared for the water activity measurements were used here. The salt content of the samples and the resulting mixture densities are presented in Tables S3.12-S3.14.

#### **3.2.4. Theoretical approach**

##### **PC-SAFT EoS**

SAFT is a thermodynamic approach derived from Wertheim's first-order thermodynamic perturbation theory,<sup>265–268</sup> proposed by Chapman and co-workers.<sup>255,256</sup> Since the original

SAFT version, several modifications have been proposed. In particular, PC-SAFT proposed by Gross and Sadowski in 2001<sup>259</sup> that uses a system of freely jointed hard spheres as reference (designated as hard-chain system), which may be perturbed by dispersive and association interactions. The PC-SAFT model attracted much attention from researchers since it was already successfully applied to a wide variety of systems. Compared to the original SAFT model, PC-SAFT modeling results demonstrate good improvements of long-chain molecules, like polymers or ILs, and even of substances of low molecular weight.<sup>259,269</sup>

In general, SAFT-type equations are written in terms of residual molar Helmholtz energy,  $a^{res}$ , defined as the difference between the total molar Helmholtz energy and that of an ideal gas at the same temperature and molar density:

$$\frac{a^{res}}{RT} = \frac{a}{RT} - \frac{a^{id}}{RT} \quad (3.11)$$

The residual Helmholtz energy is, in PC-SAFT, defined as the sum of different contributions from different molecular forces:

$$\frac{a^{res}}{RT} = \frac{a^{hc}}{RT} + \frac{a^{disp}}{RT} + \frac{a^{assoc}}{RT} \quad (3.12)$$

In Equation 3.12, the superscripts refer to the terms accounting for the residual, hard-chain fluid, dispersive and associative interactions, respectively. An EoS written in terms of the Helmholtz energy has the advantage that the calculation of all the thermodynamic properties is possible by using only derivatives and ideal-gas integrals.

In PC-SAFT model, a non-associating component  $i$  is characterized by three-pure component parameters, namely the segment number,  $m_i^{seg}$ , the segment diameter,  $\sigma_i$ , and the van der Waals dispersion energy parameter between two segments,  $u_i$ . For associating components, two additional parameters are required, namely the association-energy parameter,  $\epsilon^{AiBi}$ , and the association-volume parameter,  $\kappa^{AiBi}$ . Additionally, a

proper association scheme specifying number/type and allowed interactions must be assigned to each associating component.

When describing mixtures, the conventional Lorenz-Berthelot combining rules were used to determine the mixture parameters where one adjustable binary interaction parameter,  $k_{ij}$ , for correction of the cross-dispersion energy can be used whenever required.

$$\sigma_{ij} = \frac{1}{2}(\sigma_i + \sigma_j) \quad (3.13)$$

$$u_{ij} = (1 - k_{ij})\sqrt{u_i u_j} \quad (3.14)$$

Simple combining rules for the cross-association interactions between the two components, proposed by Wolbach and Sandler,<sup>270</sup> were further applied when dealing with mixtures.

$$\varepsilon^{AiBj} = \frac{1}{2}(\varepsilon^{AiBi} + \varepsilon^{AjBj})(1 - k_{ij\_eps}) \quad (3.15)$$

$$K^{AiBj} = \sqrt{K^{AiBi} \cdot K^{AjBj}} \left( \frac{\sqrt{\sigma_{ii} \cdot \sigma_{jj}}}{\frac{1}{2}(\sigma_{ii} + \sigma_{jj})} \right)^3 \quad (3.16)$$

A binary interaction parameter,  $k_{ij\_eps}$ , for correction of the cross-association energy can be also applied, when required, to account for the deviations from the value calculated through the original mixing rule. It is important to highlight that either in the dispersive or association interactions only energy-related binary parameters were applied in this work since the use of size-related binary parameters is unusual and not recommended.<sup>271</sup>

### PC-SAFT pure-component parameter estimation

Ji et al.,<sup>272</sup> Nann et al.<sup>273</sup> and Passos et al.<sup>274</sup> reported the use of PC-SAFT to model IL solutions while Zubeir et al.<sup>261</sup> used this EoS to model the CO<sub>2</sub> solubilities in DES with [Ch]Cl, and different symmetrical quaternary ammonium chlorides serving as HBA. The various authors treated ILs as molecules with associative behavior by using a 2B

association scheme (according to Huang and Radosz<sup>275</sup>), where to each molecule two association sites (mimicking the cation and the anion) are assigned and association interactions between unlike sites are allowed.

The molecular parameters for [N<sub>1111</sub>]Cl and [N<sub>2222</sub>]Cl were directly taken from reference<sup>261</sup> and the same approach was here followed to obtain the [N<sub>3333</sub>]Cl parameters. Thus, the association scheme (2B) and the corresponding association parameters from [N<sub>1111</sub>]Cl and [N<sub>2222</sub>]Cl were applied to [N<sub>3333</sub>]Cl. The remaining parameters  $m_i^{seg}$ ,  $\sigma_i$ , and  $u_i$  as well as one temperature-independent binary interaction parameter  $k_{ij}$  between water and [N<sub>3333</sub>]Cl were fitted to experimental water activity coefficients (at 298.15 K, Table S3.11) and mixtures densities of water + [N<sub>3333</sub>]Cl solutions (Table S3.14). The result of the parameter estimation is depicted in Figure 3.13, and the PC-SAFT parameters for the quaternary ammonium chlorides are summarized in Table 3.10.

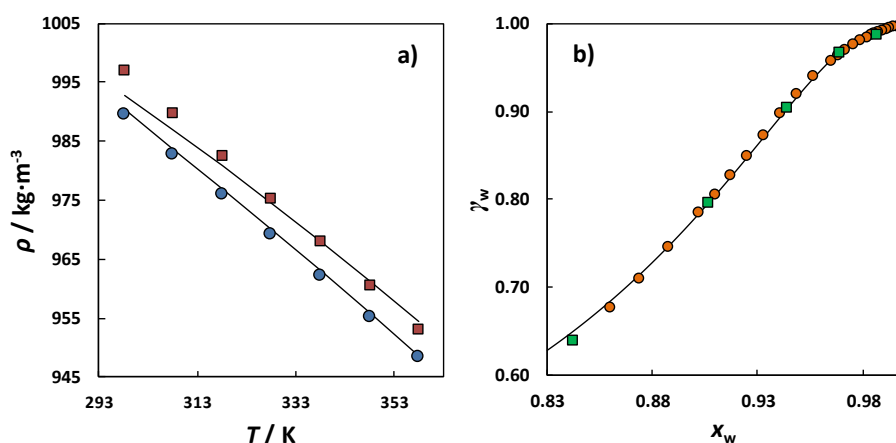


**Figure 3.13.** a) Experimental densities of aqueous solutions of [N<sub>3333</sub>]Cl measured in this work at atmospheric pressure: ■,  $x_{IL}=0.0931$ ; ●,  $x_{IL}=0.1608$ . b) Water activity coefficients at 298.15 K: ◆, Lindenbaum et al.<sup>276</sup>; ▲, this work. Symbols represent experimental data while the solid lines depict the PC-SAFT results using  $k_{ij}= -0.1167$  between water and [N<sub>3333</sub>]Cl and the water parameters also used in reference<sup>274</sup>.



**Table 3.10.** PC-SAFT molecular parameters for symmetrical quaternary ammonium chlorides (2B association scheme).

Salt	$M_w$ (g / mol)	$m_i^{seg}$	$\sigma_i$ (Å)	$u_i$ (K)	$\varepsilon^{AiBi}$ (K)	$\kappa^{AiBi}$	%ARD( $\gamma_w$ ) <sup>a</sup>	%ARD( $\rho_L$ ) <sup>a</sup>
[N <sub>1111</sub> ]Cl <sup>b</sup>	109.60	6.597	2.9160	451.63	5000	0.1	-	-
[N <sub>2222</sub> ]Cl <sup>b</sup>	165.70	17.670	2.3510	278.06	5000	0.1	-	-
[N <sub>3333</sub> ]Cl	221.81	17.789	2.6151	217.95	5000	0.1	0.40	0.12

<sup>a</sup>ARD, average relative deviation. <sup>b</sup>Parameters taken from Zubeir et al.<sup>261</sup>

The phase behavior of carboxylic acids is complex due to their strong hydrogen-bonding character. Their particular association behavior results in two hydrogen bonds formed simultaneously, which leads to a dimerization in the vapor phase. Kleiner et al.<sup>277</sup> addressed this subject by applying and comparing two different association schemes (1A and 2B) to some carboxylic acids. While the former enables the formation of only dimers, the latter also allows the formation of clusters with more than two acid molecules. The results by Kleiner et al.<sup>277</sup> showed that both association schemes provided good results but using a one-site association scheme yielded an improved description of vapor-pressure data. Nevertheless, this specific thermodynamic feature is more important especially for carboxylic acids of lower molecular weight. In fact, Albers et al.<sup>278</sup> applied the 2B association scheme to model different carboxylic acids achieving a good description of the experimental data by considering that each acid molecule contains two different association sites: an acceptor site at the oxygen atom and a donor site mimicking the hydroxyl group. Thus, the 2B association scheme was applied also for the carboxylic acids studied in this work, and the deviations [%ARD( $\rho_L$ ) and %ARD( $P^*$ ) in table 3.11] were found to be much lower compared to modeling with the 1A association scheme (results not shown in this work).

Thus, the pure-component parameters for lauric acid and myristic acid were inherited from Albers et al.,<sup>278</sup> while pure-component parameters for capric acid, palmitic acid and stearic acid were adjusted in the present work by regression to pure fluid liquid-density  $\rho_L$  and vapor pressure,  $P^*$ , data. The results obtained are depicted in Figure 3.14 and the parameters reported in Table 3.11, along with the deviations to the experimental data.

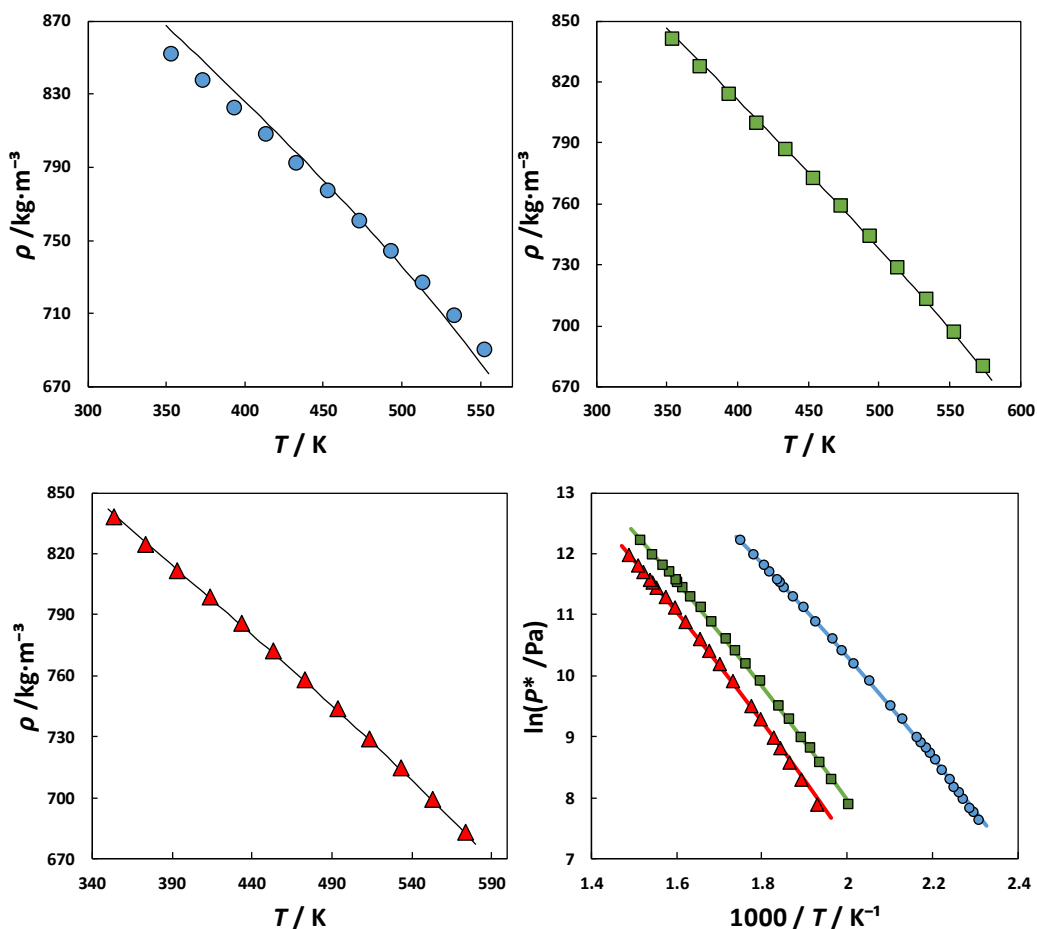


**Figure 3.14.** Densities and vapor pressures of pure monocarboxylic acids. The symbols represent experimental data from ref.<sup>279</sup> while the solid lines represent the PC-SAFT results for capric acid (●), palmitic acid (■) and stearic acid (▲), respectively.

**Table 3.11.** PC-SAFT pure-component parameters for monocarboxylic acids (2B association scheme).

Acid	$M_w$ (g / mol)	$m_i^{seg}$	$\sigma_i$ (Å)	$u_i$ (K)	$\varepsilon^{AiBi}$ (K)	$\kappa^{AiBi}$	%ARD( $\rho_L$ )	%ARD( $P^*$ )
Capric	172.26	7.1472	3.3394	242.46	2263.0	0.02	0.96	1.90
Lauric <sup>b</sup>	200.32	7.2547	3.5244	252.97	3047.5	0.00338	0.34 <sup>278</sup>	0.60 <sup>278</sup>
Myristic <sup>b</sup>	228.37	7.4126	3.6719	256.48	2252.5	0.04399	0.57 <sup>278</sup>	0.46 <sup>278</sup>
Palmitic	256.42	7.5599	3.8092	267.52	2291.4	0.02	0.17	1.70
Stearic	284.48	7.6146	3.9536	275.20	2351.6	0.02	0.10	2.20

<sup>a</sup>ARD, average relative deviation. <sup>b</sup> Parameters taken from Albers et al.<sup>278</sup>

Furthermore, as commonly observed for homologous series, the optimized molecular parameters of SAFT-type equations can be correlated with the compounds molecular weight. This allows predicting pure-component parameters for compounds of different chain length or decreasing the number of parameters to be included in the parameter estimation procedure. Thus, the non-associative pure-component parameters reported in Table 3.11 were correlated with the molecular weight of the carboxylic acids and linear trends were observed as described by Equations 3.17 to 3.19.

$$m_i^{seg} = 0.0044198M_w + 6.3885 ; R^2 = 0.9808 \quad (3.17)$$

$$m_i^{seg} \sigma_i^3 (\text{\AA}^3) = 1.8145M_w - 46.551 ; R^2 = 0.9999 \quad (3.18)$$

$$m_i^{seg} u_i (K) = 3.2523M_w + 1174.7 ; R^2 = 0.9933 \quad (3.19)$$

This supports the physical meaning behind the adjusted PC-SAFT parameters. Additionally, the associative parameters can often be set to constant values for components within a homologous series since the associative behavior and interactions in the pure fluid are generally not strongly influenced by the compounds chain length (except for the components with very small chain length). Thus, the association volume was set to a value of 0.02 for palmitic acid, capric acid, and stearic acid, and similar values for the association energy parameter were obtained for these carboxylic acid in the parameter estimation (see Table 3.11).

### Solid-Liquid Equilibrium Modeling

All the DES constituents considered in this work (quaternary ammonium salts and carboxylic acids) are solids at room temperature. Their solubility in a liquid solvent can be described by a simplified thermodynamic expressions for solid–liquid equilibria according to:<sup>280</sup>

$$x_i^l \gamma_i^l = \exp \left[ \left( \frac{\Delta H_i^{sl}}{RT_{mi}} \right) \left( \frac{T - T_{mi}}{T} \right) \right] \quad (3.20)$$

where  $x_i^l$  is the mole fraction of the component  $i$  in the liquid phase (solubility),  $\gamma_i^l$  is the activity coefficient of the component  $i$  in the liquid phase,  $T_{mi}$  and  $\Delta H_i^{sl}$  are the melting temperature (K) and melting enthalpy ( $J \cdot mol^{-1}$ ) of the pure component  $i$ ,  $T$  is the melting temperature (K) of the mixture, and  $R$  is the ideal gas constant ( $8.314 J \cdot mol^{-1} \cdot K^{-1}$ ). This equation considers that pure compounds do not present polymorphic forms, what is acceptable since the solid-solid transition temperature of the fatty acids are very close to the melting temperature, or below the eutectic point.<sup>281–283</sup> Additionally, the effect of the difference between specific heats of the solid and liquid phases was neglected since the heat capacities for fatty acids, and salts, are commonly much lower than their enthalpy values.<sup>284–286</sup> Moreover, Equation 3.20 assumes that the pure compounds are independently crystallized in the solid phase as expected from an eutectic-type phase diagram. Therefore, the solid phase can be assumed as composed by two pure components without presence of mixed crystals, such that the activity in the solid phase  $x_i^s \gamma_i^s = 1$ .

An ideal mixture is characterized by activity coefficients in the liquid phase that are equal to one ( $\gamma_i^l = 1$ ). Although clearly non-ideal, the mixtures under investigation were also treated as ideal mixtures to evaluate the non-ideality of the compounds in the liquid phase.

The liquidus lines can be obtained through Equation 3.20 where the activity coefficients need to be considered due to the non-ideality of the studied systems. Applying Equation 3.20 allows determination of an experimental value for the activity coefficients, which can be used to validate thermodynamic models (in this work PC-SAFT)

Using PC-SAFT, the activity coefficients are calculated from the fugacity coefficients through Equation 3.21.

$$\gamma_i = \frac{\varphi_i}{\varphi_i^0} \quad (3.21)$$

where  $\varphi_i$  and  $\varphi_i^0$  are the fugacity coefficients of component  $i$  in the mixture and that of the pure compound, respectively. Fugacity coefficients in the mixture depend on the components, mixture composition, density and temperature, and were derived from the residual Helmholtz energy  $a^{res}$  using thermodynamic standard relations.

To evaluate the accuracy of PC-SAFT, the deviations between PC-SAFT modeled melting temperatures  $T^{calc}$  and experimental data  $T^{exp}$  are expressed in terms of *AAD* (average absolute deviation) applying Equation 3.22 where  $N_{exp}$  is the total number of experimental points in the mixture (excluding the melting points of the pure components):

$$AAD(K) = \frac{1}{N_{exp}} \sum_{k=1}^{N_{exp}} |T_k^{calc}(K) - T_k^{exp}(K)| \quad (3.22)$$

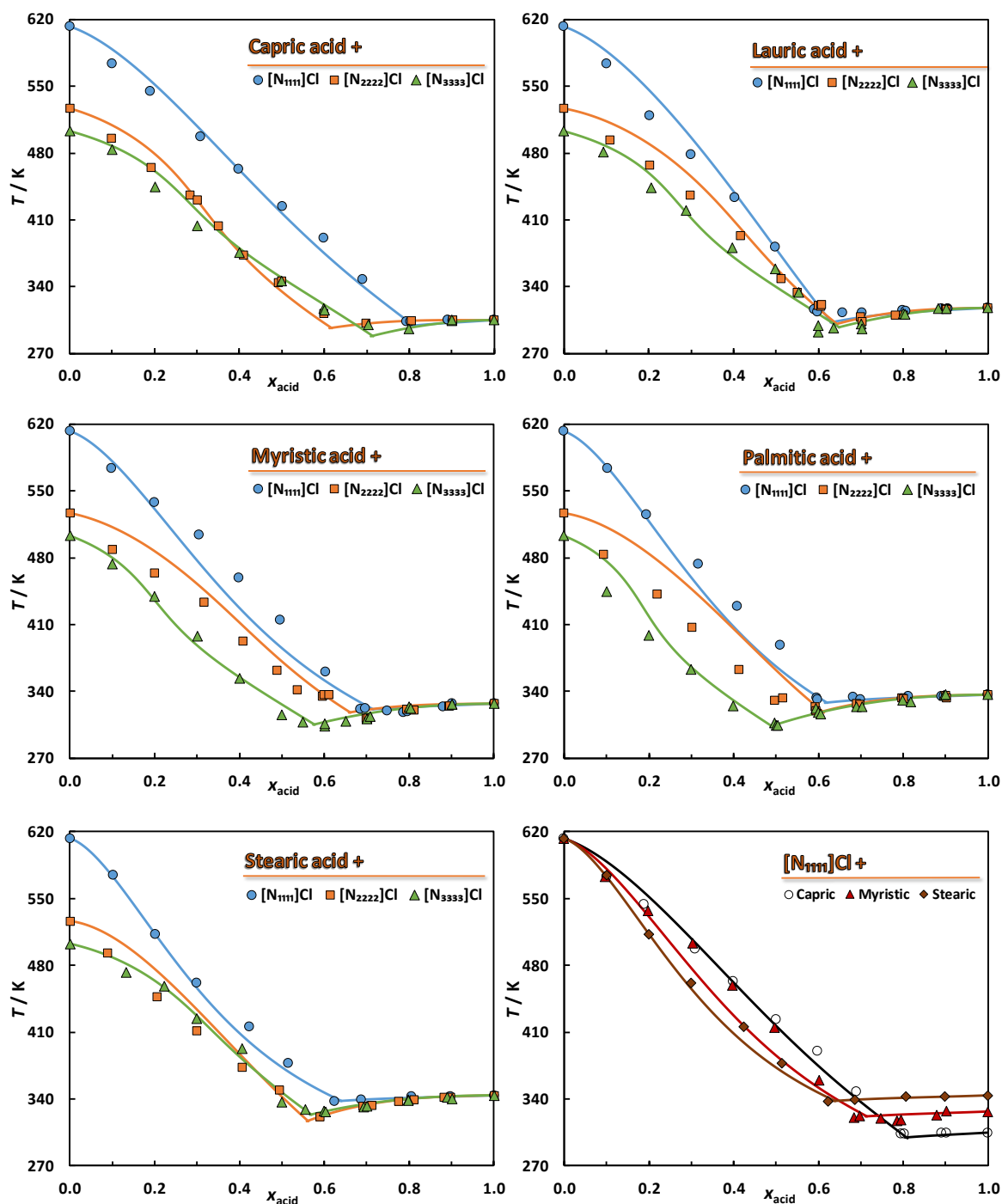
### 3.2.5. Results and discussion

Table 3.12 presents the melting temperatures and enthalpies for the pure compounds studied in this work as well as values from literature. The melting properties of the carboxylic acids under study are in very good agreement with those from literature. Melting temperatures of the quaternary ammonium salts are very scarce in literature, and melting enthalpy data for these compounds were not found in the open literature. The values for the melting points of the three quaternary ammonium salts under study were measured by DSC and confirmed with the melting points measured by the Büchi apparatus. [N<sub>1111</sub>]Cl decomposed upon heating and it was thus impossible to measure its melting enthalpy, that was fitted to the experimental data for the SLE phase diagrams measured, using the activity coefficients estimated by the COSMO-RS model.<sup>287</sup>

Figure 3.15 shows the 15 SLE phase diagrams measured in this work. They exhibited a phase behavior characterized by a single eutectic point, with a melting temperature much lower than that of the quaternary ammonium salt used, like commonly found in DES. The detailed melting experimental data obtained for each mixture are reported in Appendix 3 (Tables S3.8 to S3.10).

**Table 3.12.** Melting properties for pure compounds measured in this work and comparison with literature.

Components	$T_m / K$			$\Delta H^{sl} (kJ / mol)$		
	This work	Literature	Ref.	This work	Literature	Ref.
Quaternary ammonium salts						
[N <sub>1111</sub> ]Cl	612.87 ± 6.16	693.15	<sup>288</sup>	20.49	-	-
[N <sub>2222</sub> ]Cl	526.78 ± 1.03	-	-	51.24 ± 0.02	-	-
[N <sub>3333</sub> ]Cl	503.07 ± 2.56	416.15 - 418.15	<sup>289</sup>	66.58 ± 2.10	-	-
Fatty acids						
Capric Acid	304.75 ± 0.05	305.48	<sup>175</sup>	27.50 ± 1.29	27.23	<sup>175</sup>
		305.30	<sup>290</sup>		28.00	<sup>290</sup>
		303.80	<sup>291</sup>		28.30	<sup>291</sup>
		304.95	<sup>292</sup>		28.60	<sup>292</sup>
Lauric Acid	317.48 ± 0.14	318.48	<sup>175</sup>	37.83 ± 0.20	34.62	<sup>175</sup>
		316.20	<sup>291</sup>		36.10	<sup>291</sup>
		317.82	<sup>293</sup>		34.69 <sup>b</sup>	<sup>293</sup>
		317.45	<sup>294</sup>		36.30	<sup>294</sup>
Myristic Acid	327.03 ± 0.04	328.93	<sup>175</sup>	41.29 ± 0.38	43.95	<sup>175</sup>
		326.50	<sup>291</sup>		45.00	<sup>291</sup>
		326.20	<sup>295</sup>		45.75 <sup>b</sup>	<sup>295</sup>
		327.45	<sup>294</sup>		45.20	<sup>294</sup>
Palmitic Acid	336.84 ± 0.10	336.36	<sup>176</sup>	51.02 ± 0.22	53.02	<sup>176</sup>
		337.69	<sup>296</sup>		51.37	<sup>296</sup>
		335.44	<sup>297</sup>		55.85	<sup>297</sup>
		335.40	<sup>298</sup>		53.90	<sup>298</sup>
Stearic Acid	343.67 ± 0.07	344.04	<sup>176</sup>	61.36 ± 0.42	61.10	<sup>176</sup>
		343.65	<sup>299</sup>		59.96	<sup>299</sup>
		343.85	<sup>300</sup>		59.96	<sup>300</sup>
		342.75	<sup>301</sup>		61.30	<sup>301</sup>



**Figure 3.15.** Solid-liquid phase diagrams of DES composed of monocarboxylic acids and symmetrical quaternary ammonium chlorides. Symbols represent the experimental data measured in this work while the solid lines depict the PC-SAFT modelling.

Taking into account the simple eutectic behavior observed for these systems, they were modeled with Equation 3.20 by two methods: i) considering ideal liquid phase ( $\gamma_i = 1$ ) and

ii) as non-ideal liquid phase with activity coefficients calculated with PC-SAFT EoS. The SLE modeling results with activity coefficients obtained from PC-SAFT for the systems under study are illustrated in Figure 3.15, while the comparison with the ideal solubility curves is depicted in Figure 3.16 for the system  $[N_{2222}]Cl$  + lauric acid, and in Appendix 3 for all other systems under study (Figures S3.6 to S3.10).

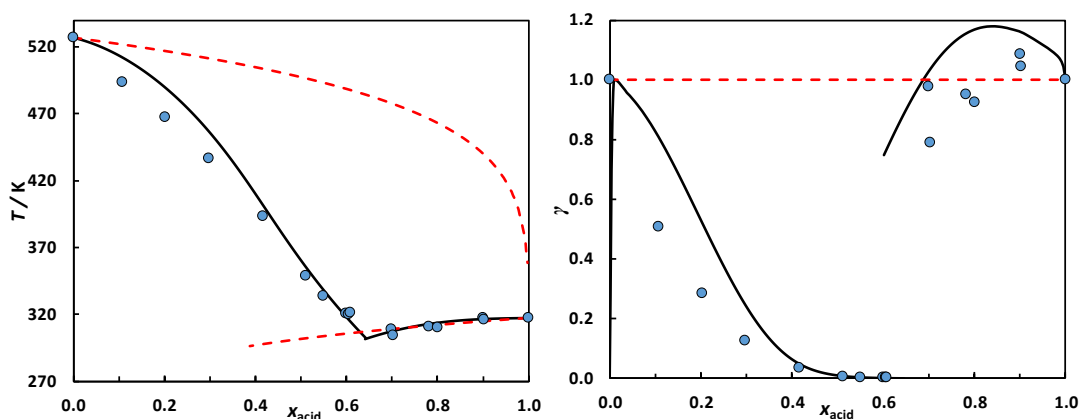


**Figure 3.16.** Solid-liquid equilibrium (left) and activity coefficients (right) for the DES  $[N_{2222}]Cl$  + lauric acid. Legend: ●, experimental; —, PC-SAFT; ---, ideal.

Figure 3.15 shows that PC-SAFT is able to provide a good description of the experimental data using either one or two binary parameters (accounting for corrections to the cross-dispersion energy and/or cross-association energy). The binary parameters are listed in Table 3.13. They were obtained by optimizing an objective function that equaled to a minimization of the  $AAD(T)$  given in Equation 3.22 using all the experimental SLE data listed in Tables S3.8-S3.10. Using the pure-component parameters listed in Table 3.10 and Table 3.11, the melting properties in Table 3.12 and the binary interaction parameters in Table 3.13, Equation 3.20 allows to accurately describe the experimental data. The highly unsymmetrical non-ideal behavior that characterizes these mixtures is correctly described with PC-SAFT. That is, the solubility curves of the quaternary ammonium salts are much more non-ideal than the solubility curves of the carboxylic acids. This is also graphically illustrated in Figure 3.16 by the values of the activity coefficients in the system  $[N_{2222}]Cl$  + lauric acid: these values are very low (close to zero) for the quaternary ammonium salts whereas values by one order of magnitude higher can be observed for the carboxylic acid.



**Table 3.13.** Binary parameters applied within PC-SAFT model.

Systems	PC-SAFT binary parameters	
	$k_{ij}$	$k_{ij\_eps}$
[N <sub>1111</sub> ]Cl + capric acid	-0.178	----
[N <sub>1111</sub> ]Cl + lauric acid	-0.210	----
[N <sub>1111</sub> ]Cl + myristic acid	-0.220	----
[N <sub>1111</sub> ]Cl + palmitic acid	-0.220	----
[N <sub>1111</sub> ]Cl + stearic acid	-0.220	----
[N <sub>2222</sub> ]Cl + capric acid	-0.085	-0.270
[N <sub>2222</sub> ]Cl + lauric acid	-0.100	-0.180
[N <sub>2222</sub> ]Cl + myristic acid	-0.120	-0.140
[N <sub>2222</sub> ]Cl + palmitic acid	-0.140	-0.096
[N <sub>2222</sub> ]Cl + stearic acid	-0.160	-0.060
[N <sub>3333</sub> ]Cl + capric acid	-0.050	-0.280
[N <sub>3333</sub> ]Cl + lauric acid	-0.050	-0.250
[N <sub>3333</sub> ]Cl + myristic acid	-0.050	-0.290
[N <sub>3333</sub> ]Cl + palmitic acid	-0.050	-0.320
[N <sub>3333</sub> ]Cl + stearic acid	-0.050	-0.220

This highly unsymmetrical non-ideality was observed for all systems under study, and is presented in Figures S3.6-S3.10 of the Appendix 3. Besides some small quantitative differences between the activity coefficients of the quaternary ammonium salts in the systems under study, a big qualitative difference between the activity coefficients of the carboxylic acids in the DES under study becomes obvious. In the systems containing [N<sub>1111</sub>]Cl, very small deviations to ideality can be found as the activity coefficients of the carboxylic acids are close to one, and usually values  $\gamma_{acid}^L > 1.0$ ) were observed. However, upon increasing the chain length of the alkyl groups of the quaternary ammonium salt, negative deviations to ideality were also observed based on the fact that the values  $\gamma_{acid}^L \ll 1.0$ . That is, the attractive interactions strongly increase with increasing chain length of the quaternary ammonium salt, and a moderate increase can also be observed with increasing chain length of carboxylic acid. This behavior suggests a strengthening of the HBA:HBD complex due to the weakening of the coulombic interactions between the cation and anion of the salt with the increase of its alkyl chains, which has been described

by Kurnia et al.<sup>202</sup> for the interactions of ionic liquids and water through hydrogen bonding.

In general, extreme strong negative deviations from ideal mixture behavior is found in all DES under study causing a large decrease in the system melting temperature. Strong associative interactions (hydrogen bonding) between the two DES constituents are the main reason for the observed negative deviations to ideality. Cross-association occurs between the carboxylic acid that acts as H-bonding donor and the quaternary ammonium salt that acts as H-bonding acceptor. These strong cross interactions explain very low activity coefficients. However, activity coefficients of the carboxylic acids are larger than one at very high concentration of carboxylic acid in the mixture. In these concentration regions, self-association interactions between the carboxyl groups become stronger than in the pure-component state, and cross-association interactions play a minor role.<sup>282,290</sup> Thus, the melting-point depressions are higher the higher the amount of quaternary ammonium salt present in the mixture. This explains the behavior of the almost horizontal liquidus line of carboxylic acid shown in Figure 3.15. In fact, the eutectic behavior observed in these systems is not trivial, as the complex interaction behavior is additionally confronted by very large differences between the melting temperatures of the DES constituents. This prevents high melting-point depressions in regions with high concentration of carboxylic acid, which forces the eutectic temperature close to the melting temperature of the pure carboxylic acid<sup>302</sup> (note in Figures S3.6 to S3.10 that the ideal solubility curves exhibit this behavior).

In contrast to the close-to-ideal phase behavior at high concentrations of carboxylic acids, negative deviations to ideality are very high at higher concentrations of quaternary ammonium salt. The deviations to the experimental data (in terms of AAD, in K) applying Equation 3.20 under the assumption of ideal mixture behavior is depicted in Figure 3.17. High deviations to the experimental data can be observed due to the significant negative deviations from ideal behavior at high concentrations of quaternary ammonium salt. Thus, advanced thermodynamic models such as PC-SAFT are required in order to quantify activity coefficients and to improve the accuracy of Equation 3.20. PC-SAFT allows for a good description of most systems with a global AAD (K) of only 7.39 K for all the systems

studied in this work. Taking into account the large temperature ranges studied (about 300 K), these results can be considered as a very satisfactory result.

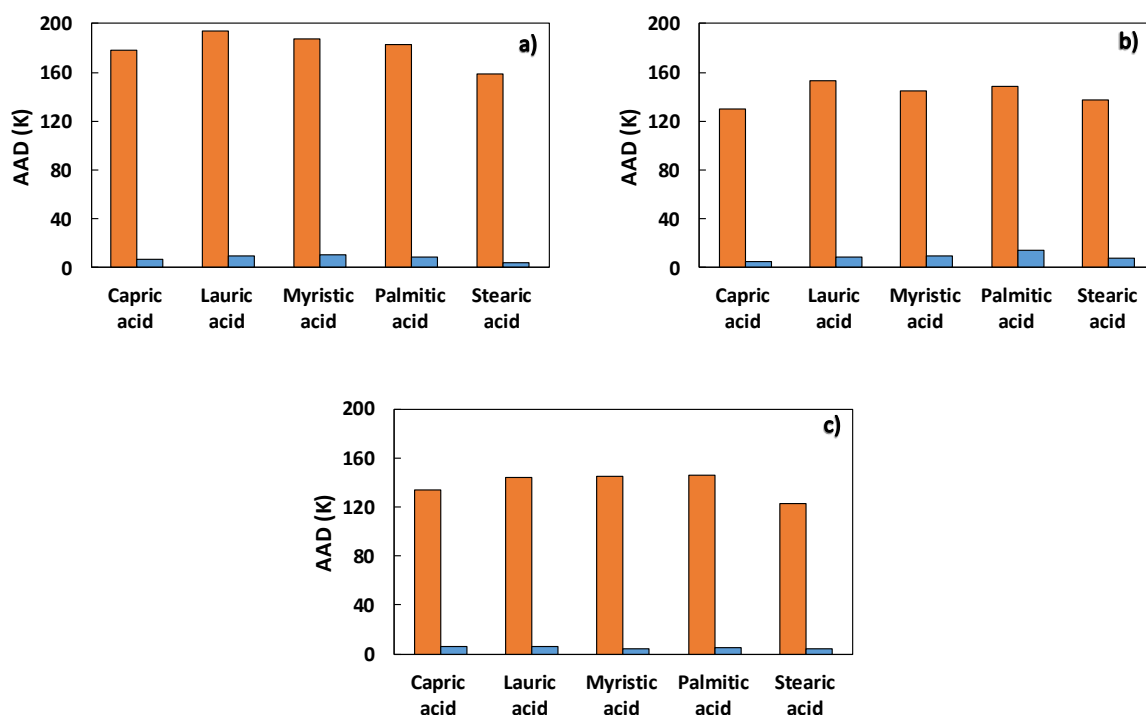


**Figure 3.17.** Deviations to the experimental data measured in this work: ■, ideal; ■, PC-SAFT for a) [N<sub>1111</sub>]Cl + carboxylic acids b) [N<sub>2222</sub>]Cl + carboxylic acids c) [N<sub>3333</sub>]Cl + carboxylic acids.

One drawback of the measurements is the time they consume. A huge number of measurements is required to quantify the eutectic point (eutectic temperature  $T^E$  and composition  $x^E$ ), allowing also to assess the temperature difference between ideal  $T^E$  and real  $T^E$  (assigned with  $\Delta T^E$ ). To overcome this time limitation, PC-SAFT was applied in this work in order to estimate the eutectic point of the DES under study. For that purpose, the pure-component parameters in Table 3.10 and Table 3.11 and the binary parameters in Table 3.13 were used. The modeling results are depicted in Figure 3.18. Figure 3.18 suggests that the eutectic composition is shifted towards lower mole fractions of acid upon increasing alkyl chain of both, the acid and the quaternary ammonium salt. In spite of the uncertainties of experimental data and PC-SAFT modelling associated to these estimates it can be stated that a fixed stoichiometric relationship between carboxylic acid

and quaternary ammonium salt is not observed. This is not surprising as the systems under study do not obey co-crystal formation with a fixed stoichiometric composition. It is possible however to state that the liquid mixture seems to be dominated by associates with molar ratios of 2:1 for the considered DES carboxylic acid / quaternary ammonium salt.

The eutectic temperature increases with increasing chain length of the carboxylic acid. This is expected as the pure-acid melting temperature limits the eutectic temperature of the system, i.e. the lower the melting temperature for the pure acid, the lower  $T^E$  values. Further, it can be observed from Figure 3.18 that  $T^E$  decreases from  $[N_{1111}]Cl$  to  $[N_{3333}]Cl$ , which can be explained by the decrease of melting points of the quaternary ammonium salts from  $[N_{1111}]Cl$  to  $[N_{3333}]Cl$  combined with the increased non-ideality of the liquid phase from  $[N_{1111}]Cl$  to  $[N_{3333}]Cl$  (see Appendix 3).

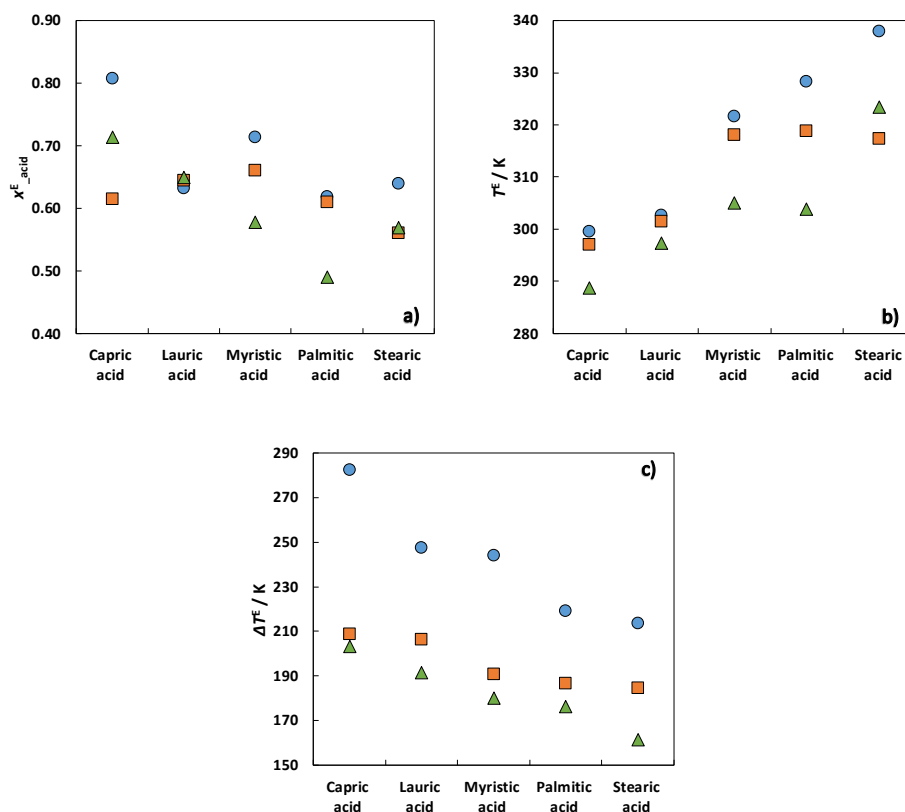


**Figure 3.18.** a) Eutectic compositions b) eutectic temperatures c) melting-temperature depression of the various DES studied, estimated by PC-SAFT. ●,  $[N_{1111}]Cl$ ; ■,  $[N_{2222}]Cl$ ; ▲,  $[N_{3333}]Cl$ .

Concerning the temperature difference  $\Delta T^E$  (i.e. the difference between the eutectic temperature estimated by PC-SAFT and that calculated considering an ideal liquid phase for the estimated eutectic composition), an increase following the order:  $[N_{1111}]Cl > [N_{2222}]Cl > [N_{3333}]Cl$  can be observed from Figure 3.18, which is mainly due to the melting temperatures of the pure quaternary ammonium salts. In contrast, activity coefficients of the salts decrease in the order  $[N_{1111}]Cl > [N_{2222}]Cl > [N_{3333}]Cl$ , as illustrated in Figures S3.6 – S3.10. Thus, the strength of cross interactions increase in the order  $[N_{1111}]Cl < [N_{2222}]Cl < [N_{3333}]Cl$  between the salt and the carboxylic acid. The very large temperature difference observed are a strong evidence that the systems studied here are, in fact, deep eutectic mixtures.

These observations are further reinforced by the binary parameters estimated for quantitative PC-SAFT modeling. As already known, one of the advantages of using these coarse-grained models is the enhanced physical meaning of the model parameters, when compared to activity coefficients models. The binary  $k_{ij\_eps}$  accounts for deviations in the cross-association energy obtained through the conventional mixing rules. The fact that  $k_{ij\_eps}$  takes negative values applied confirms the strong cross-association between acid and salt in the considered DES. According to Table 3.13, the  $k_{ij\_eps}$  values become more negative in the order  $[N_{1111}]Cl < [N_{2222}]Cl < [N_{3333}]Cl$ , supporting the interpretation for an increase of the cross-association strength in that order.

Despite the importance of hydrogen bonding, also dispersion forces are important in the DES under study. To quantitatively model the phase diagrams shown in Figure 3.15 and Figure 3.16, one binary interaction parameter  $k_{ij}$ , that accounts for deviations to the mixture's dispersive energy, was applied to each mixture. According to Table 3.13, the values obtained were also negative, which means an increased mixture's dispersive energy compared to the ideal combining rule and points to very strong cross-dispersion interactions. As often observed for a series of mixtures with mixing partner from one family (e.g. water-alkane, gas-alkane and many more), the parameter  $k_{ij}$  can be correlated with molecular weight of the mixing partner. In the DES studied in this work,

$k_{ij}$  values become more negative upon increasing the alkyl chain length of the carboxylic acid. In Table 3.13, an exception can be found for the DES with [N<sub>3333</sub>]Cl, where  $k_{ij}$  values were applied that were independent of the chain length of the carboxylic acid. For these mixtures, cross-association interactions obviously dominate the physical behavior of the mixtures, and dispersion interactions are less important compared to the DES with [N<sub>1111</sub>]Cl or [N<sub>2222</sub>]Cl. In this work, the binary parameters applied were found to follow these dependencies on molecular weight of the carboxylic acid:

$$k_{ij}(N_{1111}Cl) = 6.715 \times 10^{-6} \times M_{w\_acid}^2 - 3.402 \times 10^{-3} \times M_{w\_acid} + 0.2066 \quad (R^2 = 0.9634) \quad (3.23)$$

$$k_{ij}(N_{2222}Cl) = -6.773 \times 10^{-4} \times M_{w\_acid} + 0.03367 \quad (R^2 = 0.9972) \quad (3.24)$$

$$k_{ij}(N_{3333}Cl) = -0.05 \quad (3.25)$$

$$k_{ij\_eps}(N_{2222}Cl) = 0.4063 \times \ln(M_{w\_acid}) - 2.350 \quad (R^2 = 0.9823) \quad (3.26)$$

These correlations allow predicting interaction parameters for mixtures that are not presented in this work, or alternatively to decrease the number of required binary parameters, reducing considerably the amount of experimental data to be gathered in order to correctly describe the SLE behavior of this type of DES.

### 3.2.6. Conclusion

(Solid+liquid) phase equilibrium diagrams for 15 different DES composed of carboxylic acids and symmetrical quaternary ammonium chlorides were measured by a combination of DSC and visual methods. The experimental data obtained showed that these systems present a single-eutectic type behavior, with a eutectic temperature very close to the melting temperature of pure carboxylic acid, and a very large negative deviation from ideal-mixture behavior, that becomes more relevant as the salt alkyl chain increases. This behavior suggests a strengthening of the HBA:HBD complex upon weakening the coulombic interactions between the cation and anion of the salt with the increase of its alkyl chain length.

The modelling of the studied systems was performed applying the molecular based PC-SAFT EoS. The pure-component PC-SAFT parameters were either taken from literature, or fitted to experimental data of the pure compound for the acids, or, in the case of the salts, to activity data and density data of their aqueous solutions. The pure-compound parameters taken from literature showed transferability of the molecular parameters to different mixtures, phases or phase equilibria. By using one or two binary parameters (that in most cases can be kept constant or correlated to the molecular weight of the fatty acid), a good quantitative description (an average AAD of only 7.39 K) of the experimental data was achieved, despite the complex cross-association and large asymmetry of the studied mixtures. PC-SAFT modeling allowed to estimate the eutectic points of the DES under study. The physical meaning of the parameters within this model was also enhanced and insights into the molecular interactions in the systems were given. In more detail, the binary parameters accounting for deviations in the cross-association energy and cross-dispersion energy suggested the increase in cross-association (cross-dispersion) as the number of CH<sub>2</sub> groups in the salt (acid) increased.

The results here reported show that PC-SAFT can be a valuable tool in the description of the SLE of DES, and allows for a better understanding of phase behavior and interactions within this type of deep eutectic mixtures.

### **3.3. Indirect assessment of the fusion properties of choline chloride from solid-liquid equilibria data**

Luis Fernandez, Liliana P. Silva, Mónica A. R. Martins, Olga Ferreira, Juan Ortega, Simão P. Pinho & João A. P. Coutinho, *Fluid Phase Equilibria*, in press (2017), DOI: 10.1016/j.fluid.2017.03.015.

#### **3.3.1. Abstract**

The temperature and enthalpy of fusion of choline chloride  $-\text{[Ch]Cl}-$  are not measurable directly since the compound decomposes upon melting. Yet, given the wide use of this compound in the preparation of deep eutectic solvents (DES), its thermophysical fusion properties are very important for a better understanding of these mixtures and the

thermodynamic description of their solid-liquid phase diagrams. In this work, the fusion properties of choline chloride were estimated using the solubility curves of choline chloride in ten different ionic compounds, forming simple binary eutectic mixtures with quasi-ideal liquid phases. Experimental solid-liquid equilibria data for these systems - [Ch]Cl+ionic compounds- were measured, and the ideality of the systems assessed through the quantification of the activity coefficients and their comparison in each pair of binary solutions. The values estimated for the fusion properties of choline chloride are  $T_{fus,[Ch]Cl}=597\pm 7$  K and  $\Delta_{fus}H_{[Ch]Cl}=4300\pm 600$  J·mol<sup>-1</sup>. These were additionally checked by thermodynamic consistency tests and by the prediction of the solid-liquid curves with COSMO-RS model. The results obtained with both procedures allow us to guarantee the usefulness and robustness of the estimated data.

### 3.3.2. Introduction

Deep eutectic solvents (DES) formed by choline chloride ([Ch]Cl) and organic hydrogen donors<sup>130,148,303</sup> have been proposed as green solvents for a wide range of applications<sup>131,132,304</sup> due to their interesting properties, such as good solvent capacity, low cost, and low eco-toxicity.<sup>305</sup> The knowledge of the melting properties of [Ch]Cl is necessary to thermodynamically characterize the choline-based DES, which includes the estimation of the eutectic points and the complete description of their solid-liquid phase diagrams. This is relevant for the design and optimization of processes involving DES, including the search and selection of the best DES for a particular application. However, the decomposition temperature of [Ch]Cl before/upon melting<sup>306</sup> prevents the use of direct technics for the measurement of fusion properties.

In this work an indirect method to estimate the fusion temperature and enthalpy of [Ch]Cl was used. This is based on the evaluation of the solid-liquid phase equilibria of a set of quasi-ideal binary solutions formed by [Ch]Cl and other ionic compounds. Previous works<sup>302,307,308</sup> have shown that mixtures of ionic liquids, even with melting points above 100 °C, often form quasi-ideal mixtures. For this purpose, the solubility curves of ten eutectic systems formed by [Ch]Cl and the ionic compounds (IC): choline acetate ([Ch][Ac]), choline propanoate ([Ch][Prop]), choline butanoate ([Ch][Buta]),



tetrabutylammonium chloride ([N<sub>4444</sub>]Cl), tetrabutylphosphonium chloride ([P<sub>4444</sub>]Cl), benzyldimethyl(2-hydroxyethyl)-ammonium chloride ([BzCh]Cl), 1-butyl-1-methylpyrrolidinium chloride ([C<sub>4</sub>m<sub>pyr</sub>]Cl), choline bis(trifluoromethylsulfonyl)imide ([Ch][NTf<sub>2</sub>]), 1-ethyl-3-methylimidazolium chloride ([C<sub>2</sub>mim]Cl) and 1-(2-hydroxyethyl)-3-methylimidazolium chloride, ([C<sub>2</sub>OHmim]Cl), were measured. The quasi-ideality of each mixture was firstly assessed calculating the activity coefficients by COSMO-RS,<sup>218</sup> and using the experimental data to compare the similarity of [Ch]Cl activity coefficients in each pair of binary systems. The solubility data were then used to estimate the fusion properties of [Ch]Cl by linear regression of the solid-liquid equilibrium equation, and the final results were checked using two independent procedures: 1) evaluation of the thermodynamic consistency of the experimental data, and 2) estimation of the solid-liquid phase diagrams by COSMO-RS and comparison with the experimental phase equilibria diagrams.

### 3.3.3. Experimental

#### 3.3.3.1. Materials

The source, purity and temperature of fusion of the compounds used in this work are described in Table 3.14. [Ch][Prop] and [Ch][Buta] were synthesized in our laboratory following standard procedures presented in Appendix 3.3. Before use, all individual compounds were purified under vacuum (0.1 Pa and 298 K), for at least 72 h. The water content was then measured by Karl-Fisher and was found to be always lower than 600 ppm.

#### 3.3.3.2. Methods

The melting temperatures were determined with an automatic glass capillary device model M-565 from Buchi (100-240 V, 50-60 Hz, 150 W), which has a temperature resolution of 0.1 K. Since many ionic compounds are highly hygroscopic, in particular choline chloride, mixtures were prepared inside a dry-argon glove-box, at room temperature using an analytical balance model ALS 220-4N from Kern with an accuracy of  $\pm 0.002$  g. Vials with mixtures were, whenever

possible, heated under stirring until complete melting and then recrystallized. The solid mixtures were ground in the glove-box and the powder filled into a capillary. A temperature gradient of  $0.5 \text{ K}\cdot\text{min}^{-1}$  was used in all cases, and the melting procedure repeated at least two times. The estimated uncertainty of the melting temperatures is better than 1.2 K. This technique was also used to determine the degradation temperature of pure [Ch]Cl, where different temperature gradients were used (see Table S3.15 and Figure S3.11 of Appendix 3).

**Table 3.14.** Pure component properties.

Compound	Source	Purity / %	$T_{\text{fus}} / \text{K}$		$\Delta_{\text{fus}}H / \text{J}\cdot\text{mol}^{-1}$
			exp.	lit.	
[Ch]Cl	Acros Organics	98		575.15 <sup>130</sup>	-
[Ch][Ac]	Iolitec	> 99	362.62 <sup>a</sup>	324.15 <sup>309</sup> /345.15 <sup>310</sup>	8881.7 <sup>d</sup>
[Ch][Prop] <sup>c</sup>	-	-	282.57 <sup>b</sup>	-	2238.6 <sup>b</sup>
[Ch][Buta] <sup>c</sup>	-	-	315.98 <sup>b</sup>	318.15 <sup>311</sup>	8793.6 <sup>b</sup>
[N <sub>4444</sub> ]Cl	Sigma-Aldrich	97	342.82 <sup>a</sup>	348.15 <sup>312</sup>	19430 <sup>d</sup>
[P <sub>4444</sub> ]Cl	Cytec	97	339.46 <sup>a</sup>	338.15 <sup>313</sup>	-
[BzCh]Cl	Aldrich	97	351.42 <sup>a</sup>	-	8730 <sup>d</sup>
[C <sub>4</sub> mpyr]Cl	Iolitec	99	472.98 <sup>a</sup>	>387.15 <sup>314</sup>	30896 <sup>d</sup>
[Ch][NTf <sub>2</sub> ]	Iolitec	99	305.65 <sup>b</sup>	303.15 <sup>315</sup>	1226.5 <sup>b</sup>
[C <sub>2</sub> mim]Cl	Iolitec	98	350.42 <sup>a</sup>	363.15 <sup>316</sup>	8588 <sup>d</sup>
[C <sub>2</sub> OHmim]Cl	Iolitec	99	358.88 <sup>a</sup>	335.15 <sup>114</sup>	20974 <sup>d</sup>

<sup>a</sup>Visual detection, <sup>b</sup>DSC, <sup>c</sup>Synthesized in this work, <sup>d</sup>Estimated from experimental data using Eq.3.28 and the experimental points with  $x_{\text{IC}} > 0.6$ .

In a few specific cases indicated in Table 3.14, differential scanning calorimetry (DSC) was used. The melting properties were determined using a Hitachi DSC7000X model working at atmospheric pressure. Samples of approximately 5 mg tightly sealed in aluminium pans were submitted at least to 3 repeated cooling–heating cycles at  $2 \text{ K}\cdot\text{min}^{-1}$ . The thermal transitions temperatures were taken as the peak temperature. The temperature uncertainty calculated through the average of the standard deviation of several consecutive measurements was better than  $\pm 0.1 \text{ K}$ . The equipment was previously calibrated with several standards with weight fraction purities higher than 99%.

### 3.3.4. Theoretical approach

For eutectic systems with complete immiscibility in the solid phase the phase equilibrium can be described by 3.27:<sup>177</sup>

$$\ln(x_i \gamma_i^L) = \frac{\Delta_{fus} H}{R} \left( \frac{1}{T_{fus}} - \frac{1}{T} \right) + \frac{\Delta_{fus} C_p}{R} \left( \frac{T_{fus}}{T} - \ln \frac{T_{fus}}{T} - 1 \right) \quad (3.27)$$

where  $x_i$  is the mole fraction solubility of compound  $i$  and  $\gamma_i^L$  its activity coefficient in the liquid phase,  $\Delta_{fus} H$  and  $T_{fus}$  are the enthalpy and temperature of fusion, respectively,  $R$  is the ideal gas constant,  $T$  is the absolute temperature, and  $\Delta_{fus} C_p$  is the difference between the heat capacity of the compound  $i$  in liquid and solid phases. Since values for the heat capacities of most compounds here studied have not yet been measured, and for [Ch]Cl it is not measurable since the compound decomposes before melting, the last term in Eq. 3.27 is neglected in this work. Moreover, even when that data is available, the contribution of this term to the phase equilibrium calculations has been shown to be very small.<sup>178,179</sup> If the liquid phase is an ideal mixture, Eq. 3.27 becomes,

$$\ln(x_i) = \frac{\Delta_{fus} H}{R} \left( \frac{1}{T_{fus}} - \frac{1}{T} \right) \quad (3.28)$$

Eq. 3.28 shows a linear relationship between  $\ln(x_i)$  and  $1/T$  and thus, a linear regression of a set of experimental data for the solubility of choline chloride, in ideal systems, can provide an indirect estimation of the [Ch]Cl fusion properties. In the same way, Eq. 3.28 provides an estimation of the enthalpies of fusion for the other components for which these data are not available. These estimated enthalpies of fusion are shown in Table 3.14.

#### Assessment of the systems ideality

The use of Eq. 3.28 implies that the experimental data used in the regression must come from systems with an ideal, or quasi-ideal, liquid phase. In this work, from a

set of 21 binary systems containing [Ch]Cl, a group of 10 was selected after checking the ideality of the liquid phase of those systems using, initially, COSMO-RS.

COSMO-RS allows the prediction of the activity coefficients of each compound in a mixture without any empirical data. The activity coefficients at 300, 400 and 500 K of the [Ch]Cl(1)+IC(2) systems were estimated by COSMO-RS and this information used to assess the ideality of the solutions. Before the estimations, all the IC structures were optimized.<sup>317</sup> The ions of each compound were optimized simultaneously as an ion pair. On a second step, the COSMO file of each structure was generated by Gaussian, computing the ideal screening charges on the molecular surface at the BVP86/TZVP/DGA level.<sup>317</sup>

Despite its usefulness, COSMO-RS is a predictive tool and thus, additional experimental-based verifications must be performed. For this reason, an empirical procedure named  $\Upsilon$ -method was further employed to check the similarity of the behavior of each pair of binary solutions. This approach is based on the constancy of the second term of the equilibrium in Eq. 3.27, when the solid phase is the same, in this study [Ch]Cl, and so the product  $x_i \gamma_i^L$  is independent of the second compound in solution. This allows us to establish the equality between the activities of [Ch]Cl in two different binary solutions at the same temperature:

$$x_{[Ch]Cl,A} \gamma_{[Ch]Cl,A} = x_{[Ch]Cl,B} \gamma_{[Ch]Cl,B} \quad (3.29)$$

where *A* and *B* are two different ionic compounds forming binary solutions with [Ch]Cl. To compare magnitudes,  $\Upsilon$ , is defined as the ratio of the mole fractions of [Ch]Cl in both systems, which is equivalent to the ratio of the [Ch]Cl activity coefficients:

$$\Upsilon = \frac{x_{[Ch]Cl,A}}{x_{[Ch]Cl,B}} = \frac{\gamma_{[Ch]Cl,B}}{\gamma_{[Ch]Cl,A}} \quad (3.30)$$

From two experimental binary data sets, interpolated values for the [Ch]Cl mole fractions at the same temperature can be found, and  $\Upsilon$  calculated, showing similar magnitudes of [Ch]Cl activity coefficients, when the ratio is close to one.

### Consistency of estimated properties

Beyond the uncertainty of the fusion properties, which can be high due to the nature of the studied substances as well as of the indirect method applied, a very important concept is their reliability, in terms of the error introduced by the use of these properties in the equilibrium calculations. A check of this reliability was performed through the thermodynamic consistency tests proposed by Kang et al.<sup>318</sup> and Cunico et al.<sup>319</sup>, which apply pure compound fusion properties to check the quality of the data. These methods are described briefly in Appendix 3.3.

### 3.3.5. Results and discussion

#### Solid-liquid phase diagrams

The phase diagrams measured for the ten selected systems –[Ch]Cl(1)+IC(2)– retained for the assessment of [Ch]Cl fusion properties are plotted in Figure 3.19 and listed in Table S3.16 of Appendix 3.

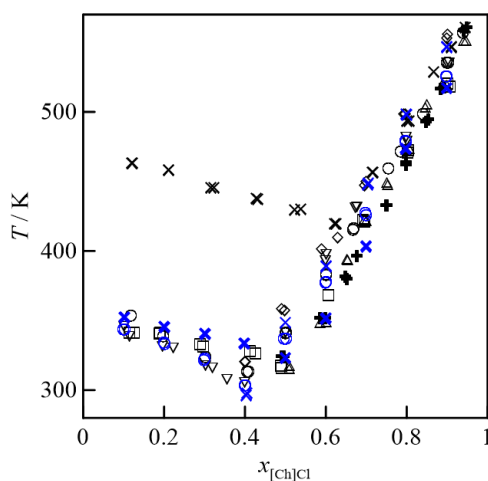


**Figure 3.19.** Solid-liquid phase diagrams for the [Ch]Cl+Ionic compounds systems studied. [Ch]Cl(1)+ (○) [Ch][Ac](2); (+) [Ch][Prop](2); (◇) [Ch][Buta](2); (□) [N<sub>4444</sub>][Cl](2); (△) [P<sub>4444</sub>][Cl](2); (▽) [BzCh][Cl](2); (×) [C<sub>4</sub>m<sub>pyr</sub>][Cl](2); (×) [Ch][NTf<sub>2</sub>](2); (○) [C<sub>2</sub>mim][Cl](2); (+) [C<sub>2</sub>OHmim][Cl](2).

Data show a similar behavior in all the solubility curves. The solubility curve of [Ch][Prop] was not possible to measure because this compound is liquid at room temperature, preventing the use of the experimental methodology applied in this work. The eutectic points of all the other systems studied depend essentially on the fusion properties of the IC in solution.

#### **Evaluation of the ideality of the studied systems: estimation of the activity coefficients by COSMO-RS**

The activity coefficients of [Ch]Cl at equimolar composition were estimated by COSMO-RS at three temperatures ( $T=300, 400$  and  $500$  K) and are reported in Table S3.17, while the curves at the full composition range can be found in Figure S3.14 of Appendix 3.

According to the equimolar data, all systems show a quasi-ideal behavior with exception of the mixture containing [N<sub>4444</sub>]Cl. However, the value of the activity coefficients of these systems is still adequate in the concentrated [Ch]Cl composition region (see Figure S3.14), and thus they were also considered in this work. The system [Ch]Cl+[Ch][Ac] presents a strong negative deviation to the ideal behavior at low temperatures, which decreases rapidly with increasing temperature. Therefore, a quasi-ideal behavior is expected close to the fusion temperature of [Ch]Cl and the data were also considered.

The experimental activity coefficients of the ten systems studied were calculated by Eq. 3.27 and are reported in Table S3.16 along with the solubility data. These values further confirm the ideality of the studied systems.

#### **Evaluation of the ideality of the studied systems: $\Upsilon$ -method**

All the possible combinations for comparing two different binary systems were explored, and for each system, the values of  $\Upsilon$  that present maximum deviation from unity are summarized in Table S3.18. The systems showing the most different behavior between each other are [Ch]Cl+[Ch][Buta] and [Ch]Cl+[C<sub>2</sub>OHmim]Cl and [Ch]Cl+[Ch][Buta] and [Ch]Cl+[N<sub>4444</sub>]Cl. Four pairs of systems show a value of  $\Upsilon=1$ :

[Ch]Cl+[Ch][Prop] and [Ch]Cl+[N<sub>4444</sub>]Cl or [C<sub>2</sub>OHmim]Cl, [Ch]Cl+[N<sub>4444</sub>]Cl + [C<sub>2</sub>OHmim]Cl and [P<sub>4444</sub>]Cl + [C<sub>2</sub>mim]Cl, but all the others are close enough to 1 to consider that they have a very similar behavior, and so to be used in the assessment of the fusion properties.

### Assessment of the fusion properties of [Ch]Cl

After the establishment of the quasi-ideality of the ten systems selected, the experimental data were fitted using Eq. 3.28. To do so, only the experimental information, for each binary system, comprising choline chloride mole fractions higher than 0.6, was considered. Figure 3.20 shows the results of the linear regression.

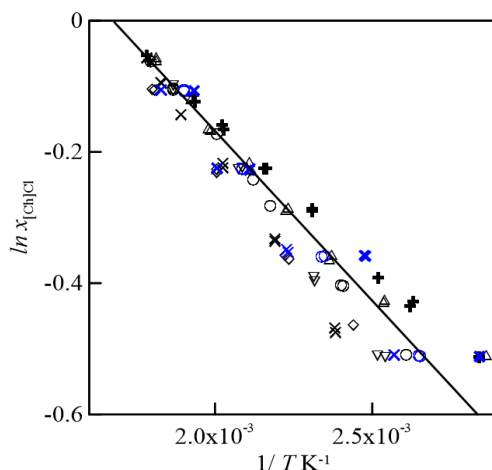


**Figure 3.20.** Plot of the regression by equation 3.29 of the experimental data for the solubility of [Ch]Cl in [Ch]Cl+Ionic compounds systems. [Ch]Cl(1)+ (○) [Ch][Ac](2); (+) [Ch][Prop](2); (◇) [Ch][Buta](2); (□) [N<sub>4444</sub>]Cl(2); (△) [P<sub>4444</sub>]Cl(2); (▽) [BzCh]Cl(2); (×) [C<sub>4</sub>mpyr]Cl(2); (×) [Ch][NTf<sub>2</sub>](2); (○) [C<sub>2</sub>mim]Cl(2); (+) [C<sub>2</sub>OHmim]Cl(2). (—) ideal solution ( $T_{\text{fus},[\text{Ch}]\text{Cl}} = 597 \text{ K}$ ,  $\Delta_{\text{fus}}H_{[\text{Ch}]\text{Cl}} = 4300 \text{ J}\cdot\text{mol}^{-1}$ ).

The calculated fusion properties of choline chloride are  $T_{\text{fus},[\text{Ch}]\text{Cl}} = 597 \pm 7 \text{ K}$  and  $\Delta_{\text{fus}}H_{[\text{Ch}]\text{Cl}} = 4300 \pm 600 \text{ J}\cdot\text{mol}^{-1}$ . The deviation of these values to those obtained by applying Eq. 3.28 to each individual system (Table S3.19) are:  $s(T_{\text{fus},[\text{Ch}]\text{Cl}}) = 11 \text{ K}$  and  $s(\Delta_{\text{fus}}H_{[\text{Ch}]\text{Cl}}) = 593 \text{ J}\cdot\text{mol}^{-1}$ , close to the uncertainty of the estimated properties.

The deviations increase for lower concentrations of [Ch]Cl, where an increase deviation to ideality is observed. However, all curves converge for concentrated choline chloride mixtures, with the experimental data showing small deviations from the fit and allowing a good estimation of the fusion properties. Given that the compound decomposes before melting there are no literature data of the enthalpy of fusion of [Ch]Cl to compare with the values here estimated. Abbott et al.<sup>130</sup> proposed a value for the fusion temperature of [Ch]Cl, that is probably a decomposition temperature. This is somewhat lower than the value estimated in this work ( $\Delta T \approx 18$  K), but nevertheless again within the uncertainty of the estimation.

### Validation of the results

The values of the three quality factors described in Appendix 3.3 [(S3.4), (S3.7) and (S3.10)] are presented in Table S3.20. The NRTL model<sup>320</sup> was used to fit the solid-liquid equilibria diagrams (parameters given in Table S3.21). All systems show very satisfactory quality factors by the three consistency tests. The system which shows a lower quality is [Ch]Cl+[P<sub>4444</sub>]Cl.

An additional verification of the results was performed through the reproduction of the solid-liquid phase equilibria of all systems by COSMO-RS model. For that, the properties estimated for [Ch]Cl and the other components shown in Table 3.14 (experimental and estimated) were used. Figure S3.15 presents all the resulting diagrams obtained, showing a very satisfactory representation of the experimental data, with three exceptions: the solubility curves of the systems [Ch]Cl+[Ch][Ac] and [Ch][NTf<sub>2</sub>] do not intersect because of the low value of the activity coefficients at low temperatures, and the system [Ch]Cl+[N<sub>4444</sub>]Cl presents a curious concavity resulting from a large deviation of the ideality estimated by COSMO-RS, which is in total disagreement with the quasi-ideal behavior found from the experimental solid-liquid equilibrium data.

The eutectic points obtained from the experimental data, and the different models used (NRTL and COSMO-RS) are presented in Table S3.22, showing relevant



differences as COSMO-RS is a pure predictive model. These results also show the importance to find the eutectic coordinates experimentally.

Finally, is important to reinforce that the methodology here proposed can potentially be expanded to other ionic compounds that decompose upon melting, giving tools for a much better analysis, thermodynamic representation and eventually screening of new DES.

### **3.3.6. Conclusion**

The experimental solid-liquid equilibria data of choline chloride in ten different ionic compounds was measured and the solubility curves used to estimate the fusion properties of choline chloride:  $T_{fus,[Ch]Cl}=597\pm 7$  K and  $\Delta_{fus}H_{[Ch]Cl}=4300\pm 600$  J·mol<sup>-1</sup>. These were additionally checked by thermodynamic consistency tests and by the prediction of the solid-liquid curves with COSMO-RS model. Results obtained guarantee the usefulness and robustness of the estimated data.

### **3.4. Solid-liquid phase diagrams of eutectic solvents based on choline chloride and fatty acids or alcohols**

Mónia A. R. Martins, Liliana P. Silva, Olga Ferreira, Simão P. Pinho & João A. P. Coutinho, in preparation.

#### **3.4.1. Abstract**

The solid-liquid equilibria phase diagrams of eight eutectic systems formed by choline chloride and a fatty alcohol or a fatty acid were measured. All systems show slight deviations to ideal behavior, especially for the non-ionic compounds, resulting from the sum of the hydrogen bonding between the acid/alcohol groups with the chloride anion (attractive) and the dispersion forces (repulsive). In most of the cases, experimental eutectic points present temperatures higher than those obtained for ideal mixtures, showing that these systems cannot be considered as deep eutectic solvents.

### 3.4.2. Introduction

In spite of the very large number of eutectic solvents reported in the literature, the actual number of solid-liquid phase diagrams investigated is surprisingly scarce despite the important information they can provide on the donor-acceptor interactions, and the range of compositions and temperatures for operating these systems.<sup>130,303</sup> This limits the systems characterization and the development of models to describe the liquid phase non-ideality, and the ability to design new eutectic solvents using computer aided molecular design approaches, instead of the trial and error currently used. Additionally, to screen solvents with particular characteristics and specific ranges of eutectic temperatures, knowledge on the relationship between the structural characteristics of organic compounds and the eutectic points is necessary. Thus, studies of solid-liquid phase diagrams focused on comparable systems (same functional groups and different chain lengths, or same chain lengths and different functional groups, etc.) are required.

In this work, the solid-liquid phase diagrams of eight eutectic solvents formed by choline chloride and fatty alcohols or fatty (monocarboxylic) acids are reported. The experimental data were measured using a visual detection technique and the thermodynamic consistency verified using tests available in literature.<sup>318,319</sup>

### 3.4.3. Experimental

#### 3.4.3.1. Materials

The properties of the compounds used in this work are detailed in Table 3.15. Experimental melting temperatures for the fatty alcohols and fatty acids obtained in this work were compared with literature showing a good agreement. For choline chloride the melting properties proposed in section 3.3 were used.<sup>321</sup> Choline chloride was purified before use under vacuum (0.1 Pa and 298 K) and constant stirring, for at least 72 h. The water content was measured using a Metrohm 831 Karl Fischer coulometer, with the analyte Hydranal® – Coulomat AG from Riedel-de Haën, and was found to be below 700ppm.

**Table 3.15.** Pure component properties.

Compound	Source	Purity %	$T_{\text{fus}} / \text{K}$		$\Delta_{\text{fus}}H / \text{J}\cdot\text{mol}^{-1}$
			exp.	lit.	
[Ch]Cl	Acros Organic	98	-	597 <sup>321</sup>	4300 <sup>321</sup>
1-tetradecanol	Aldrich	<i>n.a.</i>	311.7 ± 0.3	311.10 <sup>175</sup>	45810 <sup>175</sup>
1-hexadecanol	Aldrich	99	324.4 ± 0.2	322.90 <sup>176</sup>	60960 <sup>176</sup>
1-octadecanol	Aldrich	99	332.9 ± 0.4	331.34 <sup>176</sup>	65350 <sup>176</sup>
Decanoic acid	Alfa Aesar	99	304.6 ± 0.2	305.48 <sup>175</sup>	27230 <sup>175</sup>
Dodecanoic acid	Acros Organics	99	317.5 ± 0.3	318.48 <sup>175</sup>	34620 <sup>175</sup>
Tetradecanoic acid	Acros Organics	99	327.4 ± 0.2	328.93 <sup>175</sup>	43950 <sup>175</sup>
Hexadecanoic acid	Riedel de Haen	98	336.2 ± 0.2	336.36 <sup>176</sup>	53020 <sup>176</sup>
Octadecanoic acid	Acros Organics	97	343.4 ± 0.3	344.04 <sup>176</sup>	61100 <sup>176</sup>

*n.a.* not available.

### 3.4.3.2. Methods

The solid-liquid phase diagrams were measured using a melting point device model M-565 by Buchi (100-240 V, 50-60 Hz, 150 W) with a temperature resolution of 0.1 K. Temperature gradients of 0.1 and 0.5 K·min<sup>-1</sup> were used for pure components and mixtures, respectively. All samples were measured at least two times. Mixtures were prepared at room temperature inside a dry-argon glove-box, using an analytical balance model ALS 220-4N from Kern with an accuracy of ±0.002 g. Whenever possible mixtures were heated under stirring until complete melting and then recrystallized and mashed. The powder was filled into a glass capillary. The estimated reproducibility of the measurements is better than 1 K.

### 3.4.4. Theoretical approach

The activity coefficient,  $\gamma_i$ , at a certain composition,  $x_i$ , is related with the experimental temperature,  $T$ , and the fusion properties ( $T_{\text{fus}}$  – melting temperature,  $\Delta_{\text{fus}}H$  – enthalpy of fusion) of the pure compound by the following equation,<sup>177</sup>

$$\ln(x_i \gamma_i^L) = \frac{\Delta_{\text{fus}}H}{R} \left( \frac{1}{T_{\text{fus}}} - \frac{1}{T} \right) + \frac{\Delta_{\text{fus}}C_p}{R} \left( \frac{T_{\text{fus}}}{T} - \ln \frac{T_{\text{fus}}}{T} - 1 \right) \quad (3.31)$$

where  $R$  is the universal gas constant, and  $\Delta_{\text{fus}} C_p$  is the difference between the heat capacity of compound  $i$  in the liquid and solid states.

This equation assumes that the solid phases of each compound are not miscible. In general, the last term has a negligible value when compared with the second<sup>178,179</sup> and thus, it was not considered in this work. The enthalpies of fusion for the pure compounds were taken from literature and are summarized in Table 3.15.

### 3.4.5. Results and discussion

The solid-liquid experimental data for the systems [Ch]Cl + fatty alcohols or fatty acids are listed in Table 3.16 and presented in Figure 3.21. Data were checked using the consistency tests proposed by Kang et al.<sup>318</sup> and Cunico et al.<sup>319</sup> with the modification proposed in a previous work,<sup>321</sup> and the NRTL parameters shown in Table S3.23. The results ensure an acceptable quality of the experimental data (see Table S3.24 of the Appendix 3).

**Table 3.16.** Experimental ( $x_1$ ,  $T$ ) and calculated ( $\gamma_1$ ) data of the solid-liquid equilibria for the systems investigated in this work.

$x_1$	$T / K$	$\gamma_2$	$x_1$	$T / K$	$\gamma_1$
[Ch]Cl+1-Tetradecanol					
0.109	310.92	1.07	0.461	319.48	1.02
0.202	310.32	1.16	0.505	331.28	0.99
0.288	306.55	1.03	0.551	353.18	1.00
0.419	303.15	1.03	0.600	390.25	1.05
			0.643	414.08	1.06
			0.711	443.85	1.04
			0.742	456.58	1.03
			0.796	483.52	1.03
			0.835	494.78	1.00
			0.893	520.08	0.99
[Ch]Cl+1-Hexadecanol					
0.113	326.08	1.27	0.583	334.62	0.87
0.132	323.35	1.07	0.591	335.42	0.86
0.202	325.15	1.32	0.650	351.25	0.84
0.306	322.55	1.27	0.679	368.55	0.86
0.332	322.28	1.29	0.681	371.45	0.87
0.396	320.95	1.30	0.691	369.28	0.85

Chapter 3 – Extraction, Production and Deterpenation

0.408	320.78	1.31	0.750	415.78	0.91
0.486	325.92	2.16	0.759	426.45	0.93
0.500	318.55	1.32	0.800	452.72	0.95
			0.808	451.65	0.94
			0.860	488.25	0.96
			0.878	487.75	0.94
			0.898	513.25	0.97
			0.899	511.18	0.96
			0.944	536.25	0.96
[Ch]Cl+1-Octadecanol					
0.098	332.42	1.07	0.567	333.68	0.89
0.135	337.95	1.65	0.587	344.82	0.90
0.203	331.12	1.10	0.599	341.25	0.87
0.211	329.35	0.98	0.600	339.48	0.86
0.302	330.55	1.21	0.632	363.25	0.91
0.319	330.58	1.24	0.650	373.95	0.92
0.394	329.52	1.30	0.685	383.65	0.90
0.403	329.98	1.36	0.748	418.65	0.92
0.492	328.48	1.43	0.750	413.78	0.91
0.502	328.32	1.45	0.751	413.48	0.91
			0.798	460.15	0.97
			0.800	456.75	0.96
			0.841	480.75	0.96
			0.850	477.25	0.95
			0.888	508.55	0.97
			0.901	510.18	0.96
			0.939	541.55	0.97
[Ch]Cl+Decanoic acid					
0.101	304.60	1.11	0.456	328.75	1.08
0.212	304.45	1.26	0.485	343.30	1.09
0.296	304.10	1.40	0.540	373.60	1.10
0.342	309.25	1.79	0.592	395.55	1.09
0.399	304.70	1.67	0.642	413.70	1.06
			0.675	427.85	1.05
			0.761	453.70	1.00
			0.786	473.55	1.02
			0.850	499.80	0.99
			0.896	520.95	0.98
			0.938	543.95	0.98
[Ch]Cl+Dodecanoic acid					
0.100	316.48	1.07	0.446	324.20	1.08
0.198	315.88	1.17	0.497	343.85	1.06
0.297	313.38	1.20	0.561	373.75	1.06
0.345	313.20	1.28	0.594	405.62	1.12

Chapter 3 – Extraction, Production and Deterpenation

0.411	316.05	1.60	0.658	423.45	1.06
			0.691	444.35	1.08
			0.748	473.40	1.07
			0.792	483.78	1.03
			0.840	505.70	1.02
			0.877	513.35	0.99
			0.953	543.55	0.96
[Ch]Cl+Tetradecanoic acid					
0.101	326.65	1.07	0.550	338.85	0.94
0.208	326.20	1.19	0.579	373.62	1.03
0.311	325.95	1.35	0.653	395.40	0.98
0.405	325.45	1.53	0.667	413.52	1.02
0.491	323.30	1.60	0.745	443.25	0.99
			0.799	473.45	1.00
			0.839	483.95	0.97
			0.897	523.82	0.99
			0.944	543.75	0.97
[Ch]Cl+Hexadecanoic acid					
0.112	334.50	1.02	0.449	338.85	1.15
0.221	330.75	0.94	0.527	366.05	1.10
0.309	329.00	0.96	0.554	393.88	1.16
0.409	323.60	0.81	0.603	418.85	1.15
			0.652	438.48	1.12
			0.673	443.48	1.10
			0.750	473.58	1.06
			0.803	502.18	1.06
			0.850	517.95	1.03
			0.895	539.52	1.02
[Ch]Cl+Octadecanoic acid					
0.108	342.45	1.06	0.452	355.52	1.23
0.189	341.72	1.11	0.505	388.62	1.25
0.297	340.68	1.20	0.574	400.88	1.14
0.386	339.55	1.28	0.596	433.78	1.21
			0.650	443.85	1.14
			0.695	463.58	1.12
			0.746	483.82	1.09
			0.787	493.68	1.06
			0.844	523.92	1.05
			0.896	543.68	1.03

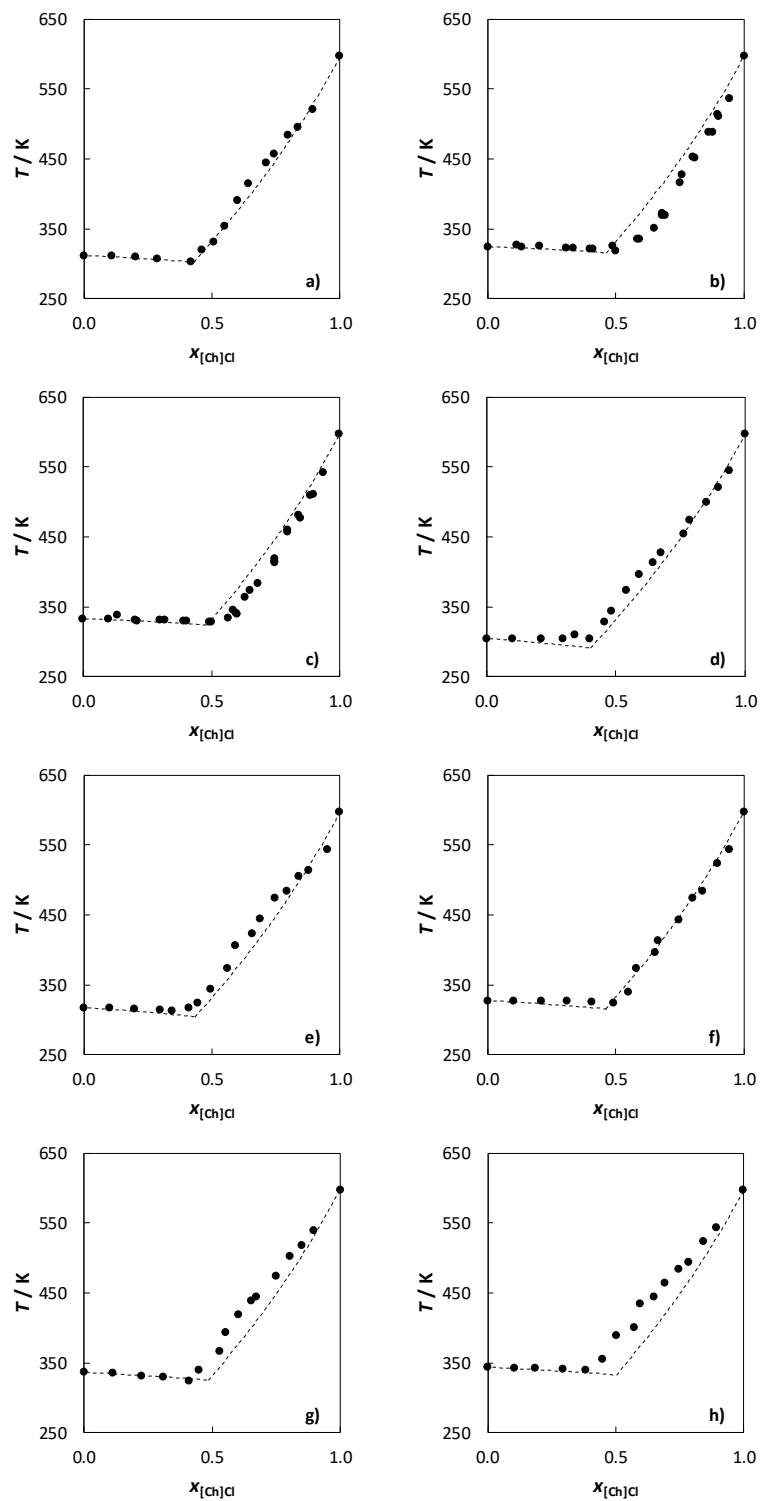


**Figure 3.21.** Solid-liquid phase diagrams of  $[Ch]Cl$  + fatty alcohols and fatty acids. (●) Experimental data, (- - -) Ideal solution.  $[Ch]Cl$  + (a) 1-tetradecanol; (b) 1-hexadecanol; (c) 1-octadecanol; (d) Decanoic acid; (e) Dodecanoic acid; (f) Tetradecanoic acid; (g) Hexadecanoic acid; (h) Octadecanoic acid.

The activity coefficients of each compound in the solutions were calculated from the experimental data, using equation 3.31, and the resulting values are also presented in Table 3.16. In general, small deviations from ideal behavior are observed. For the non-ionic compounds, in general, low positive deviations are obtained except for the system containing hexadecanoic acid. In this case, the negative deviations reflect a higher temperature decrease from the pure acid melting point up to the eutectic point. As can be seen in Figure 3.21, by comparing systems containing the fatty acid or the fatty alcohol with the same chain length, the systems [Ch]Cl+1-tetradecanol and [Ch]Cl + tetradecanoic acid are very well described by the ideal solubility curve in this composition range. For systems containing 16 or 18 carbon atoms,  $\gamma_1$  are slightly lower than 1 for the fatty alcohols systems and slightly higher than 1 for the fatty acids.

Table 3.17 presents the experimental and ideal eutectic compositions and temperatures of the measured systems. Experimental temperatures are all below 339.6 K and any mixture is liquid at room temperature. The differences between the experimental and the ideal-solution eutectic temperatures, show that only the system [Ch]Cl + hexadecanoic acid show depression in the eutectic point. The experimental eutectic points of the remaining systems have higher temperature than the corresponding ideal ones. These differences are considerably higher in the fatty acids series. Both the experimental and ideal predictions of the eutectic compositions are closer to equimolar composition, suggesting the formation of 1:1 complexes.

**Table 3.17.** Eutectic points, experimental and obtained by the ideal liquid phase model.

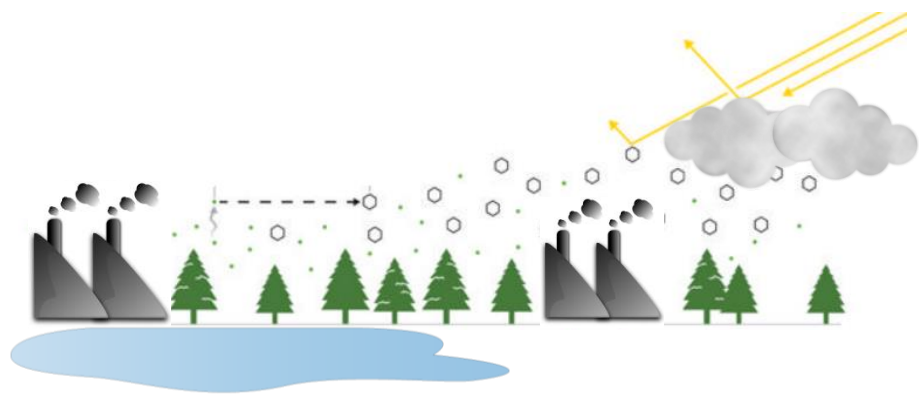
Compound	Experimental		Ideal		$\Delta T / K$
	$x_e$	$T_e / K$	$x_e$	$T_e / K$	
[Ch]Cl+1-Tetradecanol	0.42	303.15	0.43	302.00	1.1
[Ch]Cl+1-Hexadecanol	0.50	318.55	0.46	315.70	2.9
[Ch]Cl+1-Octadecanol	0.50	328.32	0.48	323.90	4.4
[Ch]Cl+Decanoic Acid	0.40	304.70	0.40	290.70	14.0
[Ch]Cl+Dodecanoic Acid	0.41	316.05	0.43	304.30	11.8
[Ch]Cl+Tetradecanoic Acid	0.49	323.30	0.46	315.30	8.0
[Ch]Cl+Hexadecanoic Acid	0.41	323.60	0.48	324.90	-1.3
[Ch]Cl+Octadecanoic Acid	0.39	339.55	0.50	332.60	6.9



### **3.4.6. Conclusion**

The solid-liquid equilibria of eight eutectic systems composed by choline chloride and fatty acids or fatty alcohols was measured and analyzed. Low positive deviations from the ideal behavior are observed, especially for the non-ionic compounds. In most of the cases, eutectic points present temperatures higher than those obtained for ideal liquid mixtures showing that these systems cannot be considered as deep eutectic solvents. All mixtures investigated remain solid in all composition range and the eutectic composition was found to be near to the equimolar composition.

# Chapter 4 – Environmental Impact





#### **4.1. Critical properties of terpenes and terpenoids**

Mónia A. R. Martins, Mariana B. Oliveira, Pedro J. Carvalho, Urszula Domańska, João A. P. Coutinho & Simão P. Pinho, submitted to Industrial & Engineering Chemistry Research.

##### **4.1.1. Abstract**

The knowledge of critical properties is fundamental in engineering process calculations, due to their use in equations of state for the prediction of thermodynamic properties and phase equilibria. A literature survey shows a large number of methods for predicting critical properties of different classes of compounds, but no indications are yet available to help deciding which are the most suitable for terpenes and terpenoids. In this work, Joback, Constantinou and Gani and Wilson and Jasperson group-contribution methods were applied to terpenes and terpenoids, and tested through Peng-Robinson (PR) and Soave-Redlich-Kwong (SRK) equations of state predictions of density and vapor pressure data with the critical properties estimated by Joback method presenting the best results. On other hand, density and vapor pressure data were also used to estimate the critical properties directly by the same equations of state, allowing a comparison between both estimation procedures. Densities were measured at atmospheric pressure in the temperature range (278.15 to 368.15) K for pure compounds, showing high agreement to literature values. The first approach indicates that the best combination is the Joback method and the Peng-Robinson EoS, even if vapor pressure calculations show high relative deviations and density predictions show problems at low temperatures. Following the second approach, the set of critical properties and acentric factors estimated is able to adequately correlate the experimental data. Both equations show a similar capability to correlate the data with SRK EoS presenting a global %ARD of 3.16 and 0.62 for vapor pressure and density, respectively; while PR EoS presented 3.61 and 0.66 %, respectively for the same properties.

##### **4.1.2. Introduction**

Despite being widely used and investigated by researchers there is still an enormous lack of experimental thermodynamic properties for systems containing terpenes and

terpenoids. Aqueous solubilities, vapor pressures, and octanol-water partition coefficients – required to assess environment fate and transport – and critical properties – used as the basis for the estimation of a large variety of thermodynamic, volumetric and transport properties using the corresponding states principle – are required.

Critical temperature and pressure data provide valuable information for the regression and prediction of vapor pressures and are essential for the description of pure component and mixture behavior by equations of state (EoS).<sup>322</sup> However, their experimental determination is complex, expensive, and in many cases impossible, since large and strongly associating components usually decompose before the critical point is reached. Thus experimental data are usually only available for smaller molecules, and predictive methods must be used to the most part of the substances.<sup>323–325</sup>

Considering terpenes, to the best of our knowledge only the critical volume and temperature for limonene,  $\alpha$ -pinene and 3-carene have been published in the open literature,<sup>326</sup> and the results may be considerably uncertain since terpenes are unstable at their critical point.<sup>327</sup> In literature, when critical properties of terpenes are needed, usually to derivate properties through cubic equations of state, most of the authors use different contribution methods to estimate them.<sup>328–330</sup>

Due to their practical and theoretical importance, estimation of critical properties has attracted the interest of researchers and a wide variety of estimation methods is available in the open literature. Riedel<sup>331</sup> and Lydersen<sup>332</sup> were the first authors to develop group-contribution methods for critical property data estimation, followed by many others.<sup>323–325,333–343</sup> Moreover, there are also publications related with the use of quantitative structure property relation (QSPR) correlations and popular mathematical methods like neural networks. A broad overview of these methods together with a detailed discussion of their reliability have been published during the past years.<sup>344,345</sup> In addition, some authors have evaluated the performance of models utilizing a large common set of experimental data.<sup>322</sup>

Due to the scarcity of experimental critical data for terpenes, the use of group-contribution schemes seems to be the adequate approach to obtain reliable results. Most

of the estimation techniques require only the molecular structure and, additionally, other relevant properties as the normal boiling point.<sup>344</sup> The main issue is how the different estimated values compare and what is their performance in terms of volumetric properties or vapor pressure estimations through a cubic equation of state (EoS).

If accurate critical properties can be found, their use in corresponding state methods, like the Lee-Kesler generalized correlation<sup>346</sup> and cubic Equations of State,<sup>347–350</sup> to the prediction of many thermodynamic properties, significantly important for reliable phase equilibrium calculations, is straightforward. These EoS play an important role in chemical engineering design and nowadays, the Peng-Robinson (PR)<sup>350</sup> and Soave-Redlich-Kwong (SRK)<sup>349</sup> equations of state are still widely used in process simulators as Aspen-Plus and ChemCad.<sup>351</sup> Several advantages can be related with how they can accurately and easily represent the relation among temperature, pressure, and phase compositions in binary and multicomponent systems, requiring only the critical properties and acentric factor as generalized parameters.

The aim of this work is to choose a good set of critical properties (critical temperature, critical pressure), and acentric factor, of a group of terpenes and terpenoids to be used with the Soave-Redlich-Kwong<sup>349</sup> and Peng-Robinson<sup>350</sup> equations of state. Two approaches were followed (Figure 4.1):

- 1) Apply the estimated critical properties using the group contribution methods developed by Joback,<sup>323</sup> Constantinou and Gani,<sup>325</sup> and Wilson and Jasperson<sup>333</sup>, to calculate densities and vapor pressure through equations of state, and compare both experimental and calculated sets;
- 2) Use experimental densities and vapor pressures to estimate the critical properties by the same equations of state.

Density data were here measured experimentally at atmospheric pressure, while vapor pressure values were taken from literature.

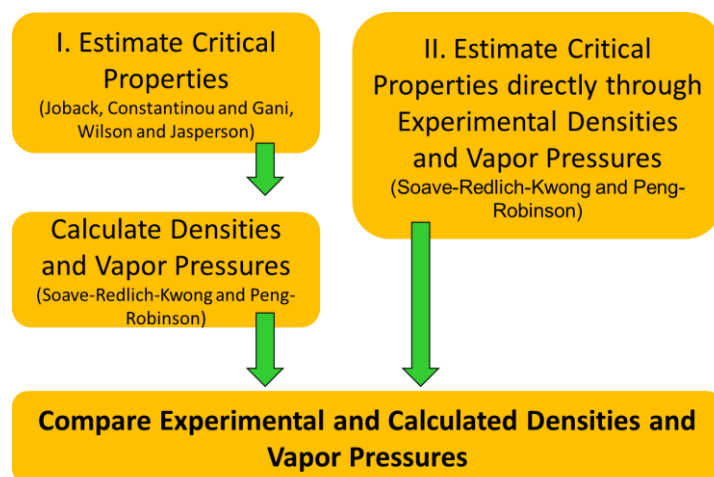


**Figure 4.1.** Schematic representation of the procedure followed in this work.

### 4.1.3. Experimental

#### 4.1.3.1. Material

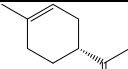
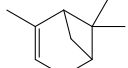
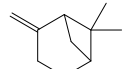
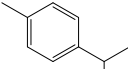
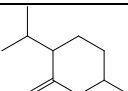
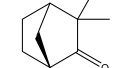
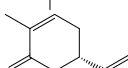
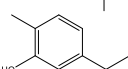
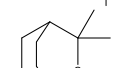
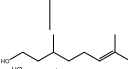
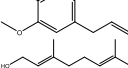
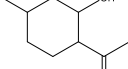
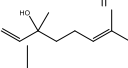
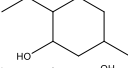
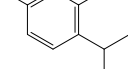


Detailed information about the terpenes and terpenoids investigated in this work is presented in Table 4.1. Compounds were used without any further purification.

#### 4.1.3.2. Methods

##### Density measurements

Densities measurements of the pure terpenes and terpenoids were carried out at atmospheric pressure and in the (278.15 to 368.15) K temperature range, using an Anton Paar GmbH 4500 vibrating-tube densimeter (Graz, Austria). Two integrated Pt 100 platinum thermometers provided good precision of the internal control of temperature ( $\pm 0.01$  K) and the densimeter includes an automatic correction for the viscosity of the sample. The apparatus is precise to within  $\pm 1 \cdot 10^{-5}$  g·cm<sup>-3</sup>, and the overall uncertainty of the measurements was estimated to be better than  $\pm 5 \cdot 10^{-5}$  g·cm<sup>-3</sup>. Additional details related with the equipment can be found elsewhere.<sup>352</sup> The density of (R)-(+)-limonene and *p*-cymene was measure using an automated SVM 3000 Anton Paar rotational Stabinger viscometer–densimeter (temperature uncertainty:  $\pm 0.02$  K; absolute density uncertainty:  $\pm 5 \cdot 10^{-4}$  g·cm<sup>-3</sup>) at atmospheric pressure and in the same temperature range.

**Table 4.1.** Names, structures, sources, molar mass ( $M$ ), boiling points<sup>a</sup> ( $T_{BP}$ ) and mass fraction purities (declared by the supplier) of the terpenes and terpenoids used.

Chemicals	Supplier	CAS	$M / \text{g}\cdot\text{mol}^{-1}$	$T_{BP}^a / \text{K}$	wt %	
Terpenes						
(R)-(+)-limonene		Aldrich	5989-27-5	136.23	449.65	97
$\alpha$ -pinene		Sigma-aldrich	80-56-8	136.23	429.29	98
$\beta$ -pinene		Sigma-aldrich	18172-67-3	136.23	439.19	99
<i>p</i> -cymene		Aldrich	99-87-6	134.22	450.28	99
Terpenoids						
(-)-menthone		Fluka	14073-97-3	154.25	483.15	$\geq 99$
(1R)-(-)-fenchone		Aldrich	7787-20-4	152.23	466.15	$\geq 98$
(S)-(+)-carvone		Merck	218-827-2	150.22	504.15	96
Carvacrol		SAFC	499-75-2	150.22	510.15	99
Eucalyptol		Aldrich	470-82-6	154.25	449.55	99
DL-citronellol		Sigma	106-22-9	156.26	496.40	$\approx 95$
Eugenol		Aldrich	97-53-0	164.20	526.35	99
Geraniol		Sigma-aldrich	106-24-1	154.25	503.15 <sup>a</sup>	98
(-)-isopulegol		SAFC	89-79-2	154.25	480.98	$\geq 98$
Linalool		Aldrich	78-70-6	154.25	470.15	97
L(-)-menthol		Acros	2216-51-5	156.26	487.40	99.7
Thymol		Sigma	89-83-8	150.22	505.65	$\geq 99.5$
$\alpha$ -pinene oxide		Aldrich	1686-14-2	152.23	489.51	97

<sup>a</sup>Taken from Yaws<sup>353</sup>.



#### 4.1.4. Theoretical approach

##### Critical Properties

The following sections will briefly introduce the methods used in this work to estimate the critical temperature,  $T_c$ , and the critical pressure,  $P_c$ , of terpenes and terpenoids, namely Joback (1984; 1987),<sup>323,339</sup> Constantinou and Gani (1994),<sup>325</sup> and Wilson and Jasperson (1996).<sup>333</sup>

##### Joback Method

Joback<sup>323,339</sup> proposed a group-contribution method based on the Lydersen's group-contribution scheme,<sup>332</sup> adding new functional groups, and establishing new parameter values. In this method no interactions between groups is assumed and the elemental contributions are mainly determined by the bonds within and among small groups of atoms, according to the following set of equations,

$$T_c(K) = T_b \left[ 0.584 + 0.965 \left\{ \sum_k N_k(tck) \right\} - \left\{ \sum_k N_k(tck) \right\}^2 \right]^{-1} \quad (4.1)$$

$$P_c(\text{bar}) = \left[ 0.113 + 0.0032N_{atoms} - \sum_k N_k(pck) \right]^{-2} \quad (4.2)$$

where  $tck$  and  $pck$  are the Joback contributions for the critical properties,  $N_k$  is the number of groups of type  $k$  in the molecule and  $N_{atoms}$  is the number of atoms in the compound. Table S4.1 of Appendix 4 presents the structural groups and their respective contributions for each property estimated in this work. For  $T_c$  a value of the normal boiling point,  $T_b$ , is needed (Table 4.1).

##### Constantinou and Gani (CG) Method

In 1994, Constantinou and Gani<sup>325</sup> developed an advanced group-contribution method based on UNIFAC and in a two level estimation scheme. The basic level has contributions from first-order functional groups and the next level has second-order groups, which

provide further information about the molecular structure of the compound. The CG formulations are:

$$T_c(K) = 181.128 \ln \left[ \sum_k N_k(tc1k) + W \sum_j M_j(tc2j) \right] \quad (4.3)$$

$$P_c(\text{bar}) = \left[ \sum_k N_k(pc1k) + W \sum_j M_j(pc2j) + 0.10022 \right]^{-2} + 1.3705 \quad (4.4)$$

where,  $tc1k$  and  $pc1k$  are the contributions of first order, and  $tc2j$  and  $pc2j$  the contributions of second order of groups  $j$ .  $M_j$  is the number of groups of type  $j$  with second order group contributions in the molecule. The constant  $W$  is assigned a value of zero for a first-order approximation and unity in the second-order approximation. Table S4.2 of Appendix 4 presents the set of groups and the respective contributions for each property used in this work.

#### Wilson and Jasperson Method

The method reported by Wilson and Jasperson (WJ)<sup>333</sup> uses the nature of the atoms involved to determine the elemental contributions. It can be applied to both organic and inorganic species. The first order method uses atomic contributions along with boiling point and number of rings, while the second order method also includes group contributions. The first order and second order contributions use the following equations:

$$T_c = \frac{T_b}{\left[ 0.048271 - 0.019846N_r + \sum_k N_k(\Delta tck) + \sum_j M_j(\Delta tcj) \right]^{0.2}} \quad (4.5)$$

$$P_c = \frac{0.018623T_c}{\left[ -0.96601 + \exp \left( -0.00922295 - 0.0290403N_r + 0.04 \left[ \sum_k N_k(\Delta pck) + \sum_j M_j(\Delta pcj) \right] \right) \right]} \quad (4.6)$$

where  $N_r$  is the number of rings in the compound and  $\Delta tck$  and  $\Delta pck$  are the first order atomic contributions, while  $\Delta tcj$  and  $\Delta pcj$  are the second order group contributions. Values of the contributions used in this work are given in Table S4.3 of Appendix 4.

### Acentric Factor

Along with the critical properties, a commonly used pure component constant for property estimation is the acentric factor,  $\omega$ . According with Poling et al.<sup>344</sup>, the most accurate technique to estimate the acentric factor is using the critical constants:

$$\omega = -\frac{\ln(P_c/1.01325) + f^{(0)}(T_b/T_c)}{f^{(1)}(T_b/T_c)} \quad (4.7)$$

$$f^{(0)} = \frac{-5.97616(1-T_b/T_c) + 1.29874(1-T_b/T_c)^{1.5} - 0.60394(1-T_b/T_c)^{2.5} - 1.06841(1-T_b/T_c)^5}{T_b/T_c} \quad (4.8)$$

$$f^{(1)} = \frac{-5.03365(1-T_b/T_c) + 1.11505(1-T_b/T_c)^{1.5} - 5.41217(1-T_b/T_c)^{2.5} - 7.46628(1-T_b/T_c)^5}{T_b/T_c} \quad (4.9)$$

### Equations of State (EoS)

EoS are used to relate temperature, pressure and volume, the macroscopically measurable properties in a system. In this work, Soave-Redlich-Kwong<sup>349</sup> and the Peng-Robinson<sup>350</sup> EoS were selected.

#### Soave-Redlich-Kwong (SRK)

In 1972, Soave<sup>349</sup> suggested the replacing of a term of the Redlich-Kwong<sup>348</sup> equation with one more general temperature-dependence, and the introduction of the acentric factor in the cubic equation of state, Eqs. 4.10-4.13. With this modification, the new equation is able to predict the phase behavior of mixtures in the critical region and improved the accuracy of the calculated critical properties of mixtures.

$$P = \frac{RT}{V_m - b} - \frac{a\alpha}{V_m(V_m + b)} \quad (4.10)$$

$$a = \frac{0.42748R^2T_c^2}{P_c} \quad (4.11)$$

$$b = \frac{0.08664RT_c}{P_c} \quad (4.12)$$

$$\sqrt{\alpha} = 1 + \left(0.48508 + 1.55171\omega - 0.15613\omega^2\right) \left(1 - \left(\frac{T}{T_c}\right)^{0.5}\right) \quad (4.13)$$

### Peng-Robinson (PR)

Since the van der Waals equation in 1873, many other approaches have been proposed. For the most part, the term ‘ $a$ ’ was replaced by semi-empirical corrections with the temperature. One of the most successful examples was the approach of Peng and Robinson<sup>350</sup> in 1976, Eqs. 4.14-4.17.

$$P = \frac{RT}{V_m - b} - \frac{a\alpha}{V_m^2 + 2bV_m - b^2} \quad (4.14)$$

$$a = \frac{0.457235R^2T_c^2}{P_c} \quad (4.15)$$

$$b = \frac{0.077796RT_c}{P_c} \quad (4.16)$$

$$\sqrt{\alpha} = 1 + \left(0.37464 + 1.54226\omega - 0.26992\omega^2\right) \left(1 - \left(\frac{T}{T_c}\right)^{0.5}\right)^2 \quad (4.17)$$

According with Poling et al.,<sup>344</sup> the PR equation of state slightly improves the prediction of liquid volumes. Peng and Robinson<sup>350</sup> gave examples of the use of their equation for predicting the vapor pressure and volumetric behavior of single-component systems, and the phase behavior and volumetric behavior of the binary, ternary, and multicomponent system and concluded that it can be used to accurately predict the vapor pressures of pure substances and equilibrium ratios of mixtures.

Along this work, the accuracy of the estimations was evaluated by using the statistical parameter average relative deviation (%ARD):

$$\%ARD = \frac{1}{N} \sum_{i=1}^N \left| \frac{X^{\text{exp}} - X^{\text{calc}}}{X^{\text{calc}}} \right| \quad (4.18)$$

where  $X^{\text{exp}}$  and  $X^{\text{cal}}$  refers to the experimental and calculated property, respectively, and  $N$  is the number of data points.

#### 4.1.5. Results and discussion

##### Density

Density measurements for the terpenes and terpenoids here studied were carried out in the temperature range (278.15 to 368.15) K and at atmospheric pressure. Results are reported in the Table S4.4 of Appendix 4 and depicted in Figure 4.2. As expected the density decreases linearly with increasing temperature, being eugenol and (R)-(+)-limonene the more and less dense, respectively. The phenylpropene eugenol is the only compound with densities higher than 1 throughout the temperature range studied.

Although new density data of terpenes and terpenoids were measured in this work, it should be remarked that many other authors already reported this property for the same terpenes at different temperatures. Nevertheless, no data was found concerning carvacrol, thymol or  $\alpha$ -pinene oxide. The maximum relative deviations between the experimental values measured in this work and those reported in the literature are presented in Figure 4.3 and Table 4.2. As can be seen a good agreement is found for all compounds, with an average relative deviation of 0.14 % and a maximum relative deviation of 0.62 %.

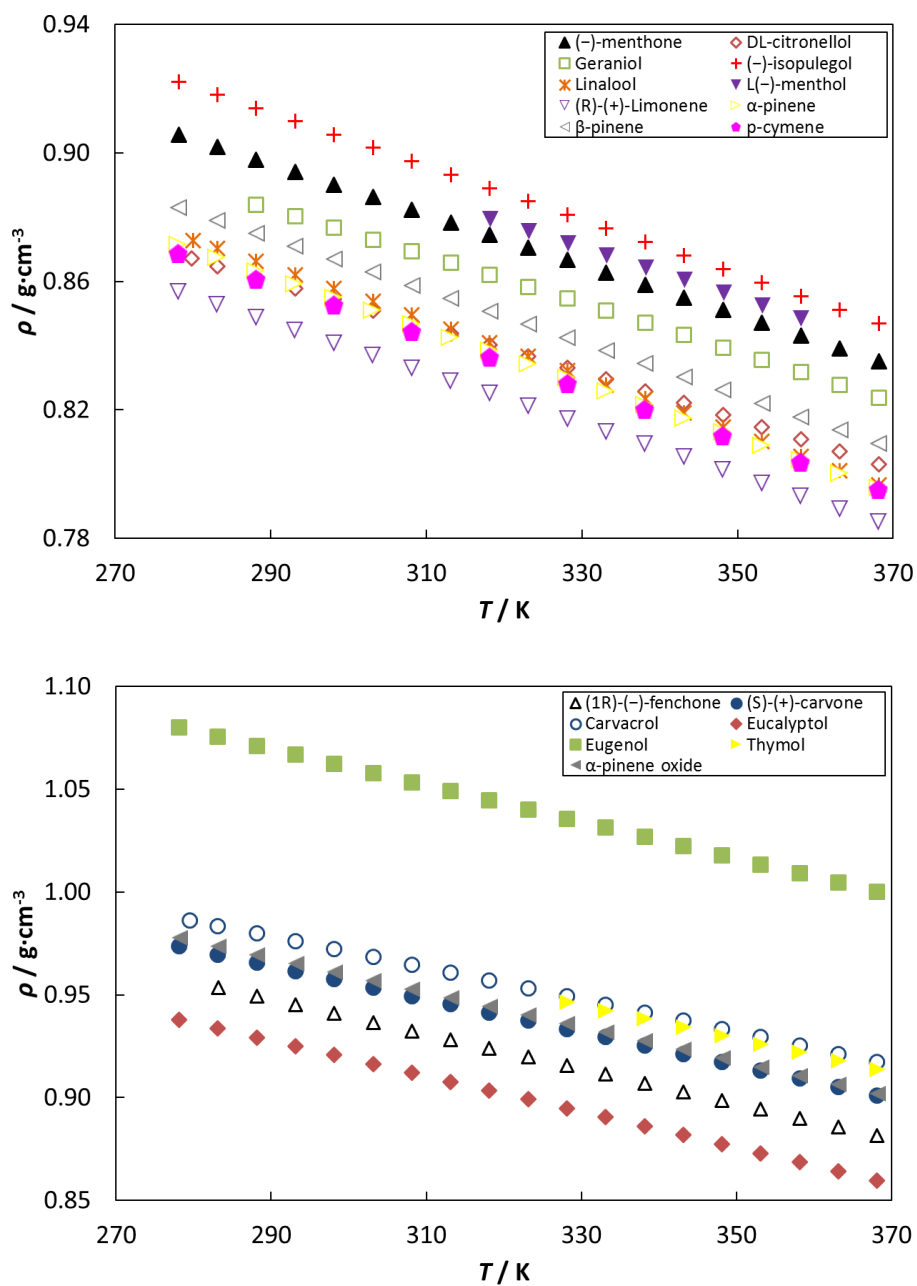


**Figure 4.2.** Density,  $\rho$ , of pure terpenes and terpenoids as a function of temperature and at 0.1 MPa.

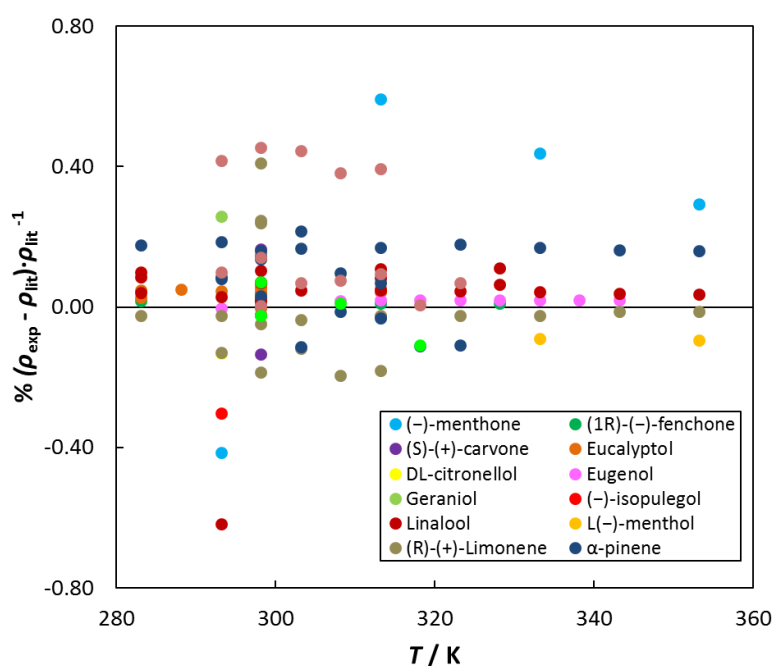


**Figure 4.3.** Percentage relative deviations between density data determined here and those from literature (references on Table 4.2).

**Table 4.2.** Maximum relative deviations between the experimental values measured in this work and those reported in the literature.

Substance	Maximum relative deviation (%)	Substance	Maximum relative deviation (%)
(-)-menthone	0.59 <sup>354</sup>	(-)-isopulegol	0.30 <sup>355</sup>
(1R)-(-)-fenchone	0.02, <sup>356</sup> 0.04, <sup>357</sup> 0.01 <sup>358</sup>	Linalool	0.62, <sup>355</sup> 0.11, <sup>330</sup> 0.07, <sup>359</sup> 0.02, <sup>89</sup> 0.03, <sup>360</sup> 0.05, <sup>361</sup> 0.09 <sup>362</sup>
(S)-(+)-carvone	0.14, <sup>359</sup> 0.16 <sup>363</sup>	L(-)-menthol	0.10 <sup>354</sup>
Eucalyptol	0.05, <sup>364</sup> 0.05, <sup>365</sup> 0.01, <sup>366</sup> 0.04, <sup>367</sup> 0.06, <sup>360</sup> 0.06 <sup>368</sup>	(R)-(+)-limonene	0.25, <sup>357</sup> 0.20, <sup>369</sup> 0.24, <sup>359</sup> 0.41, <sup>89</sup> 0.05 <sup>361</sup>
DL-citronellol	0.13 <sup>355</sup>	α-pinene	0.22, <sup>369</sup> 0.19, <sup>361</sup> 0.14, <sup>368</sup> 0.11 <sup>370</sup>
Eugenol	0.02, <sup>371</sup> 0.01 <sup>372</sup>	β-pinene	0.46, <sup>369</sup> 0.02, <sup>359</sup> 0.01, <sup>368</sup> 0.14 <sup>370</sup>
Geraniol	0.26 <sup>355</sup>	p-cymene	0.03, <sup>368</sup> 0.11 <sup>370</sup>

Terpenes and terpenoids vapor pressures (liquid – vapor) used in this work were collected from literature – Figure S4.1. Due to the lack of vapor pressure data of  $\alpha$ -pinene oxide, this compound was not considered in the following calculations.

### Critical Properties and Acentric Factor

#### *1. Estimation of critical properties using group contribution methods and EoS*

Following the approach described before, the critical properties of terpenes and terpenoids were estimated using the group contribution methods of Joback,<sup>323</sup> Constantinou and Gani (CG),<sup>325</sup> and Wilson and Jasperson (WJ).<sup>333</sup> Results are shown in Table 4.3, alongside with the acentric factor and a structural analysis is presented in Figure 4.4. Joback and CG methods cannot be applied to all the substances studied due to the absence of some groups.

**Table 4.3.** Critical properties of terpenes and terpenoids estimated with different contribution methods.

	$T_c / K$			$P_c / MPa$			$\omega$		
	Joback	CG	WJ	Joback	CG	WJ	Joback	CG	WJ
(-)-menthone	689.70	679.35	727.31	2.60	2.43	2.79	0.412	0.459	0.218
(1R)-(-)-fenchone	679.18		707.95	3.08		2.81	0.388		0.189
(S)-(+)-carvone		688.74	772.76		2.40	3.16		0.619	0.198
Carvacrol	722.20	734.81	716.34	3.44	2.85	2.93	0.581	0.408	0.553
Eucalyptol	661.05		635.70	3.02		2.44	0.339		0.432
DL-citronellol	657.87	675.94	672.09	2.45	2.19	2.30	0.848	0.591	0.657
Eugenol	735.58	772.46	733.37	3.58	2.71	2.93	0.676	0.306	0.599
Geraniol	671.67	682.12	684.75	2.57	2.18	2.42	0.820	0.617	0.648
Isopulegol	656.76	682.75	667.43	2.77	2.36	2.56	0.698	0.398	0.558
Linalool	633.30	650.00	639.84	2.58	2.16	2.26	0.755	0.494	0.612
L(-)-menthol	661.63	679.32	672.52	2.66	2.38	2.50	0.716	0.496	0.580
R-(+)-Limonene		639.85	649.99		2.41	2.72		0.394	0.373
Thymol	715.83	734.76	710.02	3.44	2.84	2.91	0.581	0.367	0.549
$\alpha$ -pinene		657.01	620.56		3.37	2.60		0.224	0.354
$\beta$ -pinene		651.26	634.87		3.22	2.66		0.329	0.363
<i>p</i> -cymene	656.89	664.29	655.59	2.91	2.47	2.84	0.359	0.249	0.358



Figure 4.4 shows some discrepancy between the results, possibly related with limitations associated to each method which was previously verified by other authors.<sup>373</sup> Globally, acentric factors present higher deviations than critical properties especially for aromatic monocyclic terpenes, with eugenol being a patent outlier. Regarding critical temperatures and pressures the highest deviations are presented by (S)-(+)-carvone and (-)-menthone. Non-cyclic compounds have the lowest deviations indicating that linear compounds are more easily described by group contribution methods available. Critical pressures from Joback method are usually larger than those by CG and WJ methods, while generally is clear that Joback and WJ methods present, for this set of compounds, more uniform results among the three tested methods.

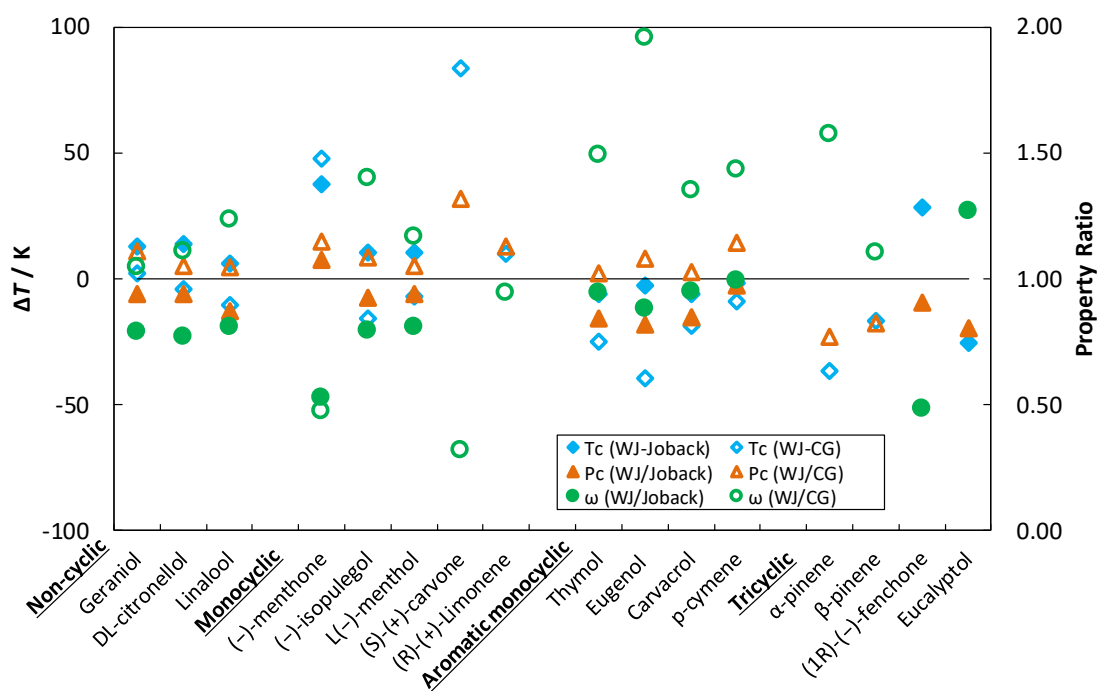


**Figure 4.4.** Temperature change ( $\Delta T / K$ ) and critical pressure and acentric factor ratio for the different contribution methods and compounds studied.

In his initial study, Joback employed only 41 molecular groups, which oversimplifies the molecular structure, thus making several types of isomers indistinguishable. Overall this is insufficient to capture the structural effects of organic molecules and is the main reason for some inaccuracy of the method. Moreover, in CG method a group appearing in an aliphatic ring is considered equivalent to its non-ring counterpart. These groups cannot

distinguish between special configurations such as multiple groups located close to each other, and resonance structures. WJ method requires additional information apart from structure and boiling point, what makes it more complex and sensitive to errors.

As pointed out, all group contribution methods present weaknesses. Therefore, to choose the best model to represent terpenes and terpenoids, the estimated sets of Table 4.3 were used to calculate densities and vapor pressures through the Soave-Redlich-Kwong and Peng-Robinson EoS. The calculated values were compared with the experimental and a global summary is displayed in Figure 4.5. Individual %ARD for each substance studied are presented in Table S4.5 of Appendix 4.

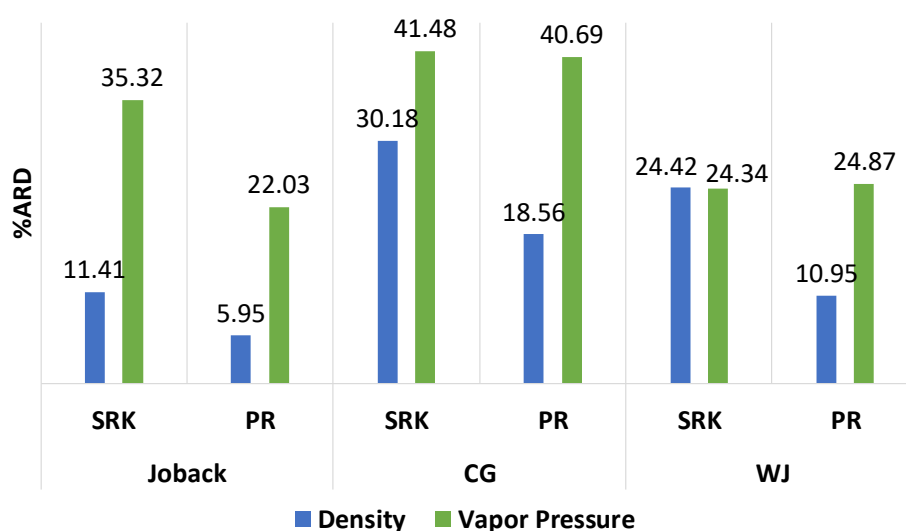


**Figure 4.5.** Global average relative deviation between the experimental and the predicted densities and vapor pressures, calculated using the PR and SRK EoS, with critical properties estimated by Joback, CG, and WJ methods

Globally, the PR EoS presents better results than the SRK. Regarding the group-contribution methods, for both properties, the smaller error was obtained with Joback. Moreover, is important to emphasize that the error obtained for vapor pressures is much higher than for density.

So far the best combination found is the PR EoS with the Joback method. Thus, in order to further investigate the results obtained, calculated and experimental densities and vapor pressures, for some terpenes and terpenoids presenting consistent data, are depicted in

Figure S4.2 and S4.3 of Appendix 4, respectively. In general, the approach is able to establish a ranking for the magnitude of the density and vapor pressure values of the different terpenes, in conformity to the experimental observed rank, and a correct temperature trend for vapor pressures (Figure S4.3). However, concerning the densities at low temperatures the correct temperature dependency is not always obtained showing that this cubic EoS should be used with precaution to estimate densities of liquids. Both EoS combined with the three method contribution groups here studied led to incorrect temperature dependency descriptions of the terpenes isopulegol, (-)-menthone, (S)-(+)-carvone, carvacrol, DL-citronellol, eugenol, geraniol and linalool. Moreover, using the SRK EoS, the experimental densities are always higher than the correspondent calculated ones; while the calculated vapor pressures are most of the times superior to the experimental. The same is observed using the EoS PR, with the exception of the Joback method, where the calculated densities are often superior to the experimental.

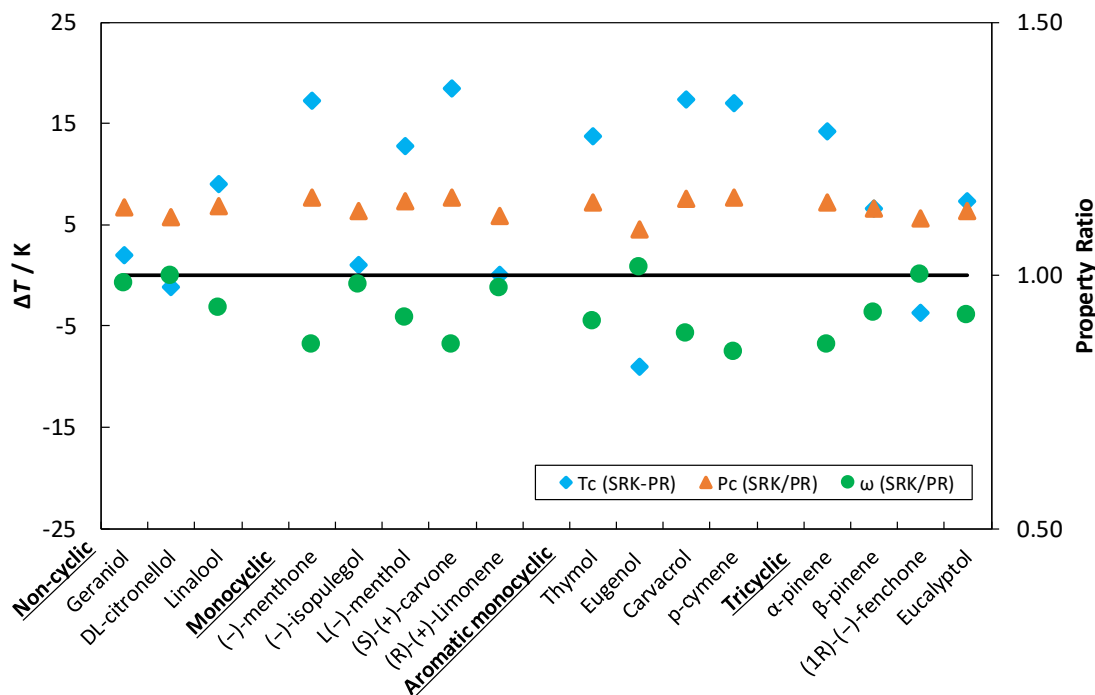
#### *II. Estimation of critical properties using experimental data and EoS*

In the second approach proposed, experimental densities and vapor pressures were used to estimate the critical properties and the acentric factor directly by EoS Soave-Redlich-Kwong and Peng-Robinson – Table 4.4. The critical properties obtained in previous section were used as initial estimates and the calculations performed until the minimum error between experimental and estimated data was obtained (equation 4.18). The values of the estimated critical properties are generally in the same range to those estimated by group contributions methods.

In Figure 4.6 the critical temperature changes and critical pressure and acentric factor property ratio between the two EoS applied is displayed. While critical pressures are always higher in SRK equation than in PR, acentric factors are almost always lower. Critical temperatures are almost always superior using SRK EoS.

**Table 4.4.** Critical properties and acentric factor of terpenes estimated according with the approach II.

	SRK			PR		
	$T_c / K$	$P_c / MPa$	$\omega$	$T_c / K$	$P_c / MPa$	$\omega$
(-)-menthone	702.09	3.16	0.391	684.83	2.75	0.453
(1R)-(-)-fenchone	671.30	3.36	0.403	675.00	3.02	0.403
(S)-(+)-carvone	743.14	3.65	0.389	724.76	3.17	0.452
Carvacrol	744.38	3.69	0.479	727.07	3.20	0.542
Eucalyptol	643.72	3.10	0.398	636.37	2.75	0.432
DL-citronellol	698.11	2.94	0.650	699.27	2.64	0.651
Eugenol	771.00	3.87	0.477	780.03	3.55	0.470
Geraniol	679.01	3.02	0.770	677.01	2.66	0.782
Isopulegol	690.01	3.22	0.490	689.05	2.86	0.500
Linalool	624.38	2.74	0.751	615.43	2.41	0.803
L(-)-menthol	659.80	2.94	0.713	647.03	2.56	0.779
R-(+)-Limonene	655.51	3.27	0.385	655.50	2.93	0.395
Thymol	713.60	3.57	0.576	699.92	3.12	0.634
$\alpha$ -pinene	629.57	3.23	0.338	615.39	2.83	0.392
$\beta$ -pinene	642.53	3.34	0.345	635.97	2.95	0.372
<i>p</i> -cymene	673.01	3.44	0.311	656.06	2.99	0.367

**Figure 4.6.** Temperature change ( $\Delta T / K$ ) and critical pressure and acentric factor ratio between Soave-Redlich-Kwong and Peng-Robinson EoS for the compounds studied.

Individual %ARD between the calculated and experimental densities and vapor pressures using SRK and PR EoS are presented in Figure 4.7. Globally both equations show a similar correlation capability, with the SRK EoS presenting an %ARD of 3.16 and 0.62 % for vapor pressure and density, respectively; while Peng Robinson EoS presented 3.61 and 0.66 %, for the same properties.

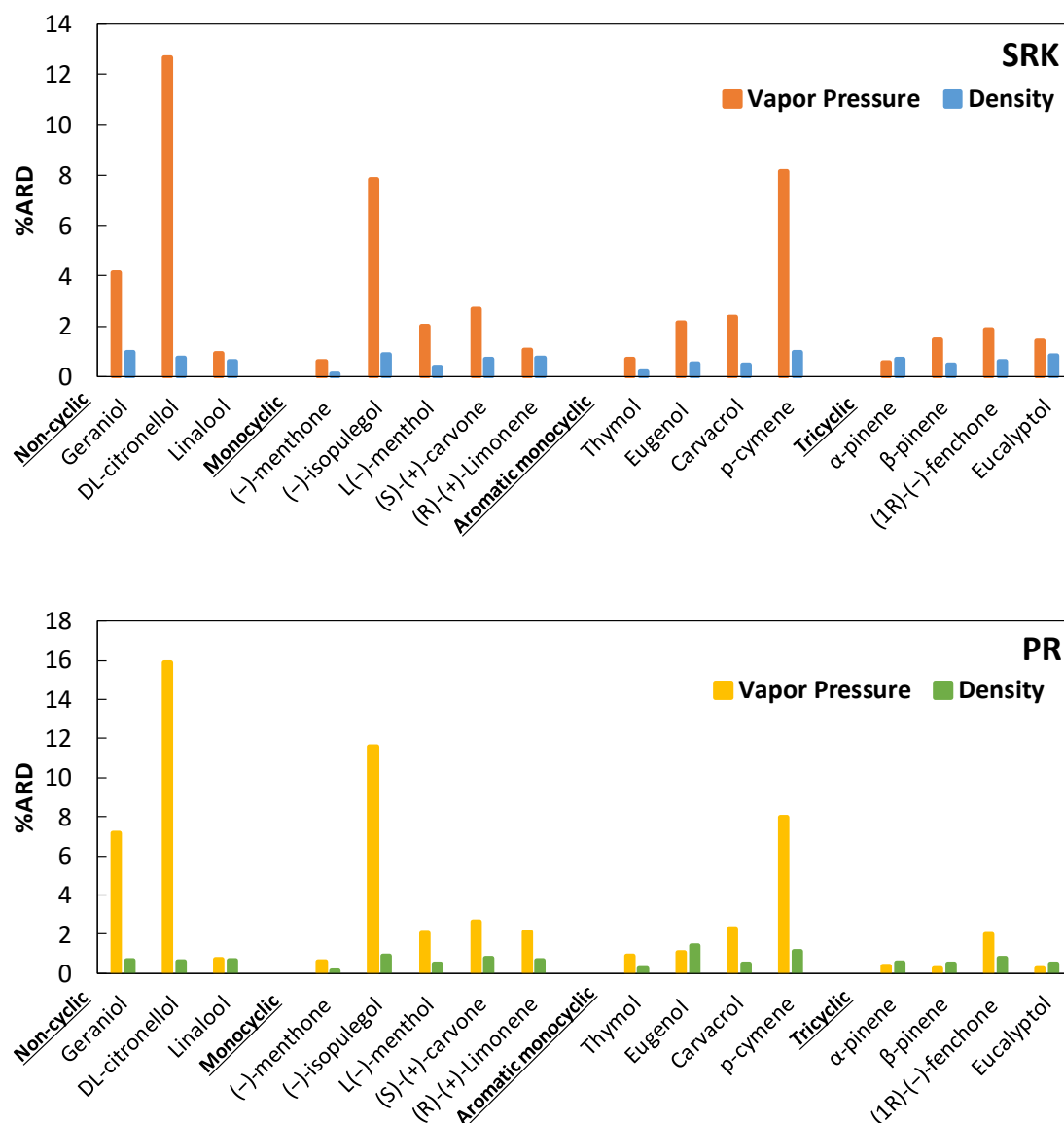


**Figure 4.7.** Average relative deviation between the experimental and the predicted densities and vapor pressures, calculated using the SRK and the PR, with critical properties estimated by the same EoS.

The vapor pressure of DL-citronellol, geraniol, (-)-isopulegol, and *p*-cymene show %ARD higher than the other compounds. Table S4.6 shows that there is a decrease followed by an increase in the %ARD with the temperature indicating an intersection of the series. For *p*-cymene the %ARD are randomly distributed with temperature. These are compounds with very low vapor pressures or for which data is available in a larger temperature range. This somehow stresses the difficulty of measuring vapor pressure and the need of new experimental data in this field.

Figure S4.4 and S4.5 of Appendix 4 show a comparison between calculated and experimental densities and vapor pressures, for some terpenes and using the EoS Peng-Robinson. Concerning vapor pressure, this second approach is able to establish a ranking for the magnitude of values in conformity to the experimental observed rank, and a correct temperature trend, while for density an important improvement is observed when compared with results shown before.

#### *Methods Comparison*

Comparing the critical properties and the acentric factor obtained by the group contribution methods and the EoS – Table 4.5 – is it possible to see that the differences between critical temperatures are minor. The absolute error obtained for critical pressure shows higher deviations between the contribution methods and the EoS SRK. The opposite is verified for acentric factors; however, the effect is less pronounced.

**Table 4.5.** Critical properties and acentric mean absolute error between those calculated by group contribution methods and those estimated by the SRK and PR EoS.

		PR	SRK
T <sub>c</sub> / K	Joback	17.61	17.09
	CG	19.58	17.68
	WJ	19.39	18.18
P <sub>c</sub> / MPa	Joback	0.15	0.33
	CG	0.45	0.74
	WJ	0.23	0.61
ω	Joback	0.08	0.08
	CG	0.16	0.12
	WJ	0.10	0.09

### Literature Analysis

For terpenes and terpenoids, experimental critical data is very rarely available, as only one work was found in the open literature.<sup>326</sup> The reason for this, is that higher molecular weight and strongly associating components readily decompose before the critical point is reached. This makes experimental measurements rather difficult and experimental errors very considerable. Table 4.6 presents, however, a comparison of critical temperatures estimated by the methods studied in this work, with the few experimental results, and some of the estimated values found in the literature for the same compounds.

**Table 4.6.** Comparison between estimated and experimental critical temperatures.

$T_c / K$	(R)-(+)-Limonene	$\alpha$ -pinene
CG	639.9	657.0
This Work	WJ	649.99
	SRK	655.51
	PR	655.50
Experimental <sup>326</sup>	653.0	644.0
Yaws <sup>246</sup>	640.0, 630.0	632.0, 644.0

Within this very limited set of experimental values, and taking into account the decomposition problem of this class of compounds, any further comparisons are premature. Regarding the estimated literature values, these are included in order to show the high variance of the critical properties values proposed in the literature, what establishes the importance of finding rational recommended values for the critical properties of terpenes and terpenoids.

#### 4.1.6. Conclusions

In this work three group-contribution methods for the estimation of critical properties are applied and analyzed for terpenes and terpenoids. As expected, the variance between the results is high and therefore, their suitability is tested through cubic equations of state, calculating densities and vapor pressure and comparing with experimental data. Results

indicate that the best combination is the Joback method and the Peng-Robinson EoS. Vapor pressure calculations globally showed higher average relative deviations between the predicted and the experimental values, when compared to density predictions. However, density predictions show problems at low temperatures. In the second part of this work, experimental densities and vapor pressures were used to estimate the critical properties and the acentric factor directly by EoS Soave-Redlich-Kwong and Peng-Robinson. The two equations show a similar correlation ability for densities and vapor pressures with SRK EoS presenting a global %ARD of 3.16 and 0.62 for vapor pressure and density, respectively; while Peng Robinson EoS presented 3.61 and 0.66 %, respectively for the same properties.

### **Clarifying note**

The next sections are related with the aqueous solubility of organic compounds, aiming the selection of the best methodology to apply to terpenes and thus contribute to the development of accurate models for the fate of these compounds in the environment. Since ILs have been studied to extract and fractionate terpenes, their mutual solubilities, densities and viscosities were measured (4.2) for a range of ILs and water. The same experimental method was applied to measure the solubility of terpenes in water that proved however to be inappropriate due to the formation of emulsions after stirring, which caused sampling problems. Thus, a new technique was implemented and firstly applied to sparingly soluble *N*-(diethylaminothiocarbonyl)benzimidazole derivatives (4.3) providing accurate results, and thus applied to determining the solubility of terpenes in water (4.4).

## **4.2. Mutual solubilities, densities and viscosities of ionic liquids and water**

### **4.2.1. Introduction**

Over the last years, ionic liquids (ILs) have been the subject of intensive investigations as a new class of neoteric solvents. Their thermodynamic data such as liquid–liquid equilibrium (LLE) and thermophysical properties have been widely study since they can be



used to develop thermodynamic models<sup>374</sup> and allow better understanding of the ILs nature, their benefits and limitations at an industrial scale.<sup>114</sup> Moreover, it is well-known that the ILs phase equilibrium and their thermophysical properties are significantly influenced by the presence of water,<sup>374,375</sup> a factor that makes the knowledge of the thermophysical and thermodynamic properties of water-saturated ILs very important together with the information that it provides on their environmental impact, toxicity and bioaccumulation.<sup>376</sup> Albeit non-volatile, even strongly hydrophobic ILs, such as the bis(trifluoromethylsulfonyl)imide-based fluids, present some solubility in water<sup>377</sup> and thus may create environmental problems in case of their accidental release into the environment.

In what concerns the IL-water miscibilities, the IL anion plays a major role although the cation also influences the hydrophobicity or hydrogen-bonding ability of the IL and can be further used to fine tune this property.<sup>378–387</sup> For instance, the 1-butyl-3-methylimidazolium cation, [C<sub>4</sub>C<sub>1</sub>im]<sup>+</sup>, in combination with anions like Cl<sup>-</sup>, Br<sup>-</sup>, [CF<sub>3</sub>SO<sub>3</sub>]<sup>-</sup> or [BF<sub>4</sub>]<sup>-</sup> are totally miscible with water at room temperature; yet, combined with [C(CN)<sub>3</sub>]<sup>-</sup>, [PF<sub>6</sub>]<sup>-</sup> or [NTf<sub>2</sub>]<sup>-</sup> they tend to phase separate at the same temperature.<sup>380</sup> However, if the alkyl side chain of the IL cation is sufficiently long, the IL-water system also display two phases, as happens with the [C<sub>6-10</sub>C<sub>1</sub>im][BF<sub>4</sub>] ILs.<sup>384,385</sup> Therefore, the wide array of possible cation-anion combinations allows a flexibility in designing new ionic fluids and in optimizing their physical/chemical properties for particular applications.

Densities and viscosities have been investigated over the last years, and a significant number of works have been published on the relationships between the structures of ILs and their fundamental properties.<sup>180,182,214,284,374,375,388–393</sup> On the other hand, systematic studies on the effect of water on the ILs densities and viscosities were also studied but are still scarce.<sup>214,235,392–397</sup> In all situations it was found that the water content has a strong effect on the viscosity of the ILs, while the effect is less significant on their densities.<sup>180,182,214,284,374,375,392,393</sup>

The works presented in this section are extensions of our investigation into water-ILs miscibility for ILs containing the bis(trifluoromethylsulfonyl)imide anion.<sup>182,378,380–382</sup> The

systems studied so far showed a very low solubility of ILs in the water-rich phase, considerable water mole fraction solubility in the IL-rich phase, and an upper critical solution behavior. As part of our ongoing work on the LLE between [NTf<sub>2</sub>]-based ILs and water, we present here new data for ILs that have been hitherto poorly investigated, focused on the structural variations of the cation, namely the number of alkyl side chains and their structural isomerism. Moreover, the densities and viscosities of binary mixtures of water and ILs, namely for ILs composed of the common anion bis(trifluoromethylsulfonyl)imide, are discussed.

#### 4.2.2. Experimental methods

##### Mutual solubilities

The mutual solubilities between water and ILs were determined in the temperature range from (288.15 to 318.15) K and at atmospheric pressure using a LLE method previously detailed.<sup>378,380</sup> The ionic liquid and water phases were initially vigorously stirred and allowed to settle and equilibrate for at least 48 h.<sup>374</sup> This period of time proved to be enough to guarantee a complete separation of the two phases, as well as their saturation. The samples, in tightly-closed glass vials with a septum cap, were put inside an aluminum block specially designed for this purpose, as schematically depicted in Figure 4.8. The isolated air bath is capable of maintaining the temperature within  $\pm 0.01$  K. The temperature control was achieved with a PID temperature controller driven by a calibrated Pt100 (class 1/10) temperature sensor inserted in the aluminium block. A Julabo (model F25-HD) refrigerated bath and circulator was used as the cooling source of the thermostated aluminium block. The temperature accuracy was  $\pm 0.01$  K. Both phases were sampled at each temperature from the equilibrium vials using glass syringes maintained dry and kept at the same temperature of the measurements.

The solubility of water in the IL-rich phase was measured by KF titration, whereas the solubility of IL in the water-rich phase was measured by UV-Vis spectroscopy, using a SHIMADZU UV-1700 PharmaSpec Spectrometer ( $\lambda = 209$  nm for [C<sub>1</sub>im][NTf<sub>2</sub>] and [C<sub>2</sub>im][NTf<sub>2</sub>]; and 211 nm for all other ILs). This wavelength was found to be the maximum UV absorption wavelength for the imidazolium-based ILs investigated here.

Approximately 0.1 g of the IL-rich phase was sampled and directly injected in the KF coulometric titrator to determine the water content. For the water-rich phase, *ca.* 0.5 g of each sample was taken and diluted in (250-500) cm<sup>3</sup> of ultrapure water. At each temperature, each measurement was repeated at least 5 times, and the results are reported as the average solubility value along with the respective standard deviations. In case of observing large standard deviations, new equilibrium phases were produced and new measured values added.

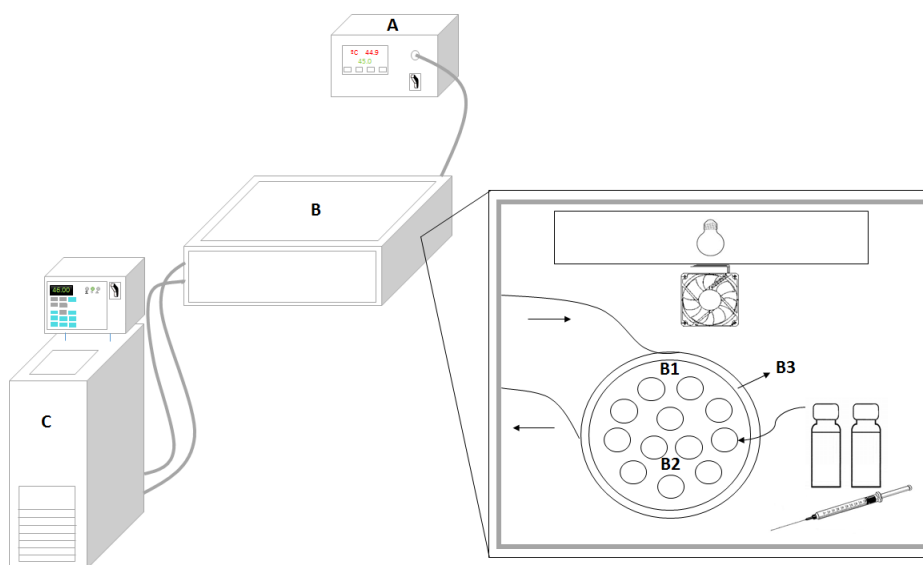


**Figure 4.8.** Scheme of the apparatus used for the mutual solubility measurements. (A), PID temperature controller; (B), Isolated air bath; (B1) Aluminum block; (B2), Pt100 (class 1/10) temperature sensor; (B3), Thermostatic fluid; (C), Refrigerated bath.

### Densities and viscosities

Densities and viscosities measurements of water-saturated ILs (of the IL-rich phase) were carried out at atmospheric pressure and in the (298.15 and 363.15) K temperature range using an automated SVM3000 Anton Paar rotational Stabinger viscometer-densimeter. The uncertainty of temperature is  $\pm 0.02$  K, the relative uncertainty in the dynamic viscosity is  $\pm 0.35\%$ , and the absolute uncertainty in density is  $\pm 5 \cdot 10^{-4}$  g·cm<sup>-3</sup>. Saturated solutions were prepared, at 298.15 K, by mixing ILs and water in excess amounts and allowing the mixture to reach the equilibrium by the complete separation of the two phases, and for at least 48h.<sup>374</sup>

### 4.2.3. Theoretical approach

#### COSMO-RS

COSMO-RS is a predictive method developed by Klamt and co-workers for providing the thermodynamic equilibrium of fluids and mixtures and that uses a statistical thermodynamic approach based on the results of unimolecular quantum chemical calculations.<sup>200,218</sup> The model can be used to predict the phase behavior of binary mixtures and subsequently the concentration of each component in a given phase.<sup>197,398</sup> Previously we used COSMO-RS to predict the equilibrium behavior of ILs and water and confirmed its high capability as a predictive tool.<sup>377,380</sup>

The standard procedure of COSMO-RS calculations employed in this work consisted essentially in two steps: (i) the continuum solvation COSMO calculations of electronic density and molecular geometry that were performed with the TURBOMOLE 6.1 program package on the density functional theory level, utilizing the BP functional B88-P86 with a triple- $\zeta$  valence polarized basis set (TZVP) and the resolution of identity standard (RI) approximation;<sup>220</sup> (ii) the estimation of the phase diagrams of binary mixtures of ILs and water performed with the COSMOtherm program using the parameter file BP\_TZVP\_C20\_0111 (COSMOlogic GmbH & Co KG, Leverkusen, Germany).<sup>399</sup> The detailed calculation of the phase equilibrium using COSMOtherm is explained in our previous work.<sup>400</sup> In all calculations, the ILs were always treated as isolated ions at the quantum chemical level. In a previous work,<sup>401</sup> the best predictions of the experimental data were obtained with the lowest energy conformations or with the global minimum for both cation and anion. Thus, in this work, the lowest energy conformations of all the species involved were used in the COSMO-RS calculations.

#### Temperature dependence and thermodynamic functions of solution

To describe the temperature dependence of the experimental mutual solubilities aiming at determining the thermodynamic functions of solution, two correlations were employed. The solubility of water in the IL-rich phase is described by Equation 4.19, while the solubility of IL in the water-rich phase is expressed using Equation 4.20,<sup>402</sup>

$$\ln x_1 = A + \frac{B}{T/K} \quad (4.19)$$

$$\ln x_2 = C + \frac{D}{T/K} + E \ln(T/K) \quad (4.20)$$

where  $x_1$  is the mole fraction solubility of water in the ionic liquid;  $x_2$  is the mole fraction solubility of the ionic liquid in water;  $T$  is the absolute temperature; and  $A$ ,  $B$ ,  $C$ ,  $D$ , and  $E$  are fitted parameters. For the solubility of water in the IL-rich phase, it is assumed that the process occurs at constant molar enthalpy of solution while for the solubility of the ILs in water, there is a significant dependence on temperature for the enthalpy of solution.

Aiming at exploring the molecular mechanisms behind the solvation phenomena, the molar thermodynamic properties of solution, namely the standard molar Gibbs energy ( $\Delta_{sol}G_m^0$ ), enthalpy ( $\Delta_{sol}H_m^0$ ) and entropy ( $\Delta_{sol}S_m^0$ ) of solution were derived. These thermodynamic properties are associated with changes that occur in the solute neighborhood when one solute molecule is transferred from an ideal gas phase to a diluted ideal solution and were calculated using Equations 4.21-4.23<sup>378</sup> for the water-rich phase, where the solute could be considered at infinite dilution. In the IL-rich phase, the solubility of water is higher and the associated thermodynamic molar functions cannot be determined.

$$\Delta_{sol}G_m^0 = -RT \ln(x_2)_p \quad (4.21)$$

$$\frac{\Delta_{sol}H_m^0}{RT^2} = \left( \frac{\partial \ln x_2}{\partial T} \right)_p \quad (4.22)$$

$$\Delta_{sol}S_m^0 = R \left[ \frac{\partial (T \ln x_2)}{\partial T} \right]_p \quad (4.23)$$

where  $x_2$  is the mole fraction solubility of ionic liquid in water,  $R$  is the ideal gas constant, subscript  $p$  indicates isobaric condition during the process and the subscript  $m$  refers to molar quantity.

Furthermore, when dealing with liquid-liquid equilibrium, the standard molar properties of solvation can be estimated using the following equations:<sup>378</sup>

$$\Delta_{sol}H_m^0 = \Delta_{svt}H_m^0 + \Delta_l^gH_m^0 \quad (4.24)$$

$$\Delta_{svt}G_m^0 = \Delta_{sol}G_m^0 + RT \ln\left(\frac{p(s2,T)}{p^0}\right) \quad (4.25)$$

$$\Delta_{svt}S_m^0 = \frac{\Delta_{svt}H_m^0 - \Delta_{svt}G_m^0}{T} \quad (4.26)$$

where  $p(s2,T)$  is the vapor pressure of the solute at the temperature  $T$  and  $p^0$  is the standard pressure of  $10^5$  Pa.

The standard molar enthalpy of solution,  $\Delta_{sol}H_m^0$ , is a sum of the standard molar enthalpy of solvation,  $\Delta_{svt}H_m^0$ , that reflects the solute-solvent interaction, and the standard molar enthalpy of vaporization of the solute to form an ideal gas,  $\Delta_l^gH_m^0$ . The standard molar Gibbs energy of solvation,  $\Delta_{svt}G_m^0$ , can be then derived using the hypothetical reference state for the solute, which considers the solute in the gas phase and at the standard pressure.

### Density

From the linear dependency of the density with temperature, at 0.1 MPa, the isobaric thermal expansion coefficient,  $\alpha_p$  (which considers the volumetric changes with temperature), can be calculated according to Equation 4.28, that is further derived from Equation 4.27 used to correlate the density as a function of temperature,

$$\ln \rho = A_0 + A_1 T \quad (4.27)$$

$$\alpha_p = -\frac{1}{\rho} \left( \frac{\partial \rho}{\partial T} \right)_p = -\left( \frac{\partial \ln \rho}{\partial T} \right)_p = -A_1 \quad (4.28)$$

where  $A_0$ , and  $A_1$  are fitting parameters,  $\rho$  is the density in  $\text{kg}\cdot\text{m}^{-3}$  and  $T$  is the absolute temperature in K.

Methods to estimate the mutual solubilities of ILs and water are of utmost importance due to the enormous possible combinations of cations and anions to form ILs and, consequently, the extended number of experimental measurements necessary. For the prediction of the solubility of ILs in the water-rich phase, several methods have been proposed.<sup>403</sup> However, and as a consequence of the dominant hydrogen-bonding interactions, the solubility of water in the IL-rich phase is more difficult to predict. In this sense, a faster, easier, and reliable method supported on the densities of pure and water-saturated ILs can be used.<sup>375</sup> Thus, and assuming that the excess molar volumes are negligible in the narrow mole fraction solubility range, the ILs water solubility can be estimated using the following equations,

$$V_{m,mixture} = V_{m,IL} \times (1 - x_w) + V_{m,w} \times x_w \quad (4.29)$$

$$V_{m,mixture} = \frac{(1 - x_w) \times M_{IL} + x_w \times M_w}{\rho_{mixture}} \quad (4.30)$$

where  $M$  is the molecular weight in  $\text{kg}\cdot\text{mol}^{-1}$  and  $V_m$  is the molar volume in  $\text{m}^3\cdot\text{mol}^{-1}$ . The subscripts  $IL$ ,  $w$ , and  $mixture$  are IL, water and water-saturated ILs, respectively.

### Viscosity

The viscosity describes the internal resistance of a fluid to a shear stress, and as it is well-known, most ILs display higher viscosities than common molecular solvents. The ILs high viscosities are a direct consequence of their high molecular weights as well as their multiple intermolecular interactions (H-bonding, dispersive and electrostatic interactions). The energy barrier ( $E$ ) is the energy value that must be overcome in order for the ions to move past each other in the fluid.<sup>181</sup> The larger is  $E$ , the harder it is for the ions to move past each other, which is inherently related with the interactions occurring in the fluid. The energy barrier can thus be correlated with structural information on the IL, and can be determined based on the viscosity dependence with temperature using the following equation,<sup>182</sup>

$$E = R \frac{\partial(\ln[\eta(T)])}{\partial(1/T)} \quad (4.31)$$

where  $\eta$  is viscosity in mPa's, and  $R$  is the gas constant.

In order to calculate the energy barrier of the water-saturated ILs studied in this work, the experimental viscosity data were initially correlated through the Vogel–Tammann–Fulcher (VTF) model,<sup>180</sup> expressed by equation 4.32,

$$\eta(T) = A_{\eta} \exp\left[\frac{B_{\eta}}{T - C_{\eta}}\right] \quad (4.32)$$

where  $A_{\eta}$ ,  $B_{\eta}$ , and  $C_{\eta}$  are adjustable parameters estimated from experimental data.

#### 4.2.4. Impact of the cation symmetry on the mutual solubilities between water and imidazolium-based ionic liquids

Mónia A. R. Martins, Catarina M. S. S. Neves, Kiki A. Kurnia, Andreia Luís, Luís M. N. B. F. Santos, Mara G. Freire, Simão P. Pinho & João A. P. Coutinho, *Fluid Phase Equilibria* 375 161–167 (2014), DOI: 10.1016/j.fluid.2014.05.013

##### 4.2.4.1. Abstract

Aiming at the evaluation of the impact of the ionic liquids (ILs) cation symmetry on their phase behavior, in this work, novel mutual solubilities with water of the symmetric series of  $[C_nC_n\text{im}][\text{NTf}_2]$  (with  $n = 1-5$ ) were determined and compared with their isomeric forms of the asymmetric  $[C_nC_1\text{im}][\text{NTf}_2]$  group. While the solubility of isomeric ILs in water was found to be similar, the solubility of water in ILs follows the same trend up to a maximum cation alkyl side chain length. For  $n \geq 4$  in  $[C_nC_n\text{im}][\text{NTf}_2]$  the solubility of water in the asymmetric ILs is slightly higher than that observed in the asymmetric counterparts. The thermodynamic properties of solution and solvation derived from the experimental solubility data of ILs in water at infinite dilution, namely the free Gibbs energy, enthalpy and entropy were used to evaluate the cation symmetry effect on the ILs solvation. It is shown that the solubility of ILs in water is entropically driven and highly influenced by the cation size. Accordingly, it was found that the ILs solubility in water of both the symmetric and asymmetric series depends on their molecular volume. Based on these findings, a



linear correlation between the logarithm of the solubility of ILs in water and their molar volume is here proposed for the [NTf<sub>2</sub>]-based ILs at a fixed temperature.

#### 4.2.4.2. Chemicals

The experimental mutual solubilities with water were carried out for the 5 ILs presented in Table 4.7. The chemical structures of the studied compounds are presented in Figure 4.9. To reduce their impurities, individual samples of ILs were dried under vacuum at 0.1 Pa and 353.15 K, under constant stirring, and for a minimum period of 48 h. After, the purity of each IL was checked by <sup>1</sup>H, <sup>13</sup>C, and <sup>19</sup>F NMR. The water content of the dried ILs was determined using a Metrohm 831 Karl Fischer (KF) coulometer, with the analyte Hydranal® - Coulomat AG from Riedel-de Haën, and was found to be below 100 ppm for all samples. Ultrapure water, double distilled, passed by a reverse osmosis system and further treated with a MilliQ plus 185 water purification apparatus, was used throughout the mutual solubility experiments ( $M(\text{H}_2\text{O}) = 18.01528 \text{ g}\cdot\text{mol}^{-1}$ ). The water used presents a resistivity of 18.2 MΩ·cm, a TOC smaller than 5 µg·dm<sup>-3</sup> and is free of particles > 0.22 µm.

**Table 4.7.** Investigated ionic liquids: name, abbreviation, source, molecular mass ( $M$ ), and purity.

Chemical Name	Abbreviation	Source	$M$ (g·mol <sup>-1</sup> )	Purity (mass %)
1,3-dimethylimidazolium bis((trifluoromethyl)sulfonyl)imide	[C <sub>1</sub> C <sub>1</sub> im][NTf <sub>2</sub> ]	Iolitec	377.29	> 99
1,3-diethylimidazolium bis((trifluoromethyl)sulfonyl)imide	[C <sub>2</sub> C <sub>2</sub> im][NTf <sub>2</sub> ]	Iolitec	405.34	> 99
1,3-dipropylimidazolium bis((trifluoromethyl)sulfonyl)imide	[C <sub>3</sub> C <sub>3</sub> im][NTf <sub>2</sub> ]	Iolitec	433.39	> 99
1,3-dibutylimidazolium bis((trifluoromethyl)sulfonyl)imide	[C <sub>4</sub> C <sub>4</sub> im][NTf <sub>2</sub> ]	Iolitec	461.45	> 99
1,3-dipentylimidazolium bis((trifluoromethyl)sulfonyl)imide	[C <sub>5</sub> C <sub>5</sub> im][NTf <sub>2</sub> ]	Iolitec	489.50	> 99

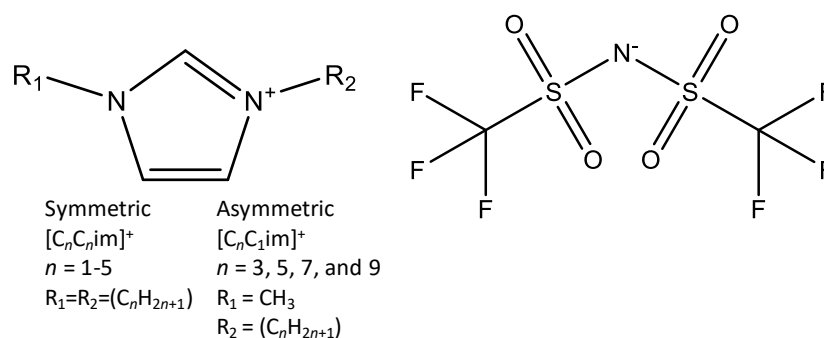


**Figure 4.9.** Chemical structures of the studied imidazolium-based ILs.

#### 4.2.4.3. Results and discussion

##### Mutual solubilities between ionic liquids and water

The novel experimental solubility data for the series  $[C_nC_n\text{im}][\text{NTf}_2]$  (with  $n = 1-5$ ), along with the respective standard deviations, are presented in Table 4.8 and 4.9. The solubility data for the asymmetric imidazolium-based ILs,  $[C_nC_1\text{im}][\text{NTf}_2]$  (with  $n = 2-8$ ) were previously reported,<sup>378</sup> and are here used for comparison purposes.

**Table 4.8.** Experimental mole fraction solubility of water ( $x_w$ ) in ILs as a function of temperature and at 0.10 KPa.<sup>a</sup>

$T / \text{K}$	$[C_1C_1\text{im}][\text{NTf}_2]$	$[C_2C_2\text{im}][\text{NTf}_2]$	$[C_3C_3\text{im}][\text{NTf}_2]$	$[C_4C_4\text{im}][\text{NTf}_2]$	$[C_5C_5\text{im}][\text{NTf}_2]$
	$x_w$	$x_w$	$x_w$	$x_w$	$x_w$
288.15	0.312 (0.002)	0.241 (0.004)	0.194 (0.007)	0.159 (0.004)	0.132 (0.002)
293.15	0.335 (0.002)	0.261 (0.001)	0.206 (0.001)	0.172 (0.001)	0.148 (0.001)
298.15	0.354 (0.004)	0.277 (0.001)	0.223 (0.001)	0.184 (0.003)	0.158 (0.001)
303.15	0.376 (0.001)	0.290 (0.001)	0.240 (0.002)	0.196 (0.002)	0.170 (0.001)
308.15	0.395 (0.001)	0.305 (0.002)	0.255 (0.002)	0.207 (0.002)	0.184 (0.002)
313.15	0.424 (0.006)	0.322 (0.002)	0.270 (0.001)	0.219 (0.006)	0.197 (0.001)
318.15	0.451 (0.007)	0.341(0.001)	0.285 (0.003)	0.233 (0.002)	0.209 (0.002)

<sup>a</sup>The correspondent standard deviation is presented between brackets. Standard uncertainties,  $u$ , are  $u(T) = 0.01 \text{ K}$ , and  $u_r(p) = 0.05 \text{ KPa}$ .

**Table 4.9.** Experimental mole fraction solubility of ionic liquid ( $x_{IL}$ ) in water as a function of temperature and at 0.10 KPa.<sup>a</sup>

$T / K$	[C <sub>1</sub> C <sub>1</sub> im][NTf <sub>2</sub> ]	[C <sub>2</sub> C <sub>2</sub> im][NTf <sub>2</sub> ]	[C <sub>3</sub> C <sub>3</sub> im][NTf <sub>2</sub> ]	[C <sub>4</sub> C <sub>4</sub> im][NTf <sub>2</sub> ]	[C <sub>5</sub> C <sub>5</sub> im][NTf <sub>2</sub> ]
	$10^3 \cdot x_{IL}$	$10^4 \cdot x_{IL}$	$10^4 \cdot x_{IL}$	$10^5 \cdot x_{IL}$	$10^5 \cdot x_{IL}$
288.15	1.38 (0.03)	5.23 (0.04)	1.82 (0.02)	6.89 (0.02)	1.94 (0.03)
293.15	1.42 (0.01)	5.31 (0.03)	1.86 (0.01)	7.03 (0.02)	2.05 (0.08)
298.15	1.49 (0.01)	5.36 (0.01)	1.92 (0.02)	7.25 (0.01)	2.11 (0.02)
303.15	1.60 (0.02)	5.79 (0.04)	2.00 (0.01)	7.62 (0.01)	2.23 (0.01)
308.15	1.69 (0.01)	6.13 (0.05)	2.06 (0.04)	7.90 (0.07)	2.35 (0.01)
313.15	1.72 (0.01)	6.50 (0.06)	2.14 (0.02)	9.00 (0.06)	2.50 (0.02)
318.15	2.03 (0.02)	7.04 (0.08)	2.25 (0.02)	9.61 (0.07)	2.71 (0.04)

<sup>a</sup>The correspondent standard deviation is presented between brackets. Standard uncertainties,  $u$ , are  $u(T) = 0.01$  K, and  $u_r(p) = 0.05$  KPa.

The inspection of Table 4.8 indicates that the solubility of water in the IL is always above 0.1 in mole fraction, despite the “hydrophobic” label usually attributed to the [NTf<sub>2</sub>]-based ILs. Table 4.9, on the other hand, indicates that the mole fraction solubility of ILs in water is in the order of  $10^{-3}$  to  $10^{-5}$ , and therefore the dissolved ILs can be considered at infinite dilution.

The liquid-liquid phase diagrams of all the [C<sub>*n*</sub>C<sub>*n*</sub>im][NTf<sub>2</sub>] ILs studied, along with the [C<sub>*n*</sub>C<sub>1</sub>im][NTf<sub>2</sub>] previously investigated,<sup>380</sup> are depicted in Figure 4.10. Concerning the phase diagrams, two features must be highlighted: (i) the studied ILs and water binary systems display a common UCST behavior asymmetrically centered in the low-concentration region of the ILs; (ii) the mutual solubilities between ILs and water, in both series, decrease with increasing the cation alkyl side chain of ILs. This is the expectable behavior given the increasing hydrophobic nature of ILs with the aliphatic moiety increase. These features are also observed in the phase behavior of water with other imidazolium-based ILs combined with the [BF<sub>4</sub>]<sup>-</sup> or [PF<sub>6</sub>]<sup>-</sup> anions.<sup>380,384,404</sup>

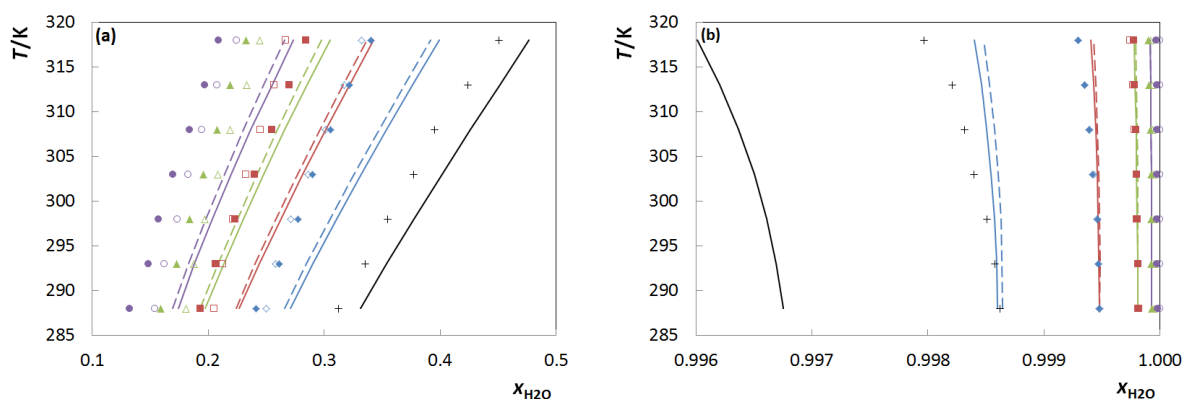


**Figure 4.10.** Liquid-liquid phase diagrams of water and ionic liquids: (a) ionic-liquid-rich phase; and (b) water-rich phase. Symbols (experimental data): (+),  $[C_1C_1im][NTf_2]$ ; ( $\blacklozenge$ ),  $[C_2C_2im][NTf_2]$ ; ( $\blacklozenge$ ),  $[C_3C_1im][NTf_2]$ ; ( $\blacksquare$ ),  $[C_3C_3im][NTf_2]$ ; ( $\square$ ),  $[C_5C_1im][NTf_2]$ ; ( $\blacktriangle$ ),  $[C_4C_4im][NTf_2]$ ; ( $\blacktriangle$ ),  $[C_7C_1im][NTf_2]$ ; ( $\bullet$ ),  $[C_5C_5im][NTf_2]$ ; and ( $\circ$ ),  $[C_9C_1im][NTf_2]$ . The matching color full and dashed lines represent, respectively, the COSMO-RS predictions for the ILs containing asymmetric and symmetric cations.

In order to check the validity of the results obtained, a literature revision was made. Data for the mutual solubilities with water of  $[C_1C_1im][NTf_2]$ <sup>405</sup> and  $[C_2C_2im][NTf_2]$ <sup>406</sup> were found and are represented in Figure 4.11 together with the experimental values. As can be seen, in the ionic liquid rich phase, Figure 4.11a, the discrepancy is not significant for both ionic liquids, and taking in account the different experimental conditions we can conclude that values are in agreement. However, in the water rich-phase, Figure 4.11b, the values presented for Gardas and co-workers<sup>405</sup> are considerably distinct. These data don't present an upper critical solution temperature behavior as was expected and as was already proved in some works.<sup>380,384,404</sup> It is worth to say that Domańska and co-workers<sup>406</sup> also presented two points in the water-rich phase, but the temperatures used are much different from the ones used in the present work and, thus, they do not allow a reasonable comparison.

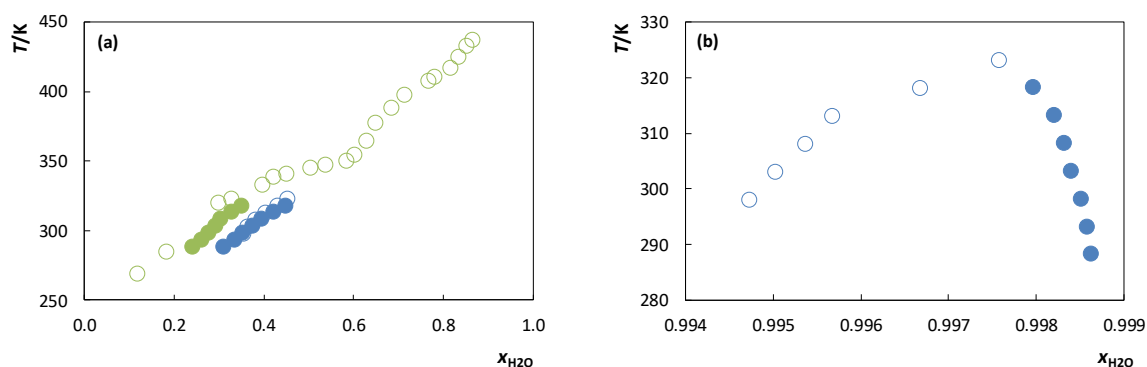


**Figure 4.11.** Comparison with literature data: (a) ionic-liquid-rich phase; and (b) water-rich phase. Symbols: (●), [C<sub>1</sub>C<sub>1</sub>im][NTf<sub>2</sub>] this work; (○), [C<sub>1</sub>C<sub>1</sub>im][NTf<sub>2</sub>]<sup>405</sup>; (●), [C<sub>2</sub>C<sub>2</sub>im][NTf<sub>2</sub>] this work; and (○), [C<sub>2</sub>C<sub>2</sub>im][NTf<sub>2</sub>]<sup>406</sup>.

The main goal of this work is to provide a better understanding of the impact of the symmetry of the IL cation and, to this end, two series of ILs are compared: symmetric and asymmetric ones with the same number of total methylene groups in the alkyl side chains. Figure 4.10a shows that the solubility of water in [C<sub>2</sub>C<sub>2</sub>im][NTf<sub>2</sub>] and [C<sub>3</sub>C<sub>3</sub>im][NTf<sub>2</sub>] are similar to those of their structural analogues or isomers, [C<sub>3</sub>C<sub>1</sub>im][NTf<sub>2</sub>] and [C<sub>5</sub>C<sub>1</sub>im][NTf<sub>2</sub>], respectively. On the other hand, water presents a somewhat lower solubility in [C<sub>4</sub>C<sub>4</sub>im][NTf<sub>2</sub>] and [C<sub>5</sub>C<sub>5</sub>im][NTf<sub>2</sub>] than on [C<sub>7</sub>C<sub>1</sub>im][NTf<sub>2</sub>] and [C<sub>9</sub>C<sub>1</sub>im][NTf<sub>2</sub>].<sup>407</sup> Thus, for the long alkyl chain length isomers, the ILs with an asymmetric cation are able to dissolve a higher content of water. A symmetry-asymmetry effect was also recently reported for other properties of the same ILs series, such as density and viscosity,<sup>182</sup> volatility,<sup>408</sup> heat capacity,<sup>409,410</sup> surface tension,<sup>411,412</sup> and refractive index.<sup>413</sup>

The solubility of isomeric ILs in water is essentially identical, as shown in Figure 4.10b. The solubility of poorly soluble compounds in water, is known to be primarily controlled by their molar volume.<sup>382</sup> Since the molar volume for isomeric ILs is identical, containing either symmetric or asymmetric cations, their solubilities in water are very close. The effect of the molar volume,  $V_m$ , on the solubility of ionic liquids in water has been discussed in our previous works.<sup>377,381</sup> The  $V_m$  of each ionic liquid at 298.15 K was determined based on experimental density data taken from literature,<sup>182</sup> and the aqueous solubility experimental data used were those obtained in this work along with

other results taken from the literature.<sup>378</sup> The dependence of the IL solubility in the water-rich phase with the IL molar volume, at 298.15 K, is shown in Figure 4.12. A very good correlation between the logarithm of the solubility,  $\ln(x_{\text{IL}})$ , and the molar volume,  $V_m$ , was obtained while covering a wide range of magnitudes regarding the solubility mole fraction data. Thus, it is here shown that a large range of solubilities of [NTf<sub>2</sub>]-based ILs in water can be estimated using their molar volumes and the equation provided in Figure 4.12 caption.

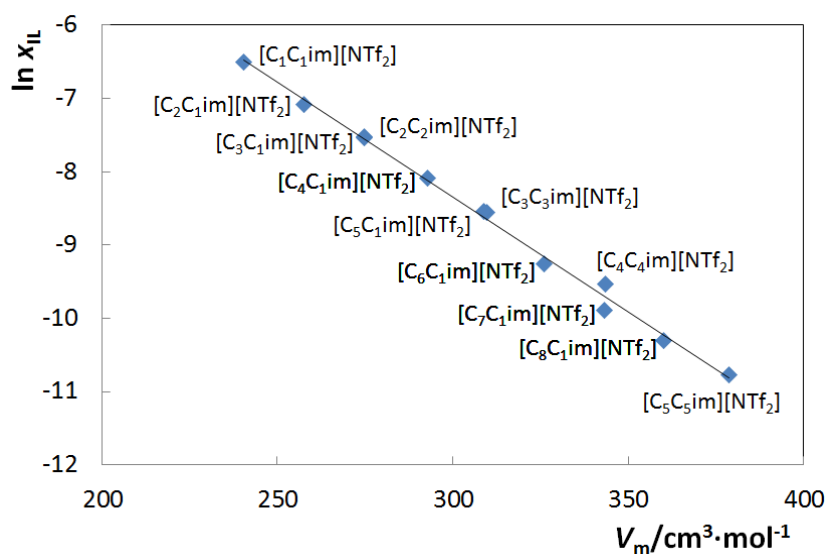


**Figure 4.12.** Solubility of [NTf<sub>2</sub>]-based ILs in water (expressed in mole fraction) as function of the IL molar volume:  $\ln(x_{\text{IL}}) = -0.0309 (V_m/\text{cm}^3 \cdot \text{mol}^{-1}) + 0.9357$ ;  $R^2 = 0.9947$ . All data are at 298.15 K.

### Temperature dependence and thermodynamic functions of solution

The fitted parameters of equations 4.19 and 4.20 along with their standard deviations are presented in Table 4.10. The proposed correlations present a maximum relative deviation in the experimental mole fraction data of 2 and 3%, for the water-rich and IL-rich phases, respectively.

The molar thermodynamic properties of the ionic liquid solvation in water are reported in Table 4.11 at 298.15 K.

**Table 4.10.** Estimated parameters for the mole fraction of water in the IL-rich phase and IL in the water-rich phase estimated using Equations 4.19 and 4.20, respectively.<sup>a</sup>

Ionic liquid	A	B / K	C	D / K	E
[C <sub>1</sub> C <sub>1</sub> im][NTf <sub>2</sub> ]	2.65 (0.08)	-1098 (23)	-337 (83)	13938 (3744)	50 (12)
[C <sub>2</sub> C <sub>2</sub> im][NTf <sub>2</sub> ]	2.11 (0.09)	-1102 (28)	-359 (73)	15065 (3322)	53 (11)
[C <sub>3</sub> C <sub>3</sub> im][NTf <sub>2</sub> ]	2.52 (0.08)	-1197 (24)	-131 (28)	4954 (1240)	19 (4)
[C <sub>4</sub> C <sub>4</sub> im][NTf <sub>2</sub> ]	2.12 (0.07)	-947 (34)	-462 (96)	19516 (4309)	68 (14)
[C <sub>5</sub> C <sub>5</sub> im][NTf <sub>2</sub> ]	2.76 (0.15)	-1372 (38)	-217 (45)	8495 (2022)	31 (7)

<sup>a</sup>The correspondent standard deviation is presented between brackets.

**Table 4.11.** Standard thermodynamic molar properties of solution of ionic liquids in water at 298.15 K.<sup>a</sup>

	$\Delta_{sol}H_m^0 / \text{kJ} \cdot \text{mol}^{-1}$	$\Delta_{sol}G_m^0 / \text{kJ} \cdot \text{mol}^{-1}$	$\Delta_{sol}S_m^0 / \text{J} \cdot \text{K}^{-1} \cdot \text{mol}^{-1}$
[C <sub>1</sub> C <sub>1</sub> im][NTf <sub>2</sub> ]	7.6 (1.5)	16.131 (0.017)	-28.6 (5.0)
[C <sub>2</sub> C <sub>2</sub> im][NTf <sub>2</sub> ]	5.8 (1.5)	18.672 (0.014)	-43.3 (5.0)
[C <sub>3</sub> C <sub>3</sub> im][NTf <sub>2</sub> ]	4.7 (1.5)	21.218 (0.026)	-55.2 (5.0)
[C <sub>4</sub> C <sub>4</sub> im][NTf <sub>2</sub> ]	6.0 (1.5)	23.629 (0.003)	-59.2 (5.0)
[C <sub>5</sub> C <sub>5</sub> im][NTf <sub>2</sub> ]	7.0 (1.5)	26.687 (0.024)	-66.1 (5.0)

<sup>a</sup>The correspondent standard deviation is presented between brackets.

At 298.15 K, the standard Gibbs energy of solution of the ILs in water increases with the alkyl chain leading to a lower solubility in water with the increase of the respective aliphatic moieties. The enthalpies of solution derived from experimental data show that the dissolution of ionic liquids in water is an endothermic process, thus leading to an UCST-type of phase diagram. As previously shown, the enthalpies of solution of ILs in water are very little dependent on the alkyl side chain length of the cation,<sup>378</sup> and this trend is also observed with the symmetric [C<sub>n</sub>C<sub>n</sub>im][NTf<sub>2</sub>] series of ILs. These results confirm that the solubility of ILs in water is entropically driven, as previously observed for [C<sub>n</sub>C<sub>1</sub>im][NTf<sub>2</sub>]<sup>378</sup> and [PF<sub>6</sub>]-based ILs.<sup>380</sup> Figure 4.13 presents the experimental entropies of [C<sub>n</sub>C<sub>n</sub>im][NTf<sub>2</sub>], [C<sub>n</sub>C<sub>1</sub>im][NTf<sub>2</sub>],<sup>378</sup> and [C<sub>n</sub>C<sub>1</sub>im][PF<sub>6</sub>]<sup>380</sup> as function of total methylene groups in the two alkyl side chains, *N*. The entropies of solution of these three series of ILs

in water exhibit a small decrease in the entropy of solution of approximately  $-5 \text{ J}\cdot\text{K}^{-1}\cdot\text{mol}^{-1}$  per methylene addition to the cation. In addition, the entropies of solution of ILs in water decrease with increasing cation alkyl side chain length, regardless of the anion. Thus, it can be concluded that the decrease of the ILs solubility with the increase of the alkyl side chain length is driven by the linear decrease of the entropy of solution, related with the increase of the cavitation entropy very identical to that the observed in the solvation of linear alkanes and alcohols in water.<sup>414,415</sup>

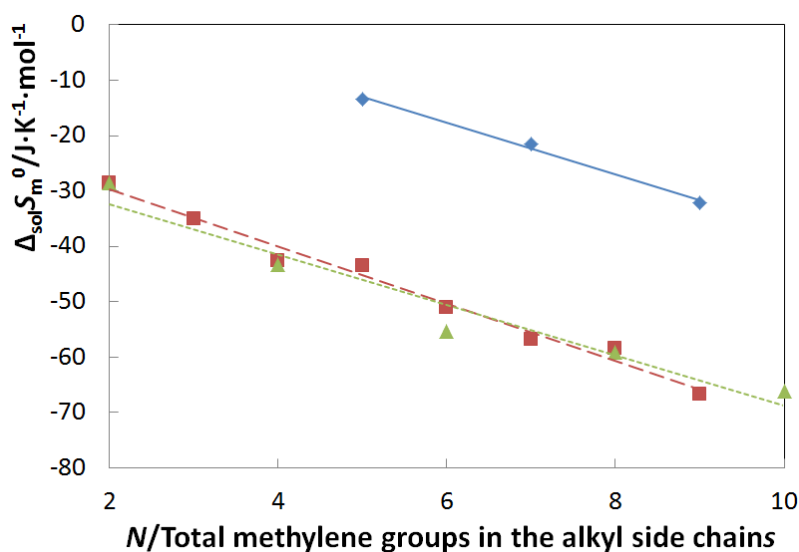


**Figure 4.13.** Standard molar entropy of solution,  $\Delta_{sol}S_m^0$ , as function of total methylene groups in the alkyl side chains,  $N$ , of ILs. Symbols: ( $\blacklozenge$ , solid line),  $[\text{C}_n\text{C}_1\text{im}][\text{PF}_6]$ ,<sup>380</sup>  $\Delta_{sol}S_m^0 = -4.7 \cdot N + 10.3$ ,  $R^2 = 0.9931$ ; ( $\blacksquare$ , dashed line),  $[\text{C}_n\text{C}_1\text{im}][\text{NTf}_2]$ ,<sup>378</sup>  $\Delta_{sol}S_m^0 = -5.2 \cdot N + 19.4$ ,  $R^2 = 0.9832$ ; and ( $\blacktriangle$ , dotted line),  $[\text{C}_n\text{C}_n\text{im}][\text{NTf}_2]$ ,  $\Delta_{sol}S_m^0 = -4.5 \cdot N - 23.2$ ,  $R^2 = 0.9459$ . The symbols and line represents the estimated  $\Delta_{sol}S_m^0$  calculated using Equation 4.23 and dependency of  $\Delta_{sol}S_m^0$  as function of  $N$ , respectively. All data are at 298.15 K.

The conventional standard molar properties of solvation were determined through the reported vapor pressures and the standard molar enthalpy of vaporization of each IL studied at 298.15 K.<sup>408,416</sup> The reported vapor pressures were used to extrapolate them to 298.15 K using the Clarke and Glew equation. The conventional solvation thermodynamic functions at 298.15 K, and for the ILs studied, are presented in Table 4.12.



**Table 4.12.** Standard molar properties of solvation of ionic liquids in water at 298.15 K. <sup>a</sup>

	$\Delta_{svl} H_m^0 / \text{kJ} \cdot \text{mol}^{-1}$	$\Delta_{svl} G_m^0 / \text{kJ} \cdot \text{mol}^{-1}$	$\Delta_{svl} S_m^0 / \text{J} \cdot \text{K}^{-1} \cdot \text{mol}^{-1}$
[C <sub>1</sub> C <sub>1</sub> im][NTf <sub>2</sub> ]	-128.8 (1.8)	-63.775 (0.017)	-218.1 (4.5)
[C <sub>2</sub> C <sub>2</sub> im][NTf <sub>2</sub> ]	-123.3 (1.8)	-57.017 (0.024)	-222.3 (4.5)
[C <sub>3</sub> C <sub>3</sub> im][NTf <sub>2</sub> ]	-131.3 (1.8)	-55.226 (0.026)	-255.1 (4.5)
[C <sub>4</sub> C <sub>4</sub> im][NTf <sub>2</sub> ]	-134.8 (1.8)	-53.867 (0.003)	-271.4 (4.5)
[C <sub>5</sub> C <sub>5</sub> im][NTf <sub>2</sub> ]	-143.6 (1.8)	-54.087 (0.024)	-300.3 (4.5)

<sup>a</sup>The correspondent standard deviation is presented between brackets.

The standard molar Gibbs energies of solvation increase with the alkyl chain length (decrease of the IL solubility in water). The results show, with exception of the outlier IL, [C<sub>1</sub>C<sub>1</sub>im][NTf<sub>2</sub>], a regular decrease the molar enthalpies and entropies of solvation as a function of the alkyl chain length, highlighting the role of the entropy in the solvation of ionic liquids in water.

### COSMO-RS

Figure 4.10 presents the COSMO-RS predicted phase diagrams of the binary mixtures composed of ionic liquids and water. The results obtained with COSMO-RS show an acceptable qualitative agreement with the experimental data, and as previously observed.<sup>374,377–380</sup> The same hydrophobic character increase, at the water-rich side, is observed both in the experimental data and in the predictions. Furthermore, the similar trends of mole fraction solubility of water in symmetric and asymmetric ionic liquids are also well predicted by COSMO-RS. Higher relative deviations were observed in the water-rich phase due to the very low solubility of the studied ionic liquids in water. In spite of the quantitative deviations obtained with COSMO-RS from experimental data the model is able to correctly display the alkyl chain length and cation symmetry impact in these mutual solubilities. Thus, COSMO-RS proved to be a useful predictive method for the a priori screening of ionic liquids to find suitable candidates for a given task, before extensive experimental measurements.

It is worth mentioning that we also used the latest COSMO file parameterization, BP\_TZVP\_C30\_1301 and the results are given in Figure S4.6 of Appendix 4. Despite the new parameterization being able to correctly predict the trend of water mole fraction in the IL-rich phase, the phase diagram of ILs in the water-rich phase deviates much more from the experimental results. Moreover, the predicted phase diagrams behavior displays a wrong trend with temperature.

#### **4.2.5. Analysis of the isomerism effect on the mutual solubilities of bis(trifluoromethylsulfonyl)imide-based ionic liquids with water**

Mónia A. R. Martins, Catarina M. S. S. Neves, Kiki A. Kurnia, Luís M. N. B. F. Santos, Mara G. Freire, Simão P. Pinho & João A. P. Coutinho, *Fluid Phase Equilibria* 381 28–35 (2014), DOI: 10.1016/j.fluid.2014.08.007

##### **4.2.5.1. Abstract**

The knowledge of the liquid-liquid equilibria (LLE) between ionic liquids (ILs) and water is of utmost importance for environmental monitoring, process design and optimization. Therefore, in this work, the mutual solubilities with water, for the ILs combining the 1-methylimidazolium,  $[C_1im]^+$ ; 1-ethylimidazolium,  $[C_2im]^+$ ; 1-ethyl-3-propylimidazolium,  $[C_2C_3im]^+$ ; and 1-butyl-2,3-dimethylimidazolium,  $[C_4C_1C_1im]^+$  cations with the bis(trifluoromethylsulfonyl)imide anion, were determined and compared with the isomers of the symmetric 1,3-dialkylimidazolium bis(trifluoromethylsulfonyl)imide ( $[C_nC_nim][NTf_2]$ , with  $n = 1-3$ ) and of the asymmetric 1-alkyl-3-methylimidazolium bis(trifluoromethylsulfonyl)imide ( $[C_nC_1im][NTf_2]$ , with  $n = 2-5$ ) series of ILs. The results obtained provide a broad picture of the impact of the IL cation structural isomerism, including the number of alkyl side chains at the cation, on the water-IL mutual solubilities. Despite the hydrophobic behavior associated to the  $[NTf_2]^-$  anion, the results show a significant solubility of water in the IL-rich phase, while the solubility of ILs in the water-rich phase is much lower. The thermodynamic properties of solution indicate that the solubility of ILs in water is entropically driven and highly influenced by the cation size. Using the results obtained here in addition to literature data, a correlation between the solubility of  $[NTf_2]$ -based ILs in water and their molar volume, for a large range of cations,

is proposed. The CONductor like Screening MOdel for Real Solvents (COSMO-RS) was also used to estimate the LLE of the investigated systems and proved to be a useful predictive tool for the *a priori* screening of ILs aiming at finding suitable candidates before extensive experimental measurements.

#### 4.2.5.2. Chemicals

The ILs studied in this work are displayed in Table 4.13 and their chemical structure is presented in Figure 4.14.

**Table 4.13.** Investigated ionic liquids: name, abbreviation, source, molecular mass (M), and purity.

Chemical Name	Abbreviation	Source	M (g·mol <sup>-1</sup> )	Purity (mass %)
1-methylimidazolium bis(trifluoromethylsulfonyl)imide	[C <sub>1</sub> im][NTf <sub>2</sub> ]	Iolitec	363.25	> 99
1-ethylimidazolium bis(trifluoromethylsulfonyl)imide	[C <sub>2</sub> im][NTf <sub>2</sub> ]	Iolitec	377.28	> 99
1-ethyl-3-propylimidazolium bis(trifluoromethylsulfonyl)imide	[C <sub>2</sub> C <sub>3</sub> im][NTf <sub>2</sub> ]	Iolitec	419.37	> 99
1-butyl-2,3-dimethylimidazolium bis(trifluoromethylsulfonyl)imide	[C <sub>4</sub> C <sub>1</sub> C <sub>1</sub> im][NTf <sub>2</sub> ]	Iolitec	433.39	> 99

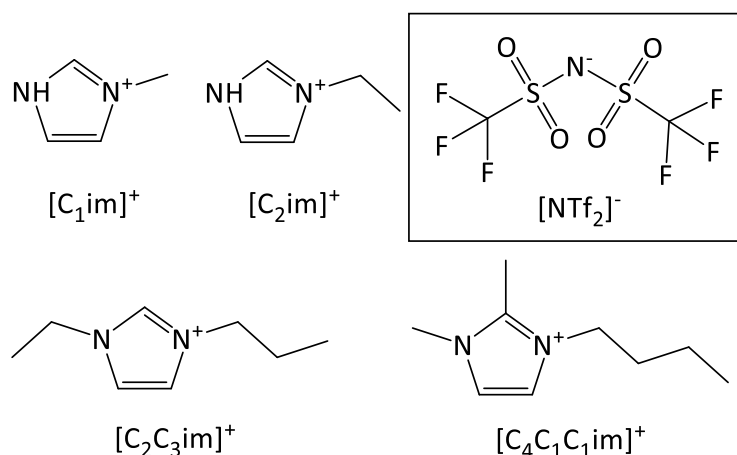


**Figure 4.14.** Schematic representation of chemical structure of the studied imidazolium-based ionic liquids.

To reduce the water and volatile compounds content to insignificant values, individual samples of ILs were dried under vacuum at 1 Pa and constant stirring at 353 K, for a minimum of 48 h. After, the purity of each ionic liquid was further checked by  $^1\text{H}$ ,  $^{13}\text{C}$ , and  $^{19}\text{F}$  NMR spectra. A Metrohm 831 Karl Fischer coulometer using the analyte Hydranal<sup>®</sup> - Coulomat AG, from Riedel-de Haën, was used to determine the water content of the dried ionic liquids, and was found to be below 100 ppm for all samples. The water used in the measurements was double distilled, passed by a reverse osmosis system and further treated with a MilliQ plus 185 water purification apparatus, presenting a resistivity of 18.2  $\text{M}\Omega\cdot\text{cm}$ , a TOC smaller than  $5\ \mu\text{g}\cdot\text{dm}^{-3}$  and free of particles larger than  $0.22\ \mu\text{m}$  ( $M(\text{H}_2\text{O})=18.01528\ \text{g}\cdot\text{mol}^{-1}$ ).

#### 4.2.5.3. Results and discussion

##### Mutual solubilities between ionic liquids and water

The experimental data for the mutual solubility between water and the studied ILs, along with the respective standard deviations, are given in Table 4.14 and 4.15.

The analysis of Table 4.14 reveals a significant mole fraction solubility of water in the IL-rich phase, and above 0.5 for the  $[\text{C}_1\text{im}][\text{NTf}_2]$  and  $[\text{C}_2\text{im}][\text{NTf}_2]$  ILs. Thus, in spite of the hydrophobic character usually associated to the bis(trifluoromethylsulfonyl)imide anion, it is shown here that monosubstituted ILs dissolve large amounts of water. The change on the nature and acidity of the imidazolium cation by and “extra” “N-H” acidic site leads to a saturation limit above 1:1 for the pair water-IL. The water solubility in  $[\text{C}_2\text{C}_3\text{im}][\text{NTf}_2]$  and  $[\text{C}_4\text{C}_1\text{C}_1\text{im}][\text{NTf}_2]$  is of the same order observed previously in the  $[\text{C}_n\text{C}_1\text{im}][\text{NTf}_2]$  and  $[\text{C}_n\text{C}_n\text{im}][\text{NTf}_2]$  series.<sup>378,403</sup> On the opposite side of the phase diagram, the mole fraction solubility of ILs in the water-rich phase is much lower, in the order of  $10^{-3}$  to  $10^{-4}$ , which may be considered as an almost pure phase with the IL close to infinite dilution.

In general, when comparing the data obtained for  $[\text{C}_1\text{im}][\text{NTf}_2]$  and  $[\text{C}_2\text{im}][\text{NTf}_2]$ , the mutual solubilities with water decrease with the increase on the alkyl side chain length of the cation due to an increase in the IL hydrophobic character. For all the studied ILs, the mutual solubilities increase with temperature, displaying an upper critical solution

temperature behavior. This is the expectable behavior, and also observed with other imidazolium-based ILs combined with the  $[\text{BF}_4]^-$  or  $[\text{PF}_6]^-$  anions.<sup>380,384,404</sup> Watanabe and Katsuta (2014)<sup>417</sup> reported the solubility of  $[\text{C}_4\text{C}_1\text{C}_1\text{im}][\text{NTf}_2]$  in water at 298.15 K. The relative deviation to the experimental value measured in this work is only 5%.

**Table 4.14.** Experimental mole fraction solubility of water in ionic liquids,  $x_w$ , at different temperatures and at 0.10 MPa.<sup>a</sup>

$T / \text{K}$	$[\text{C}_1\text{im}][\text{NTf}_2]$	$[\text{C}_2\text{im}][\text{NTf}_2]$	$[\text{C}_2\text{C}_3\text{im}][\text{NTf}_2]$	$[\text{C}_4\text{C}_1\text{C}_1\text{im}][\text{NTf}_2]$
	$x_w$	$x_w$	$x_w$	$x_w$
288.15	0.627 (0.009)	0.604 (0.010)	0.209 (0.002)	0.168 (0.001)
293.15	0.648 (0.003)	0.612 (0.010)	0.222 (0.002)	0.183 (0.002)
298.15	0.667 (0.005)	0.628 (0.006)	0.239 (0.001)	0.191 (0.001)
303.15	0.686 (0.001)	0.641 (0.004)	0.256 (0.001)	0.212 (0.001)
308.15	0.709 (0.001)	0.659 (0.005)	0.278 (0.006)	0.229 (0.001)
313.15	0.720 (0.003)	0.673 (0.007)	0.296 (0.003)	0.244 (0.002)
318.15	0.736 (0.010)	0.682 (0.012)	0.314 (0.003)	0.263 (0.001)

<sup>a</sup>The correspondent standard deviation is presented between brackets. Standard uncertainties,  $u$ , are  $u(T) = 0.01 \text{ K}$ , and  $u_r(p) = 0.05$ .

**Table 4.15.** Experimental mole fraction solubility of ionic liquids in water,  $x_{\text{IL}}$ , at different temperatures and at 0.10 MPa.<sup>a</sup>

$T / \text{K}$	$[\text{C}_1\text{im}][\text{NTf}_2]$	$[\text{C}_2\text{im}][\text{NTf}_2]$	$[\text{C}_2\text{C}_3\text{im}][\text{NTf}_2]$	$[\text{C}_4\text{C}_1\text{C}_1\text{im}][\text{NTf}_2]$
	$10^3 x_{\text{IL}}$	$10^3 x_{\text{IL}}$	$10^3 x_{\text{IL}}$	$10^3 x_{\text{IL}}$
288.15	4.132 (0.037)	2.360 (0.004)	0.311 (0.001)	0.203 (0.002)
293.15	4.206 (0.027)	2.388 (0.019)	0.317 (0.001)	0.206 (0.008)
298.15	4.359 (0.011)	2.451 (0.008)	0.325 (0.001)	0.209 (0.001)
303.15	4.499 (0.053)	2.549 (0.001)	0.336 (0.002)	0.217 (0.003)
308.15	4.811 (0.032)	2.669 (0.019)	0.351 (0.002)	0.237 (0.001)
313.15	5.393 (0.020)	2.979 (0.060)	0.387 (0.002)	0.246 (0.003)
318.15	5.945 (0.026)	3.233 (0.010)	0.410 (0.014)	0.270 (0.001)

<sup>a</sup>The correspondent standard deviation is presented between brackets. Standard uncertainties,  $u$ , are  $u(T) = 0.01 \text{ K}$ , and  $u_r(p) = 0.05$ .

Aiming at studying the impact of the structural variation of ILs toward their mutual solubility with water, Figure 4.15 depicts the phase diagrams of the studied ILs along with the corresponding isomers previously reported.<sup>378,403</sup> The ionic liquids studied in this work and the symmetric and asymmetric series with the same number of methylene groups in the alkyl side chains are compared, enabling us to investigate the impact of structural isomers toward their mutual solubilities with water. As depicted in Figure 4.15a, the mole fraction solubility of water in the ionic liquid  $[\text{C}_2\text{C}_3\text{im}][\text{NTf}_2]$  is similar to that of  $[\text{C}_4\text{C}_1\text{im}][\text{NTf}_2]$ . Considering now the IL  $[\text{C}_4\text{C}_1\text{C}_1\text{im}][\text{NTf}_2]$  with the respective structural isomers,  $[\text{C}_3\text{C}_3\text{im}][\text{NTf}_2]$  and  $[\text{C}_5\text{C}_1\text{im}][\text{NTf}_2]$ , the trialkyl-substituted IL presents a lower solubility of water whereas the disubstituted ILs present similar solubility values. The introduction of a third aliphatic moiety substituting the most acidic hydrogen clearly reduces the hydrogen-bonding ability between the imidazolium cation and water with an impact on the water solubility. However, smaller differences are observed for the pair,  $[\text{C}_3\text{C}_3\text{im}][\text{NTf}_2]$  and  $[\text{C}_5\text{C}_1\text{im}][\text{NTf}_2]$  that contain the same number of aliphatic tails. Moreover, it is interesting to notice the significant differentiation of the solubility of water in  $[\text{C}_2\text{im}][\text{NTf}_2]$  and in  $[\text{C}_1\text{C}_1\text{im}][\text{NTf}_2]$ , also structural isomers. The change in the chemical nature of the cation and the presence of a N-H group increases the water solubility in the IL to a mole fraction higher than 0.5 (above 1:1, water:IL) that is an indication of a strong affinity and hydrogen-bonding between N-H and  $\text{H}_2\text{O}$ .

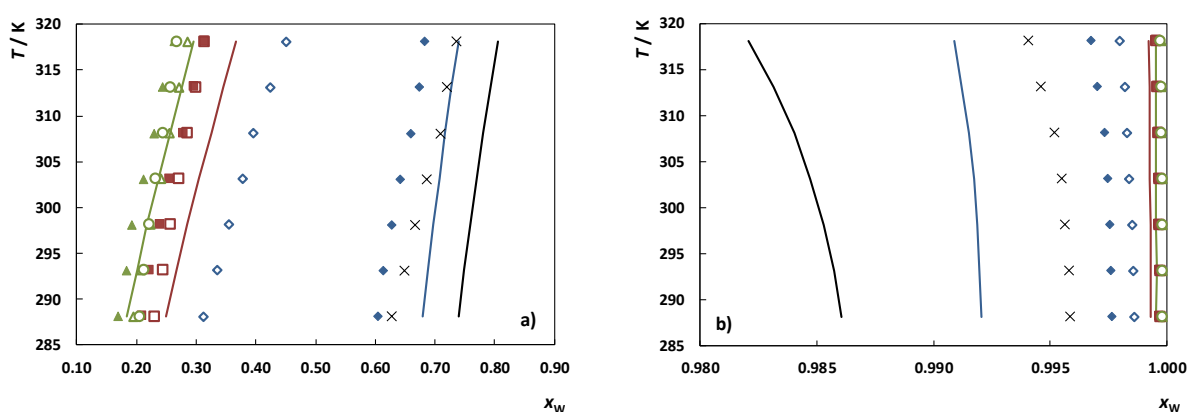


**Figure 4.15.** Liquid-liquid phase diagram for water and ionic liquids: (a), ionic-liquid-rich phase; and (b) water-rich phase: (x),  $[\text{C}_1\text{im}][\text{NTf}_2]$ ; (◆),  $[\text{C}_2\text{im}][\text{NTf}_2]$ ; (◇),  $[\text{C}_1\text{C}_1\text{im}][\text{NTf}_2]$ ; (■),  $[\text{C}_2\text{C}_3\text{im}][\text{NTf}_2]$ ; (□),  $[\text{C}_4\text{C}_1\text{im}][\text{NTf}_2]$ ; (▲),  $[\text{C}_4\text{C}_1\text{C}_1\text{im}][\text{NTf}_2]$ ; (△),  $[\text{C}_3\text{C}_3\text{im}][\text{NTf}_2]$ ; and (○),  $[\text{C}_5\text{C}_1\text{im}][\text{NTf}_2]$ .

(○), [C<sub>5</sub>C<sub>1</sub>im][NTf<sub>2</sub>]. The lines at the same colors represent the COSMO-RS predictions for the compounds measured in this work.

The mole fraction solubility of the different ionic liquids in water is presented in Figure 4.15b. Also here, as noted in the IL-rich phase, the mole fraction solubility in water of the ionic liquid [C<sub>2</sub>C<sub>3</sub>im][NTf<sub>2</sub>] is similar to that of [C<sub>4</sub>C<sub>1</sub>im][NTf<sub>2</sub>]. In the case of the trialkyl-substituted IL, [C<sub>4</sub>C<sub>1</sub>C<sub>1</sub>im][NTf<sub>2</sub>], and their structural isomers [C<sub>5</sub>C<sub>1</sub>im][NTf<sub>2</sub>] and [C<sub>3</sub>C<sub>3</sub>im][NTf<sub>2</sub>], the solubility in water of the [C<sub>4</sub>C<sub>1</sub>C<sub>1</sub>im][NTf<sub>2</sub>] is slightly larger than the respective isomers, contrary to what happens in the IL-rich phase. The solubility of the disubstituted isomers [C<sub>3</sub>C<sub>3</sub>im][NTf<sub>2</sub>] and [C<sub>5</sub>C<sub>1</sub>im][NTf<sub>2</sub>] is similar as they contain the same number of aliphatic tails. Finally, concerning the solubility in water of [C<sub>2</sub>im][NTf<sub>2</sub>] and [C<sub>1</sub>C<sub>1</sub>im][NTf<sub>2</sub>], and similarly to what observed in the IL-rich phase a large significant difference, can be observed. Once again the strong affinity and hydrogen-bonding between “N-H” and H<sub>2</sub>O increases the ionic liquid solubility in water.

In order to more thoroughly understand the impact of the structural variations of ionic liquids on their mutual solubilities with water, the solubility variations are summarized in Figure 4.16. The ionic liquids investigated in this work, together with the symmetric ([C<sub>n</sub>C<sub>n</sub>im][NTf<sub>2</sub>], with *n* = 1-3) and asymmetric ([C<sub>n</sub>C<sub>1</sub>im][NTf<sub>2</sub>], with *n* = 2-5) series are analyzed in order to evaluate the variations in the mutual solubilities when adding a methyl group.

As observed in Figure 4.16, in both phases, whenever a methyl group is introduced, the solubility decreases. In the IL-rich phase, this reduction is within the range 5-16%, if the introduction of the methyl group takes place in the aliphatic chains, and 26-52%, if directly attached to the aromatic ring. Concerning the water-rich phase, the reduction is more pronounced but less distinct; 36-44% for an addition of a methyl to the aliphatic chains, and 32-66% if to the aromatic ring. When the methyl group is added to the aromatic ring, the highest percent decrease correspond to the pair [C<sub>2</sub>im][NTf<sub>2</sub>] / [C<sub>2</sub>C<sub>1</sub>im][NTf<sub>2</sub>] and the lowest to [C<sub>4</sub>C<sub>1</sub>im][NTf<sub>2</sub>] / [C<sub>4</sub>C<sub>1</sub>C<sub>1</sub>im][NTf<sub>2</sub>], i.e., the introduction of a third aliphatic moiety has a less impact than the elimination of the “N-H” bond.

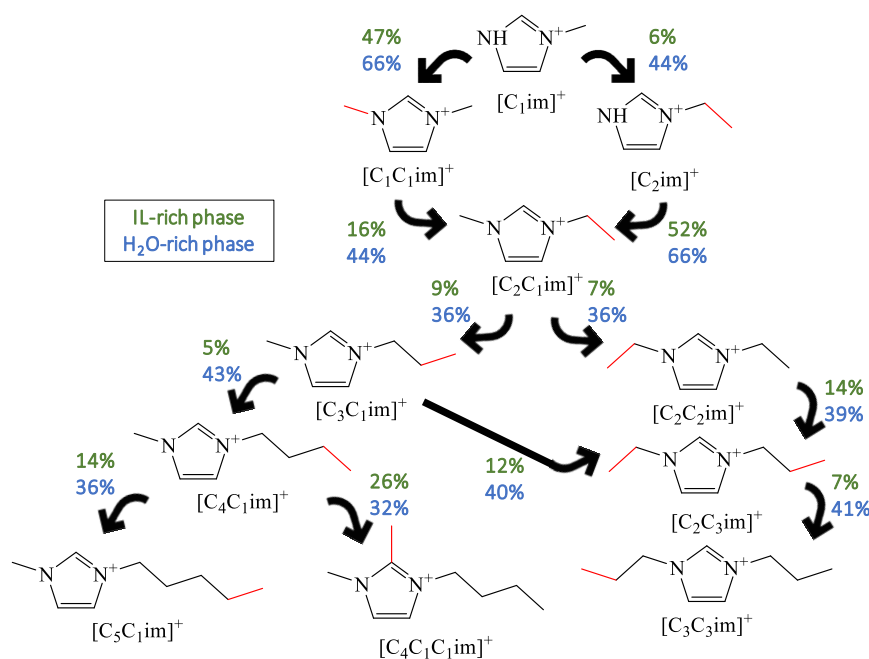


**Figure 4.16.** Schematic representation of the percent decrease in the mutual solubilities of ILs with water, when introducing a methyl group.

Concerning the IL-rich phase, when adding a methyl group to [C<sub>1</sub>im][NTf<sub>2</sub>] in the aliphatic chain the variation is 6%, but, if this addition causes the elimination of the “N-H” bond, the variation is 47%. In the same way, the variation in the solubility to obtain [C<sub>2</sub>C<sub>1</sub>im][NTf<sub>2</sub>] from a monosubstituted IL ([C<sub>2</sub>im][NTf<sub>2</sub>]) is much larger than from a disubstituted IL ([C<sub>1</sub>C<sub>1</sub>im][NTf<sub>2</sub>]). The addition of methyl groups to obtain the symmetric and asymmetric series causes a more or less constant variation in the solubility (5-14%), being [C<sub>4</sub>C<sub>1</sub>im][NTf<sub>2</sub>]/ [C<sub>5</sub>C<sub>1</sub>im][NTf<sub>2</sub>] the pair where the greatest variation occurs. Lastly the [C<sub>4</sub>C<sub>1</sub>im][NTf<sub>2</sub>], where the introduction of a third aliphatic moiety to obtain [C<sub>4</sub>C<sub>1</sub>C<sub>1</sub>im][NTf<sub>2</sub>], reduce the hydrogen-bonding ability and, consequently, causes a significant decrease in the solubility.

On the other hand, in the water-rich phase although the changes are larger than in the IL-rich phase, these seem more similar the different isomers. For instance, when adding a methyl group to the monosubstituted IL [C<sub>1</sub>im][NTf<sub>2</sub>] the variations are 44 for the addition to the aliphatic chain and 66 % if the addition takes place directly in the aromatic ring. To obtain [C<sub>2</sub>C<sub>1</sub>im][NTf<sub>2</sub>] the addition of a methyl group to [C<sub>2</sub>im][NTf<sub>2</sub>] cause a variation of 66% while the addition to [C<sub>1</sub>C<sub>1</sub>im][NTf<sub>2</sub>] causes a variation of only 44%. Again, the



additions of methyl groups to obtain the symmetric and asymmetric series, causes approximately constant variations in the solubility (36-43%). Concerning the trialkyl-substituted IL, [C<sub>4</sub>C<sub>1</sub>C<sub>1</sub>im][NTf<sub>2</sub>], the addition of a methyl group to [C<sub>4</sub>C<sub>1</sub>im][NTf<sub>2</sub>] causes merely a reduction of 32% in the IL solubility. Moreover, is interesting to note that the variation on the solubility between the pairs [C<sub>3</sub>C<sub>1</sub>im][NTf<sub>2</sub>]/[C<sub>2</sub>C<sub>3</sub>im][NTf<sub>2</sub>] and [C<sub>2</sub>C<sub>2</sub>im][NTf<sub>2</sub>]/[C<sub>2</sub>C<sub>3</sub>im][NTf<sub>2</sub>] is almost the same in each phase, and four times higher in the water-rich phase.

### Temperature dependence and thermodynamic functions of solution

The fitted parameters of equations 4.19 and 4.20 as well as their standard deviations are listed in Table 4.16. The maximum relative deviation to the experimental data is 2%, for both the water-rich and the ionic liquid-rich phases.

**Table 4.16.** Correlation parameters for the mole fraction solubility of water in the IL-rich phase and IL in the water-rich phase.<sup>a</sup>

IL	A	B / K	C	D / K	E
[C <sub>1</sub> im][NTf <sub>2</sub> ]	1.252 (0.055)	-494.1 (16.6)	-554.0 (62.7)	23802.9 (2826.8)	82.3 (9.3)
[C <sub>2</sub> im][NTf <sub>2</sub> ]	0.853 (0.051)	-392.4 (15.5)	-503.6 (60.9)	21623.2 (2746.8)	74.6 (9.1)
[C <sub>2</sub> C <sub>3</sub> im][NTf <sub>2</sub> ]	2.860 (0.084)	-1277.7 (25.3)	-382.0 (61.3)	16139.1 (2764.5)	56.1 (9.1)
[C <sub>4</sub> C <sub>1</sub> C <sub>1</sub> im][NTf <sub>2</sub> ]	2.987 (0.145)	-1376.3 (43.9)	-390.6 (68.7)	16495.2 (3098.6)	57.4 (10.2)

<sup>a</sup>The correspondent standard deviation is presented between brackets.

The molar thermodynamic functions for the IL solution in water were estimated at 298.15 K and are reported in Table 4.17.

**Table 4.17.** Standard molar properties of solution of ILs in water, at 298.15 K.<sup>a</sup>

	$\Delta_{sol}H_m^0 / \text{kJ} \cdot \text{mol}^{-1}$	$\Delta_{sol}G_m^0 / \text{kJ} \cdot \text{mol}^{-1}$	$\Delta_{sol}S_m^0 / \text{J} \cdot \text{K}^{-1} \cdot \text{mol}^{-1}$
[C <sub>1</sub> im][NTf <sub>2</sub> ]	6.0 (1.5)	13.475 (0.006)	-25.0 (5.1)
[C <sub>2</sub> im][NTf <sub>2</sub> ]	5.2 (1.5)	14.901 (0.008)	-32.7 (5.1)
[C <sub>2</sub> C <sub>3</sub> im][NTf <sub>2</sub> ]	5.0 (1.5)	19.910 (0.010)	-50.1 (5.1)
[C <sub>4</sub> C <sub>1</sub> C <sub>1</sub> im][NTf <sub>2</sub> ]	5.1 (1.5)	21.000 (0.017)	-53.1 (5.1)

<sup>a</sup>The correspondent standard deviation is presented between brackets.

At 298.15 K, the  $\Delta_{sol}H_m^0$  of the studied ILs in water, remains approximately constant with the increase of the aliphatic moiety, because when the ionic liquid is in aqueous solution the interactions occur mainly with the charged head and are much less dependent on the alkyl chain. The experimental enthalpies of solution also show that the solubilisation of ILs in water is an endothermic process, leading to an upper critical solution temperature behavior type phase diagram. On the other hand, the standard Gibbs energy of solution increases with the alkyl chain length leading to a lower solubility of the heavier ILs in water. The molar entropies of solution are shown to be negative and dependent on the cation structure, decreasing with increasing the alkyl chain length (approximately  $-5 \text{ J}\cdot\text{K}^{-1}\cdot\text{mol}^{-1}$  per methylene addition to the cation and as shown previously<sup>378,380–382</sup>). Therefore, the solubility of the ILs in water is driven by the entropy of solution; the higher (less negative) the entropic change, the higher the solubility of the ILs in water.

The significant increase of solubility of the  $[\text{C}_1\text{im}][\text{NTf}_2]$  and  $[\text{C}_2\text{im}][\text{NTf}_2]$  in water is also entropically driven and is a results of the quite significant increase of the entropy of solution of  $\sim (+25 \text{ kJ}\cdot\text{K}^{-1}\cdot\text{mol}^{-1})$  when compared with their isomers<sup>378,403</sup> and other members of the  $[\text{NTf}_2]$ -series of ILs as well as combined with other anions. The significant increase in the entropy of solution is also related with the expected cation to water interaction via the N-H group that leads to a better solvation interaction with water and to a decrease of the cavitation entropy penalty (more hydrophilic).

### **COSMO-RS**

The predicted phase diagrams of the binary mixtures composed of water and the studied ILs using COSMO-RS are presented in Figure 4.15. The same increase on the hydrophobic character is observed for the experimental data and COSMO predictions. COSMO-RS is thus able to qualitatively predict the trend on the ILs affinity for water. The only exception found was for the prediction of the solubility change with the temperature for the ionic liquid containing the cation  $[\text{C}_4\text{C}_1\text{C}_1\text{im}]^+$  in water. In opposition to the experimental information, COSMO-RS predicts a solubility decrease with rising temperature. This irregularity can be related to the fact that simple empirical interaction

potentials are used in COSMO-RS to describe the weaker interactions of the ILs with water, which is expected to poorly describe their effective complexity.

Figure 4.17 plots the calculated *versus* experimental solubility for several [NTf<sub>2</sub>]-based ILs, at both rich phases, and at 298.15 K. From the close correlations depicted in Figure 4.17 it can be concluded that COSMO-RS can predict the mutual solubilities between the studied ILs and water.

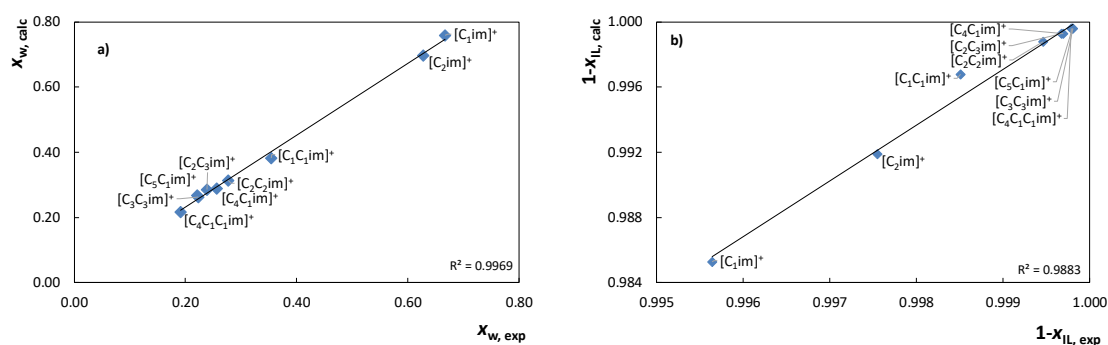


**Figure 4.17.** Calculated *versus* experimental solubility of bis(trifluoromethylsulfonyl)imide-based ionic liquids at 298.15 K in (a) IL-rich phase and (b) water-rich phase.

It should be pointed out here that the latest COSMO file parameterization, BP\_TZVP\_C30\_1401, was also used to predict the LLE of the binary systems investigated in this work, *cf.* Figure S4.7 of Appendix 4, presenting a global relative deviations of 35.3 and 2.8 % for the solubility of water in ILs and ILs in water, respectively. However, this COSMO-RS parameterization is also unable to correctly describe the solubility change with the temperature for the ILs [C<sub>4</sub>C<sub>1</sub>C<sub>1</sub>im][NTf<sub>2</sub>] and [C<sub>2</sub>C<sub>3</sub>im][NTf<sub>2</sub>] in water. With the file parameterization, BP\_TZVP\_C21\_0110 the global relative deviations obtained were 16.8 and 1.2 %. Since the latest version of COSMO-RS predicts the phase diagrams with a larger deviation from the experimental results and wrong trends, the oldest version is preferred and was used here. Despite some regular deviations, COSMO-RS shows to be a useful tool in the prediction of the binary systems behavior, and able to correctly display the alkyl chain length and IL cation isomeric effect, and as previously observed.<sup>374,377,378,380</sup>

### Correlation for the solubility of bis(trifluoromethylsulfonyl)imide-based ionic liquids in water

The solubility of hydrophobic solutes in water, near infinite dilution, is controlled and strongly correlated to their molar volume.<sup>377,381,382</sup> For isomeric ILs, the molar volume is identical and, consequently, the solubilities are essentially the same. In this context, in our previous work<sup>403</sup> we have start to investigate the relevance of the solutes molar volume on the solubility of the [NTf<sub>2</sub>]-based ionic liquids in water, at 298.15 K, and a correlation was proposed. Here, new points were plotted together with the correlation obtained,<sup>403</sup> in order to verify if it can be also used for more diverse systems, as shown in Figure 4.18. The molar volumes were calculated based on density data taken from literature<sup>182,397,418</sup> and the aqueous solubility data used were those obtained in this work along with data previously published.<sup>378,381,382,403</sup> Data relative to other cations (pyridinium-, pyrrolidinium- and piperidinium-based<sup>381,382,397,418</sup>) combined with the same anion where also included in order to verify the robustness of the correlation proposed.

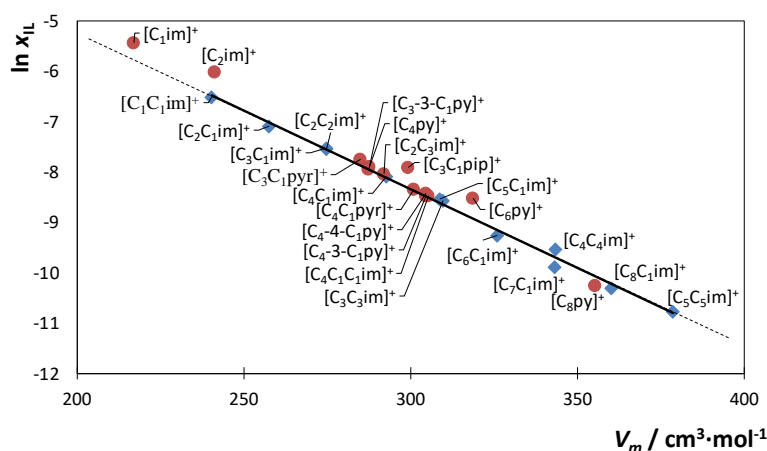


**Figure 4.18.** Solubility of bis(trifluoromethylsulfonyl)imide-based ionic liquids in water as a function of the ionic liquid molar volume:  $\ln(x_{IL}) = -0.0309 (V_m/\text{cm}^3 \cdot \text{mol}^{-1}) + 0.9357$ ;  $R^2 = 0.9947$ ,<sup>403</sup> at 298.15 K. (◆), data used in the correlation; and (●), new data.

Despite the different cations families, the correlation<sup>403</sup> is able to correctly describe the solubility of [NTf<sub>2</sub>]-based ILs in water. However, it is observed that cations with different cores, i.e. with a more different chemical nature (like pyridinium-, pyrrolidinium- and

piperidinium-based) and the mono substituted imidazolium IL deviate more from the proposed correlation that was constructed with imidazolium-based fluids only. On Figure 4.18 the isomerism effect can also be analyzed and, as can be seen, ionic liquids with the same molar volume present similar solubility in water. Exceptions are only the pair [C<sub>2</sub>im][NTf<sub>2</sub>]/[C<sub>1</sub>C<sub>1</sub>im][NTf<sub>2</sub>], which is understood due to the elimination of a 'N-H' bond in the imidazolium ring like explored before, and for ILs with a different core than imidazolium, namely, [C<sub>3</sub>C<sub>1</sub>pip][NTf<sub>2</sub>] and [C<sub>6</sub>py][NTf<sub>2</sub>].

#### **4.2.6. Densities, viscosities and derived thermodynamic properties of water-saturated imidazolium-based ionic liquids**

Mónia A. R. Martins, Catarina M. S. S. Neves, Kiki A. Kurnia, Pedro J. Carvalho, Marisa A. A. Rocha, Luís M. N. B. F. Santos, Simão P. Pinho & Mara G. Freire, *Fluid Phase Equilibria* 407 188–196 (2016), DOI: 10.1016/j.fluid.2015.05.023

##### **4.2.6.1. Abstract**

In order to evaluate the impact of the alkyl side chain length and symmetry of the cation on the thermophysical properties of water-saturated ionic liquids (ILs), densities and viscosities as a function of temperature were measured at atmospheric pressure and in the (298.15 to 363.15) K temperature range, for systems containing two series of bis(trifluoromethylsulfonyl)imide-based compounds: the symmetric [C<sub>n</sub>C<sub>n</sub>im][NTf<sub>2</sub>] (with *n* = 1-8 and 10) and asymmetric [C<sub>n</sub>C<sub>1</sub>im][NTf<sub>2</sub>] (with *n* = 2-5, 7, 9 and 11) ILs. For water-saturated ILs, the density decreases with the increase of the alkyl side chain length while the viscosity increases with the size of the aliphatic tails. The saturation water solubility in each IL was further estimated with a reasonable agreement based on the densities of water-saturated ILs, further confirming that for the ILs investigated the volumetric mixing properties of ILs and water follow a near ideal behavior. The water-saturated symmetric ILs generally present lower densities and viscosities than their asymmetric counterparts. From the experimental data, the isobaric thermal expansion coefficient and energy barrier were also estimated. A close correlation between the difference in the energy barrier values between the water-saturated and pure ILs and the water content in each IL

was found, supporting that the decrease in the viscosity of ILs in presence of water is directly related with the decrease of the energy barrier.

#### 4.2.6.2. Chemicals

The densities and viscosities of water-saturated ILs were measured for the following bis(trifluoromethylsulfonyl)imide-based compounds: 1,3-dialkylimidazolium,  $[C_nC_n\text{im}][\text{NTf}_2]$  (with  $n = 1-8$  and 10); and 1-alkyl-3-methylimidazolium,  $[C_nC_1\text{im}][\text{NTf}_2]$  (with  $n = 2-5, 7, 9$  and 11). The ILs investigated in this work are displayed in Table 4.18 and their chemical structure are depicted in Figure 4.19. In general, two series of fluids were investigated: (i) ILs with symmetric alkyl side chains at the imidazolium cation; and (ii) a group of ILs with alkyl side chains of different length at the cation and where one aliphatic moiety is always a methyl group. All ILs were purchased from Iolitec with mass fraction purities higher than 99%. To reduce the impurities, all ILs were dried and purified under vacuum (1 Pa) and at moderate temperature (353 K) for a minimum period of 48 h before the experimental measurements. The purity of each IL was further confirmed by us by  $^1\text{H}$ ,  $^{13}\text{C}$ , and  $^{19}\text{F}$  NMR. Ultra-pure water, double distilled, passed by a reverse osmosis system and further treated with a MilliQ plus 185 water purification apparatus was used. It presented a resistivity of 18.2  $\text{M}\Omega\cdot\text{cm}$ , a TOC (Total Organic Content) smaller than 5  $\mu\text{g}\cdot\text{dm}^{-3}$  and was free of particles  $> 0.22 \mu\text{m}$ .

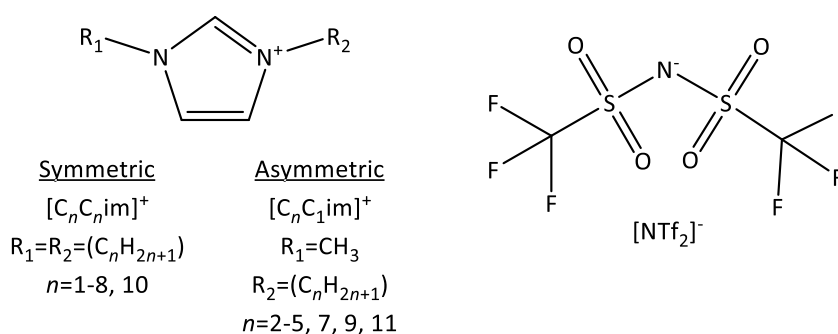


**Figure 4.19.** Schematic representation of the chemical structure of the studied imidazolium-based ILs.

**Table 4.18.** Investigated ionic liquids: chemical name, abbreviation, source, molecular weight ( $M_w$ ) and purity.

Chemical Name	Abbreviation	Source	$M_w$ / (g·mol <sup>-1</sup> )	Purity / (wt %)
1-ethyl-3-methylimidazolium bis((trifluoromethyl)sulfonyl)imide	[C <sub>2</sub> C <sub>1</sub> im][NTf <sub>2</sub> ]	Iolitec	391.31	> 99
1-methyl-3-propylimidazolium bis((trifluoromethyl)sulfonyl)imide	[C <sub>3</sub> C <sub>1</sub> im][NTf <sub>2</sub> ]	Iolitec	405.34	> 99
1-butyl-3-methylimidazolium bis((trifluoromethyl)sulfonyl)imide	[C <sub>4</sub> C <sub>1</sub> im][NTf <sub>2</sub> ]	Iolitec	419.37	> 99
1-methyl-3-pentylimidazolium bis((trifluoromethyl)sulfonyl)imide	[C <sub>5</sub> C <sub>1</sub> im][NTf <sub>2</sub> ]	Iolitec	433.39	> 99
1-heptyl-3-methylimidazolium bis((trifluoromethyl)sulfonyl)imide	[C <sub>7</sub> C <sub>1</sub> im][NTf <sub>2</sub> ]	Iolitec	461.45	> 99
1-methyl-3-nonylmethylimidazolium bis((trifluoromethyl)sulfonyl)imide	[C <sub>9</sub> C <sub>1</sub> im][NTf <sub>2</sub> ]	Iolitec	489.50	> 99
1-methyl-3-undecylimidazolium bis((trifluoromethyl)sulfonyl)imide	[C <sub>11</sub> C <sub>1</sub> im][NTf <sub>2</sub> ]	Iolitec	517.55	> 99
1,3-dimethylimidazolium bis((trifluoromethyl)sulfonyl)imide	[C <sub>1</sub> C <sub>1</sub> im][NTf <sub>2</sub> ]	Iolitec	377.29	> 99
1,3-diethylimidazolium bis((trifluoromethyl)sulfonyl)imide	[C <sub>2</sub> C <sub>2</sub> im][NTf <sub>2</sub> ]	Iolitec	405.34	> 99
1,3-dipropylimidazolium bis((trifluoromethyl)sulfonyl)imide	[C <sub>3</sub> C <sub>3</sub> im][NTf <sub>2</sub> ]	Iolitec	433.39	> 99
1,3-dibutylimidazolium bis((trifluoromethyl)sulfonyl)imide	[C <sub>4</sub> C <sub>4</sub> im][NTf <sub>2</sub> ]	Iolitec	461.45	> 99
1,3-dipentylimidazolium bis((trifluoromethyl)sulfonyl)imide	[C <sub>5</sub> C <sub>5</sub> im][NTf <sub>2</sub> ]	Iolitec	489.50	> 99
1,3-dihexylimidazolium bis((trifluoromethyl)sulfonyl)imide	[C <sub>6</sub> C <sub>6</sub> im][NTf <sub>2</sub> ]	Iolitec	517.55	> 99
1,3-diheptylimidazolium bis((trifluoromethyl)sulfonyl)imide	[C <sub>7</sub> C <sub>7</sub> im][NTf <sub>2</sub> ]	Iolitec	545.60	> 99
1,3-dioctylimidazolium bis((trifluoromethyl)sulfonyl)imide	[C <sub>8</sub> C <sub>8</sub> im][NTf <sub>2</sub> ]	Iolitec	573.66	> 99
1,3-didecylimidazolium bis((trifluoromethyl)sulfonyl)imide	[C <sub>10</sub> C <sub>10</sub> im][NTf <sub>2</sub> ]	Iolitec	629.76	> 99

#### 4.2.6.3. Results and discussion

Although the density and viscosity values determined in this work majorly correspond to novel ILs saturated with water at 298.15 K, it should be remarked that Jacquemin et al.<sup>396</sup> already reported the density and viscosity of the water-saturated [C<sub>2</sub>C<sub>1</sub>im][NTf<sub>2</sub>] and [C<sub>4</sub>C<sub>1</sub>im][NTf<sub>2</sub>] at several temperatures. The maximum relative deviations between the experimental values measured in this work and those reported in the literature<sup>396</sup> are 0.2% and 9.0% for the water-saturated [C<sub>2</sub>C<sub>1</sub>im][NTf<sub>2</sub>], and 0.4% and 14.9% for the water-

saturated  $[\text{C}_4\text{C}_1\text{im}][\text{NTf}_2]$ , for density and viscosity, respectively. Moreover, the equipment used by us was already validated and proven to be adequate for the measurements of densities and viscosities of IL-rich phases.<sup>180,374,375</sup>

The ILs water content, *i.e.*, the saturation values of water in each IL at 298.15 K, used in the density and viscosity measurements, are presented in Table 4.19.

### Density of Water-Saturated Ionic Liquids

The new experimental density data for the water-saturated ILs are presented in the Table S4.7 and S4.8 of Appendix 4. Figure 4.20 depicts the density results obtained in this work alongside with the relative deviations between the pure ILs, reported previously by us,<sup>182</sup> and the water-saturated ones. As previously observed with the pure fluids,<sup>182</sup> also in both series of the water-saturated ILs, the density decreases with the increase on temperature.

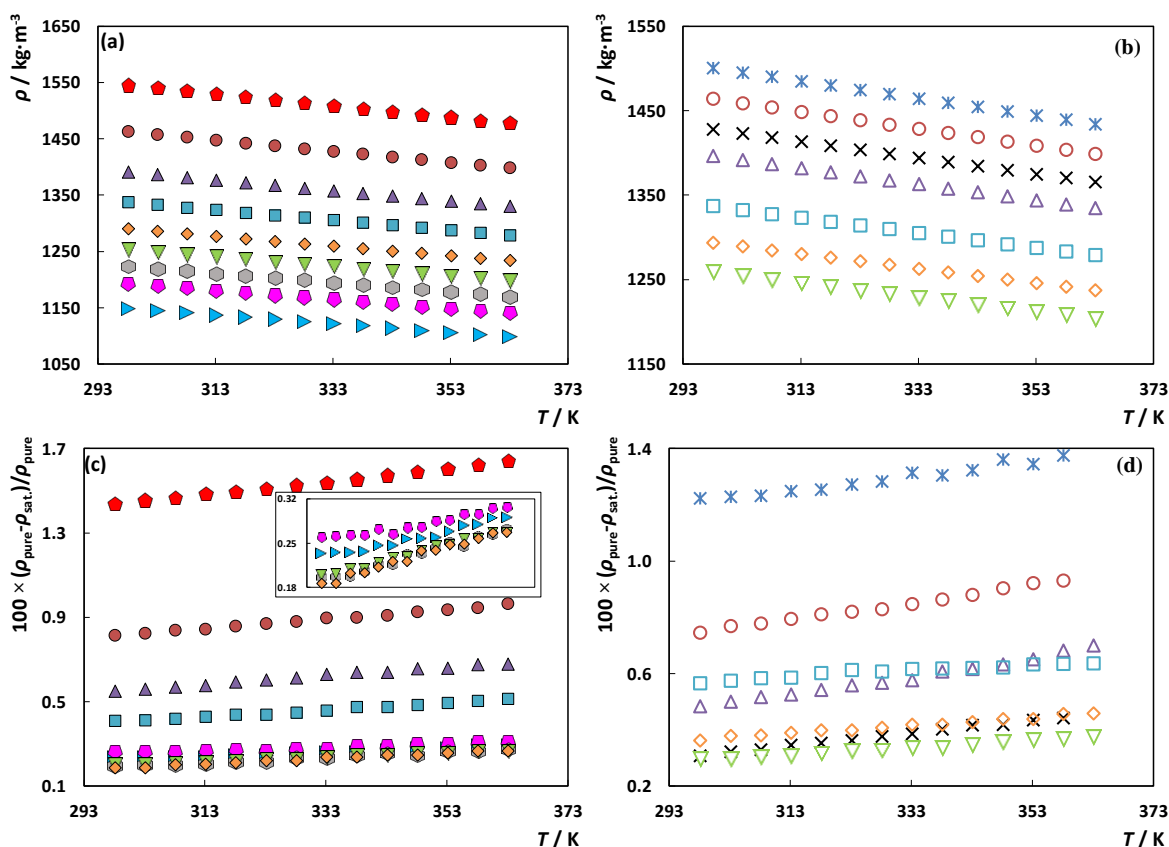


**Figure 4.20.** Density of the symmetric and asymmetric water-saturated ILs as function of temperature, (a, b), respectively; and density relative deviations between the pure<sup>182</sup> and



the symmetric and asymmetric water-saturated ILs, (c, d), respectively: (◆), [C<sub>1</sub>C<sub>1</sub>im][NTf<sub>2</sub>]; (●), [C<sub>2</sub>C<sub>2</sub>im][NTf<sub>2</sub>]; (▲), [C<sub>3</sub>C<sub>3</sub>im][NTf<sub>2</sub>]; (■), [C<sub>4</sub>C<sub>4</sub>im][NTf<sub>2</sub>]; (◇), [C<sub>5</sub>C<sub>5</sub>im][NTf<sub>2</sub>]; (▽), [C<sub>6</sub>C<sub>6</sub>im][NTf<sub>2</sub>]; (⊖), [C<sub>7</sub>C<sub>7</sub>im][NTf<sub>2</sub>]; (◆), [C<sub>8</sub>C<sub>8</sub>im][NTf<sub>2</sub>]; (▶), [C<sub>10</sub>C<sub>10</sub>im][NTf<sub>2</sub>]; (\*), [C<sub>2</sub>C<sub>1</sub>im][NTf<sub>2</sub>]; (○), [C<sub>3</sub>C<sub>1</sub>im][NTf<sub>2</sub>]; (×), [C<sub>4</sub>C<sub>1</sub>im][NTf<sub>2</sub>]; (Δ), [C<sub>5</sub>C<sub>1</sub>im][NTf<sub>2</sub>]; (□), [C<sub>7</sub>C<sub>1</sub>im][NTf<sub>2</sub>]; (◇), [C<sub>9</sub>C<sub>1</sub>im][NTf<sub>2</sub>]; and (▽), [C<sub>11</sub>C<sub>1</sub>im][NTf<sub>2</sub>].

In general, and for both symmetric and asymmetric series of ILs, the density decreases with the increase of the alkyl chain length, which is a direct effect of the increasing fraction of methylene groups (-CH<sub>2</sub>). In addition, the presence of water leads to a decrease on the density of ILs ranging between (0.19 to 1.6)% - values that depend on the IL hydrophobicity and associated water content. This decrease on density is more pronounced in ILs with shorter alkyl chains, and it is related with the higher water solubility in these ILs when compared to those with longer alkyl chains – *cf.* Table 4.19. For instance, at 298.15 K, the density relative deviations of the pure ILs in respect to the water-saturated samples are 1.4% and 0.23% for [C<sub>1</sub>C<sub>1</sub>im][NTf<sub>2</sub>] and [C<sub>10</sub>C<sub>10</sub>im][NTf<sub>2</sub>], respectively, and 0.75% and 0.29% for [C<sub>3</sub>C<sub>1</sub>im][NTf<sub>2</sub>] and [C<sub>11</sub>C<sub>1</sub>im][NTf<sub>2</sub>], respectively.

When addressing the results obtained for the structural pairs of isomers some discussions and conclusions can be drawn. For all the isomeric pairs, the asymmetric series present slightly higher values of densities than the corresponding symmetric ones. The more pronounced differences in densities were observed for the pairs [C<sub>3</sub>C<sub>3</sub>im][NTf<sub>2</sub>]/[C<sub>5</sub>C<sub>1</sub>im][NTf<sub>2</sub>] and [C<sub>6</sub>C<sub>6</sub>im][NTf<sub>2</sub>]/[C<sub>11</sub>C<sub>1</sub>im][NTf<sub>2</sub>]. A similar behavior on densities was already reported for the pure ILs.<sup>182</sup> In general, and due to the slightly differences between the isomeric pairs (which most of the times fall within the densities uncertainty), it can be postulated that the cation isomerism, at least derived from symmetric/asymmetric series of imidazolium-based ILs, does significantly lead to different densities – whereas the contribution of the -CH<sub>2</sub> groups towards the IL molar volume seems to be independent on its localization at one of the aliphatic tails.<sup>419,420</sup>

**Table 4.19.** Experimental and estimated mole fraction solubility of water ( $x_w$ ) in the investigated ILs, at 298.15 K and 0.10 MPa.

Ionic Liquid	$x_w$		$x_{Dev}^b$
	Estimated	Experimental <sup>a</sup> [29-31]	
[C <sub>2</sub> C <sub>1</sub> im][NTf <sub>2</sub> ]	0.345 (0.002)	0.298 (0.009)	0.0467
[C <sub>3</sub> C <sub>1</sub> im][NTf <sub>2</sub> ]	0.264 (0.002)	0.272 (0.007)	-0.0079
[C <sub>4</sub> C <sub>1</sub> im][NTf <sub>2</sub> ]	0.142 (0.002)	0.257 (0.006)	-0.1149
[C <sub>5</sub> C <sub>1</sub> im][NTf <sub>2</sub> ]	0.225 (0.002)	0.221 (0.005)	0.0042
[C <sub>7</sub> C <sub>1</sub> im][NTf <sub>2</sub> ]	0.298 (0.002)	0.197 (0.004)	0.1010
[C <sub>9</sub> C <sub>1</sub> im][NTf <sub>2</sub> ]	0.248 (0.002)	0.174 (0.001)	0.0748
[C <sub>11</sub> C <sub>1</sub> im][NTf <sub>2</sub> ]	0.244 (0.002)	0.157 (0.001)	0.0871
[C <sub>1</sub> C <sub>1</sub> im][NTf <sub>2</sub> ]	0.354 (0.002)	0.355 (0.004)	-0.0011
[C <sub>2</sub> C <sub>2</sub> im][NTf <sub>2</sub> ]	0.282 (0.002)	0.277 (0.001)	0.0043
[C <sub>3</sub> C <sub>3</sub> im][NTf <sub>2</sub> ]	0.251 (0.002)	0.223 (0.001)	0.0277
[C <sub>4</sub> C <sub>4</sub> im][NTf <sub>2</sub> ]	0.235 (0.002)	0.184 (0.003)	0.0508
[C <sub>5</sub> C <sub>5</sub> im][NTf <sub>2</sub> ]	0.147 (0.002)	0.158 (0.001)	-0.0109
[C <sub>6</sub> C <sub>6</sub> im][NTf <sub>2</sub> ]	0.183 (0.002)	0.149 (0.001)	0.0337
[C <sub>7</sub> C <sub>7</sub> im][NTf <sub>2</sub> ]	0.208 (0.002)	0.137 (0.001)	0.0711
[C <sub>8</sub> C <sub>8</sub> im][NTf <sub>2</sub> ]	0.297 (0.002)	0.125 (0.001)	0.1728
[C <sub>10</sub> C <sub>10</sub> im][NTf <sub>2</sub> ]	0.349 (0.002)	- <sup>c</sup>	-

<sup>a</sup>Standard deviation between brackets. Uncertainties are  $u(T) = 0.01$  K and  $u_r(p) = 0.05$ .

<sup>b</sup> $x_{Dev} = x_{w(Estimated)} - x_{w(Experimental)}$ .

<sup>c</sup>Not experimentally determined at 298.15 K due to the higher melting temperature of this ionic liquid. However, the water solubility in [C<sub>10</sub>C<sub>10</sub>im][NTf<sub>2</sub>] at 308.15 K is 0.1337 (in mole fraction).<sup>407</sup>

Figure 4.21 depicts the dependency of the ILs density at a fixed temperature along with the cation's alkyl side chain length. In both series of ILs, larger differences in densities amongst the pure and water-saturated ILs are observed in compounds with shorter alkyl side chains. This is a major result of a higher water content in ILs with alkyl side chains of smaller size as highlighted before. Overall, the densities of the water-saturated and pure ILs, in both series, become almost equal for  $N = 8$  (where  $N$  represents the total number of carbon atoms in the two aliphatic tails).

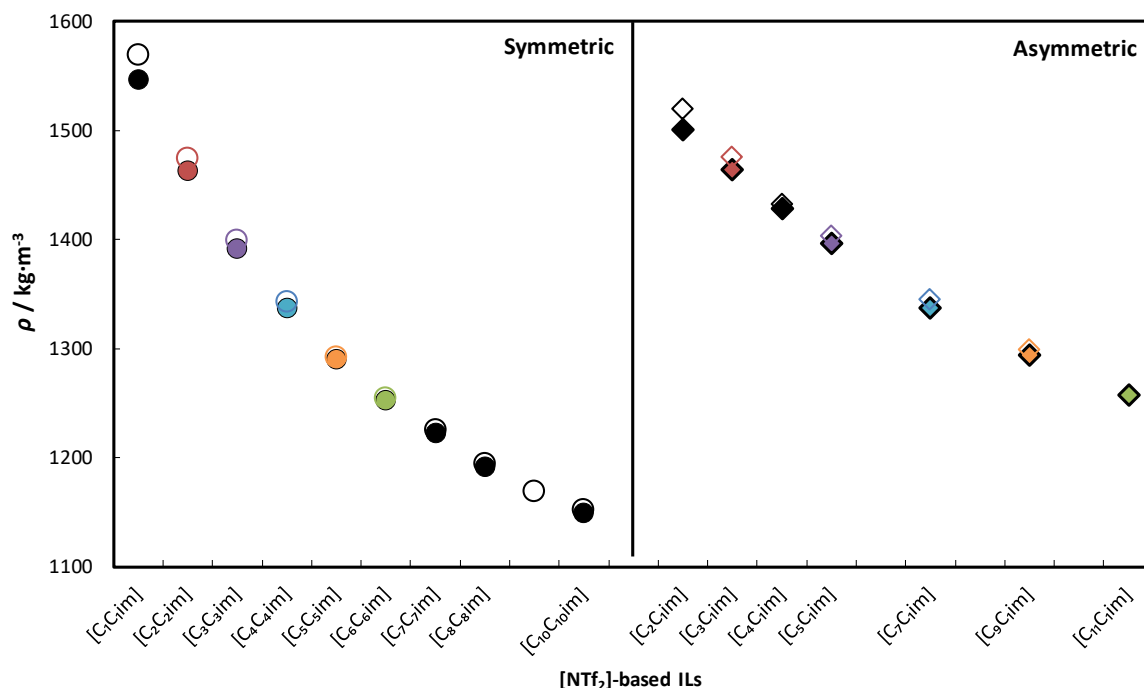


**Figure 4.21.** Density of the studied pure<sup>182</sup> (empty symbols) and water-saturated (full symbols) [NTf<sub>2</sub>]-based ILs as a function of the cation structure (alkyl side chain length increase) at 298.15 K. Colorful symbols correspond to isomers, and black symbols correspond to ILs with no corresponding isomers.

Despite the current debate surrounding the application of a linear correlation or a second order polynomial equation to describe the density data of ILs,<sup>180</sup> it was found that the use of a linear equation satisfactorily describes the experimental data within the temperature studied in this work. The fitting parameters of Equation 4.27 are given in Table S4.9 of Appendix 4.

Table 4.20 lists the thermal expansion coefficients calculated at 323.15 K and 0.1 MPa, using Equation 4.28, for all the studied water-saturated ILs, together with the values previously reported for the corresponding pure ILs.<sup>182</sup> This temperature was chosen to allow a direct comparison of all ILs at their liquid state. Even though similar thermal expansion coefficients for both symmetric and asymmetric ILs are observed, the presence of water leads to a slightly increase on  $\alpha_p$ . The  $\alpha_p$  for water-saturated ILs varies between  $(6.82 \text{ and } 7.00) \times 10^{-4} \text{ K}^{-1}$ , *i.e.*, between [C<sub>7</sub>C<sub>1</sub>im][NTf<sub>2</sub>] and [C<sub>3</sub>C<sub>1</sub>im][NTf<sub>2</sub>], respectively.

**Table 4.20.** Thermal expansion coefficients,  $\alpha_p$ , of pure<sup>182</sup> and water-saturated ILs, estimated using Equation 4.28 at 323.15 K and 0.1 MPa.<sup>a</sup>

Ionic Liquid	$10^4 \cdot (\alpha_{p,water-saturated} \pm \sigma)^b / K^{-1}$	$10^4 \cdot (\alpha_{p,pure} \pm \sigma)^b / K^{-1}$	%AD <sup>c</sup>
[C <sub>2</sub> C <sub>1</sub> im][NTf <sub>2</sub> ]	6.959 ± 0.012	6.69 ± 0.09	4.01
[C <sub>3</sub> C <sub>1</sub> im][NTf <sub>2</sub> ]	7.003 ± 0.007	6.71 ± 0.09	4.37
[C <sub>4</sub> C <sub>1</sub> im][NTf <sub>2</sub> ]	6.893 ± 0.004	6.67 ± 0.12	3.35
[C <sub>5</sub> C <sub>1</sub> im][NTf <sub>2</sub> ]	6.981 ± 0.005	6.67 ± 0.09	4.66
[C <sub>7</sub> C <sub>1</sub> im][NTf <sub>2</sub> ]	6.819 ± 0.006	6.72 ± 0.16	1.48
[C <sub>9</sub> C <sub>1</sub> im][NTf <sub>2</sub> ]	6.840 ± 0.004	6.72 ± 0.13	1.79
[C <sub>11</sub> C <sub>1</sub> im][NTf <sub>2</sub> ]	6.889 ± 0.004	6.78 ± 0.11	1.61
[C <sub>1</sub> C <sub>1</sub> im][NTf <sub>2</sub> ]	6.925 ± 0.003	6.63 ± 0.11	4.44
[C <sub>2</sub> C <sub>2</sub> im][NTf <sub>2</sub> ]	6.966 ± 0.003	6.75 ± 0.07	3.19
[C <sub>3</sub> C <sub>3</sub> im][NTf <sub>2</sub> ]	6.939 ± 0.008	6.75 ± 0.09	2.80
[C <sub>4</sub> C <sub>4</sub> im][NTf <sub>2</sub> ]	6.855 ± 0.004	6.71 ± 0.09	2.16
[C <sub>5</sub> C <sub>5</sub> im][NTf <sub>2</sub> ]	6.870 ± 0.007	6.75 ± 0.08	1.77
[C <sub>6</sub> C <sub>6</sub> im][NTf <sub>2</sub> ]	6.893 ± 0.005	6.80 ± 0.14	1.36
[C <sub>7</sub> C <sub>7</sub> im][NTf <sub>2</sub> ]	6.878 ± 0.004	6.77 ± 0.14	1.59
[C <sub>8</sub> C <sub>8</sub> im][NTf <sub>2</sub> ]	6.898 ± 0.004	6.84 ± 0.15	0.85
[C <sub>10</sub> C <sub>10</sub> im][NTf <sub>2</sub> ]	6.947 ± 0.004	6.87 ± 0.14	1.12

<sup>a</sup>Standard uncertainties,  $u$ , are  $u(T) = 0.02$  K, and  $u_r(p) = 0.05$ .

<sup>b</sup>Expanded uncertainty with approximately 95% level of confidence.

<sup>c</sup>Percentage average relative deviation on  $\alpha_p$  between the water-saturated and pure ILs.

The representation of the thermal expansion coefficient for the water-saturated ILs along with the pure ILs,<sup>182</sup> at 323.15 K and 0.1 MPa, as a function of the cation structure and alkyl side chain length is depicted in Figure 4.22. Although a straight dependence of  $\alpha_p$  with the alkyl chain length is not observed, there are pronounced effects on general trends according to the alkyl chain length increase that agree well those observed with pure ILs.<sup>182</sup>

The results obtained from the estimation of the solubility using equations 4.29 and 4.30 at 298.15 K are reported in Table 4.19. Albeit with some deviations, this approximation can be used to estimate water saturation values when no experimental data are available while foreseeing an initial screening on ILs to be applied in a particular application. These close values are also an indication that the volumetric mixing properties of the two IL series and water follow a near ideal behavior.

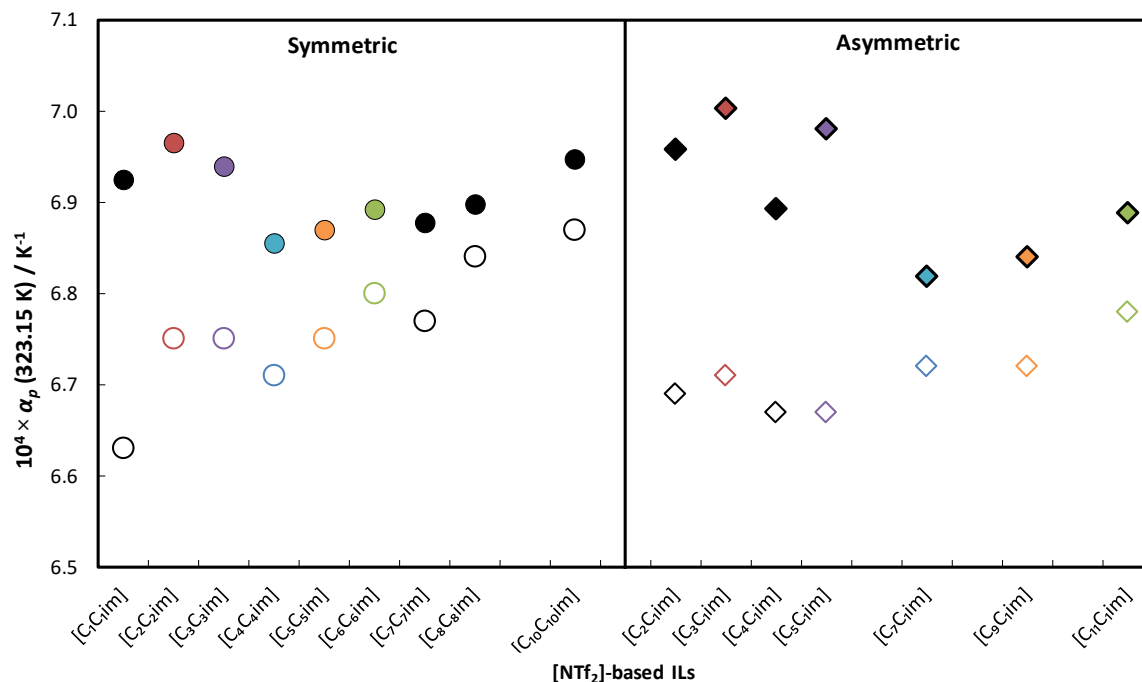


**Figure 4.22.** Thermal expansion coefficient of pure<sup>182</sup> and water-saturated ILs at 323.15 K and 0.1 MPa as a function of the cation structure (alkyl side chain length increase). The full and empty symbols represent water-saturated and pure ILs, respectively. Colorful symbols correspond to isomers, and black symbols correspond to ILs with no corresponding isomers.

### Viscosity of Water-Saturated Ionic Liquids

The viscosity data for water-saturated ILs were determined from (298.15 to 363.15) K and the detailed values are given in Tables S4.10 and S4.11 of Appendix 4. Figure 4.23 shows the viscosity results obtained in this work alongside with the deviations between the pure ILs, previously reported,<sup>182,421</sup> and the water-saturated ILs. The viscosity of water-saturated ILs increases with the increase on the size of the alkyl side chain, following the general trend already shown for pure ILs.<sup>182</sup>

It is striking to see the impact of water content in the viscosity of ILs, which significantly decreases (from 16% to 51%). Figure 4.23 also reveals the higher viscosity of water-saturated asymmetric ILs compared to the symmetric isomeric pairs, a pattern already reported for pure ILs.<sup>182</sup> The isomeric pair [C5C1im][NTf2]/[C3C3im][NTf2] presents the

smallest differences for their viscosities at the same temperature, whereas the other pairs exhibit more noticeable differences. These differences decrease with increasing temperature and increase with the length of the alkyl chain for both series of ILs. Moreover, the difference in viscosity between pure and water-saturated ILs is higher in the asymmetric series.

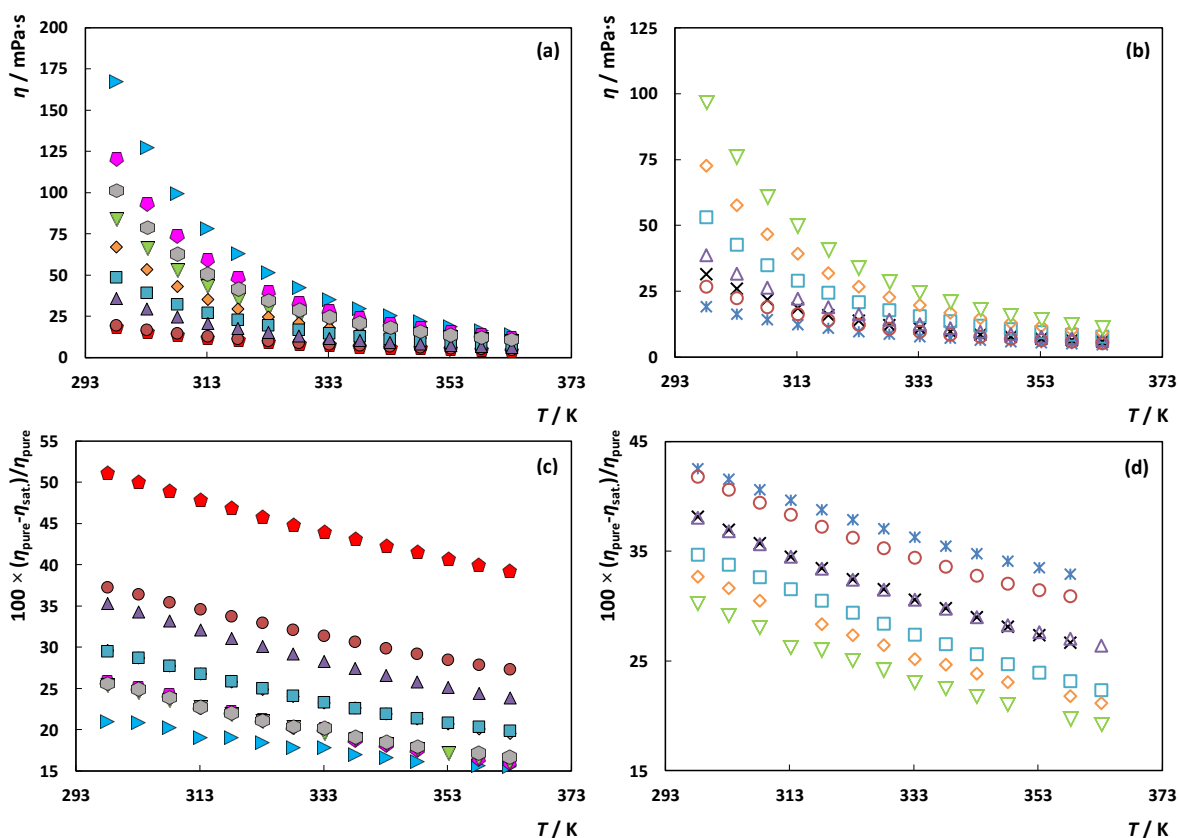


**Figure 4.23.** Viscosity of the of the symmetric and asymmetric water-saturated ILs as function of temperature, (a, b), respectively, and viscosity relative deviations between the pure<sup>182,421</sup> and the symmetric and asymmetric water-saturated ILs (c, d), respectively: (◆), [C<sub>1</sub>C<sub>1</sub>im][NTf<sub>2</sub>]; (\*), [C<sub>2</sub>C<sub>1</sub>im][NTf<sub>2</sub>]; (○), [C<sub>3</sub>C<sub>1</sub>im][NTf<sub>2</sub>]; (●), [C<sub>2</sub>C<sub>2</sub>im][NTf<sub>2</sub>]; (×), [C<sub>4</sub>C<sub>1</sub>im][NTf<sub>2</sub>]; (△), [C<sub>5</sub>C<sub>1</sub>im][NTf<sub>2</sub>]; (▲), [C<sub>3</sub>C<sub>3</sub>im][NTf<sub>2</sub>]; (□), [C<sub>7</sub>C<sub>1</sub>im][NTf<sub>2</sub>]; (■), [C<sub>4</sub>C<sub>4</sub>im][NTf<sub>2</sub>]; (◇), [C<sub>9</sub>C<sub>1</sub>im][NTf<sub>2</sub>]; (◆), [C<sub>5</sub>C<sub>5</sub>im][NTf<sub>2</sub>]; (▽), [C<sub>11</sub>C<sub>1</sub>im][NTf<sub>2</sub>]; (▽), [C<sub>6</sub>C<sub>6</sub>im][NTf<sub>2</sub>]; (◐), [C<sub>7</sub>C<sub>7</sub>im][NTf<sub>2</sub>]; (◆), [C<sub>8</sub>C<sub>8</sub>im][NTf<sub>2</sub>]; and (▶), [C<sub>10</sub>C<sub>10</sub>im][NTf<sub>2</sub>].

In recent works we have shown, not only for viscosity but also for other properties, such as vapor pressures, heat capacity and surface tension,<sup>182,416,422,423</sup> that both the asymmetric [C<sub>n</sub>C<sub>1</sub>im][NTf<sub>2</sub>] and symmetric [C<sub>n</sub>C<sub>n</sub>im][NTf<sub>2</sub>] series of ILs present a trend shift

in these properties along the alkyl side chain length increase.<sup>182,422,423</sup> Similarly to the case of the pure ILs viscosity,<sup>182</sup> this trend shift for the water-saturated ILs occurs around  $[C_6C_1im][NTf_2]$  for the asymmetric ILs and  $[C_6C_6im][NTf_2]$  for the symmetric ones, as depicted in Figure 4.24. This trend shift is related with the structural organization of the liquid above a critical alkyl size (CAS) and, similar to the pure ILs viscosity, it is particularly emphasized in the cations with higher symmetry. Some molecular dynamics studies for the asymmetric series aiming at understanding the structural shifts observed have been already performed,<sup>424</sup> while demonstrating the progressive increase and segregation of the nonpolar parts (tails) of the cations as the alkyl side chains become larger. The pure ILs with shorter alkyl chain lengths also display a clearly discernible odd-even effect on the viscosities,<sup>182</sup> that albeit the presence of water seems to smooth, is also observed in the water-saturated ILs.

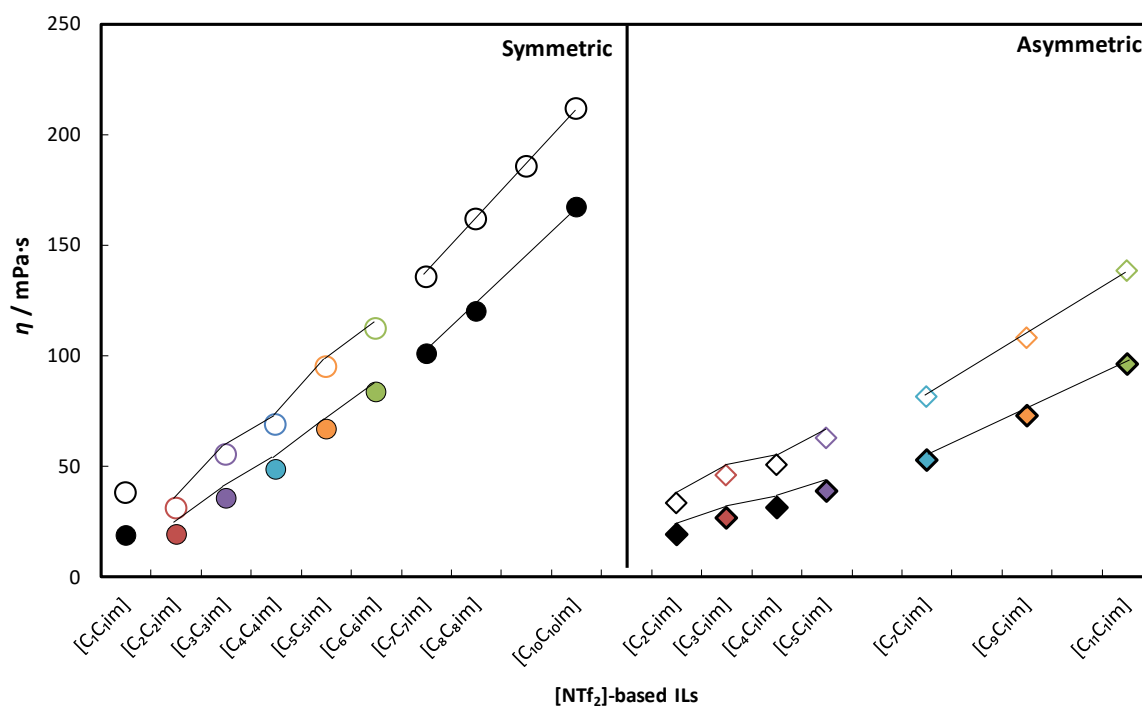


**Figure 4.24.** Viscosity dependence of the pure<sup>182,421</sup> and water-saturated  $[NTf_2]$ -based ILs studied, at 298.15 K, as a function of the cation structure (alkyl side chain length increase). The matching empty and colorful symbols represent, respectively, the pure and water-saturated ILs. Colorful symbols correspond to isomers, and black symbols correspond to ILs with no corresponding isomers.

The fitting parameters resulting from the application of the VFT model are presented in Table 4.21. The maximum absolute relative deviation between the correlated and experimental values is 2.08%, with an average absolute relative deviation of 0.17%. Thus, the application of the Vogel-Tammann-Fulcher correlation to the viscosity data<sup>180</sup> provides a good description of the viscosity dependence of water-saturated ILs as well.

**Table 4.21.** Fitting coefficients of the VTF equation and derived energy barrier,  $E$ , of pure<sup>182,421</sup> and water-saturated ILs at 323.15 K and 0.1 MPa.<sup>a</sup>

Ionic Liquid	$(A_{\eta} \pm \sigma)^b / \text{mPa}\cdot\text{s}$	$(B_{\eta} \pm \sigma)^b / \text{K}$	$(C_{\eta} \pm \sigma)^b / \text{K}$	$(E_{\text{water-saturated}} \pm \sigma)^b / \text{kJ}\cdot\text{mol}^{-1}$	$(E_{\text{pure}} \pm \sigma)^b / \text{kJ}\cdot\text{mol}^{-1}$	%AD <sup>c</sup>
[C <sub>2</sub> C <sub>1</sub> im][NTf <sub>2</sub> ]	0.203 ± 0.007	645.7 ± 11.5	155.8 ± 1.4	20.03 ± 0.76	22.35 ± 0.24	2.32
[C <sub>3</sub> C <sub>1</sub> im][NTf <sub>2</sub> ]	0.181 ± 0.006	671.4 ± 10.2	163.6 ± 1.2	22.90 ± 0.77	25.48 ± 0.15	2.58
[C <sub>4</sub> C <sub>1</sub> im][NTf <sub>2</sub> ]	0.184 ± 0.004	678.0 ± 5.8	166.2 ± 0.7	23.89 ± 0.46	26.41 ± 0.31	2.52
[C <sub>5</sub> C <sub>1</sub> im][NTf <sub>2</sub> ]	0.158 ± 0.002	734.0 ± 3.1	164.8 ± 0.3	25.40 ± 0.24	27.87 ± 0.16	2.47
[C <sub>7</sub> C <sub>1</sub> im][NTf <sub>2</sub> ]	0.164 ± 0.005	742.2 ± 9.1	169.6 ± 0.9	27.34 ± 0.75	29.83 ± 0.09	2.49
[C <sub>9</sub> C <sub>1</sub> im][NTf <sub>2</sub> ]	0.116 ± 0.028	880.0 ± 74.1	161.5 ± 6.5	29.23 ± 5.30	31.50 ± 0.54	2.27
[C <sub>11</sub> C <sub>1</sub> im][NTf <sub>2</sub> ]	0.115 ± 0.012	906.8 ± 31.3	163.5 ± 2.6	30.89 ± 2.31	32.99 ± 0.74	2.10
[C <sub>1</sub> C <sub>1</sub> im][NTf <sub>2</sub> ]	0.227 ± 0.007	600.0 ± 9.3	162.0 ± 1.2	20.06 ± 0.68	23.15 ± 0.37	3.09
[C <sub>2</sub> C <sub>2</sub> im][NTf <sub>2</sub> ]	0.165 ± 0.005	717.1 ± 10.3	147.6 ± 1.2	20.20 ± 0.59	22.33 ± 0.47	2.13
[C <sub>3</sub> C <sub>3</sub> im][NTf <sub>2</sub> ]	0.178 ± 0.003	681.8 ± 5.1	169.5 ± 0.6	25.07 ± 0.43	27.43 ± 0.16	2.36
[C <sub>4</sub> C <sub>4</sub> im][NTf <sub>2</sub> ]	0.144 ± 0.004	768.6 ± 9.3	166.1 ± 0.9	27.07 ± 0.72	28.92 ± 0.25	1.85
[C <sub>5</sub> C <sub>5</sub> im][NTf <sub>2</sub> ]	0.117 ± 0.002	846.5 ± 6.3	164.8 ± 0.6	29.31 ± 0.48	31.21 ± 0.44	1.90
[C <sub>6</sub> C <sub>6</sub> im][NTf <sub>2</sub> ]	0.105 ± 0.001	899.6 ± 2.0	163.6 ± 0.2	30.66 ± 0.15	32.34 ± 0.54	1.68
[C <sub>7</sub> C <sub>7</sub> im][NTf <sub>2</sub> ]	0.093 ± 0.004	953.7 ± 13.3	161.7 ± 1.1	31.75 ± 0.95	33.30 ± 1.30	1.55
[C <sub>8</sub> C <sub>8</sub> im][NTf <sub>2</sub> ]	0.095 ± 0.003	962.7 ± 10.4	163.4 ± 0.8	32.74 ± 0.76	34.47 ± 0.92	1.73
[C <sub>10</sub> C <sub>10</sub> im][NTf <sub>2</sub> ]	0.083 ± 0.004	1034.3 ± 15.5	162.3 ± 1.1	34.70 ± 1.11	35.70 ± 2.70	1.00

<sup>a</sup>Uncertainties are  $u(T) = 0.02$  K, and  $u_r(p) = 0.05$ .

<sup>b</sup>Expanded uncertainty with an approximately 95% level of confidence. The energy barrier values for the pure ionic liquids are from reference.<sup>182</sup>

<sup>c</sup>Percentage average absolute deviation on  $E$  between the pure and the water-saturated ILs.

The calculated energy barrier for the water-saturated ILs, at 323.15 K, together with the data for the pure ILs (reported in a previous work<sup>182,421</sup>), are listed in Table 4.21 and depicted in Figure 4.25.



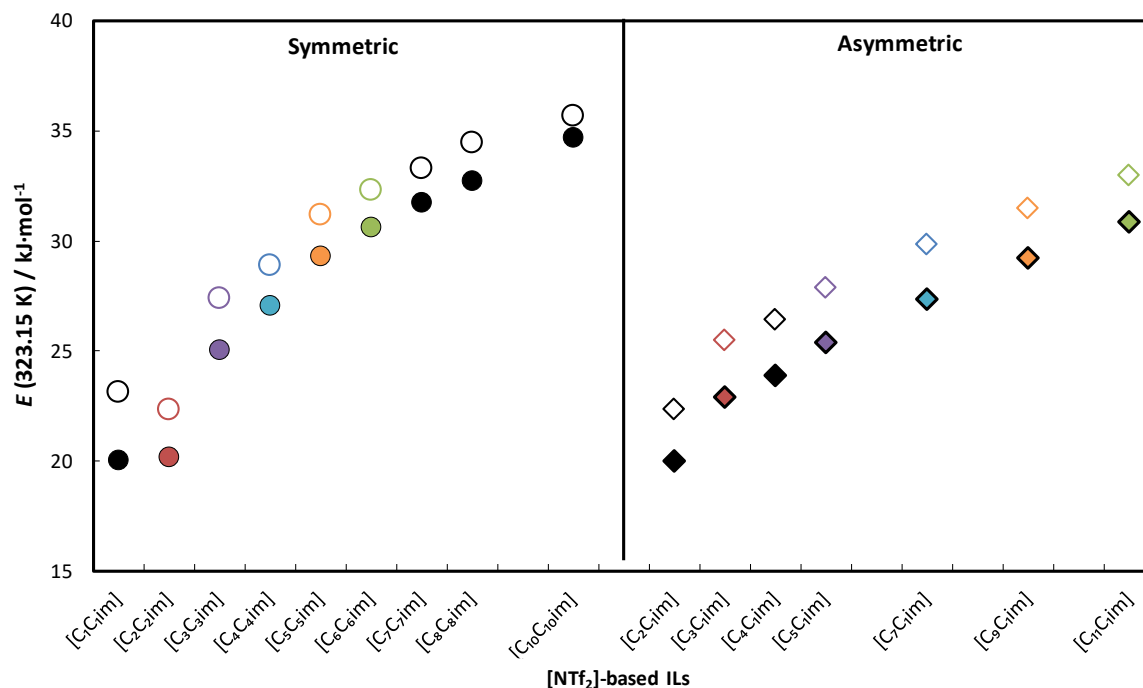


**Figure 4.25.** Energy barrier of pure<sup>182,421</sup> and water-saturated ILs at 323.15 K and 0.1 MPa, as a function of the cation structure (alkyl side chain length increase). The matching empty and colorful symbols represent, respectively, the pure and water-saturated ILs. Colorful symbols correspond to isomers, and black symbols correspond to ILs with no corresponding isomers.

As can be seen in Figure 4.25, and in both series of ILs, the energy barrier increases monotonically with the cation alkyl side chain length increase since the van der Waals interactions start to overwhelm the cation-anion electrostatic interactions. [C<sub>1</sub>C<sub>1</sub>im][NTf<sub>2</sub>] has an outlier behavior for the viscosity and energy barrier according to the increase on the alkyl side chains size due to its high charge density afforded by two small methyl groups, and as already proved for the same properties regarding the pure IL.<sup>182</sup> For ILs with the same number of carbon atoms at the aliphatic moieties, *i.e.*, structural isomers, the symmetric series of water-saturated ILs display lower energy barrier values, following the same trend observed in pure ILs.<sup>182</sup> Figure 4.25 also reveals that the presence of water reduces the energy barrier of the respective ILs.

In general, the difference in the energy barrier between water-saturated and pure ILs values, correlates well with the total number of carbons in the alkyl side chains, *N*, either

for the symmetric or asymmetric series of ILs – Figure 4.26a. Moreover, the difference of the energy barriers at 323.15 K slightly correlates with the mole fraction of water in each IL (including both series of compounds) - Figure 4.26b. The observed correlation is a clear indication that the presence of water is a major factor contribution for the decreasing of the energy barrier in all the ILs investigated, as well as a strong indication that the water molecules are solvated and mainly interacting with the polar regions of the IL (IL anion and imidazolium high-charge region). In fact, the lower is the energy barrier, the less difficult is for the ions to move past each other, which seems to be favored in the presence of water due to the weakening of IL-IL interactions. The decrease of viscosity in ILs in presence of water is thus a result of a decrease on the energy barrier, which is further connected to the water content in each IL.

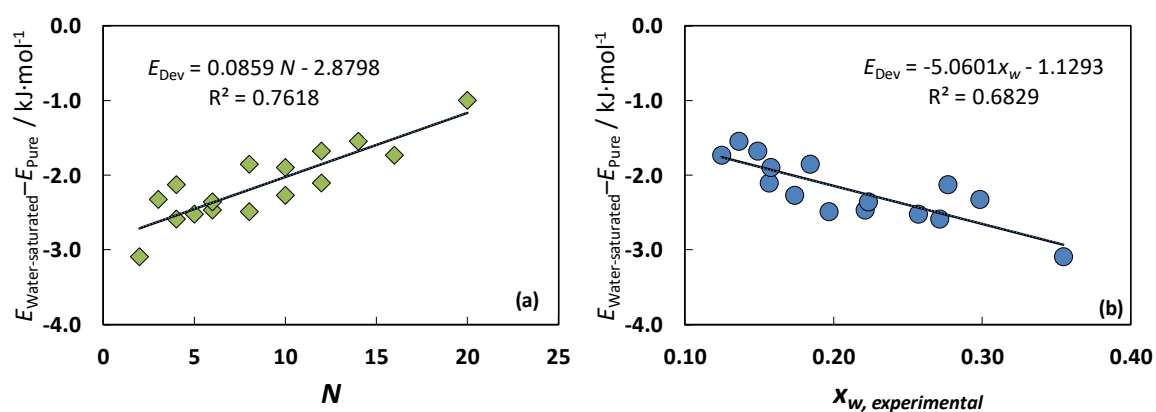


**Figure 4.26.** Deviation ( $E_{Dev}$ ) between the water-saturated and the pure ILs energy barriers at 323.15 K, as a function of: (a) the total number of carbons in the alkyl chain length,  $N$ ; and (b) the experimental mole fraction water solubility,  $x_w$  (at 298.15 K).

#### 4.2.7. Conclusions

The impact of the cation symmetry on the mutual solubilities between ILs and water was here evaluated. Despite the hydrophobic label attributed to  $[\text{NTf}_2]$ -based ILs, both series dissolve a large amount of water. In particular, solubilities in the order of 0.5 (in mole fraction) were found for the monosubstituted ILs. The impact of the structural variation of the ILs cations toward their mutual solubilities with water were analyzed and showed that the introduction of a methyl group always decreases the solubility. This decrement is

more pronounced when the addition of the methyl group is carried to an “N-H” bond. Moreover, the solubilities of ILs in water with the same total number of carbons in the alkyl side chain are comparable, as they have similar molar volumes, and a useful correlation between the solubility of [NTf<sub>2</sub>]-based ILs and their molar volume was evaluated. The thermodynamic functions of solution and solvation were also derived, indicating that the solution of the studied ILs in water is entropically driven, and the symmetric and asymmetric series of ILs display an increase of circa  $-5 \text{ J}\cdot\text{K}^{-1}\cdot\text{mol}^{-1}$  *per* methylene addition in the aliphatic moieties similar to that observed in the alkanes and alcohols in water. The predictive results obtained with COSMO-RS for the LLE of the systems here studied are in good agreement with the experimental data supporting the applicability of this model to predict the solubility of other ionic liquids and water not experimentally available.

For both pure and water-saturated ILs, the density and viscosity values decrease with increasing temperature. The density decreases with the increase of the alkyl side chain length while the viscosity increases with the size of the aliphatic tails – trend observed either for the pure or water-saturated ILs. Although the density is only slightly affected by the presence of water, the water solubility in each IL was estimated in a reasonable agreement with the experimental solubility data being an indication that the volumetric mixing properties of ILs and water follow a near ideal behavior. Furthermore, the water-saturated symmetric series of ILs generally present lower densities and viscosities than their asymmetric counterparts. The water effect on the viscosity trends shows that for pure and water-saturated ILs there is a trend shift along the alkyl side chain length. Moreover, the presence of water also affects the derived properties, leading to an increase of 2% in the thermal expansion coefficients, while the energy barrier is reduced. The latter property reveals that the symmetric series of ILs require less energy to move freely in the bulk than the asymmetric counterparts. The differences in the energy barrier values between the water-saturated and pure ILs closely correlate with the water content, meaning that the decrease on viscosity is a direct consequence of the presence of water which favor the ions to move past each other.

### 4.3. Aqueous solubilities of five *N*-(diethylaminothiocarbonyl)benzimidido derivatives at $T = 298.15$ K

Bernd Schröder, Mónia A. R. Martins, João A. P. Coutinho & Simão P. Pinho, *Chemosphere* 160, 45–53 (2016), DOI: 10.1016/j.chemosphere.2016.06.042

#### 4.3.1. Abstract

*N*-(diethylaminothiocarbonyl)benzimidido derivatives are polar multifunctional substances. A set of these compounds was synthesized by successive substitution on the enamine side, resulting in similar substances with different polarities, providing a set of model compounds with respect to the study of substituent effects on physico-chemical properties. Experimental aqueous solubility data, at  $T = 298.15$  K, of *N*-(diethylaminothiocarbonyl)benzamidine,  $\text{PhCNH}_2\text{NCSNET}_2$  (1), *N*-(diethylaminothiocarbonyl)-*N'*-phenylbenzamidine,  $\text{PhCNHPhNCSNET}_2$  (2), *N*-(diethylaminothiocarbonyl)-*N'*-monoethylbenzamidine,  $\text{PhCNHEtNCSNET}_2$  (3), *N*-(diethylaminothiocarbonyl)-*N',N'*-diethylbenzamidine,  $\text{PhCNET}_2\text{NCSNET}_2$  (4), and *N*-(diethylaminothiocarbonyl)benzimidido ethylester,  $\text{PhCOEtNCSNET}_2$  (5) were measured at  $T = 298.15$  K. The obtained data are supplemented by COSMO-RS aqueous solubility predictions as well as other environmentally important partition coefficients. This information is shown in a two-dimensional chemical space diagram, providing indications about the compartment into which the bulk of the compounds is likely to concentrate. The expected quality of COSMO-RS predictions for this type of screening exercise is illustrated on a set of pesticides with established thermophysical property data.

#### 4.3.2. Introduction

*N*-(diethylaminothiocarbonyl)benzimidido derivatives are relatively stable substances belonging to the group of thiourea derivative compounds.<sup>425</sup> They are accessible through the reaction of coordinated *N*-Acythiourea with acid chlorides, followed by further derivatization. Members of this family are known chelating agents,<sup>426</sup> with potential applications e.g., radio pharmaceuticals (<sup>99m</sup>Tc).<sup>427</sup> A large number of serine proteinase inhibitors has been developed, starting from benzamidine and its derivatives.<sup>428–430</sup>

Reports on the thermochemistry of *N*-(diethylaminothiocarbonyl)benzimidazole derivatives<sup>431,432</sup> and some of their Ni-complexes<sup>433</sup> are available. More recently, they were systematically examined for their crystalline structures,<sup>434,435</sup> with intent to connect to their fusion thermodynamics.<sup>435</sup>

Here, we report on experimental aqueous solubility data, at  $T = 298.15$  K, of the following compounds: *N*-(diethylaminothiocarbonyl)benzimidazole,  $\text{PhCNH}_2\text{NCSNEt}_2$  (1), *N*-(diethylaminothiocarbonyl)-*N'*-phenylbenzimidazole,  $\text{PhCNHPhNCSNEt}_2$  (2), *N*-(diethylaminothiocarbonyl)-*N'*-monoethylbenzimidazole,  $\text{PhCNHEtNCSNEt}_2$  (3), *N*-(diethylaminothiocarbonyl)-*N',N'*-diethylbenzimidazole,  $\text{PhCNEt}_2\text{NCSNEt}_2$  (4), and *N*-(diethylaminothiocarbonyl)benzimidazole ethylester,  $\text{PhCOEtNCSNEt}_2$  (5), as shown in Figure 4.27. These compounds have all the same chemical core structure, only differentiated by successive substitution on the enamine side (1-4) or its complete replacement by an ester group (5), making them an interesting study subject. They represent a class of rather simple, but nevertheless multifunctional compounds, whose thermodynamic properties, due to the combination of their functional groups, are not easy to predict.

Cpd. No.	Name	Structural formula
1	<i>N</i> -(diethylaminothiocarbonyl)benzimidazole	
2	<i>N</i> -(diethylaminothiocarbonyl)- <i>N'</i> -phenylbenzimidazole	
3	<i>N</i> -(diethylaminothiocarbonyl)- <i>N'</i> -monoethylbenzimidazole	
4	<i>N</i> -(diethylaminothiocarbonyl)- <i>N',N'</i> -diethylbenzimidazole	
5	<i>N</i> -(diethylaminothiocarbonyl)benzimidazole ethylester	

**Figure 4.27.** Chemical structures of the title compounds.

Quite often, accurate experimental data concerning equilibrium partition constants of such substances are not available. Furthermore, given the large number of chemicals in use, accompanied by frequently incomplete data sets, reliable methods for rapid screening of substances for their persistence in the environment are required.<sup>436</sup> A first screening procedure based on physical-chemical equilibrium partitioning data between air, water and octanol can assist in identifying environmental compartments for which degradation half-lives might be needed.<sup>437</sup>

A computational tool under attention is COSMO-RS, from which a variety of environmentally important partition coefficients are available straight from a statistical thermodynamic treatment following quantum chemical COSMO calculations. The ability of the method to successfully predict environmentally important partition coefficients was demonstrated on a variety of occasions, with respect to a diversity of compounds as well as properties.<sup>438–448</sup>

Hence our principal goals are twofold: to provide a) reliable aqueous solubility data and b) check on the predicting performance of COSMO-RS regarding these compounds, with respect to the obtained experimental data. Organizing the results in the form of partition coefficients in a two-dimensional chemical space diagram provides information about the partition behavior of the title compounds once released in the environment. For the sake of comparison, structurally related, mostly urea-based pesticides, with established thermophysical property data sets were selected and also plotted in the space diagram.

### **4.3.3. Experimental**

#### **4.3.3.1. Material**

The synthesis was performed as described in detail elsewhere.<sup>425,435</sup> A resume as well as details of characterization are given in Appendix 4.2.

### 4.3.3.2. Methods

The experimental solubilities of the *N*-(diethylaminothiocarbonyl)benzimidido derivatives in water were determined at  $T = 298.15$  K and at atmospheric pressure. The experimental setup, adapted from literature,<sup>449–451</sup> is presented in Figure 4.28.

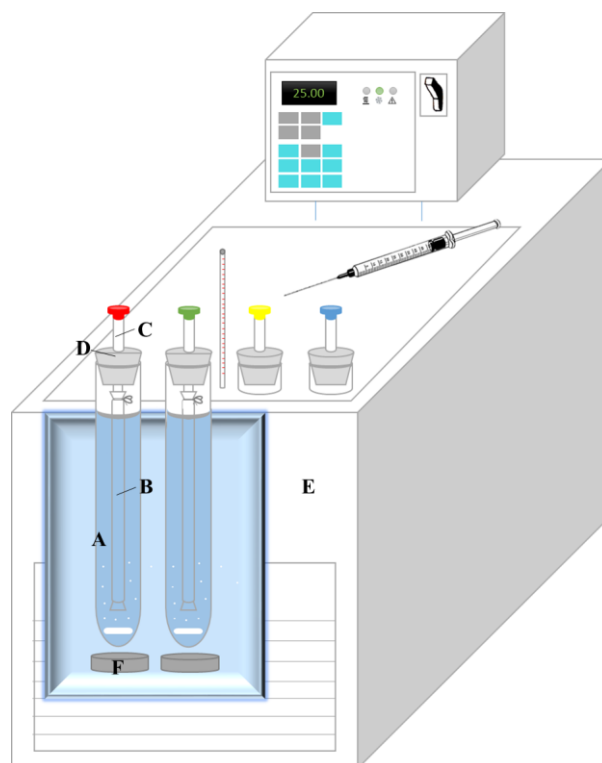


**Figure 4.28.** Experimental setup for the aqueous solubility measurements. A: Test tubes, B: dialysis tubing containing ultra-pure water, C: sampling glass tube, D: rubber cup, E: thermostated bath, F: stirrer.

Initially, test tubes (A) with solutions with an excess of solid were prepared and a dialysis tubing cellulose membrane (B) (D9277 from SIGMA), filled with ultra-pure water. The water used was double distilled, passed by a reverse osmosis system and further treated with a MilliQ plus 185 water purification apparatus (resistivity:  $18.2 \text{ M}\Omega \text{ cm}$ ;  $\text{TOC} < 5 \mu\text{g}\cdot\text{dm}^{-3}$ ; free of particles  $> 0.22 \mu\text{m}$ ). The dialysis tubing of around 10 cm length were previously humidified for at least 3 hours and cleaned according to the instructions given by the manufacturer. As shown by Figure 4.28, one end of the dialysis tubing (B) was

closed with a tight knot and the other was fixed to a glass tube (C). This glass tube allows the sampling through a rubber cup (D).

The test tubes solutions were dispersed using an isothermal ultrasonic bath (Branson 250 & 450 Sonifier) during one hour at 60%, and then allowed to equilibrate in a thermostated Julabo F38 - EH (V2) bath (E) under agitation (F) for at least 24 h, at 298.15 K. Stirring was carried out by Thermo Scientific™ Cimarec™ Micro Stirrers. This period of time proved to be enough to guarantee the saturation. The temperature accuracy of the bath was  $\pm 0.03$  K.

Samples from the inside of the dialysis membrane were collected using plastic syringes maintained at the same temperature of the saturated solution. Solute concentration was obtained by UV–vis spectroscopy, using a SHIMADZU UV-1700 PharmaSpec Spectrometer, at wavelengths of 270, 267, 269, 243, 281 for N-(diethylaminothiocarbonyl) benzamidine, N-(diethylaminothiocarbonyl)- N',N'-diethylbenzamidine, N-(diethylaminothiocarbonyl)- N'-monoethylbenzamidine, N-(diethylaminothiocarbonyl)benzimidido ethylester and N-(diethylaminothiocarbonyl)-N'-phenylbenzamidine, respectively. These wavelengths were found to be the maximum UV absorption wavelengths for the compounds investigated here. Due to the very low aqueous solubilities, solutions of known solute concentration were prepared in the binary water + methanol mixed solvent containing 65% (mass percentage in solute free basis) of methanol. Diluting this mother solution with the same mixed solvent, calibration curves were built relating absorbance and concentration, in the solute concentration range expected for aqueous solubility.

For sampling, approximately 0.5 g of saturated solution was collected from inside the dialysis tubing, and diluted in methanol, in order to have the same solvent composition as the calibration curve. At least six independent measurements were carried out for each average solubility value reported in Table 4.22, where the uncertainty is also given. Individual experimental aqueous solubility results are given in Table S4.12.



#### 4.3.4. Theoretical approach

##### Quantum chemical and COSMO-RS calculations

To obtain the necessary COSMO files, quantum-chemical optimizations were performed for all molecules in the gas phase as well as in the COSMO state, using TURBOMOLE TmoleX v.4.0.1.<sup>452,453</sup> To generate sets of all relevant conformers, COSMOconfX v.3.0<sup>454</sup> was utilized. The encountered most stable conformers are presented in Table S4.13. The possible existence of tautomeric species in the title compounds was subject to previous studies. All solid structures of 1-3 exclusively show the enamine (a) structure.<sup>434,435,455,456</sup>

At the quantum-chemical level of theory relevant to COSMO-RS, the enamine structures are the energetically more favored ones. This holds for the gas-phase as well as for the COSMO state, where they are more stable than the respective imino counterparts, in a magnitude of 35-55 kJ/mol. Although no reports regarding enamine-imino tautomerism of the title compounds in solution exist, experimental work on similar tautomerisms suggested that the form with the highest dipole moment will predominate in polar solution, e.g. in the case of 3-methylcytosine<sup>457</sup> and 1-alkyladenines.<sup>458</sup>

Table S4.14 gives an overview about COSMO-RS dipole moments. From these findings, the prevalence of the imino form (b) in aqueous solution was assumed for compounds 1 and 2.

While *pK* values of a variety of structural analoga were successfully measured by *pH* potentiometry before, no data for the title compounds could be obtained.<sup>426,459</sup>

Hence, at this stage, we assume neutral species being predominant in aqueous solutions at environmentally relevant medium *pH* ranges. Furthermore, *pK* data of the title compounds were estimated using quantum-chemical calculations at the BP-TZVP level of theory in combination with a linear free energy relationship, as provided by COSMO-RS in its COSMOtherm implementation. The results are given in Table S4.14. They suggest that the initial assumption of no significant speciation for all assumed species holds, with exception of the imino form of compound 1, for which 30 % of protonated species at

$pH=7$  would require a dissociation correction of 0.005 in  $\log S$ . With respect to  $pK_1$ , no meaningful data could be produced for compound 5.

All optimizations were performed at the BP-TZVP as well as the BP-TZVPD-FINE level of theory. In order to assure to have reached a true minimum by excluding the appearance of imaginary frequencies, the encountered global gas phase minimum was subjected to vibrational frequency calculations with AOFORCE, at the respective BP-TZVP level of theory. Resulting COSMO energies of the most stable conformers are given in Table S4.13, as well. Finally, the physico-chemical properties were estimated, using the parameter file BP\_TZVP\_C30\_1401.ctd (for COSMO files created at the BP-TZVP level of theory) and BP\_TZVPD\_FINE\_C30\_1401.ctd (for COSMO files created at the quantum chemical level BP-TZVPD-FINE, with a novel hydrogen bond interaction term and a novel van der Waals dispersion term).<sup>460</sup> In our work, all COSMO-RS calculations were performed with its COSMOtherm implementation.<sup>460</sup> In the following, a few more details are given concerning the use of COSMO-RS to calculate aqueous solubility and partition coefficients.

### **Aqueous solubility**

The mole fractions of the solute are refined using the automatic solubility calculation option of COSMOtherm:

$$\log_{10}(x_2^1) = \left[ \mu_2^{(P)} - \mu_2^{(1)} - \max(0, \Delta_{\text{fus}}G) \right] / (RT \ln(10)) \quad (4.33)$$

where  $R$  is the ideal gas constant,  $T$  is the absolute temperature,  $x_2^1$  is the mole fraction of solid 2 dissolved in the solvent phase 1 at saturation,  $\mu_2^{(P)}$  is the chemical potential of pure compound 2,  $\mu_2^{(1)}$  is the chemical potential of compound 2 at infinite dilution in the solvent, compound 1. The program possesses experimental free energy of fusion data,  $\Delta_{\text{fus}}G$ .

**Air-water partition coefficient**

Common representations of the Henry's law constant are depicted in the following equations:

$$H / (\text{Pa} \cdot \text{m}^3 \cdot \text{mol}^{-1}) = \frac{P_2}{c_2} \quad (4.34)$$

with  $c_2$  as the molar concentration of the solute, and, furthermore the air-water partition coefficient ( $K_{AW}$ ) is defined accordingly to

$$\log K_{AW} / (\text{dimensionless}) = \log \left( \frac{H}{RT} \right) \quad (4.35)$$

**Octanol-water partition coefficient**

In COSMO-RS, the octanol-water partition coefficient,  $K_{OW}$ , is predicted *via* computation of the chemical potentials of the solute at infinite dilution in each of the solvents:

$$\log K_{OW} = \log_{10} \left\{ \exp \left[ \left( \mu_w^x - \mu_o^x \right) / RT \right] \frac{V_{w,m}}{V_{o,m}} \right\} \quad (4.36)$$

with  $\mu_w^x$  as the chemical potential of compound  $x$  in water, and  $\mu_o^x$  as the chemical potential of the same compound in 1-octanol. Two different  $K_{OW}$  coefficients, the so-called wet and dry, can be calculated, being the last useful to calculate the octanol-air partition coefficient ( $K_{OA}$ ). A ratio of molar volumes  $V_{w,m}/V_{o,m}$  of 0.1505 (wet) and 0.1141 (dry) was used. Besides the density difference of the solvents, their mutual solubility is taken into account in the case of  $K_{OW}$  (wet), which corresponds to 0.274 mole fraction of water in the octanol-rich phase<sup>461,462</sup> at 298.15 K.

**Octanol-air and soil sorption coefficients**

The octanol-air coefficient is frequently used to describe partitioning of organic substances between air and organic phases in soils, plants and atmospheric aerosols. It has been obtained according equation 4.37:

$$\log K_{OA} = \log K_{OW}(\text{dry}) - \log K_{AW} \quad (4.37)$$

The data for  $K_{OW}$  (dry) can be generated in COSMO-RS using the pure quantum chemical approach. Soil-sorption partition coefficients ( $K_{OC}$ ) are directly accessible from the “Environmental Property” section of the current version of the program.

#### 4.3.5. Results and discussion

##### Experimental aqueous solubilities

Experimental solubility data measured in this work is presented in Table 4.22, including the expanded uncertainty for a 95% confidence interval. As expected, uncertainty increases with decreasing solubility. The results are, however, very satisfactory since the uncertainty divided by the solubility value presents a maximum around 12.1% for substance 2, the least soluble, while that statistical parameter is lower than 5% for solubility values higher than  $1.00\text{E-}04 \text{ g/g}_{\text{H}_2\text{O}}$ .

**Table 4.22.** Experimental aqueous solubilities at 298.15 K and expanded uncertainties ( $U$ ) for a 95% confidence interval.

Substance	Experimental ( $\text{g}\cdot\text{g}_{\text{H}_2\text{O}}^{-1}$ )	$U$ ( $\text{g}\cdot\text{g}_{\text{H}_2\text{O}}^{-1}$ )
1	1.280E-04	3.597E-06
2	8.871E-06	1.071E-06
3	1.744E-04	9.575E-06
4	3.168E-04	1.082E-05
5	3.738E-05	4.199E-06

The experimental procedure followed here was used in our laboratory for the first time. In order to validate the method, the experimental determination of the solubility of naphthalene in water at 298.15 K was also carried out, which has a solubility value of the same order of magnitude of the studied substances. Exactly the same steps were

followed, and the average value of six independent measurements was  $3.219\text{E-}05 \text{ g/g}_{\text{H}_2\text{O}}$ , presenting and extended uncertainty of  $2.730\text{E-}06 \text{ g/g}_{\text{H}_2\text{O}}$ .

In the compilation book by Yalkowsky et al.,<sup>463</sup> 28 solubility values are available at 298.15 K. Eliminating four evident outliers, the solubility ranges from  $2.957\text{E-}05 \text{ g/g}_{\text{H}_2\text{O}}$  to  $3.450\text{E-}05 \text{ g/g}_{\text{H}_2\text{O}}$ , presenting an average of  $3.189\text{E-}05 \text{ g/g}_{\text{H}_2\text{O}}$ . Therefore, the results found in this work show the good reliability of the method.

### **COSMO-RS calculations: qualitative considerations**

COSMO sigma profiles (of the energetically most stable conformers) and sigma potentials of the title compounds are shown in Figure 4.29 and 4.30, respectively. The inspection of the sigma profiles highlights differences in the local polarization-charge densities, which ultimately define the differentiation in the interaction energies of the surfaces, and hence, the magnitude of all related properties to be predicted. In the histogram, the range beyond  $\sigma = \pm 0.01 \text{ e}\cdot\text{\AA}^{-2}$  is considered as being strongly polar and potentially hydrogen-bonding, while the remaining part is weakly to non-polar. All molecules display a distinct peak at  $0.011 \text{ e}\cdot\text{\AA}^{-2}$ , with exception of 3 and 4, which are slightly shifted towards  $0.014 \text{ e}\cdot\text{\AA}^{-2}$ . The peak familiar to all molecules arises mainly from the negatively polar thiocarbonyl sulphur. The largest peak belongs to 5; here, the ester oxygen contribution is adding up. On the other side of the histogram, compounds 1 to 3 show potential to form intermolecular hydrogen bonds. This is further depicted in the hydrogen-bond moments, referring to the BP-TZVP level of theory, as Table S4.14. Compounds 1 to 3 are identified being a hydrogen-bond donor. Dipole moments decrease in the order  $4 > 3 > 5 > 1b > 2b$ .

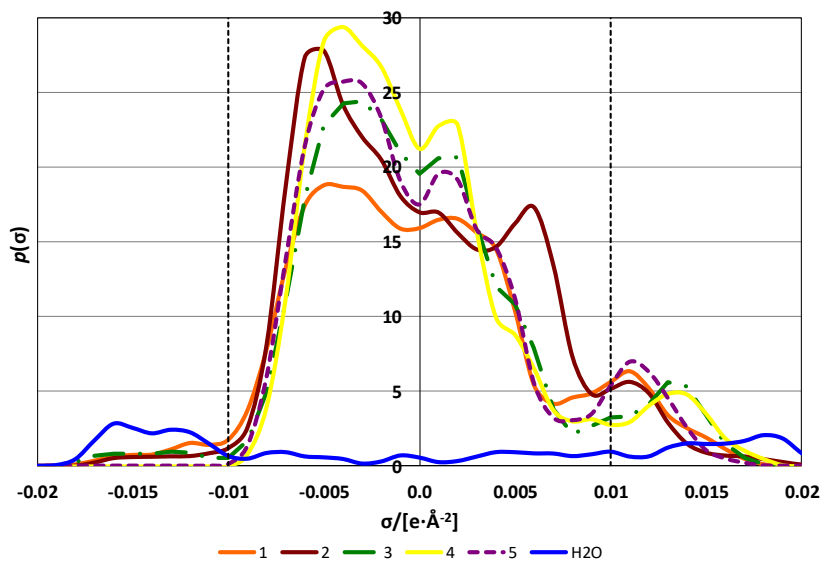


**Figure 4.29.** Sigma profiles of most stable conformers of the respective *N*-(diethylaminothiocarbonyl)benzimidazole derivatives, BP-TZVP level of theory. The sigma profile of water is plotted as reference. The range beyond  $\sigma = \pm 0.01 \text{ e}\cdot\text{\AA}^{-2}$  is considered as being strongly polar and potentially hydrogen-bonding (with a hydrogen-bond threshold value at  $\sigma_{\text{hb}} = 0.0079 \text{ e}\cdot\text{\AA}^{-2}$ ).<sup>218</sup>

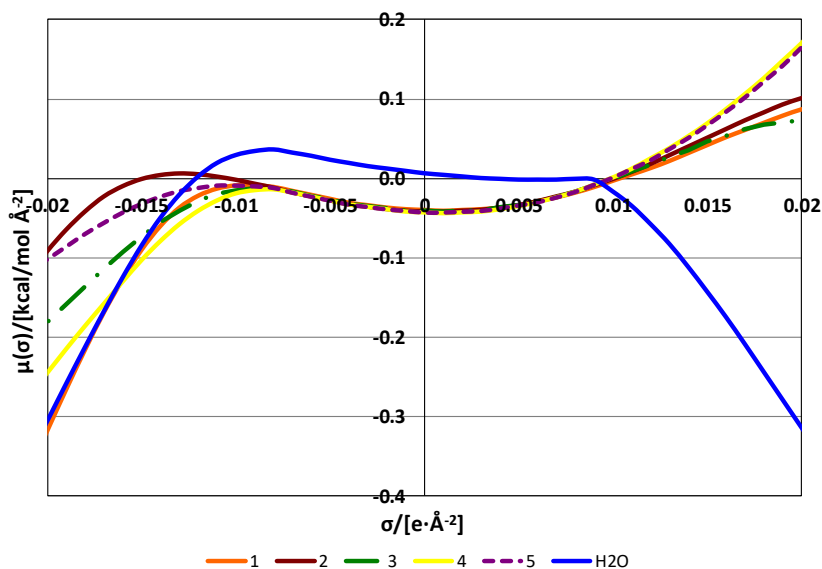


**Figure 4.30.** Sigma potentials of most stable conformers of the respective *N*-(diethylaminothiocarbonyl)benzimidazole derivatives, at  $T = 298.15 \text{ K}$ , BP-TZVP level of theory, revealing the effect of successive substitution on the enamine side of the title compounds. The sigma potential of water is plotted as reference.

The sigma potential is a measure for the affinity of the system *S* to a surface of polarity  $\sigma$ . Non-polar molecules with purely dielectric behavior exhibit a simple parabola centered at  $\sigma = 0$ . Compounds 1 to 3 indicate their hydrogen bonding donor capacity, while the other compounds show nearly parabolic behavior in the positive region. The sigma potentials of the compounds in the negative region indicate increasingly unfavorable interaction of compounds with themselves in the order  $2 > 5 > 3 > 4 > 1$ . Thermophysical data obtained in a crystal-liquid equilibrium study<sup>435</sup> of all compounds show (Table S4.15) that 4 exhibits the lowest enthalpy of fusion, followed by 1. Additionally, 4 shows a remarkably low fusion temperature when compared with the other *N*-(diethylaminothiocarbonyl)benzimidazole derivatives. These results were in agreement with the existing crystal packing constraints due to the non-existing intermolecular NH...S hydrogen-bond interactions in 4 and 1.<sup>455</sup> From all of these qualitative considerations, one could preliminarily expect 4 and 1 possessing the highest aqueous solubilities among the compounds studied here.

#### **COSMO-RS calculations: aqueous solubility calculations**

Aqueous solubilities were calculated at  $T = 298.15$  K, both at the BP-TZVP and BP-TZVPD-FINE level of theory, considering the crystalline state of the title compounds, based on the thermophysical fusion data given in Table S4.15. The results are given in Table 4.23 and compared with the obtained experimental data. Additionally, prediction results with a simpler model as provided by EPI suite WSKOWwin v 1.42 are presented, as well. WSKOWwin predicts the water solubility of an organic compound using the compounds log octanol-water partition coefficient as provided by the estimation engine from the KOWwin program, as well as the respective melting point, with the results being subject to certain structure-dependent corrections. In all cases, COSMO-RS tends to underestimate aqueous solubilities, more pronounced with the BP-TZVPD-FINE approach. Overall performance of WSKOWwin falls in-between both COSMO-RS levels of theory, underestimating aqueous solubilities for all compounds except 1.<sup>464</sup>

**Table 4.23.** Comparison of experimental data and COSMO-RS aqueous solubilities, both at the BP-TZVP and BP-TZVPD-FINE level of theory, referring to the crystalline state.

	$\log S_s/(\text{mol}\cdot\text{L}^{-1})$			
	experimental	BP-TZVP	BP-TZVPD-FINE	WSKOWwin
1	-3.266	-3.508	-3.371	-2.835
2	-4.547	-5.704	-5.730	-4.810
3	-3.180	-3.898	-4.585	-4.798
4	-2.965	-3.623	-4.981	-5.113
5	-3.851	-4.869	-5.425	-4.727
	$\sigma^a$	0.66	1.26	1.07

$$^a \sigma = \frac{1}{N_C} \sum_{i=1}^{N_C} \left| \log S_{S,\text{Exp}} - \log S_{S,\text{Calc}} \right| \text{ with } \sigma \text{ the standard error, and } N_C \text{ the number of compounds.}$$

For the title compounds, the BP-TZVP level of theory performs best overall, with a standard error  $\sigma$  of 0.66 in  $\log S$ , and a smallest deviation in  $\log S$  of 0.2 for compound 1, while the highest deviation in  $\log S$  is 1.0 for compound 5. At the BP-TZVP level of theory, the experimental finding of similar magnitudes of aqueous solubilities of compounds 1, 3 and 4 could be reproduced. For a small set of urea-based pesticides containing similar structural features and for which experimental fusion and aqueous solubility data are available, a standard error of 0.25 in  $\log S$  was obtained, slightly underestimating the solubilities in all cases except for propachlor, propanil and carbaryl, considering the BP-TZVP level of theory, as given as Table S4.16 and S4.17.

To the best of our knowledge, no vapor pressure data of the title compounds are reported, yet, neither for the (subcooled) liquid nor the crystalline state. Calorimetrically obtained standard molar enthalpies of sublimation are available, though, which represent the temperature dependence of the vapor pressure in the crystalline state, and hence might serve as an additional indicator of COSMOtherm's capability to correctly describe the energetics of the crystalline phase via the input of experimental free energy of fusion data. They are compiled in Table 4.24, together with the COSMO-RS results. The deviation for compounds 2 is biggest for both methods and rather distinct from the others. The



overall performance is good and slightly better for BP-TZVP (AAD of 5.9%) than BP-TZVPD-FINE (AAD of 9.6%).

**Table 4.24.** Standard molar enthalpies of sublimation,  $\Delta_{cr}^g H_m^0(298.15 \text{ K})$ , of *N*-(diethylaminothiocarbonyl)benzimidazole derivatives. Literature data and COSMO-RS results, both at the BP-TZVP and BP-TZVPD-FINE level of theory.

$\Delta_{cr}^g H_m^0(298.15 \text{ K}) / \text{kJ}\cdot\text{mol}^{-1}$			
Compound	Experimental	BP-TZVP	BP-TZVPD-FINE
1	$126.0 \pm 1.5^a$	117.7	115.3
2	$159.4 \pm 3.3^a$	134.8	128.4
3	$141.2 \pm 1.2^b$	139.7	130.0
4	$122.2 \pm 2.0^a$	126.0	119.3
5	$135.6 \pm 2.6^b$	130.9	122.7
AAD(%)		5.9	9.6

<sup>a</sup>Ref.<sup>431</sup>, <sup>b</sup>Ref.<sup>432</sup>

#### COSMO-RS calculations: further equilibrium partition coefficients as obtained from COSMO-RS

Today, a variety of partitioning property estimation methods is used in the attempt to prioritize substances according to their potential environmental hazards. Main targets of screening exercises are information about persistence, bioaccumulation potential, toxicity and long-range transport potential of existing and new chemicals. Equilibrium partition coefficients like  $\log K_{AW}$ ,  $\log K_{OW}$ ,  $\log K_{OA}$  and  $\log K_{OC}$  are key parameters in the process. Since experimental data are often unavailable, reliable prediction methods are of utmost importance. Current prediction methods are consistent only to a certain degree: a screening test of 529 substances using four established prediction methods showed a mere consistence for ~70% of the set members.<sup>443</sup>

Further physico-chemical data relevant for environmental purposes obtained from COSMO-RS are presented in Table S4.18. Results for the chosen urea-based pesticides are given as Table S4.19. The deviations are given in Table S4.20 and show a good performance of COSMO-RS predictions. Table S4.21 compiles data on hybrid air-water

partition coefficient of the title compounds, where the experimental component of the calculated value stems from this work aqueous solubility measurements, while vapor pressures were estimated with COSMO-RS.

The derived partition coefficients may be introduced into a two-dimensional plot describing a hypothetical chemical space as depicted in Figure 4.31. Here, the environment is modelled as volumes of air, water, and octanol, where octanol represents the organic fraction appearing in soils and sediments.<sup>437</sup> More details on the approach are given in Appendix 4.2.

The plot allows a first screening of compounds with respect to their probable distribution in the environment once (hypothetically) released. It also gives an idea about the deviation between experimental data and COSMO-RS predictions with respect to the equilibrium partition coefficients and the impact on chemical space distribution.

For the title compounds, experimental solubilities are used in the calculation of  $\log K_{AW}$ , all other properties were calculated with COSMO-RS. Since experimental  $\log K_{OW}$  (dry) data were not available,  $\log K_{OW}$  (wet) data were used throughout. The rather small deviations between both, as indicated in Table S4.18 and 4.19, justifies this approach in this qualitative screening exercise.

The 1% and 99% lines in Figure 4.31 divide the  $K_{AW}/K_{OW}$  space into regions in which partitioning is occurring almost exclusively into one medium. It is likely that degradation processes in that medium are most important, and hence, respective data are to be collected, in order to proceed with a more complete study of the compound's behavior once released into the environment. For instance, from the title compounds, 2 is to be expected to mainly partition into soil and sediment, its rather high  $\log K_{OW}$  value renders the compound prone to be persistent in the environment. The other title compounds will partially be found in the water phase, as well; especially, due to their relative lower content of carbohydrate fragments, compounds 1 and 4.

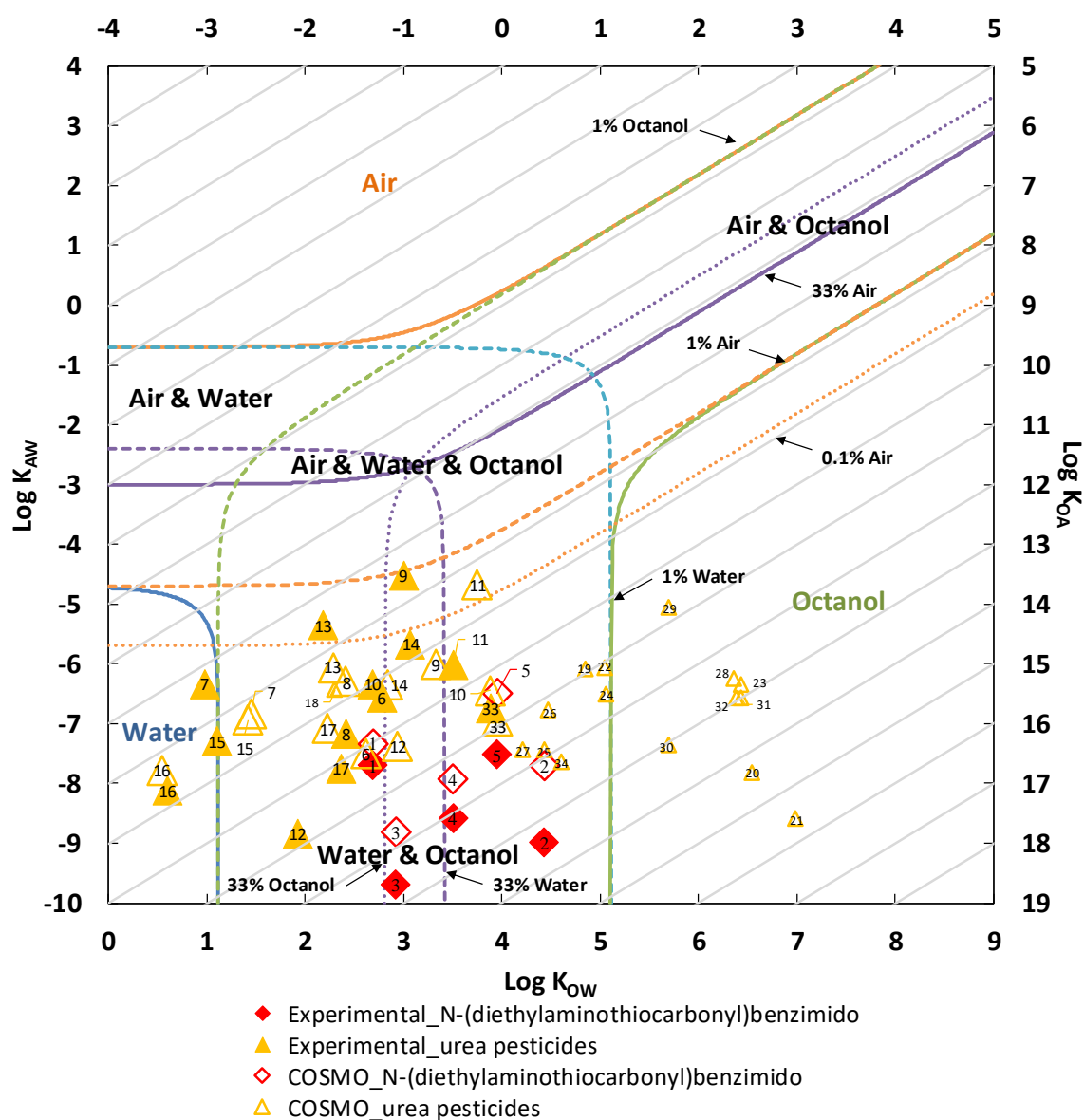


**Figure 4.31.** Chemical space diagram of the title compounds and selected urea-based pesticides (6 – Diuron; 7 – Fenuron; 8 – Fluometuron; 9 – Linuron; 10 – Barban; 11 – Chlorpropham; 12 – Diphenamid; 13 – Propachlor; 14 – Propanil; 15 – Aldicarb; 16 – Methomyl; 17 – Carbaryl; 18 – Parafluron; 19 – Triflumuron; 20 – Flufenoxuron; 21 – Chlorfluazuron; 22 – Teflubenzuron; 23 – Noviflumuron; 24 – Cyflufenamid; 25 – Penthiopyrad; 26 – Flutolanil; 27 – Fluopicolide; 28 – Etoxazole; 29 – Bistrifluron; 30 – Hexaflumuron; 31 – Lufenuron; 32 – Novaluron; 33 – Diflubenzuron; 34 – Dichlorbenzuron).

In a first approximation, the substances of the set are mainly partitioning into soil and the aquatic environment. The quality of used input data may alter the detected principal environmental compartment of their occurrence. In our example, the input only differs in  $\log K_{AW}$ , which leads to vertical shift between the data based on experimental aqueous solubility data and COSMO-RS solubilities, while all other data are obtained with COSMO-RS. The air-water partition coefficient is the compound's property most intimately related to aqueous solubility and vapor pressure. Simultaneous over (-or under)estimation of a comparable magnitude of aqueous solubilities as well as vapor pressures can largely be cancelled out in the Henry's law constant itself, as was found e.g., in the case of alkylated naphthalenes.<sup>465</sup>

Until experimental vapor pressures or experimentally determined air-water partition coefficients of the title compounds are known for confirmation, the COSMO-RS  $\log K_{AW}$  data provide a reasonable estimate. The shift resulting from the different input data sets does, in this specific case, not influence the expected environmental compartment in which the bulk of each compound will likely to partition.

In order to give indications about the adequacy of COSMO-RS to build a preliminary chemical space diagram, Figure 4.31 also includes a comparison for a set of urea-based pesticides with established consistent thermophysical property data. As can be seen the results are promising as the predictions are globally close to the experimental information. On the other hand, calculated environmental properties of some compounds show rather distinct deviations from experiment, and hence, substantially different placements in Figure 4.31. Fenuron and linuron for instance exhibit deviations in their aqueous solubilities falling within the expected range. But rather high deviations in their vapor pressure predictions are encountered, when compared to recommended data. These recommendations are known for their limited quality, e.g. solid vapor pressures of linuron.<sup>466</sup> Barban and diphenamid, with acceptable to excellent deviations concerning vapor pressures and aqueous solubilities, show a remarkable, in terms of magnitude, atypical overestimation of their lipophilicity - when compared to experiment. In such cases, COSMO-RS can serve as a screening tool for sorting out problematic experimental data, given the known difficulties in obtaining them.

Furthermore, COSMO-RS results for a set of more modern fluorine-containing pesticides<sup>467</sup> are included (Table S4.22 and S4.23). These are mostly benzoylphenyl urea derivatives used as commercial insect growth regulants (IGRs). To our best knowledge, no agreed-upon consistent thermophysical property data are available in the literature, at this point of time (except diflubenzuron). Introducing electron-withdrawing substituents often extends a compound's pesticidal spectrum, but also affects its environmental behavior. In the exemplary case of dichlorbenzuron, a 2,6-dichloro benzoyl derivative, and diflubenzuron, its 2,6-difluorinated congener, COSMO-RS calculations suggest that the substitution of chlorine by fluorine augments the vapor pressure more than it increases its aqueous solubility, in relative terms. Next to the therefore increased Henry constant, a less pronounced lipophilic character is illustrated in the lower log  $K_{ow}$  value of diflubenzuron, leading to the spatial separation of both compounds in Figure 4.31. Furthermore, dichlorbenzuron is known to degrade in soil within six to twelve months, while diflubenzuron has a half-life in soil of about three days.<sup>468</sup> The different sizes of the introduced halogens lead to distinctively different molecular structures and hence, to different metabolic pathways.<sup>469</sup>

To obtain further hints on a possible PBT character of the title compounds, another screening exercise was performed with the online-calculator PBT Profiler, whose estimates are designed for screening-level assessments on persistence (P), bioaccumulation (B), and/or toxicity (T).<sup>470</sup>

The PBT Profiler expresses (reactivity-based) persistence in single medium half-lives, measured in days, in air, water, soil, and sediment. The program first determines the media a chemical is most likely to be found in, using a Level III multi-media model where advective losses are accounted for. Furthermore, the program provides estimates regarding the bioconcentration factor (BCF) as well as the chemical's relative toxicity in the form of a long-term toxicity value (Fish ChV). The results with regard to the title compounds are given as Table S4.24 and S4.25.

They suggest that actually all title compounds might be of interest in terms of potential PBT characteristics. Their estimated half-life in soil, 75 days, exceeds the EPA criteria of  $\geq$

2 months. Therefore, they are estimated to be persistent in the environment, once released. All compounds are assigned a chronic toxicity value of fish above EPA threshold limits, except 1.

#### **4.3.6. Conclusions**

The applied aqueous solubility measurement method proved to give reliable and precise experimental data. COSMO-RS tends to underestimate aqueous solubilities of the title compounds, with respect to the experimental data, yielding best results at the BP-TZVP level of theory.

COSMO-RS is a useful tool to predict the distribution of a species between different compartments in preliminary screening exercises with the aim to prioritize compounds with potential impacts in the environment. The reliable prediction of physico-chemical properties of multi-functional substances remains a challenging task, as well as the quantification of numerical hazard estimates with respect to their uncertainties.<sup>436,471</sup>

This in turn calls for improvements in the availability of reliable experimental physico-chemical property data. Although measuring all relevant partition parameters of all multi-functional compounds is impossible, given their sheer number, the opportunity given by the technological developments in high-accuracy property determinations should be concisely applied. A concerted effort should be focused in measuring sets of polar key compounds to be defined, and re-measuring other important compounds where available data are of dubious quality, even more so as these data are supposed to serve as the future's foundation of predictive routines.

#### **4.4. Terpene solubility in water and their environmental distribution**

Mónia A. R. Martins, Liliana P. Silva, Olga Ferreira, Bernd Schröder, João A. P. Coutinho & Simão P. Pinho, submitted to *Journal of Molecular Liquids*.

##### **4.4.1. Abstract**

Terpenes and terpenoids belong to the largest and most diverse class of natural products. Due to the increasing importance of their applications and the emerging perception of

their impact on the environment, the available physico-chemical characterization is insufficient. In this work the water solubility of geraniol, linalool, DL-citronellol, thymol, eugenol, carvacrol and *p*-cymene, in the temperature range from (298.15 to 323.15) K, and at atmospheric pressure, is studied. Due to the low solubility of these compounds a novel technique was adopted for their measurements and validated using the aqueous solubility data for sparingly soluble aromatic compounds. The thermodynamic properties of solution were derived from the experimental data at infinite dilution. It is shown that the solubility of terpenes in water is an endothermic process confirming the existence of UCST phase diagrams, and only for carvacrol and eugenol is entropically driven. The experimental information is shown in a two-dimensional chemical space diagram providing indications to their probable distribution in the environment once released.

#### 4.4.2. Introduction

Terpenes, and their oxygenated derivatives, terpenoids, belong to what is probably the largest and most diverse class of natural compounds. As components of essential oils, most of them are extensively used in different industrial sectors such as flavors, fragrances, spices, perfumeries, cosmetics, or food additives, and due to their biological activity, used for pharmaceutical and medical purposes.<sup>9,22,23,30</sup>

On the other hand, on a global scale, the extensive anthropogenic use of terpenes and terpenoids associated with their natural emissions from coniferous forests, are one of the principal sources of biogenic volatile organic compounds (BVOC).<sup>24,472,473</sup> About half of global BVOC-emissions originate in isoprene, the terpenes building-block,<sup>76</sup> and their role in aerosol formation became an important research topic on the chemistry of the atmosphere, with a renewed emphasis due to the ongoing climate change debate.<sup>24,73,474</sup>

With the increase of the importance of their commercial and industrial applications, process-relevant physico-chemical data of terpenes and terpenoids have been retrieved over time. Meanwhile, with the increasing number of terpenes applications allied to their impact on the environment, right through to implications on a global scale, those data are insufficient. Furthermore, the discovery of more compounds with novel structures, and interesting bioactivities, to the already classified 55,000 terpenes, enhances the need to

establish new methods to efficiently measure the physicochemical properties of terpenes, contributing also for the development of predictive models based on molecular descriptors, quantum chemistry or equilibrium thermodynamics.

Besides vapor pressure and octanol-water partition coefficients, aqueous solubility is an important parameter to allow an ample description of the distribution of a substance amongst the different environmental compartments. Aqueous solubility is therefore an essential property in fields such as pharmaceutical sciences, environmental studies or chemical engineering. Concerning terpenes only a few works focusing exclusively SLE or LLE of binary mixtures of terpenes and water have been published. In 1980, Smyrl and LeMaguer<sup>78</sup> investigated the solubilities of three terpenic essential oil components in water, with or without dissolved solids, at three temperatures. Later, Weidenhamer and co-workers<sup>77</sup> determined the solubility of 31 biologically active monoterpenes in water by chromatography. Miller and Hawthorne<sup>475</sup> presented solubilities of D-limonene, carvone, eugenol, 1,8-cineole, and nerol in subcritical water; while Fichan et al.<sup>11</sup> and Tamura and Li<sup>476</sup> investigated water solubilities of monoterpenes at 25 °C. By searching compilation books such as “Handbook of Aqueous Solubility Data”<sup>463</sup> it is possible to gauge the limited, and high inconsistency of the available data.

Amongst the vast range of terpenes, in this work seven showing similar structures and important properties or applications, were selected. Geraniol, linalool and DL-citronellol are non-cyclic monoterpenoids usually used as repellents.<sup>10</sup> Moreover, linalool is used as a scent in 60-80% of the perfumed cleaning agents and hygiene products, and as a synthetic precursor and chemical intermediate of vitamin D. DL-citronellol is also used as raw material for the synthesis of other terpenes.<sup>10,30</sup> Thymol, eugenol, carvacrol and *p*-cymene are monoterpenoids (*p*-cymene is a monoterpene) that present an aromatic ring. *p*-Cymene occurs in the ethereal oils and is used to improve the odor of soaps, and as a solvent for dyes and varnishes. Carvacrol is a major component of oregano, and is applied as a disinfectant while eugenol is a component of clove and cinnamon oils, and both used in flavors and in dentistry. Finally, thymol occurs in the oil of thyme and oregano and it is applied as a topical antiseptic and antihelmintic.<sup>477</sup> This work reports their water solubility in the temperature range from (298.15 to 323.15) K using an experimental method



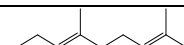
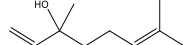
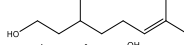
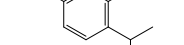
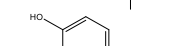
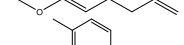
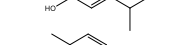
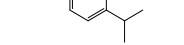
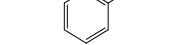
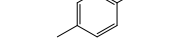
recently adapted by us for sparingly soluble solid compounds, and here applied for the first time to study the solubility of liquids in water. The new technique was validated against data for some well-studied aromatic compounds and the data reported is compared with literature values. Additionally, a thermodynamic analysis through the thermodynamic properties of solution is explored, and the terpenes first distribution in the environmental, predicted.

### 4.4.3. Experimental

#### 4.4.3.1. Material

The description of the chemicals used in this work is presented on Table 4.25. All compounds were stored at 278.15 K and used as received. However, the purity of each terpene was checked by  $^1\text{H}$ , and  $^{13}\text{C}$  NMR spectra and GC-MS. The water used was double distilled, passed by a reverse osmosis system and further treated with a MilliQ plus 185 water purification apparatus (resistivity: 18.2 M $\Omega$  cm; TOC < 5  $\mu\text{g}\cdot\text{dm}^{-3}$ ; free of particles > 0.22  $\mu\text{m}$ ). Toluene and *p*-xylene were used in order to validate the new application of the experimental method.

**Table 4.25.** Name, structure, supplier, CAS, molar mass (*M*), and purity (declared by the supplier) of the investigated compounds.

Chemicals	Supplier	CAS	<i>M</i> / g·mol <sup>-1</sup>	Mass fraction purity	Wavelength / nm
Geraniol 	Sigma-Aldrich	106-24-1	154.25	0.98	242
Linalool 	Aldrich	78-70-6	154.25	0.97	293
DL-citronellol 	Sigma	106-22-9	156.26	≈0.95	238
Thymol 	Sigma	89-83-8	150.22	≥0.995	276
Eugenol 	Aldrich	97-53-0	164.20	0.99	282
Carvacrol 	SAFC	499-75-2	150.22	0.99	275
<i>p</i> -cymene 	Aldrich	99-87-6	134.22	0.99	274
Toluene 	Sigma-Aldrich	108-88-3	92.14	0.998	262
<i>p</i> -xylene 	Acros Organics	1330-20-7	106.16	0.99	275
Methanol 	Fisher Chemical	67-56-1	32.04	0.9999	-

#### 4.4.3.2. Methods

Due to the low solubility values of the compounds under study, an approach adapted from Andersson and Schröder (1999); Etzweiler et al. (1995); and Schröder and Andersson (2001)<sup>449–451</sup> was here adopted. The experimental setup was previously presented (Figure 4.28)<sup>478</sup> and proved to be efficient in the determination of aqueous solubilities of solid substances. In this work, toluene and *p*-xylene, which have a similar structure and solubility values of the same order of magnitude with the compounds under analysis, were used to validate the method for measuring solubilities of sparingly soluble liquid compounds in water.

The experimental procedure is described in section 4.3.3.2 since it is the same used in the previous work. The wavelengths corresponding to the maximum UV absorption are indicated in Table 4.25.

The main advantage of the present technique is to avoid sampling of solute not dissolved, but present in micro-emulsions, a common experimental error, which often leads to overestimated solubility values.

#### 4.4.4. Results and discussion

##### Method validation

The experimental procedure used for the aqueous solubility determination was validated in the last chapter for solid substances. In this work it is validated for liquid compounds using toluene and *p*-xylene, molecules with similar structure and solubilities values of the same order of magnitude of the substances under study. The procedure described above was followed, and the solubility in water of toluene and *p*-xylene determined at various temperatures. Results are presented in Table 4.26 and compared in Figure 4.32 with values from the extensive and detailed study by Góral et al.<sup>479</sup> The results obtained by Neely et al.,<sup>480</sup> published after that study were also included. As shown in Figure 4.32, the results obtained demonstrate the reliability of the method for the measurement of the water solubility of sparingly soluble liquid substances.

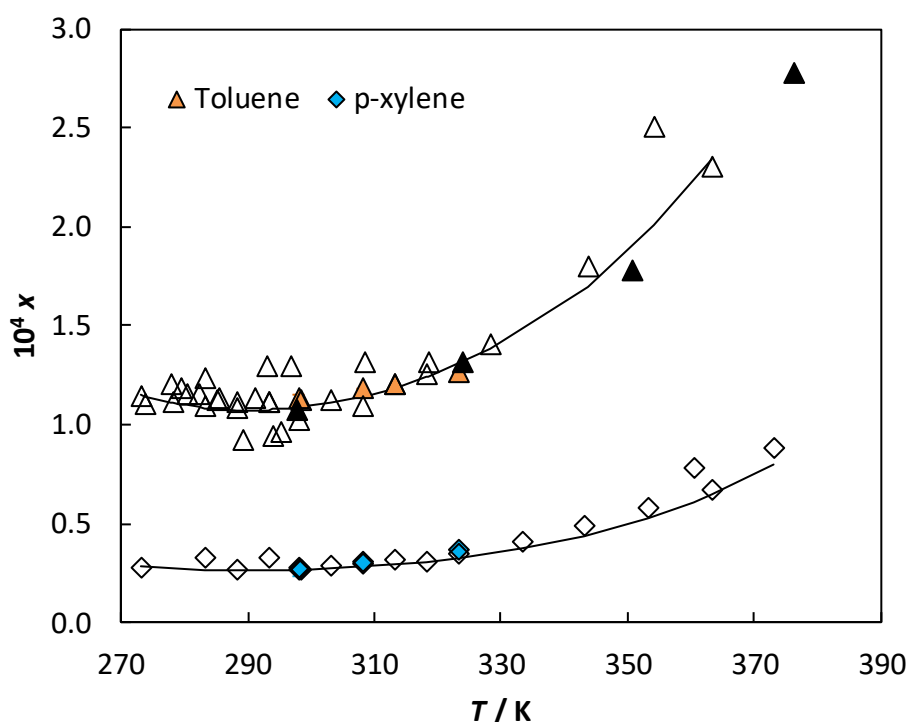


**Figure 4.32.** Comparison of the experimental aqueous solubilities of toluene and *p*-xylene with data from literature. The colorful filled symbols represent experimental points measured in this work and the open symbols and lines represent experimental and calculated data compiled and selected by Góral et al.<sup>479</sup> The black filled triangles correspond to values measured by Neely et al.<sup>480</sup>

### Aqueous Solubilities

The novel experimental aqueous solubility data for the terpenes under study, along with the uncertainty for a 95% confidence interval, are presented in Table 4.26 and Figure S4.8 of Appendix 4. Despite the lower solubilities, results are very satisfactory since the coefficient of variation defined as the ratio between the standard deviation to the average presents a maximum of 10.8% for linalool at 298.15 K. It is important to mention that among the compounds investigated in this work, thymol is the only one that is solid at room temperature, with a melting point above 500 K.

As shown in Table 4.26, with the exception of DL-citronellol the solubility of terpenes in water show a monotonical increase with temperature. Moreover, mole fraction

solubilities are in the order of  $10^{-4}$ , confirming the “hydrophobic” label usually attributed to this class of compounds and showing that the dissolved terpenes can be considered at infinite dilution. Concerning the compounds structures, at 298.15 K, the terpene *p*-cymene, an alkylbenzene, presents the lowest solubilities while the terpenoid eugenol, a phenylpropene, presents the highest, what can be attributed to the presence of oxygenated groups. This is the expectable behavior given the increasing hydrophobic nature as we move from molecules with oxygenated groups to hydrocarbons. However, the temperature dependencies of the solubilities varies widely amongst the various compounds studied. From 298.15 to 325.15 K the solubility of geraniol increases around 12 times, while for DL-citronellol, eugenol and carvacrol only double their solubility, turning the measurements more difficult.

**Table 4.26.** Experimental mole fraction ( $x_{\text{terpene}}$ ) of terpenes in water as a function of temperature and at atmospheric pressure.<sup>a</sup>

	$10^4 x_{\text{terpene}}$					
	298.15 K	303.15 K	308.15 K	313.15 K	318.15 K	325.15 K
<b>Geraniol</b>	1.027(0.330)	1.390(0.066)	3.747(0.366)	6.429(0.099)	9.222(0.315)	12.652(0.087)
<b>Linalool</b>	1.808(1.756)	3.320(0.406)	4.723(0.236)	5.920(0.424)	8.438(0.849)	11.080(1.306)
<b>DL-citronellol</b>	2.177(0.114)	1.874(0.391)	1.866(0.327)	2.082(0.028)	2.487(0.068)	3.084(0.044)
<b>Thymol</b>	1.180(0.060)	1.327(0.047)	1.457(0.069)	1.689(0.150)	1.890(0.050)	-
<b>Eugenol</b>	2.280(0.083)	2.305(0.522)	2.538(0.275)	2.539(0.150)	2.856(0.932)	3.118(0.920)
<b>Carvacrol</b>	1.440(0.173)	1.547(0.073)	1.642(0.098)	1.687(0.163)	1.703(0.090)	1.717(0.054)
<b><i>p</i>-cymene</b>	0.048(0.002)	0.069(0.003)	0.099(0.005)	0.124(0.004)	0.151(0.016)	0.189(0.007)
<b>Toluene</b>	1.127(0.048)	-	1.178(0.020)	1.203(0.038)	-	1.257(0.026)
<b><i>p</i>-xylene</b>	0.262(0.028)	-	0.307(0.006)	-	-	0.365(0.009)

<sup>a</sup>The expanded uncertainty for a 95% confidence interval is presented between brackets. The standard uncertainty of temperature is  $u(T) = 0.02$  K.

Carvacrol-thymol and geraniol-linalool are positional isomers and, as expected, their solubilities present similar values. However, while from 298.15 to 313.15 K carvacrol presents the highest solubility, at 318.15 and 323.15 K thymol is more soluble. Concerning the linear alcohols, linalool presents higher solubilities than the others up to 308.15 K, above which geraniol is the most soluble.

Among the non-cyclic terpenes studied, in general, DL-citronellol is the one presenting lower solubilities. This compound presents one double bond less when compared with linalool and geraniol, being more soluble at the lowest temperature only. In fact, it is relevant to mention the difficulty of measuring the solubility of DL-citronellol at low temperatures, due to the very small change in its solubility in that temperature range, and some enthalpic effects can be associated when comparing the solubility magnitudes of these three compounds. Regarding the aromatic terpenes group, *p*-cymene and eugenol present the lowest and highest solubilities in water, as stated before. Thymol and carvacrol present similar solubilities, between those of the other compounds.

The compounds *p*-cymene, *p*-xylene and toluene present very similar structures as can be seen in Figure 4.33, and that was the reason why the last two were chosen to validate the experimental method here adopted. Like expected, the solubility decreases from toluene to *p*-cymene, with the increase of the number of CH<sub>2</sub> groups.

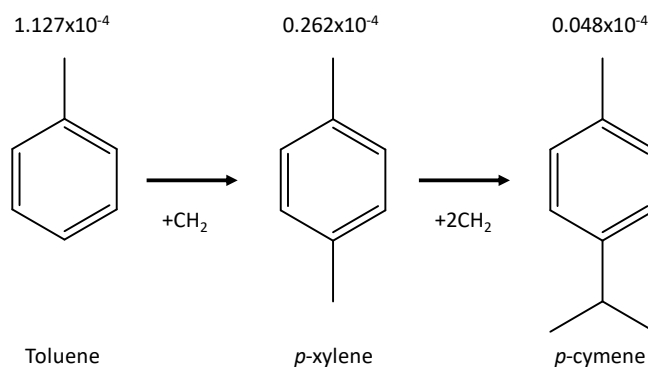


**Figure 4.33.** Structures and mole fraction water solubilities of toluene, *p*-xylene and *p*-cymene at 298.15 K.

One important objective of this work is to provide accurate experimental data of terpenes solubilities in water. However, as mentioned above, the number of terpenes known today is about 55,000. It is thus impracticable the study of all these molecules, and predictive models, or simple empirical correlations with some readily available parameters, would be of great help.

Computational methods as COSMO-RS,<sup>218</sup> SPARC,<sup>481</sup> UNIFAC<sup>482</sup> and EPI Suite,<sup>483</sup> were tested in order to predict or estimate the solubility of the studied terpenes in water. However, as can be seen in Table 4.27, none of them was able to predict satisfactorily the solubility values, nor even the solubility ranking among the different compounds studied. In particular, UNIFAC predicts a decrease on the solubility values when the temperature increases. The experimental data here presented is not only of enormous importance to assess modeling approaches, but more notably to include modifications in the description of these type of molecules, within models such as COSMO-RS, to improve the prediction capabilities concerning this vast family of compounds.

**Table 4.27.** Experimental and calculated mole fraction ( $x_{\text{terpene}}$ ) of terpenes in water at 298.15 K.

$10^4 x_{\text{terpene}}$	This Work	COSMO-RS	SPARC	UNIFAC	EPI Suite
Geraniol	1.027	0.727	0.140	1.738	0.300
Linalool	1.808	0.615	0.344	6.579	0.801
DL-citronellol	2.177	0.653	0.222	1.967	0.122
Thymol	1.180	0.284	1.370	-	0.526
Eugenol	2.280	0.235	0.267	-	0.830
Carvacrol	1.440	2.501	2.027	-	0.362
<i>p</i> -cymene	0.048	0.031	0.027	-	0.038

Several correlations of the solubility of terpenes in water with some of their properties, such as dipolar moment, octanol-water partition coefficient, solubility parameter or molar volume at several temperatures were attempted. However, no interesting results were achieved.

### Comparison with Literature

Literature values on terpenes water solubilities were previously reported and are listed in Table S4.26 and Figure S4.9 of Appendix 4, along with the experimental values from this work. Only experimental data at atmospheric pressure were selected (data points predicted or estimated were omitted). Up to date, and to the best of our knowledge, only

the values displayed in Table S4.26 were reported. For each terpene only a few reliable literature data are available, which poorly or roughly illustrates the behavior with temperature and makes the comparison with literature extremely difficult.

With a few exceptions, linalool and thymol, for which more literature information is available, show satisfactory agreement with the data measured in this work. Carvacrol presents a maximum relative deviation ( $RD / \% = |x_{exp} - x_{lit}| \cdot x_{lit}^{-1}$ ) of 20% at 298.15 K. Data for DL-citronellol reported in the overlapping temperatures to our measurements, deviate more than 100%; with the exception of the value measured by Knobloch et al.<sup>484</sup> which present RD of about 35%. RD for eugenol range between 16 and more than 100%, and for *p*-cymene range between 32 and 90%, revealing also the high inconsistency among data reported by different researchers. The same can be seen in geraniol, where at 298.15 K the RD varies between 3-25%, and at 313.15 K is more than 100%.

The large discrepancies between literature data and the experimental values here reported, and between the literature values themselves can be assigned to different experimental conditions and techniques used, and to the fact that most of the literature values are rather old. In general, taking into account the nature of the compounds here investigated, errors may be attributed to deficient saturation and sampling techniques. Thus, in this work a special procedure was applied where the use of an isothermal ultrasonic bath to speed up the dispersion guarantee the saturation; a binary solvent of water and methanol used in dilutions and calibration curves avoid dissolution problems what is very important given the hydrophobicity of these compounds; and the use of dialysis membranes avoid sampling of non-dissolved solute, which lead to overestimated solubility values, usually found by us before its use. In fact, the validation methodology implemented by studying the solubility of toluene and *p*-xylene, also support the data presented in this work.

### **Thermodynamic Functions**

In order to describe the experimental solubility of terpenes in water and taking into account the significant dependence on temperature for the enthalpy of solution, several correlations were attempted as those proposed by Tsonopoulos,<sup>402</sup> Góral<sup>479</sup> and

Maczynski et al.<sup>485</sup> However, the most suitable was found to be a linear equation that considers the harmonic temperature:<sup>486,487</sup>

$$\ln x_{\text{terpene}} = A + B \left( \frac{1}{T} - \frac{1}{T_{hm}} \right) \quad (4.38)$$

where  $T$  and  $T_{hm}$  are the absolute and harmonic temperatures, respectively; and  $A$  and  $B$  are the fitted parameters.

Table 4.28 presents the fitted parameters along with the corresponding errors considering a confidence level of 95%; where the absolute average relative deviation in the experimental mole fraction data is of 5.4 %.

**Table 4.28.** Estimated parameters for the mole fraction of terpenes in water estimated using Equation 4.38, along with the corresponding errors at the 95% confidence level.

	<b>A</b>	<b>B / K<sup>-1</sup></b>
Geraniol	-7.83 ± 0.23	-10361.19 ± -2554.61
Linalool	-7.60 ± 0.12	-6674.68 ± -1312.55
DL-citronellol	-8.41 ± 0.16	-1456.00 ± -1858.73
Thymol	-8.78 ± 0.05	-1931.58 ± -547.11
Eugenol	-8.26 ± 0.04	-1210.40 ± -479.49
Carvacrol	-8.73 ± 0.03	-663.14 ± -345.81
<i>p</i> -cymene	-11.49 ± 0.08	-5216.52 ± -859.38
Toluene	-9.04 ± 0.01	-420.01 ± -36.83

Through the temperature dependence of the experimental solubility data and assuming infinite dilution of the solubility in water, it is possible to derive the standard molar thermodynamic functions of solution: Gibbs energy ( $\Delta_{sol}G_m^0$ ), enthalpy ( $\Delta_{sol}H_m^0$ ) and entropy ( $\Delta_{sol}S_m^0$ ), using equations 4.39 – 4.41. Results are presented in Table 4.29.

$$\Delta_{sol}G_m^0 = -RT \ln(x)_p \quad (4.39)$$

$$\frac{\Delta_{sol}H_m^0}{RT^2} = \left( \frac{\partial \ln x}{\partial T} \right)_p \quad (4.40)$$



$$\Delta_{sol}S_m^0 = R \left[ \frac{\partial(T \ln x)}{\partial T} \right]_p \quad (4.41)$$

where  $R$  is the ideal gas constant and subscripts  $p$  and  $m$  indicates isobaric condition and constant composition during the process, respectively.

**Table 4.29.** Standard thermodynamic molar properties of solution of terpenes in water at  $T_{hm} = 310.42$  K together with the errors at the 95% confidence level.

	$\Delta_{sol}H_m^0 / \text{kJ} \cdot \text{mol}^{-1}$	$\Delta_{sol}G_m^0 / \text{kJ} \cdot \text{mol}^{-1}$	$T_{hm}\Delta_{sol}S_m^0 / \text{kJ} \cdot \text{mol}^{-1}$
Geraniol	$86.15 \pm 21.24$	$23.70 \pm 0.83$	$62.45 \pm 21.26$
Linalool	$55.50 \pm 10.91$	$22.24 \pm 2.51$	$33.25 \pm 11.20$
DL-citronellol	$12.11 \pm 15.45$	$21.76 \pm 0.14$	$-9.66 \pm 15.45$
Thymol	$16.06 \pm 4.55$	$23.34 \pm 0.13$	$-7.28 \pm 4.55$
Eugenol	$10.06 \pm 3.99$	$21.64 \pm 0.09$	$-11.58 \pm 3.99$
Carvacrol	$5.51 \pm 2.88$	$22.83 \pm 0.31$	$-17.32 \pm 2.89$
<i>p</i> -cymene	$43.37 \pm 7.15$	$31.63 \pm 0.09$	$11.74 \pm 7.15$
Toluene	$3.49 \pm 0.31$	$23.46 \pm 0.11$	$-19.97 \pm 0.33$

The molar thermodynamic properties of solution reported in Table 4.29 help to explore molecular mechanisms behind the solvation phenomena. The positive enthalpies of solution show that the dissolution of terpenes in water is an endothermic process and confirm the existence of UCST phase diagrams assumed before. Very evidently, geraniol and linalool present a very unfavorable enthalpic term when compared with all the other terpenes, while an enthalpic-entropic compensation phenomena occurs as eugenol and carvacrol show a very unfavorable entropic effect while their solution enthalpy are much smaller. Moreover, the standard Gibbs energy of solution increases with the reduction of functional groups present in the molecules. Eugenol presents the lowest standard Gibbs energy of solution, *p*-xylene the highest, while the isomers carvacrol and thymol present similar values. With only four experimental points the same procedure was applied to toluene solubility. The standard enthalpy of solution is 3.49 kJ/mol at the harmonic temperature 310.4 K, which is comparable to 4.36 kJ/mol measured by a flow micro-calorimetric method at 308.2 K,<sup>488</sup> and to 4.56 kJ/mol found using the solubility data by Neely at al.,<sup>480</sup> supporting also the good quality of the experimental data collected in this

work, as in the compilation analysis by Hefter<sup>489</sup> the enthalpy of solution at 298.15 K, calculated from different aqueous solubility sets, are in the range between 1.5 and 4.7 kJ/mol.

### Environmental Distribution

The environment is modelled as volumes of air, water, and octanol, where octanol represents the organic fraction appearing in soils and sediments. Thus, Gouin et al.<sup>437</sup> proposed a qualitative approach that allows to have a first screen of compounds with respect to their probable distribution in the environment once released. This was used by us in Chapter 4.3 and is here applied for the first time to terpenes and terpenoids. Here, octanol-water ( $\log K_{OW}$ ) and air-water ( $\log K_{AW}$ ) partition coefficients are introduced in a two-dimensional plot describing a hypothetical chemical space as represented in Figure 4.34. Additional details about this approach are given in Appendix 4.3.

The air-water partition coefficients are most intimately related to aqueous solubility and vapor pressure. The experimental aqueous solubility data from this work were used to calculate the  $\log K_{AW}$ , together with vapor pressures collected from literature.<sup>82,466,490–494</sup> Octanol-water partition coefficients were measured experimentally by Griffin et al.<sup>495</sup> Isoprene data, used here as a references, were taken from Mackay et al.<sup>466</sup>

The lines in Figure 4.34 (1% and 99%) divide the chemical space into different regions in which partitioning is occurring almost exclusively into one medium. In general, terpenes are partitioning into the three environmental compartments while toluene, *p*-xylene and isoprene partition exclusively into air due to their extremely high vapor pressure. DL-citronellol is the only compound that only partition between water and octanol phases. Its rather high value of  $\log K_{OH}$  makes it to be more persistent in the environment. Due to its high solubility in water, eugenol will partially be found in the water phase.

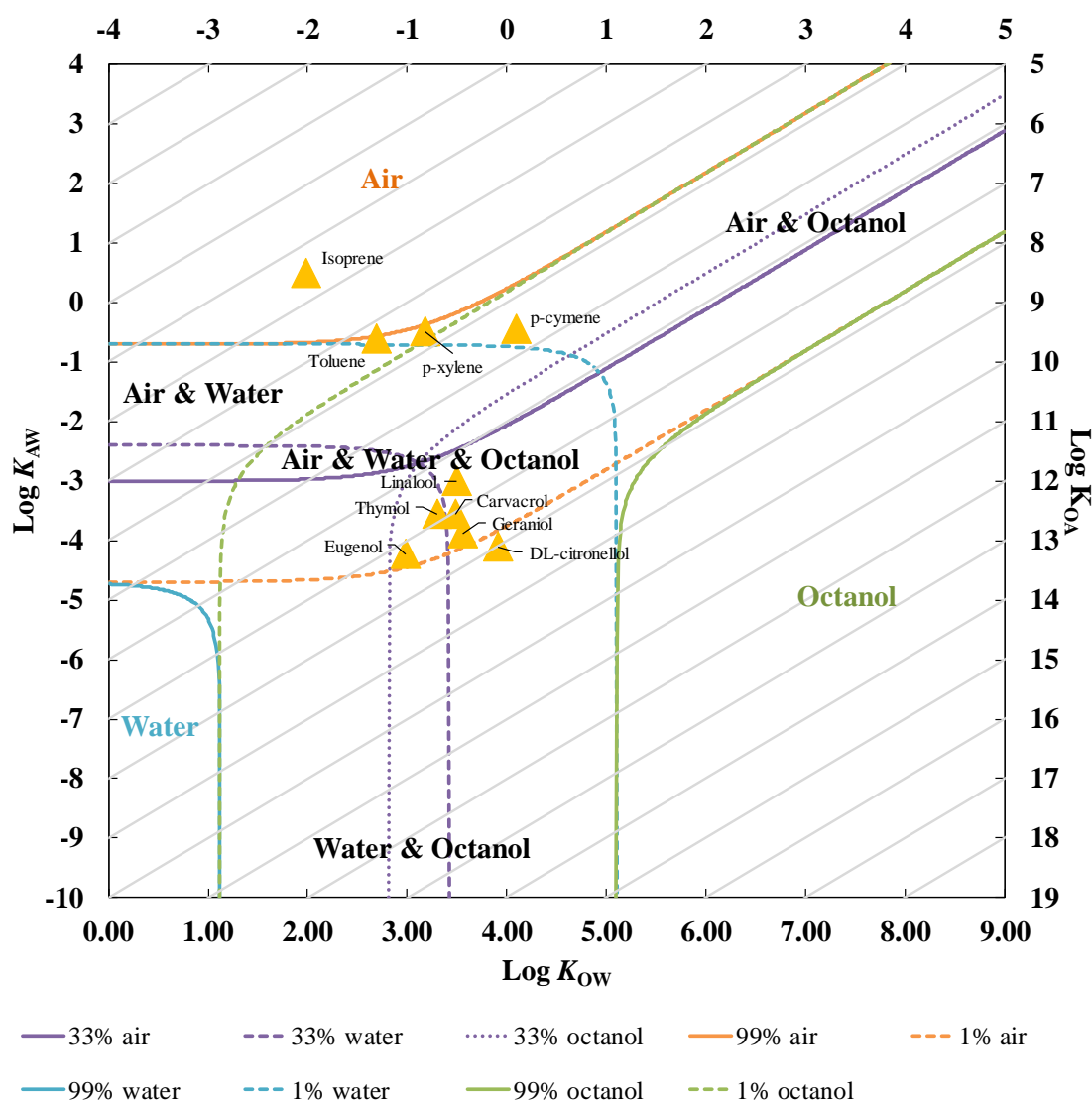


**Figure 4.34.** Chemical space diagram of the terpenes investigated in this work and some other selected compounds, namely isoprene, toluene and *p*-xylene.

#### 4.4.5. Conclusions

The solubility of seven terpenes in water at six different temperatures was evaluated using a new experimental methodology. The new experimental method was successfully validated for liquid substances using toluene and *p*-xylene as model compounds, proving to give reliable and precise experimental data. The thermodynamic properties of solution were calculated indicate that the solubility of terpenes in water is an endothermic process, confirming the existence of UCST phase diagrams and, excepting carvacrol and

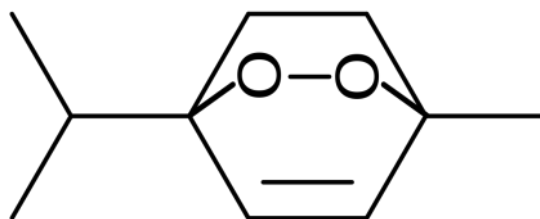
eugenol, enthalpically driven. A two-dimensional chemical space diagram shows that, in general, terpenes partition into the three environmental compartments, while toluene and *p*-xylene partition exclusively into air due to their higher vapor pressure.

This work contributes and calls for increasing the availability of reliable experimental physico-chemical property data of terpenes, which are also of enormous importance to the improvement, development and test new computational methods aiming for their prediction in such a vast family of compounds. Efforts must be focused in measuring or re-measuring basic important properties as mutual solubilities, vapor pressures, and octanol-water partition coefficients, where available, are very often of dubious quality.



# Chapter 5 – Final Remarks and Future

## Work





The present work reports a comprehensive study on terpenes properties and phase equilibria, that are a contribution for the development of novel terpenes applications, their extraction, and studies addressing their environmental fate.

First, and inspired by the lack of well characterized hydrophobic eutectic mixtures to be used in novel processes and products, sustainable hydrophobic solvents based on terpenes and monocarboxylic acids – and liquid at room temperature – were successfully prepared and characterized. Mixtures between terpenes and monocarboxylic acids form normal eutectic solvents while some mixtures of terpenes form deep eutectic solvents.

To be used in different applications pure terpenes must be extract from essential oils and subsequently fractionated, and ionic liquids were here evaluated to that purpose. Results show that ILs may replace conventional entrainers applied for the separation processes of aliphatic/aromatic hydrocarbons and, concerning terpenes the most effective ILs would require polar anions to improve selectivity and non-polar cations to increase capacity. Based on the later conclusions, it was decided to design deep eutectic solvents for the same purpose. Ammonium salts were combined with fatty alcohols or fatty acids and novel DES and simple eutectic mixtures designed and their solid-liquid phase diagrams characterized and modeled.

When envisaging large-scale applications terpenes will inevitably end in the environment. Anthropogenic releases allied to their natural emissions are concerning the environmentalists. In this context, the solubilities of terpenes in water were determined confirming their hydrophobicity and a set of critical properties was estimated and recommended. A derived two-dimensional plot describing a hypothetical chemical space shows that in general and despite their low solubility in water, terpenes are partitioning into the three environmental compartments.

Along this work a novel technique for the solubility measurement of sparingly soluble compounds in water was developed, validated and successfully applied for several compounds. Moreover, aiming at the measurement of activity coefficients at infinite dilution in the University of Aveiro, the experimental procedure used in the Warsaw University of Technology was here implemented for the first time. In the deep eutectic



solvents framework, a visual methodology to measure the solid-liquid phase diagrams of mixtures and pure compounds using an automatic glass capillary device was developed and validated.

Future investigations should be focused on the effective proving of the hydrophobicity of the new eutectic and deep eutectic mixtures formulated in chapter 2. To that end, the water content, mutual solubilities, NMR, TGA, FTIR, viscosities and densities of the pure and water saturated mixtures should be measured and evaluated. NMR and FTIR spectroscopy will help to explore the mixtures structures and purities and to confirm the interaction of the two compounds leading to the eutectic formation. Additionally, their effectiveness to extract different biomolecules and metals could be an interesting topic of study. A full work on the modeling of these systems using PC-SAFT, UNIFAC or CPA is of the utmost importance.

Another area to further investigate is the use of the new apparatus in Aveiro to measure activity coefficients at infinite dilution of terpenes and non-volatile ionic liquids or deep eutectic solvents aiming to screen these class of solvents for the terpenes extraction. COSMO-RS indicated the more suitable ILs to perform terpenes extraction and purification, and these should now be tested experimentally in both, the measurements of the activity coefficients at infinite dilution and the real extraction and purification of terpenes. Being DES an important neoteric class of solvents, these should be use to the same end and screened by using calculation tools as COSMO-RS. The fact that terpenes are hydrophobic compounds indicates that hydrophobic DES should be preferred and thus further investigated. The same characterization mentioned before for systems involving terpenes – formulation, characterization, modeling and extraction ability evaluation – must be performed to all mixtures formulated. Being vapor pressure an important property that may condition solvents used in industries, it must be additionally measured and taking into account in future studies involving DES.

Moreover, the new solubility apparatus implemented should be used to determine the solubility of more terpenes and their mixtures in water at different temperatures, an essential property to accurate predict the fate of terpenes in environment. A review

focused on the monoterpenes physico-chemical properties that is also an output of this work is a useful starting point to select the compounds and properties to investigate next. Due to the large number of terpenes, investigation on the prediction methods and empirical correlations of the properties measured should always be attempted.



## List of Publications

### **2.4 Tunable hydrophobic deep eutectic solvents and eutectic mixtures based on terpenes**

Mónia A. R. Martins, Paula V. A. Pontes, Liliana P. Silva, Guilherme J. Máximo, Eduardo A. C. Batista, Simão P. Pinho & João A. P. Coutinho, in preparation.

My contribution to this work was the measurement of the experimental data in collaboration with Paula V. A. Pontes, their interpretation and the writing of the manuscript.

### **3.1.4 Activity coefficients at infinite dilution of organic solutes and water on polar imidazolium-based ionic liquids**

Mónia A. R. Martins, João A. P. Coutinho, Simão P. Pinho & Urszula Domańska, *Journal of Chemical Thermodynamics* 91, 194–203 (2015), DOI: 10.1016/j.jct.2015.07.042

My contribution to this work was the measurement of all the experimental data, their interpretation and the writing of the manuscript.

### **3.1.5 Selection of ionic liquids to be used as separation agents for terpenes and terpenoids**

Mónia A. R. Martins, Urszula Domańska, Bernd Schröder, João A. P. Coutinho & Simão P. Pinho, *ACS Sustainable Chemistry & Engineering* 4, 548–556 (2016), DOI: 10.1021/acssuschemeng.5b01357

My contribution to this work was the measurement of all the experimental data, their interpretation and the writing of the manuscript.

### **3.2 Measurement and PC-SAFT modeling of solid-liquid equilibrium of deep eutectic solvents of quaternary ammonium chlorides and carboxylic acids**

Paula V. A. Pontes, Emanuel A. Crespo, Mónia A. R. Martins, Liliana P. Silva, Catarina M. S. S. Neves, Guilherme J. Máximo, Miriam Dupas Hubinger, Eduardo A. C. Batista, Simão P. Pinho, João A. P. Coutinho, & Christoph Held, *Fluid Phase Equilibria*, in press (2017), DOI: 10.1016/j.fluid.2017.04.007.

My contribution to this work was the measurement of part of the experimental data obtained by DSC in collaboration with Paula V. A. Pontes, the validation and supervision of the data obtained by Liliana P. Silva and the writing of part of the manuscript.

### **3.3 Indirect assessment of the fusion properties of choline chloride from solid-liquid equilibria data**

Luis Fernandez, Liliana P. Silva, Mónia A. R. Martins, Olga Ferreira, Juan Ortega, Simão P. Pinho & João A. P. Coutinho, *Fluid Phase Equilibria*, in press (2017), DOI: 10.1016/j.fluid.2017.03.015.

My contribution to this work was the validation of the procedure used for the melting points measurements, the measurement of all the DSC data, the supervision of the new data obtained by Liliana P. Silva and the writing of part of the manuscript.

### **3.4 Solid-liquid phase diagrams of eutectic solvents based on choline chloride and fatty acids or alcohols**

Mónia A. R. Martins, Liliana P. Silva, Olga Ferreira, Simão P. Pinho & João A. P. Coutinho, in preparation.

My contribution to this work was the validation of the procedure used for the melting points measurements, the supervision of the new data obtained by Liliana P. Silva and the interpretation and writing of the manuscript.

### **4.1 Critical properties of terpenes and terpenoids**

Mónia A. R. Martins, Mariana B. Oliveira, Pedro J. Carvalho, Urszula Domańska, João A. P. Coutinho & Simão P. Pinho, submitted to *Industrial & Engineering Chemistry Research*.

My contribution to this work was the measurement of all the experimental data, calculations, their interpretation and write the manuscript.

### **4.2.4 Impact of the cation symmetry on the mutual solubilities between water and imidazolium-based ionic liquids**

Mónia A. R. Martins, Catarina M. S. S. Neves, Kiki A. Kurnia, Andreia Luís, Luís M. N. B. F. Santos, Mara G. Freire, Simão P. Pinho & João A. P. Coutinho, *Fluid Phase Equilibria* 375 161–167 (2014), DOI: 10.1016/j.fluid.2014.05.013

My contribution to this work was the measurement of all the experimental data and the COSMO-RS calculations, their interpretation and write the manuscript.

#### **4.2.5 Analysis of the isomerism effect on the mutual solubilities of bis(trifluoromethylsulfonyl)imide-based ionic liquids with water**

Mónia A. R. Martins, Catarina M. S. S. Neves, Kiki A. Kurnia, Luís M. N. B. F. Santos, Mara G. Freire, Simão P. Pinho & João A. P. Coutinho, *Fluid Phase Equilibria* 381 28–35 (2014), DOI: 10.1016/j.fluid.2014.08.007

My contribution to this work was the measurement of all the experimental data and the COSMO-RS calculations, their interpretation and write the manuscript.

#### **4.2.6 Densities, viscosities and derived thermodynamic properties of water-saturated imidazolium-based ionic liquids**

Mónia A. R. Martins, Catarina M. S. S. Neves, Kiki A. Kurnia, Pedro J. Carvalho, Marisa A. A. Rocha, Luís M. N. B. F. Santos, Simão P. Pinho & Mara G. Freire, *Fluid Phase Equilibria* 407 188–196 (2016), DOI: 10.1016/j.fluid.2015.05.023

My contribution to this work was the data validation, their interpretation and the writing of the manuscript.

#### **4.3 Aqueous solubilities of five *N*-(diethylaminothiocarbonyl)benzimidazole derivatives at T = 298.15 K**

Bernd Schröder, Mónia A. R. Martins, João A. P. Coutinho & Simão P. Pinho, *Chemosphere* 160, 45–53 (2016), DOI: 10.1016/j.chemosphere.2016.06.042

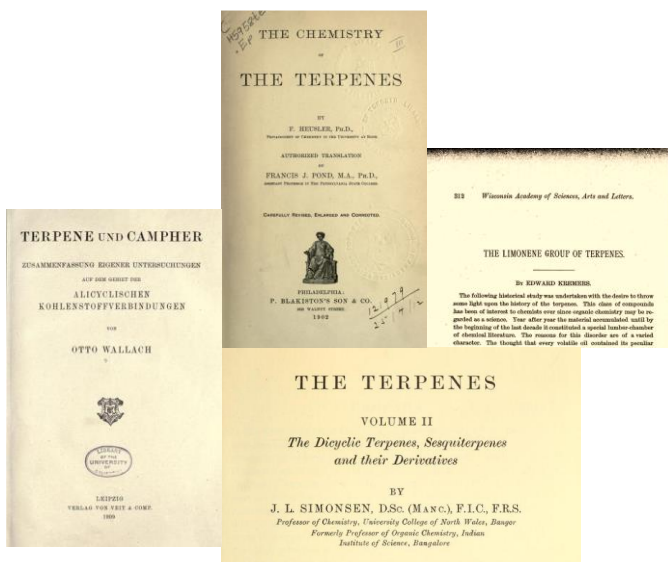
My contribution to this work was the validation of the new solubility procedure and all the experimental measurements.

#### **4.4 Terpene solubility in water and their environmental distribution**

Mónia A. R. Martins, Liliana P. Silva, Olga Ferreira, Bernd Schröder, João A. P. Coutinho & Simão P. Pinho, submitted to Journal of Molecular Liquids.

My contribution to this work was the validation of the new solubility procedure, part of the experimental measurements in collaboration with Liliana P. Silva, their interpretation and write the manuscript.

# References







- (1) Rowe, D. J. *Chemistry and Technology of Flavours and Fragrances*; Rowe, D., Ed.; Blackwell Publishing Ltd, 2005.
- (2) Associates&Leffingwell. 2011 - 2015 Flavor & Fragrance Industry Leaders [http://www.leffingwell.com/top\\_10.htm](http://www.leffingwell.com/top_10.htm) (accessed Sep 2, 2016).
- (3) Associates&Leffingwell. 2005 - 2009 Flavor & Fragrance Industry Leaders [http://www.leffingwell.com/top\\_10\\_2009.htm](http://www.leffingwell.com/top_10_2009.htm) (accessed Sep 1, 2016).
- (4) Swift, K. A. D. *Flavours and Fragrances*; Woodhead Publishing Limited: Cambridge England, 1997.
- (5) Berger, R. G. *Flavours and Fragrances: Chemistry, Bioprocessing and Sustainability*; Springer: Leipzig, Germany, 2007.
- (6) Ruzicka, L. The Isoprene Rule and the Biogenesis of Terpenic Compounds. *Experientia* **1953**, *9*, 357–367.
- (7) Silvestre, A. J. D.; Gandini, A. Chapter 2 – Terpenes: Major Sources, Properties and Applications. In *Monomers, Polymers and Composites from Renewable Resources*; Belgacem, Gandini, Eds.; Elsevier, 2008; pp 17–38.
- (8) Croteau, R. B. The Discovery of Terpenes. In *Discoveries in Plant Biology, Volume 1*; Kung, S.-D., Yang, S.-F., Eds.; World Scientific: Singapore, 1998; pp 329–343.
- (9) Zwenger, S.; Basu, C. Plant Terpenoids: Applications and Future Potentials. *Biotechnol. Mol. Biol. Rev.* **2008**, *3* (1), 1–7.
- (10) Sell, C. *A Fragrant Introduction to Terpenoid Chemistry*; The Royal Society of Chemistry: Cambridge, UK, 2003.
- (11) Fichan, I.; Larroche, C.; Gros, J. B. Water Solubility, Vapor Pressure, and Activity Coefficients of Terpenes and Terpenoids. *J. Chem. Eng. Data* **1998**, *44* (1), 56–62.
- (12) Breitmaier, E. *Terpenes: Flavors, Fragrances, Pharmaca, Pheromones*; Wiley-VCH: Germany, 2006.
- (13) Buchanan, B. B.; Gruissem, W.; Jones, R. L. *Biochemistry and Molecular Biology of Plants*; Wiley Blackwell, 2015; Vol. 2.
- (14) Burke, Y. D.; Stark, M. J.; Roach, S. L.; Sen, S. E.; Crowell, P. L. Inhibition of Pancreatic Cancer Growth by the Dietary Isoprenoids Farnesol and Geraniol. *Lipids* **1997**, *32*, 151–156.
- (15) Ćirić, A.; Karioti, A.; Koukoulitsa, C.; Soković, M.; Skaltsa, H. Sesquiterpene Lactones from *Centaurea Zuccariniana* and Their Antimicrobial Activity. *Chem. Biodivers.* **2012**, *9* (12), 2843–2853.
- (16) Dufresne, C.; Young, K.; Pelaez, F.; Gonzalez, A.; Val, D.; Valentino, D.; Graham, A.; Platas, G.; Bernard, A.; Zink, D. Illudinic Acid, a Novel Illudane Sesquiterpene Antibiotic. *J. Nat. Prod.* **1997**, *60* (2), 188–190.
- (17) Porter, J. W.; Spurgeon, S. L. *Biosynthesis of Isoprenoid Compounds, Volume 1*; Porter, J. W., Spurgeon, S. L., Eds.; Wiley-Interscience, 1981.
- (18) Guchelaar, H.-J.; Ten Napel, C. H. H.; de Vries, E. G. E.; Mulder, N. H. Clinical, Toxicological and Pharmaceutical Aspects of the Antineoplastic Drug Taxol: A Review. *Clin. Oncol.* **1994**, *6* (1), 40–48.
- (19) Zhang, L.; Demain, A. L. *Natural Products - Drug Discovery and Therapeutic Medicine*, 1st ed.; Humana Press: New Delhi, India, 2005.
- (20) Goodwin, T. W. Biosynthesis of Plant Sterols and Other Tripterpenoids. In *Biosynthesis of Isoprenoid*

- Compounds, Volume 1*; Porter, J. W., Spurgeon, S. L., Eds.; Wiley: New York, 1981; pp 443–480.
- (21) Connolly, J. D.; Overton, K. H. *Chemistry of Terpenes and Terpenoids*; Ed. Newman, Ed.; Academic Press: London, 1972.
  - (22) Bohlmann, J.; Keeling, C. I. Terpenoid Biomaterials. *Plant J.* **2008**, *54* (4), 656–669.
  - (23) Caputi, L.; Aprea, E. Use of Terpenoids as Natural Flavouring Compounds in Food Industry. *Recent Patents Food, Nutr. Agric.* **2011**, *3* (1), 9–16.
  - (24) Kesselmeier, J.; Staudt, M. Biogenic Volatile Organic Compounds (VOC): An Overview on Emission, Physiology and Ecology. *J. Atmos. Chem.* **1999**, *33* (1), 23–88.
  - (25) Buckingham, J. *Dictionary of Natural Products*; CRC Press, 1994.
  - (26) Maimone, T. J.; Baran, P. S. Modern Synthetic Efforts toward Biologically Active Terpenes. *Nat. Chem. Biol.* **2007**, *3*, 396–407.
  - (27) Werf, M. van der; Bont, J. de; Leak, D. Opportunities in Microbial Biotransformation of Monoterpenes. *Adv. Biochem. Eng. Biotechnol.* **1997**, *55*, 147–177.
  - (28) Guimarães, A. G.; Serafini, M. R.; Quintans-Júnior, L. J. Terpenes and Derivatives as a New Perspective for Pain Treatment: A Patent Review. *Expert Opin. Ther. Pat.* **2014**, *24* (3), 243–265.
  - (29) Patel, S. Plant Essential Oils and Allied Volatile Fractions as Multifunctional Additives in Meat and Fish-Based Food Products: A Review. *Food Addit. Contam. Part A* **2015**, *32* (7), 1049–1064.
  - (30) Schwab, W.; Fuchs, C.; Huang, F.-C. Transformation of Terpenes into Fine Chemicals. *Eur. J. Lipid Sci. Technol.* **2013**, *115* (1), 3–8.
  - (31) Wang, G.; Tang, W.; Bidigare, R. R. Terpenoids As Therapeutic Drugs and Pharmaceutical Agents. In *Natural Products*; Humana Press: Totowa, NJ, 2005; pp 197–227.
  - (32) Feucht, C. L. Analgesics and Anti-Inflammatory Medications in Sports: Use and Abuse. *Pediatr. Clin. North Am.* **2010**, *57* (3), 751–774.
  - (33) Monks, R. Natural Ingredients, Rapid Relief Top of Mind. *DSN: Drug Store News*. 2015.
  - (34) Hyldgaard, M.; Mygind, T.; Meyer, R. L. Essential Oils in Food Preservation: Mode of Action, Synergies, and Interactions with Food Matrix Components. *Front. Microbiol.* **2012**, *3*, 12.
  - (35) Lewis, D. F. V.; Ioannides, C.; Walker, R.; Parke, D. V. Safety Evaluations of Food Chemicals by “compact” 1. A Study of Some Acyclic Terpenes. *Food Chem. Toxicol.* **1994**, *32* (11), 1053–1059.
  - (36) Do, T.-A. L.; Vieira, J.; Hargreaves, J. M.; Wolf, B.; Mitchell, J. R. Impact of Limonene on the Physical Properties of Reduced Fat Chocolate. *J. Am. Oil Chem. Soc.* **2008**, *85* (10), 911–920.
  - (37) Beckett, S. T. Preparation of Chocolate Products with Limonene to Reduce Fat Content, 2001.
  - (38) Euromonitor International <http://www.euromonitor.com/> (accessed Sep 2, 2016).
  - (39) Berger, R. G. *Flavours and Fragrances: Chemistry, Bioprocessing and Sustainability*; Springer-Verlag Berlin Heidelberg, 2007.
  - (40) Philippopoulos, C.; Economou, D.; Economou, C.; Marangozis, J. Norbornadiene-Quadricyclane System in the Photochemical Conversion and Storage of Solar Energy. *Ind. Eng. Chem. Prod. Res. Dev.* **1983**, *22* (4), 627–633.

- (41) Payne, G. B. Preparation of 2-Exo-Hydroxy-7-oxabicyclo[2.2.1]heptanes, 1983.
- (42) Heil, M. Indirect Defence via Tritrophic Interactions. *New Phytol.* **2008**, *178* (1), 41–61.
- (43) Knudsen, J. T.; Eriksson, R.; Gershenzon, J. Diversity and Distribution of Floral Scent. *Bot. Rev.* **2006**, *72* (March), 1–120.
- (44) Gershenzon, J.; Dudareva, N. The Function of Terpene Natural Products in the Natural World. *Nat. Chem. Biol.* **2007**, *3* (7), 408–414.
- (45) Koul, O.; Walia, S.; Dhaliwal, G. S. Essential Oils as Green Pesticides: Potential and Constraints. *Biopestic. Int* **2008**, *4* (1), 63–84.
- (46) Li, Z.; Smith, K. H.; Stevens, G. W. The Use of Environmentally Sustainable Bio-Derived Solvents in Solvent Extraction applications—A Review. *Chinese J. Chem. Eng.* **2016**, *24* (2), 215–220.
- (47) Boutekedjiret, C.; Vian, M. A.; Chemat, F. Terpenes as Green Solvents for Natural Products Extraction; Springer Berlin Heidelberg, 2014; pp 205–219.
- (48) Himejima, M.; Hobson, K. R.; Otsuka, T.; Wood, D. L.; Kubo, I. Antimicrobial Terpenes from Oleoresin of Ponderosa Pine Tree *Pinus Ponderosa*: A Defense Mechanism against Microbial Invasion. *J. Chem. Ecol.* **1992**, *18*, 1809–1818.
- (49) Tamura, K.; Li, H. Mutual Solubilities of Terpene in Methanol and Water and Their Multicomponent Liquid-Liquid Equilibria. *J. Chem. Eng. Data* **2005**, *50* (6), 2013–2018.
- (50) Dejoye Tanzi, C.; Abert Vian, M.; Ginies, C.; Elmaataoui, M.; Chemat, F. Terpenes as Green Solvents for Extraction of Oil from Microalgae. *Molecules* **2012**, *17* (12), 8196–8205.
- (51) International Rubber Study Group - Home Page <http://www.rubberstudy.com/>.
- (52) Lago, S.; Rodríguez, H.; Soto, A.; Arce, A. Deterpenation of Citrus Essential Oil by Liquid-Liquid Extraction with 1-Alkyl-3-Methylimidazolium Bis(trifluoromethylsulfonyl)amide Ionic Liquids. *J. Chem. Eng. Data* **2011**, *56* (4), 1273–1281.
- (53) Francisco, M.; Lago, S.; Soto, A.; Arce, A. Essential Oil Deterpenation by Solvent Extraction Using 1-Ethyl-3-Methylimidazolium 2-(2-Methoxyethoxy) Ethylsulfate Ionic Liquid. *Fluid Phase Equilib.* **2010**, *296* (2), 149–153.
- (54) Arce, A.; Soto, A. Citrus Essential Oils: Extraction and Deterpenation. *Tree For. Sci. Biotechnol.* **2008**, *2* (Special Issue 1), 1–9.
- (55) Oliveira, C. M.; Koshima, C. C.; Capellini, M. C.; Carvalho, F. H.; Aracava, K. K.; Gonçalves, C. B.; Rodrigues, C. E. C. Liquid-liquid Equilibrium Data for the System Limonene + Carvone + Ethanol + Water at 298.2 K. *Fluid Phase Equilib.* **2013**, *360*, 233–238.
- (56) Martins, P. F.; Medeiros, H. H. R.; Sbaite, P.; Wolf Maciel, M. R. Enrichment of Oxyterpenes from Orange Oil by Short Path Evaporation. *Sep. Purif. Technol.* **2013**, *116*, 385–390.
- (57) Brose, D. J.; Chidlaw, M. B.; Friesen, D. T.; LaChapelle, E. D.; van Eikeren, P. Fractionation of Citrus Oils Using a Membrane-Based Extraction Process. *Biotechnol. Prog.* **1995**, *11* (2), 214–220.
- (58) Shimoda, M.; Shin, D. H.; Kawano, T.; Osajima, Y. Effects of ethanol as an entrainer in preparation of terpeneless oil by supercritical carbon-dioxide extraction. *Nippon Shokuhin Kogyo Gakkaishi* **1992**, *39* (4), 339–343.
- (59) Sato, M.; Goto, M.; Kodama, A.; Hirose, T. Supercritical Fluid Extraction with Reflux for Citrus Oil Processing. In *Supercritical Fluids: Extraction and Pollution Prevention*; Abraham, M. A., Sunol, A. K.,

Eds.; American Chemical Society: Washington, 1997; Vol. 670, pp 119–131.

- (60) Sato, M.; Goto, M.; Hirose, T. Fractional Extraction with Supercritical Carbon Dioxide for the Removal of Terpenes from Citrus Oil. *Ind. Eng. Chem. Res.* **1995**, *34* (11), 3941–3946.
- (61) Koshima, C. C.; Capellini, M. C.; Geremias, I. M.; Aracava, K. K.; Gonçalves, C. B.; Rodrigues, C. E. C. Fractionation of Lemon Essential Oil by Solvent Extraction: Phase Equilibrium for Model Systems at T=298.2 K. *J. Chem. Thermodyn.* **2012**, *54*, 316–321.
- (62) Koshima, C. C.; Nakamoto, K. T.; Aracava, K. K.; Oliveira, A. L.; Rodrigues, C. E. C. Fractionation of Bergamot and Lavandin Crude Essential Oils by Solvent Extraction: Phase Equilibrium at 298.2 K. *J. Chem. Eng. Data* **2015**, *60* (1), 37–46.
- (63) Lago, S.; Rodríguez, H.; Arce, A.; Soto, A. Improved Concentration of Citrus Essential Oil by Solvent Extraction with Acetate Ionic Liquids. *Fluid Phase Equilib.* **2014**, *361*, 37–44.
- (64) Lockwood, G. B. Techniques for Gas Chromatography of Volatile Terpenoids from a Range of Matrices. *J. Chromatogr. A* **2001**, *936* (1–2), 23–31.
- (65) Taylor, A. J.; Linfoth, R. S. T. *Food Flavour Technology, 2nd Edition*; Wiley-Blackwell, 2010.
- (66) Chen, W.; Viljoen, A. M. Geraniol — A Review of a Commercially Important Fragrance Material. *South African J. Bot.* **2010**, *76* (4), 643–651.
- (67) Lu, J. J.; Dang, Y. Y.; Huang, M.; Xu, W. S.; Chen, X. P.; Wang, Y. T. Anti-Cancer Properties of Terpenoids Isolated from Rhizoma Curcumae—a Review. *J. Ethnopharmacol.* **2012**, *143* (2), 406–411.
- (68) Rabi, T.; Bishayee, A. Terpenoids and Breast Cancer Chemoprevention. *Breast Cancer Res. Treat.* **2009**, *115* (2), 223–239.
- (69) Carvalho, C. C. C. R.; Fonseca, M. M. R. Carvone: Why and How Should One Bother to Produce This Terpene. *Food Chem.* **2006**, *95* (3), 413–422.
- (70) Maestre Zapata, J.; Gonzalez Del Tanago, J. On the Extraction of Terpene from Lavender Oil. *Farmacognosia* **1959**, *19*, 281–284.
- (71) *The Flavor And Fragrance High Production Volume Consortia: Revised Test Plan For Bicyclic Terpene Hydrocarbons*; The Terpene Consortium: Washington, DC, 2006.
- (72) *Kirk-Othmer Encyclopedia of Chemical Technology, 3rd Edition*; Wiley: New York, 1982.
- (73) Guenther, A.; Hewitt, C. N.; Erickson, D.; Fall, R.; Geron, C.; Graedel, T.; Harley, P.; Klinger, L.; Lerdau, M.; McKay, W. A.; Pierce, T.; Scholes, B.; Steinbrecher, R.; Tallamraju, R.; Taylor, J.; Zimmerman, P. A Global Model of Natural Volatile Organic Compound Emissions. *J. Geophys. Res. Atmos.* **1995**, *100* (D5), 8873–8892.
- (74) Ehn, M.; Thornton, J. A.; Kleist, E.; Sipilä, M.; Junninen, H.; Pullinen, I.; Springer, M.; Rubach, F.; Tillmann, R.; Lee, B.; Lopez-Hilfiker, F.; Andres, S.; Acir, I.-H.; Rissanen, M.; Jokinen, T.; Schobesberger, S.; Kangasluoma, J.; Kontkanen, J.; Nieminen, T.; Kurtén, T.; Nielsen, L. B.; Jørgensen, S.; Kjaergaard, H. G.; Canagaratna, M.; Maso, M. D.; Berndt, T.; Petäjä, T.; Wahner, A.; Kerminen, V.-M.; Kulmala, M.; Worsnop, D. R.; Wildt, J.; Mentel, T. F. A Large Source of Low-Volatility Secondary Organic Aerosol. *Nature* **2014**, *506* (7489), 476–479.
- (75) Andreae, M. O. Atmosphere. Aerosols before Pollution. *Science* **2007**, *315* (5808), 50–51.
- (76) Wiedinmeyer, C.; Guenther, A.; Harley, P.; Hewitt, N.; Geron, C.; Artaxo, P.; Steinbrecher, R.; Rasmussen, R. Global Organic Emissions from Vegetation. In *Emissions of atmospheric trace compounds*; C. Garnier, Artaxo, P., Reeves, C., Eds.; Kluwer Academic Publishers: Dordrecht,

Netherlands, 2004; pp 115–170.

- (77) Weidenhamer, J.; Macias, F.; Fischer, N.; Williamson, G. B. Just How Insoluble Are Monoterpenes? *J. Chem. Ecol.* **1993**, *19* (8), 1799–1807.
- (78) Smyrl, T. G.; LeMaguer, M. Solubilities of Terpenic Essential Oil Components in Aqueous Solutions. *J. Chem. Eng. Data* **1980**, *25* (2), 150–152.
- (79) Schmid, C.; Steinbrecher, R.; Ziegler, H. Partition Coefficients of Plant Cuticles for Monoterpenes. *Trees* **1992**, *6* (1), 32–36.
- (80) Massaldi, H. A.; King, C. J. Simple Technique to Determine Solubilities of Sparingly Soluble Organics. Solubility and Activity Coefficients of D-Limonene, Butylbenzene, and N-Hexyl Acetate in Water and Sucrose Solutions. *J. Chem. Eng. Data* **1973**, *18* (4), 393–397.
- (81) Štejfa, V.; Fulem, M.; Růžička, K.; Červinka, C.; Rocha, M. A. A.; Santos, L. M. N. B. F.; Schröder, B. Thermodynamic Study of Selected Monoterpenes. *J. Chem. Thermodyn.* **2013**, *60*, 117–125.
- (82) Štejfa, V.; Dergal, F.; Mokbel, I.; Fulem, M.; Jose, J.; Růžička, K. Vapor Pressures and Thermophysical Properties of Selected Monoterpenoids. *Fluid Phase Equilib.* **2015**, *406*, 124–133.
- (83) Li, J.; Perdue, E. M.; Pavlostathis, S. G.; Araujo, R. Physicochemical Properties of Selected Monoterpenes. *Environ. Int.* **1998**, *24* (3), 353–358.
- (84) Capello, C.; Fischer, U.; Hungerbühler, K. What Is a Green Solvent? A Comprehensive Framework for the Environmental Assessment of Solvents. *Green Chem.* **2007**, *9*, 927–934.
- (85) Breslow, R.; Breslow; Ronald. The Principles of and Reasons for Using Water as a Solvent for Green Chemistry. In *Handbook of Green Chemistry*; Wiley-VCH Verlag GmbH & Co. KGaA: Weinheim, Germany, 2010.
- (86) Anastas, P. T.; Leitner, W.; Jessop, P. G. *Handbook of Green Chemistry, Volume 4, Green Solvents, Supercritical Solvents*; Wiley-VCH, 2013.
- (87) Anastas, P. T.; Wasserscheid, P.; Stark, A. *Handbook of Green Chemistry, Volume 6, Green Solvents, Ionic Liquids*; Wiley-VCH, 2013.
- (88) Dai, Y.; van Spronsen, J.; Witkamp, G.-J.; Verpoorte, R.; Choi, Y. H. Natural Deep Eutectic Solvents as New Potential Media for Green Technology. *Anal. Chim. Acta* **2013**, *766*, 61–68.
- (89) Arce, A.; Marchiaro, A.; Soto, A. Liquid–liquid Equilibria of Linalool + Ethanol + Water, Water + Ethanol + Limonene, and Limonene + Linalool + Water Systems. *J. Solution Chem.* **2004**, *33* (5), 561–569.
- (90) Gramajo de Doz, M. B.; Cases, A. M.; Sólamo, H. N. (Liquid + Liquid) Equilibria of (Water + Linalool + Limonene) Ternary System at T = (298.15, 308.15, and 318.15) K. *J. Chem. Thermodyn.* **2008**, *40* (11), 1575–1579.
- (91) Chiyoda, C.; Capellini, M. C.; Geremias, I. M.; Carvalho, F. H.; Aracava, K. K.; Bueno, R. S.; Gonçalves, C. B.; Rodrigues, C. E. C. Deterpenation of Bergamot Essential Oil Using Liquid–Liquid Extraction: Equilibrium Data of Model Systems at 298.2 K. *J. Chem. Eng. Data* **2011**, *56* (5), 2362–2370.
- (92) Tamura, K.; Li, X.; Li, H. Temperature Dependence on Mutual Solubility of Binary (Methanol + Limonene) Mixture and (Liquid + Liquid) Equilibria of Ternary (Methanol + Ethanol + Limonene) Mixture. *J. Chem. Thermodyn.* **2009**, *41* (4), 564–568.
- (93) Tamura, K.; Li, X.; Li, H. Temperature Dependence on Mutual Solubility Data of the Binary (Methanol +  $\alpha$ -Pinene or  $\beta$ -Pinene) Systems and Ternary Liquid–Liquid Equilibria for the (Methanol + Ethanol +

- $\alpha$ -Pinene or  $\beta$ -Pinene) Systems. *J. Chem. Eng. Data* **2008**, 53 (10), 2417–2421.
- (94) Li, H.; Zhang, T.; Fu, W.; Tamura, K. Liquid–liquid Phase Behaviors of Geraniol in Aqueous Alcohol Mixtures. *J. Chem. Eng. Data* **2012**, 57 (1), 148–154.
- (95) Zhang, T.; Li, H.; Zhang, W.; Tamura, K. Ternary (Liquid+liquid) Equilibria for  $\beta$ -Citronellol in Aqueous Alcohol at Different Temperatures. *J. Chem. Thermodyn.* **2012**, 53, 16–22.
- (96) Gramajo de Doz, M. B.; Cases, A. M.; Díaz, P. A.; Sólamo, H. N. (Liquid + Liquid) Equilibria for Water + Ethanol + Citral Multicomponent System at 303.15 K. *J. Chem. Eng. Data* **2007**, 52 (5), 1710–1714.
- (97) Li, H.; Tamura, K. Ternary and Quaternary (Liquid + Liquid) Equilibria for (Water + Ethanol +  $\alpha$ -Pinene, +  $\beta$ -Pinene, or +limonene) and (Water + Ethanol +  $\alpha$ -Pinene + Limonene) at the Temperature 298.15 K. *J. Chem. Thermodyn.* **2006**, 38 (8), 1036–1041.
- (98) Li, H.; Tamura, K. Ternary Liquid–liquid Equilibria for (Water + Terpene + 1-Propanol or 1-Butanol) Systems at the Temperature 298.15 K. *Fluid Phase Equilib.* **2008**, 263 (2), 223–230.
- (99) Arce, A.; Marchiaro, A.; Martínez-Ageitos, J. M.; Soto, A. Citrus Essential Oil Deterpenation by Liquid-Liquid Extraction. *Can. J. Chem. Eng.* **2005**, 83 (2), 366–370.
- (100) Antosik, M.; Stryjek, R. Liquid-Liquid Equilibria in Ternary  $\alpha$ -Pinene +  $\Delta^3$ -Carene + Polar Compound Systems. *Fluid Phase Equilib.* **1992**, 71 (3), 321–331.
- (101) Sevgili, L. M.; Şahin, S.; Kırbaşlar, S. I. Liquid–Liquid Equilibria of (Limonene + Linalool + Ethylene Glycol or Diethylene Glycol or Triethylene Glycol or 1,2-Propylene Glycol) Ternary Systems. *J. Chem. Eng. Data* **2008**, 53 (3), 737–741.
- (102) Arce, A.; Marchiaro, A.; Rodríguez, O.; Soto, A. Liquid–liquid Equilibria of Limonene+linalool+diethylene Glycol System at Different Temperatures. *Chem. Eng. J.* **2002**, 89 (1–3), 223–227.
- (103) Arce, A.; Marchiaro, A.; Soto, A. Phase Stability of the System Limonene + Linalool + 2-Aminoethanol. *Fluid Phase Equilib.* **2004**, 226, 121–127.
- (104) Arce, A.; Marchiaro, A.; Rodríguez, O.; Soto, A. Essential Oil Terpenless by Extraction Using Organic Solvents or Ionic Liquids. *AIChE J.* **2006**, 52 (6), 2089–2097.
- (105) Arce, A.; Pobudkowska, A.; Rodríguez, O.; Soto, A. Citrus Essential Oil Terpenless by Extraction Using 1-Ethyl-3-Methylimidazolium Ethylsulfate Ionic Liquid: Effect of the Temperature. *Chem. Eng. J.* **2007**, 133 (1–3), 213–218.
- (106) Bica, K.; Gaertner, P.; Rogers, R. D. Ionic Liquids and Fragrances - Direct Isolation of Orange Essential Oil. *Green Chem.* **2011**, 13 (8), 1997–1999.
- (107) Lago, S.; Rodríguez, H.; Soto, A.; Arce, A. Alkylpyridinium Alkylsulfate Ionic Liquids as Solvents for the Deterpenation of Citrus Essential Oil. *Sep. Sci. Technol.* **2011**, 47 (2), 292–299.
- (108) Plechkova, N. V; Seddon, K. R. Applications of Ionic Liquids in the Chemical Industry. *Chem. Soc. Rev.* **2008**, 37 (1), 123–150.
- (109) Wasserscheid, P.; Welton, T. *Ionic Liquids in Synthesis*, 2nd ed.; Wiley-VCH: Darmstadt, Federal Republic of Germany, 2009; Vol. 1.
- (110) Kirchner, B. *Ionic Liquids*; Springer-Verlag Berlin Heidelberg: Heidelberg, Germany, 2010.
- (111) Walden, P. Molecular Weights and Electrical Conductivity of Several Fused Salts. *Bull. Russ. Acad. Sci.* **1914**, 8, 405–422.

- (112) Graenacher, C. Cellulose Solution, 1934.
- (113) Tao, G.; He, L.; Liu, W.; Xu, L.; Xiong, W.; Wang, T.; Kou, Y. Preparation, Characterization and Application of Amino Acid-Based Green Ionic Liquids. *Green Chem.* **2006**, *8* (7), 639.
- (114) Zhang, S. J.; Lu, X. M.; Zhou, Q.; Li, X.; Zhang, X.; Lu, S. *Ionic Liquids: Physicochemical Properties*, 1st ed.; Elsevier: Oxford - United Kingdom, 2009.
- (115) Passos, H.; Freire, M. G.; Coutinho, J. A. P. Ionic Liquid Solutions as Extractive Solvents for Value-Added Compounds from Biomass. *Green Chem.* **2014**, *16* (12), 4786–4815.
- (116) Pârvulescu, V. I.; Hardacre, C. Catalysis in Ionic Liquids. *Chem. Rev.* **2007**, *107* (6), 2615–2665.
- (117) Davey, P. Ionic Liquids in Consumer Products. *Perfum. FLAVORIST* **2008**, *33*, 34–35.
- (118) Ventura, S. P. M.; e Silva, F. A.; Quental, M. V.; Mondal, D.; Freire, M. G.; Coutinho, J. A. P. Ionic-Liquid-Mediated Extraction and Separation Processes for Bioactive Compounds: Past, Present, and Future Trends. *Chem. Rev.* **2017**, acs.chemrev.6b00550.
- (119) Forsyth, S. A.; Gunaratne, H. Q. N.; Hardacre, C.; McKeown, A.; Rooney, D. W.; Seddon, K. R. Utilisation of Ionic Liquid Solvents for the Synthesis of Lily-of-the-Valley Fragrance { $\beta$ -Lilial<sup>®</sup>; 3-(4-T-Butylphenyl)-2-Methylpropanal}. *J. Mol. Catal. A Chem.* **2005**, *231* (1), 61–66.
- (120) Petrat, F. M.; Schmidt, F.; Stutzel, B.; Kohler, G. Fragrance Composition Comprising at Least One Ionic Liquid, Method for Production and Use Thereof. US20060166856 A1, 2006.
- (121) Arlt, W.; Seiler, M.; Jork, C.; Schneider, T. IONIC LIQUIDS AS SELECTIVE ADDITIVES FOR THE SEPARATION OF CLOSE-BOILING OR AZEOTROPIC MIXTURES. US 20040133058 A1, 2002.
- (122) *Extraction of Artemisinin Using Ioniq Liquids, Project Report 003-003/3, Bioniqus Ltd, York, UK, 2008; York, UK, 2008.*
- (123) Wu, K.; Zhang, Q.; Liu, Q.; Tang, F.; Long, Y.; Yao, S. Ionic Liquid Surfactant-Mediated Ultrasonic-Assisted Extraction Coupled to HPLC: Application to Analysis of Tanshinones in *Salvia Miltiorrhiza* Bunge. *J. Sep. Sci.* **2009**, *32*, 4220–4226.
- (124) Bi, W.; Tian, M.; Row, K. H. Ultrasonication-Assisted Extraction and Preconcentration of Medicinal Products from Herb by Ionic Liquids. *Talanta* **2011**, *85* (1), 701–706.
- (125) Bi, W.; Tian, M.; Zhou, J.; Row, K. H. Task-Specific Ionic Liquid-Assisted Extraction and Separation of Astaxanthin from Shrimp Waste. *J. Chromatogr. B* **2010**, *878* (24), 2243–2248.
- (126) Liu, T.; Sui, X.; Zhang, R.; Yang, L.; Zu, Y.; Zhang, L.; Zhang, Y.; Zhang, Z. Application of Ionic Liquids Based Microwave-Assisted Simultaneous Extraction of Carnosic Acid, Rosmarinic Acid and Essential Oil from *Rosmarinus Officinalis*. *J. Chromatogr. A* **2011**, *1218* (47), 8480–8489.
- (127) Ressmann, A. K.; Strassl, K.; Gaertner, P.; Zhao, B.; Greiner, L.; Bica, K. New Aspects for Biomass Processing with Ionic Liquids: Towards the Isolation of Pharmaceutically Active Betulin. *Green Chem.* **2012**, *14* (4), 940–944.
- (128) Lin, H.; Zhang, Y.; Han, M.; Yang, L. Aqueous Ionic Liquid Based Ultrasonic Assisted Extraction of Eight Ginsenosides from Ginseng Root. *Ultrason. Sonochem.* **2013**, *20* (2), 680–684.
- (129) Onda, S.; Usuki, T.; Yoshizawa-Fujita, M.; Rikukawa, M. Ionic Liquid-Mediated Extraction of Bilobalide from Ginkgo Biloba Leaves. *Chem. Lett.* **2015**, *44* (11), 1461–1463.
- (130) Abbott, A. P.; Capper, G.; Davies, D. L.; Rasheed, R. K.; Tambyrajah, V. Novel Solvent Properties of Choline Chloride/urea Mixtures. *Chem. Commun.* **2003**, *99* (1), 70–71.



- (131) Zhang, Q.; De Oliveira Vigier, K.; Royer, S.; Jérôme, F. Deep Eutectic Solvents: Syntheses, Properties and Applications. *Chem. Soc. Rev.* **2012**, *41* (21), 7108–7146.
- (132) Smith, E. L.; Abbott, A. P.; Ryder, K. S. Deep Eutectic Solvents (DESs) and Their Applications. *Chem. Rev.* **2014**, *114* (21), 11060–11082.
- (133) Tang, B.; Row, K. H. Recent Developments in Deep Eutectic Solvents in Chemical Sciences. *Monatshefte für Chemie - Chem. Mon.* **2013**, *144* (10), 1427–1454.
- (134) Hayyan, A.; Mjalli, F. S.; Alnashef, I. M.; Al-Wahaibi, Y. M.; Al-Wahaibi, T.; Hashim, M. A. Glucose-Based Deep Eutectic Solvents: Physical Properties. *J. Mol. Liq.* **2013**, *178*, 137–141.
- (135) Francisco, M.; Bruinhorst, A. van den; Kroon, M. C. Low-Transition-Temperature Mixtures (LTTMs): A New Generation of Designer Solvents. *Angew. Chemie Int. Ed.* **2013**, *52* (11), 3074–3085.
- (136) Carriazo, D.; Serrano, M. C.; Gutiérrez, M. C.; Ferrer, M. L.; del Monte, F. Deep-Eutectic Solvents Playing Multiple Roles in the Synthesis of Polymers and Related Materials. *Chem. Soc. Rev.* **2012**, *41* (14), 4996–5014.
- (137) Tang, B.; Bi, W.; Zhang, H.; Row, K. H. Deep Eutectic Solvent-Based HS-SME Coupled with GC for the Analysis of Bioactive Terpenoids in *Chamaecyparis Obtusa* Leaves. *Chromatographia* **2014**, *77* (3–4), 373–377.
- (138) Zhang, H.; Tang, B.; Row, K. H. A Green Deep Eutectic Solvent-Based Ultrasound-Assisted Method to Extract Astaxanthin from Shrimp Byproducts. *Anal. Lett.* **2014**, *47* (5), 742–749.
- (139) Lee, Y. R.; Row, K. H. Comparison of Ionic Liquids and Deep Eutectic Solvents as Additives for the Ultrasonic Extraction of Astaxanthin from Marine Plants. *J. Ind. Eng. Chem.* **2016**, *39*, 87–92.
- (140) Jeong, K. M.; Lee, M. S.; Nam, M. W.; Zhao, J.; Jin, Y.; Lee, D.-K.; Kwon, S. W.; Jeong, J. H.; Lee, J. Tailoring and Recycling of Deep Eutectic Solvents as Sustainable and Efficient Extraction Media. *J. Chromatogr. A* **2015**, *1424*, 10–17.
- (141) Wang, M.; Wang, J.; Zhang, Y.; Xia, Q.; Bi, W.; Yang, X.; Chen, D. D. Y. *Fast Environment-Friendly Ball Mill-Assisted Deep Eutectic Solvent-Based Extraction of Natural Products*; 2016; Vol. 1443.
- (142) van den Bruinhorst, A.; Kouris, P. ; Timmer, J. M. K. ; de Croon, M. H. J. M. ; Kroon, M. . Exploring Orange Peel Treatment with Deep Eutectic Solvents and Diluted Organic Acids. *Nat. Prod. Chem. Res.* **2016**, *4* (6), 1–5.
- (143) Tereshatov, E. E.; Boltoeva, M. Y.; Folden, C. M. First Evidence of Metal Transfer into Hydrophobic Deep Eutectic and Low-Transition-Temperature Mixtures: Indium Extraction from Hydrochloric and Oxalic Acids. *Green Chem.* **2016**, *18* (17), 4616–4622.
- (144) Alexis LAVAUD, Michael LAGUERRE, Simona BIRTIC, TIXIER Anne Sylvie FABIANO, Marc Roller, Farid Chemat, A. C. B. Eutectic Extraction Solvents, Extraction Methods by Eutectigenesis Using Said Solvents, and Extracts Derived from Said Extraction Methods. WO 2016162703 A1, 2016.
- (145) Naturex group and the Personal Care market <http://www.naturex.com/BUSINESS-UNITS/Personal-Care#Eutectys> (accessed Feb 3, 2017).
- (146) Green Industrial Applications of Ionic Liquids | Robin D. Rogers | Springer <http://www.springer.com/us/book/9781402011368> (accessed Jan 31, 2016).
- (147) Florindo, C.; Oliveira, F. S.; Rebelo, L. P. N.; Fernandes, A. M.; Marrucho, I. M. Insights into the Synthesis and Properties of Deep Eutectic Solvents Based on Cholinium Chloride and Carboxylic Acids. *ACS Sustain. Chem. Eng.* **2014**, *2* (10), 2416–2425.

- (148) Maugeri, Z.; Domínguez de María, P. Novel Choline-Chloride-Based Deep-Eutectic-Solvents with Renewable Hydrogen Bond Donors: Levulinic Acid and Sugar-Based Polyols. *RSC Adv.* **2012**, *2* (2), 421–425.
- (149) Choi, Y. H.; van Spronsen, J.; Dai, Y.; Verberne, M.; Hollmann, F.; Arends, I. W. C. E.; Witkamp, G.-J.; Verpoorte, R. Are Natural Deep Eutectic Solvents the Missing Link in Understanding Cellular Metabolism and Physiology? *Plant Physiol.* **2011**, *156* (4), 1701–1705.
- (150) van Osch, D. J. G. P.; Zubeir, L. F.; van den Bruinhorst, A.; Rocha, M. A. A.; Kroon, M. C. Hydrophobic Deep Eutectic Solvents as Water-Immiscible Extractants. *Green Chem.* **2015**, *17* (9), 4518–4521.
- (151) Van Osch, D. J. G. P.; Parmentier, D.; Dietz, C. H. J. T.; Van Den Bruinhorst, A.; Tuinier, R.; Kroon, M. C. Removal of Alkali and Transition Metal Ions from Water with Hydrophobic Deep Eutectic Solvents. *Chem. Commun.* **2016**, *52* (52), 11987–11990.
- (152) Ribeiro, B. D.; Florindo, C.; Iff, L. C.; Coelho, M. A. Z.; Marrucho, I. M. Menthol-Based Eutectic Mixtures: Hydrophobic Low Viscosity Solvents. *ACS Sustain. Chem. Eng.* **2015**, *3* (10), 2469–2477.
- (153) Shen, Q.; Li, X.; Li, W.; Zhao, X. Enhanced Intestinal Absorption of Daidzein by Borneol/Menthol Eutectic Mixture and Microemulsion. *AAPS PharmSciTech* **2011**, *12* (4), 1044–1049.
- (154) Liu, J.; Fu, S.; Wei, N.; Hou, Y.; Zhang, X.; Cui, H. The Effects of Combined Menthol and Borneol on Fluconazole Permeation through the Cornea Ex Vivo. *Eur. J. Pharmacol.* **2012**, *688* (1), 1–5.
- (155) Li, F.; Feng, J.; Cheng, Q.; Zhu, W.; Jin, Y. Delivery of 125I-Cobrotoxin after Intranasal Administration to the Brain: A Microdialysis Study in Freely Moving Rats. *Int. J. Pharm.* **2007**, *328* (2), 161–167.
- (156) Gohel, M. C.; Nagori, S. A. Resolving Issues of Content Uniformity and Low Permeability Using Eutectic Blend of Camphor and Menthol. *Indian J. Pharm. Sci.* **2009**, *71* (6), 622–629.
- (157) Phaechamud, T.; Tuntarawongsa, S. Transformation of Eutectic Emulsion to Nanosuspension Fabricating with Solvent Evaporation and Ultrasonication Technique. *Int. J. Nanomedicine* **2016**, *11*, 2855–2865.
- (158) Tuntarawongsa, S.; Phaechamud, T. Menthol, Borneol, Camphor and WS-3 Eutectic Mixture. *Adv. Mater. Res.* **2012**, *506*, 355–358.
- (159) Hoang Pham, U. G.; Pham, H.; Chauhan, H. Pharmaceutical Applications of Eutectic Mixtures. *J. Dev. Drugs* **2013**, *2* (3).
- (160) Mohammadi-Samani, S.; Yousefi, G.; Mohammadi, F.; Ahmadi, F. Meloxicam Transdermal Delivery: Effect of Eutectic Point on the Rate and Extent of Skin Permeation. *Iran. J. Basic Med. Sci.* **2014**, *17* (2), 112–118.
- (161) Stott, P. W.; Williams, A. C.; Barry, B. W. Transdermal Delivery from Eutectic Systems: Enhanced Permeation of a Model Drug, Ibuprofen. *J. Control. Release* **1998**, *50* (1), 297–308.
- (162) Phaechamud, T.; Tuntarawongsa, S.; Charoensuksai, P. Evaporation Behavior and Characterization of Eutectic Solvent and Ibuprofen Eutectic Solution. *AAPS PharmSciTech* **2016**, *17* (5), 1213–1220.
- (163) Gala, U.; Chuong, M. C.; Varanasi, R.; Chauhan, H. Characterization and Comparison of Lidocaine-Tetracaine and Lidocaine-Camphor Eutectic Mixtures Based on Their Crystallization and Hydrogen-Bonding Abilities. *AAPS PharmSciTech* **2015**, *16* (3), 528–536.
- (164) Yong, C. S.; Jung, S. H.; Rhee, J.-D.; Choi, H.-G.; Lee, B.-J.; Kim, D.-C.; Choi, Y. W.; Kim, C.-K. Improved Solubility and In Vitro Dissolution of Ibuprofen from Poloxamer Gel Using Eutectic Mixture with Menthol. *Drug Deliv.* **2003**, *10* (3), 179–183.

- (165) Yong, C. S.; Oh, Y.-K.; Jung, S. H.; Rhee, J.-D.; Kim, H.-D.; Kim, C.-K.; Choi, H.-G. Preparation of Ibuprofen-Loaded Liquid Suppository Using Eutectic Mixture System with Menthol. *Eur. J. Pharm. Sci.* **2004**, *23* (4–5), 347–353.
- (166) Kaplun-Frischoff, Y.; Touitou, E. Testosterone Skin Permeation Enhancement by Menthol through Formation of Eutectic with Drug and Interaction with Skin Lipids. *J. Pharm. Sci.* **1997**, *86* (12), 1394–1399.
- (167) Kang, L.; Jun, H. W.; McCall, J. W. Physicochemical Studies of Lidocaine–menthol Binary Systems for Enhanced Membrane Transport. *Int. J. Pharm.* **2000**, *206* (1), 35–42.
- (168) Nazzal, S.; Smalyukh, I. ; Lavrentovich, O. ; Khan, M. A. Preparation and in Vitro Characterization of a Eutectic Based Semisolid Self-Nanoemulsified Drug Delivery System (SNEDDS) of Ubiquinone: Mechanism and Progress of Emulsion Formation. *Int. J. Pharm.* **2002**, *235* (1), 247–265.
- (169) Aroso, I. M.; Craveiro, R.; Rocha, Â.; Dionísio, M.; Barreiros, S.; Reis, R. L.; Paiva, A.; Duarte, A. R. C. Design of Controlled Release Systems for THEDES—Therapeutic Deep Eutectic Solvents, Using Supercritical Fluid Technology. *Int. J. Pharm.* **2015**, *492* (1), 73–79.
- (170) Aroso, I. M.; Silva, J. C.; Mano, F.; Ferreira, A. S. D.; Dionísio, M.; Sá-Nogueira, I.; Barreiros, S.; Reis, R. L.; Paiva, A.; Duarte, A. R. C. Dissolution Enhancement of Active Pharmaceutical Ingredients by Therapeutic Deep Eutectic Systems. *Eur. J. Pharm. Biopharm.* **2016**, *98*, 57–66.
- (171) Okuniewski, M.; Padoszyński, K.; Domańska, U. (Solid + Liquid) Equilibrium Phase Diagrams in Binary Mixtures Containing Terpenes: New Experimental Data and Analysis of Several Modelling Strategies with Modified UNIFAC (Dortmund) and PC-SAFT Equation of State. *Fluid Phase Equilib.* **2016**, *422*, 66–77.
- (172) Štejfa, V.; Fulem, M.; Růžička, K.; Červinka, C. Thermodynamic Study of Selected Monoterpenes II. *J. Chem. Thermodyn.* **2014**, *79*, 272–279.
- (173) Rietveld, I. B.; Barrio, M.; Veglio, N.; Espeau, P.; Tamarit, J. L.; Céolin, R. Temperature and Composition-Dependent Properties of the Two-Component System D- and L-Camphor at “ordinary” Pressure. *Thermochim. Acta* **2010**, *511* (1–2), 43–50.
- (174) Domalski, E. S.; Hearing, E. D. Heat Capacities and Entropies of Organic Compounds in the Condensed Phase. Volume III. *J. Phys. Chem. Ref. Data* **1996**, *25* (1), 1–525.
- (175) de Matos, F. C.; da Costa, M. C.; de Almeida Meirelles, A. J.; Batista, E. A. C. Binary Solid–liquid Equilibrium Systems Containing Fatty Acids, Fatty Alcohols and Triolein by Differential Scanning Calorimetry. *Fluid Phase Equilib.* **2015**, *404*, 1–8.
- (176) de Matos, F. C.; da Costa, M. C.; Meirelles, A. J. de A.; Batista, E. A. C. Binary Solid–liquid Equilibrium Systems Containing Fatty Acids, Fatty Alcohols and Trilaurin by Differential Scanning Calorimetry. *Fluid Phase Equilib.* **2016**, *423*, 74–83.
- (177) Prausnitz, J. M.; Lichtenthaler, R. N.; Azevedo, E. G. *Molecular Thermodynamics Fluid Phase Equilibria*; Prentice-Hall, 1986.
- (178) Gmehling, J.; Kolbe, B.; Kleiber, M.; Rarey, J. *Chemical Thermodynamics for Process Simulation*; Wiley-VCH, 2012.
- (179) Coutinho, J. A. P.; Andersen, S. I.; Stenby, E. H. Evaluation of Activity Coefficient Models in Prediction of Alkane Solid-Liquid Equilibria. *Fluid Phase Equilib.* **1995**, *103* (1), 23–39.
- (180) Neves, C. M. S. S.; Kurnia, K. A.; Coutinho, J. A. P.; Marrucho, I. M.; Lopes, J. N. C.; Freire, M. G.; Rebelo, L. P. N. Systematic Study of the Thermophysical Properties of Imidazolium-Based Ionic

- Liquids with Cyano-Functionalized Anions. *J. Phys. Chem. B* **2013**, *177* (35), 10271–10283.
- (181) Okoturo, O. O.; VanderNoot, T. J. Temperature Dependence of Viscosity for Room Temperature Ionic Liquids. *J. Electroanal. Chem.* **2004**, *568*, 167–181.
- (182) Rocha, M. A. A.; Neves, C. M. S. S.; Freire, M. G.; Russina, O.; Triolo, A.; Coutinho, J. A. P.; Santos, L. M. N. B. F. Alkylimidazolium Based Ionic Liquids: Impact of Cation Symmetry on Their Nanoscale Structural Organization. *J. Phys. Chem. B* **2013**, *117* (37), 10889–10897.
- (183) Yiin, C. L.; Quitain, A. T.; Yusup, S.; Sasaki, M.; Uemura, Y.; Kida, T. Characterization of Natural Low Transition Temperature Mixtures (LTTMs): Green Solvents for Biomass Delignification. *Bioresour. Technol.* **2016**, *199*, 258–264.
- (184) Domanska, U.; Pobudkowska, A.; Eckert, F. Liquid-Liquid Equilibria in the Binary Systems (1,3-Dimethylimidazolium, or 1-Butyl-3-Methylimidazolium Methylsulfate + Hydrocarbons). *Green Chem.* **2006**, *8* (3), 268–276.
- (185) Domańska, U.; Lukoshko, E. V.; Królikowski, M. Phase Behaviour of Ionic Liquid 1-Butyl-1-Methylpyrrolidinium Tris(pentafluoroethyl)trifluorophosphate with Alcohols, Water and Aromatic Hydrocarbons. *Fluid Phase Equilib.* **2013**, *345*, 18–22.
- (186) Poole, C. F. Chromatographic and Spectroscopic Methods for the Determination of Solvent Properties of Room Temperature Ionic Liquids. *J. Chromatogr. A* **2004**, *1037* (1–2), 49–82.
- (187) Letcher, T. M.; Marciniak, A.; Marciniak, M. Determination of Activity Coefficients at Infinite Dilution of Solutes in the Ionic Liquid 1-Butyl-3-Methylimidazolium Octyl Sulfate Using Gas-Liquid Chromatography at a Temperature of 298.15 K, 313.15 K, or 328.15 K. *J. Chem. Eng. Data* **2005**, *50* (4), 1294–1298.
- (188) Heintz, A.; Casás, L. M.; Nesterov, I. A.; Emelyanenko, V. N.; Verevkin, S. P. Thermodynamic Properties of Mixtures Containing Ionic Liquids. 5. Activity Coefficients at Infinite Dilution of Hydrocarbons, Alcohols, Esters, and Aldehydes in 1-Methyl-3-Butyl-Imidazolium Bis(trifluoromethyl-Sulfonyl) Imide Using Gas-Liquid Chromatography. *J. Chem. Eng. Data* **2005**, *50* (5), 1510–1514.
- (189) Marciniak, A.; Wlazło, M. Activity Coefficients at Infinite Dilution and Physicochemical Properties for Organic Solutes and Water in the Ionic Liquid 1-(2-Methoxyethyl)-1-Methylpyrrolidinium Trifluorotris(perfluoroethyl)phosphate. *J. Chem. Thermodyn.* **2013**, *60*, 114–119.
- (190) Canongia Lopes, J.; Pádua, A. H. CL&P: A Generic and Systematic Force Field for Ionic Liquids Modeling. *Theor. Chem. Acc.* **2012**, *131* (3), 1–11.
- (191) Maginn, E. J. Molecular Simulation of Ionic Liquids: Current Status and Future Opportunities. *J. Phys. Condens. Matter* **2009**, *21* (37), 373101–373118.
- (192) Sellin, M.; Ondruschka, B.; Stark, A. Hydrogen Bond Acceptor Properties of Ionic Liquids and Their Effect on Cellulose Solubility. In *Cellulose Solvents: For Analysis, Shaping and Chemical Modification*; American Chemical Society, 2010; Vol. 1033, pp 121–135.
- (193) Danten, Y.; Cabaço, M. I.; Besnard, M. Interaction of Water Highly Diluted in 1-Alkyl-3-Methyl Imidazolium Ionic Liquids with the PF<sub>6</sub><sup>-</sup> and BF<sub>4</sub><sup>-</sup> Anions. *J. Phys. Chem. A* **2009**, *113* (12), 2873–2889.
- (194) Khan, I.; Taha, M.; Ribeiro-Claro, P.; Pinho, S. P.; Coutinho, J. A. P. Effect of the Cation on the Interactions between Alkyl Methyl Imidazolium Chloride Ionic Liquids and Water. *J. Phys. Chem. B* **2014**, *118* (35), 10503–10514.
- (195) Carvalho, P. J.; Khan, I.; Morais, A.; Granjo, J. F. O.; Oliveira, N. M. C.; Santos, L. M. N. B. F.; Coutinho,

- J. A. P. A New Microbulliometer for the Measurement of the Vapor–liquid Equilibrium of Ionic Liquid Systems. *Fluid Phase Equilib.* **2013**, *354*, 156–165.
- (196) Freire, M. G.; Santos, L. M. N. B. F.; Marrucho, I. M.; Coutinho, J. A. P. Evaluation of COSMO-RS for the Prediction of LLE and VLE of Alcohols + Ionic Liquids. *Fluid Phase Equilib.* **2007**, *255* (2), 167–178.
- (197) Ferreira, A. R.; Freire, M. G.; Ribeiro, J. C.; Lopes, F. M.; Crespo, J. G.; Coutinho, J. A. P. An Overview of the Liquid–Liquid Equilibria of (Ionic Liquid + Hydrocarbon) Binary Systems and Their Modeling by the Conductor-like Screening Model for Real Solvents. *Ind. Eng. Chem. Res.* **2011**, *50* (9), 5279–5294.
- (198) Neves, C. M. S. S.; Granjo, J. F. O.; Freire, M. G.; Robertson, A.; Oliveira, N. M. C.; Coutinho, J. A. P. Separation of Ethanol–Water Mixtures by Liquid–Liquid Extraction Using Phosphonium-Based Ionic Liquids. *Green Chem.* **2011**, *13* (6), 1517–1526.
- (199) Pereira, L. M. C.; Oliveira, M. B.; Llovel, F.; Vega, L. F.; Coutinho, J. A. P. Assessing the N<sub>2</sub>O/CO<sub>2</sub> High Pressure Separation Using Ionic Liquids with the Soft-SAFT EoS. *J. Supercrit. Fluids* **2014**, *92*, 231–241.
- (200) Klamt, A.; Eckert, F. COSMO-RS: A Novel and Efficient Method for the A Priori Prediction of Thermophysical Data of Liquids. *Fluid Phase Equilib.* **2000**, *172* (1), 43–72.
- (201) Kurnia, K. A.; Pinho, S. P.; Coutinho, J. A. P. Evaluation of the Conductor-like Screening Model for Real Solvents for the Prediction of the Water Activity Coefficient at Infinite Dilution in Ionic Liquids. *Ind. Eng. Chem. Res.* **2014**, *53* (31), 12466–12475.
- (202) Kurnia, K. A.; Pinho, S. P.; Coutinho, J. A. P. Designing Ionic Liquids for Absorptive Cooling. *Green Chem.* **2014**, *16* (8), 3741–3745.
- (203) Domańska, U.; Lukoshko, E. V. Measurements of Activity Coefficients at Infinite Dilution for Organic Solutes and Water in the Ionic Liquid 1-Butyl-1-Methylpyrrolidinium Tricyanomethanide. *J. Chem. Thermodyn.* **2013**, *66*, 144–150.
- (204) Domańska, U.; Marciniak, A. Activity Coefficients at Infinite Dilution Measurements for Organic Solutes and Water in the Ionic Liquid 1-Butyl-3-Methylimidazolium Trifluoromethanesulfonate. *J. Phys. Chem. B* **2008**, *112* (35), 11100–11105.
- (205) Heintz, A.; Verevkin, S. P. Thermodynamic Properties of Mixtures Containing Ionic Liquids. 6. Activity Coefficients at Infinite Dilution of Hydrocarbons, Alcohols, Esters, and Aldehydes in 1-Methyl-3-Octyl-Imidazolium Tetrafluoroborate Using Gas–Liquid Chromatography. *J. Chem. Eng. Data* **2005**, *50* (5), 1515–1519.
- (206) David, W.; Letcher, T. M.; Ramjugernath, D.; David Raal, J. Activity Coefficients of Hydrocarbon Solutes at Infinite Dilution in the Ionic Liquid, 1-Methyl-3-Octyl-Imidazolium Chloride from Gas–Liquid Chromatography. *J. Chem. Thermodyn.* **2003**, *35* (8), 1335–1341.
- (207) Kato, R.; Gmehling, J. Activity Coefficients at Infinite Dilution of Various Solutes in the Ionic Liquids [MMIM]+[CH<sub>3</sub>SO<sub>4</sub>]-, [MMIM]+[CH<sub>3</sub>OC<sub>2</sub>H<sub>4</sub>SO<sub>4</sub>]-, [MMIM]+[(CH<sub>3</sub>)<sub>2</sub>PO<sub>4</sub>]-, [C<sub>5</sub>H<sub>5</sub>NC<sub>2</sub>H<sub>5</sub>]+[(CF<sub>3</sub>SO<sub>2</sub>)<sub>2</sub>N]- and [C<sub>5</sub>H<sub>5</sub>NH]+[C<sub>2</sub>H<sub>5</sub>OC<sub>2</sub>H<sub>4</sub>OSO<sub>3</sub>]. *Fluid Phase Equilib.* **2004**, *226*, 37–44.
- (208) Krummen, M.; Wasserscheid, P.; Gmehling, J. Measurement of Activity Coefficients at Infinite Dilution in Ionic Liquids Using the Dilutor Technique. *J. Chem. Eng. Data* **2002**, *47* (6), 1411–1417.
- (209) Domańska, U.; Królikowska, M. Measurements of Activity Coefficients at Infinite Dilution in Solvent Mixtures with Thiocyanate-Based Ionic Liquids Using GLC Technique. *J. Phys. Chem. B* **2010**, *114* (25), 8460–8466.

- (210) Domańska, U.; Królikowski, M.; Acree Jr, W. E.; Baker, G. A. Physicochemical Properties and Activity Coefficients at Infinite Dilution for Organic Solutes and Water in a Novel Bicyclic Guanidinium Superbase-Derived Protic Ionic Liquid. *J. Chem. Thermodyn.* **2013**, *58*, 62–69.
- (211) Domańska, U.; Królikowski, M. Measurements of Activity Coefficients at Infinite Dilution for Organic Solutes and Water in the Ionic Liquid 1-Ethyl-3-Methylimidazolium Methanesulfonate. *J. Chem. Thermodyn.* **2012**, *54*, 20–27.
- (212) Domańska, U.; Marciniak, A. Activity Coefficients at Infinite Dilution Measurements for Organic Solutes and Water in the Ionic Liquid 1-Ethyl-3-Methylimidazolium Trifluoroacetate. *J. Phys. Chem. B* **2007**, *111* (41), 11984–11988.
- (213) Domanska, U.; Marciniak, A. Measurements of Activity Coefficients at Infinite Dilution of Aromatic and Aliphatic Hydrocarbons, Alcohols, and Water in the New Ionic Liquid [EMIM][SCN] Using GLC. *J. Chem. Thermodyn.* **2008**, *40* (5), 860–866.
- (214) Carvalho, P. J.; Regueira, T.; Santos, L. M. N. B. F.; Fernandez, J.; Coutinho, J. A. P. Effect of Water on the Viscosities and Densities of 1-Butyl-3-Methylimidazolium Dicyanamide and 1-Butyl-3-Methylimidazolium Tricyanomethane at Atmospheric Pressure†. *J. Chem. Eng. Data* **2009**, *55* (2), 645–652.
- (215) Everett, D. H. Effect of Gas Imperfection on G.L.C. Measurements: A Refined Method for Determining Activity Coefficients and Second Virial Coefficients. *Trans. Faraday Soc.* **1965**, *61*, 1637–1645.
- (216) Cruickshank, A. J. B.; Gainey, B. W.; Hicks, C. P.; Letcher, T. M.; Moody, R. W.; Young, C. L. Gas-Liquid Chromatographic Determination of Cross-Term Second Virial Coefficients Using Glycerol. Benzene + Nitrogen and Benzene + Carbon Dioxide at 50°C. *Trans. Faraday Soc.* **1969**, *65*, 1014–1031.
- (217) Grant, D. W. *Gas-Liquid Chromatography*; van Nostrand Reinhold: London, UK, 1971.
- (218) Klamt, A. *COSMO-RS From Quantum Chemistry to Fluid Phase Thermodynamics and Drug Design*; Elsevier: Amsterdam, The Netherlands, 2005.
- (219) Diedenhofen, M.; Eckert, F.; Klamt, A. Prediction of Infinite Dilution Activity Coefficients of Organic Compounds in Ionic Liquids Using COSMO-RS. *J. Chem. Eng. Data* **2003**, *48* (3), 475–479.
- (220) University of Karlsruhe and Forschungszentrum Karlsruhe GmbH, TURBOMOLE V6.1 2009, 1989–2007, 25 GmbH, since 2007; Available from [Http://www.turbomole.com](http://www.turbomole.com).
- (221) Domańska, U.; Marciniak, A. Physicochemical Properties and Activity Coefficients at Infinite Dilution for Organic Solutes and Water in the Ionic Liquid 1-Decyl-3-Methylimidazolium Tetracyanoborate. *J. Phys. Chem. B* **2010**, *114* (49), 16542–16547.
- (222) Domańska, U.; Bogel-Łukasik, E.; Bogel-Łukasik, R. 1-Octanol/Water Partition Coefficients of 1-Alkyl-3-Methylimidazolium Chloride. *Chem. – A Eur. J.* **2003**, *9* (13), 3033–3041.
- (223) Stark, A.; Zidell, A. W.; Russo, J. W.; Hoffmann, M. M. Composition Dependent Physicochemical Property Data for the Binary System Water and the Ionic Liquid 1-Butyl-3-Methylimidazolium Methanesulfonate ([C4mim][MeSO3]). *J. Chem. Eng. Data* **2012**, *57* (12), 3330–3339.
- (224) Design Institute for Physical Properties, Sponsored by AIChE. (2005; 2008; 2009; 2010; 2011; 2012). DIPPR Project 801 - Full Version. Design Institute for Physical Property Research/AIChE. Online Version Available at: [Http://app.knovel.com/hotlink/toc/id](http://app.knovel.com/hotlink/toc/id):
- (225) Poling, B. E.; Prausnitz, J. M. *Properties of Gases and Liquids*; McGraw-Hill Publishing, 2001.

- (226) Stark, A. Ionic Liquid Structure-Induced Effects on Organic Reactions. In *Ionic Liquids*; Kirchner, B., Ed.; Springer Berlin Heidelberg, 2010; Vol. 290, pp 41–81.
- (227) Pádua, A. A. H.; Costa Gomes, M. F.; Canongia Lopes, J. N. A. Molecular Solutes in Ionic Liquids: A Structural Perspective. *Acc. Chem. Res.* **2007**, *40* (11), 1087–1096.
- (228) Domańska, U.; Królikowski, M. Determination of Activity Coefficients at Infinite Dilution of 35 Solutes in the Ionic Liquid, 1-Butyl-3-Methylimidazolium Tosylate, Using Gas-Liquid Chromatography. *J. Chem. Eng. Data* **2010**, *55* (11), 4817–4822.
- (229) Claudio, A. F. M.; Swift, L.; Hallett, J. P.; Welton, T.; Coutinho, J. A. P.; Freire, M. G. Extended Scale for the Hydrogen-Bond Basicity of Ionic Liquids. *Phys. Chem. Chem. Phys.* **2014**, *16* (14), 6593–6601.
- (230) Jork, C.; Kristen, C.; Pieraccini, D.; Stark, A.; Chiappe, C.; Beste, Y. A.; Arlt, W. Tailor-Made Ionic Liquids. *J. Chem. Thermodyn.* **2005**, *37* (6), 537–558.
- (231) Stark, A.; Ondruschka, B.; Zaitsau, D. H.; Verevkin, S. P. Biomass-Derived Platform Chemicals: Thermodynamic Studies on the Extraction of 5-Hydroxymethylfurfural from Ionic Liquids. *J. Chem. Eng. Data* **2012**, *57* (11), 2985–2991.
- (232) Moïse, J.-C.; Mutelet, F.; Jaubert, J.-N.; Grubbs, L. M.; Acree, W. E.; Baker, G. A. Activity Coefficients at Infinite Dilution of Organic Compounds in Four New Imidazolium-Based Ionic Liquids. *J. Chem. Eng. Data* **2011**, *56*, 3106–3114.
- (233) Ge, M.-L.; Chen, J.-B. Activity Coefficients at Infinite Dilution of Alkanes, Alkenes, and Alkyl Benzenes in 1-Ethyl-3-Methylimidazolium Diethylphosphate Using Gas-Liquid Chromatography. *J. Chem. Eng. Data* **2011**, *56* (7), 3183–3187.
- (234) Ge, M. L.; Song, X. J.; Li, G. M.; Li, Y. H.; Liu, F. Z.; Ma, H. L. Activity Coefficients at Infinite Dilution of Alkanes, Alkenes, and Alkyl Benzenes in 1-Butyl-3-Methylimidazolium Dibutylphosphate Using Gas-Liquid Chromatography. *J. Chem. Eng. Data* **2012**, *57* (8), 2109–2113.
- (235) Gong, Y.; Shen, C.; Lu, Y.; Meng, H.; Li, C. Viscosity and Density Measurements for Six Binary Mixtures of Water (Methanol or Ethanol) with an Ionic Liquid ([BMIM][DMP] or [EMIM][DMP]) at Atmospheric Pressure in the Temperature Range of (293.15 to 333.15) K. *J. Chem. Eng. Data* **2011**, *57* (1), 33–39.
- (236) Machida, H.; Taguchi, R.; Sato, Y.; Smith, J. R. L. Measurement and Correlation of High Pressure Densities of Ionic Liquids, 1-Ethyl-3-Methylimidazolium L-Lactate ([emim][Lactate]), 2-Hydroxyethyl-Trimethylammonium L-Lactate ([C<sub>2</sub>H<sub>4</sub>OH](CH<sub>3</sub>)<sub>3</sub>N][Lactate]), and 1-Butyl-3-Methylimidazolium Chloride ([bmim][Cl]). *J. Chem. Eng. Data* **2010**, *56* (4), 923–928.
- (237) He, R.-H.; Long, B.-W.; Lu, Y.-Z.; Meng, H.; Li, C.-X. Solubility of Hydrogen Chloride in Three 1-Alkyl-3-Methylimidazolium Chloride Ionic Liquids in the Pressure Range (0 to 100) kPa and Temperature Range (298.15 to 363.15) K. *J. Chem. Eng. Data* **2012**, *57* (11), 2936–2941.
- (238) Govinda, V.; Attri, P.; Venkatesu, P.; Venkateswarlu, P. Thermophysical Properties of Dimethylsulfoxide with Ionic Liquids at Various Temperatures. *Fluid Phase Equilib.* **2011**, *304* (1–2), 35–43.
- (239) Kavitha, T.; Vasantha, T.; Venkatesu, P.; Rama Devi, R. S.; Hofman, T. Thermophysical Properties for the Mixed Solvents of N-Methyl-2-Pyrrolidone with Some of the Imidazolium-Based Ionic Liquids. *J. Mol. Liq.* **2014**, *198*, 11–20.
- (240) Huddleston, J. G.; Visser, A. E.; Reichert, W. M.; Willauer, H. D.; Broker, G. A.; Rogers, R. D. Characterization and Comparison of Hydrophilic and Hydrophobic Room Temperature Ionic Liquids Incorporating the Imidazolium Cation. *Green Chem.* **2001**, *3* (4), 156–164.

- (241) Wytze Meindersma, G.; Podt, A.; de Haan, A. B. Selection of Ionic Liquids for the Extraction of Aromatic Hydrocarbons from Aromatic/aliphatic Mixtures. *Fuel Process. Technol.* **2005**, *87* (1), 59–70.
- (242) Lei, Z.; Arlt, W.; Wasserscheid, P. Separation of 1-Hexene and N-Hexane with Ionic Liquids. *Fluid Phase Equilib.* **2006**, *241* (1–2), 290–299.
- (243) Yu, Y.-X.; Gong, Q.; Huang, L.-L. Measurement of Activity Coefficient at Infinite Dilution of Hydrocarbons in Sulfolane Using Gas–Liquid Chromatography. *J. Chem. Eng. Data* **2007**, *52* (4), 1459–1463.
- (244) Krummen, M.; Gruber, D.; Gmehling, J. Measurement of Activity Coefficients at Infinite Dilution in Solvent Mixtures Using the Dilutor Technique. *Ind. Eng. Chem. Res.* **2000**, *39* (6), 2114–2123.
- (245) Sheldon, R. Catalytic Reactions in Ionic Liquids. *Chem. Commun.* **2001**, No. 23, 2399–2407.
- (246) Yaws, Carl L., (2012; 2013; 2014). Yaws' Critical Property Data for Chemical Engineers and Chemists. Knovel. Online Version Available at: <http://app.knovel.com/hotlink/toc/id:kpYCPDCECD/yaws-Critical-Property/yaws-Critical-Property>.
- (247) Martins, M. A. R.; Coutinho, J. A. P.; Pinho, S. P.; Domańska, U. Measurements of Activity Coefficients at Infinite Dilution of Organic Solutes and Water on Polar Imidazolium-Based Ionic Liquids. *J. Chem. Thermodyn.* **2015**, *91*, 194–203.
- (248) Goharshadi, E. K.; Hesabi, M. Estimation of Solubility Parameter Using Equations of State. *J. Mol. Liq.* **2004**, *113* (1–3), 125–132.
- (249) Zech, O.; Stoppa, A.; Buchner, R.; Kunz, W. The Conductivity of Imidazolium-Based Ionic Liquids from (248 to 468) K. B. Variation of the Anion. *J. Chem. Eng. Data* **2010**, *55* (5), 1774–1778.
- (250) Gardas, R. L.; Freire, M. G.; Carvalho, P. J.; Marrucho, I. M.; Fonseca, I. M. A.; Ferreira, A. G. M.; Coutinho, J. A. P. High-Pressure Densities and Derived Thermodynamic Properties of Imidazolium-Based Ionic Liquids. *J. Chem. Eng. Data* **2006**, *52* (1), 80–88.
- (251) Lei, Z.; Dai, C.; Zhu, J.; Chen, B. Extractive Distillation with Ionic Liquids: A Review. *AIChE J.* **2014**, *60* (9), 3312–3329.
- (252) Langa, E.; Palavra, A. M. F.; Lourenço, M. J. V.; Nieto de Castro, C. A.; Mainar, A. M. P. P, T and Heat Capacity Measurements of ( $\alpha$ -Pinene +  $\beta$ -Pinene) Mixtures over the Temperature Range 283.15 K to 358.15 K and Pressures up to 40 MPa: Experiments and Modelling. *J. Chem. Thermodyn.* **2013**, *57*, 493–499.
- (253) Sama, J. K.; Bandopadhyay, P. Development of a Simple Method for Separation of Alpha-Pinene and Beta-Pinene from Turpentine Oil and Designing Multicomponent Batch Distillation Columns. *Indian J. Chem. Technol.* **2001**, *8* (4), 260–272.
- (254) Díaz, E.; Cortiñas, J.; Ordóñez, S.; Vega, A.; Coca, J. Selectivity of Several Liquid Phases for the Separation of Pine Terpenes by Gas Chromatography. *Chromatographia* **2004**, *60* (9–10), 573–578.
- (255) Chapman, W. G.; Jackson, G.; Gubbins, K. E. Phase Equilibria of Associating Fluids Chain Molecules with Multiple Bonding Sites. *Mol. Phys.* **1988**, *65* (5), 1057–1079.
- (256) Chapman, W. G.; Gubbins, K. E.; Jackson, G.; Radosz, M. New Reference Equation of State for Associating Liquids. *Ind. Eng. Chem. Res.* **1990**, *29* (8), 1709–1721.
- (257) Müller, E. A.; Gubbins, K. E. Molecular-Based Equations of State for Associating Fluids: A Review of SAFT and Related Approaches. *Ind. Eng. Chem. Res.* **2001**, *40*, 2193–2211.



- (258) Paricaud, P.; Galindo, A.; Jackson, G. Recent Advances in the Use of the SAFT Approach in Describing Electrolytes, Interfaces, Liquid Crystals and Polymers. *Fluid Phase Equilib.* **2002**, *194*, 87–96.
- (259) Gross, J.; Sadowski, G. Perturbed-Chain SAFT: An Equation of State Based on a Perturbation Theory for Chain Molecules. *Ind. Eng. Chem. Res.* **2001**, *40* (4), 1244–1260.
- (260) Verevkin, S. P.; Sazonova, A. Y.; Frolkova, A. K.; Zaitsau, D. H.; Prikhodko, I. V.; Held, C. Separation Performance of BioRenewable Deep Eutectic Solvents. *Ind. Eng. Chem. Res.* **2015**, *54* (13), 3498–3504.
- (261) Zubeir, L. F.; Held, C.; Sadowski, G.; Kroon, M. C. PC-SAFT Modeling of CO<sub>2</sub> Solubilities in Deep Eutectic Solvents. *J. Phys. Chem. B* **2016**, *120* (9), 2300–2310.
- (262) Toledo Hijo, A. A. C.; Maximo, G. J.; Costa, M. C.; Batista, E. A. C.; Meirelles, A. J. A. Applications of Ionic Liquids in the Food and Bioproducts Industries. *ACS Sustain. Chem. Eng.* **2016**, *4* (10), 5347–5369.
- (263) Hamer, W. J.; Wu, Y. Osmotic Coefficients and Mean Activity Coefficients of Uni-univalent Electrolytes in Water at 25°C. *J. Phys. Chem. Ref. Data* **1972**, *1* (4), 1047–1100.
- (264) Archer, D. G. Thermodynamic Properties of the NaBr+H<sub>2</sub>O System. *J. Phys. Chem. Ref. Data* **1991**, *20* (3), 509–555.
- (265) Wertheim, M. S. Fluids with Highly Directional Attractive Forces. I. Statistical Thermodynamics. *J. Stat. Phys.* **1984**, *35* (1), 19–34.
- (266) Wertheim, M. S. Fluids with Highly Directional Attractive Forces. II. Thermodynamic Perturbation Theory and Integral Equations. *J. Stat. Phys.* **1984**, *35* (1), 35–47.
- (267) Wertheim, M. S. Fluids with Highly Directional Attractive Forces. III. Multiple Attraction Sites. *J. Stat. Phys.* **1986**, *42* (3), 459–476.
- (268) Wertheim, M. S. Fluids with Highly Directional Attractive Forces. IV. Equilibrium Polymerization. *J. Stat. Phys.* **1986**, *42* (3), 477–492.
- (269) Gross, J.; Sadowski, G. Application of the Perturbed-Chain SAFT Equation of State to Associating Systems Application of the Perturbed-Chain SAFT Equation of State to. *Ind. Eng. Chem. Res.* **2002**, *41*, 5510–5515.
- (270) Wolbach, J. P.; Sandler, S. I. Using Molecular Orbital Calculations To Describe the Phase Behavior of Cross-Associating Mixtures. *Ind. Eng. Chem. Res.* **1998**, *37* (8), 2917–2928.
- (271) Held, C.; Prinz, A.; Wallmeyer, V.; Sadowski, G. Measuring and Modeling Alcohol/salt Systems. *Chem. Eng. Sci.* **2012**, *68* (1), 328–339.
- (272) Ji, X.; Held, C.; Sadowski, G. Modeling Imidazolium-Based Ionic Liquids with ePC-SAFT. *Fluid Phase Equilib.* **2012**, *335*, 64–73.
- (273) Nann, A.; Held, C.; Sadowski, G. Liquid – Liquid Equilibria of 1 - Butanol / Water / IL Systems. *Ind. Eng. Chem. Res.* **2013**, *52* (51), 18472–18481.
- (274) Passos, H.; Khan, I.; Mutelet, F.; Oliveira, M. B.; Carvalho, P. J.; Santos, L. M. N. B. F.; Held, C.; Sadowski, G.; Freire, M. G.; Coutinho, J. A. P. Vapor-Liquid Equilibria of Water plus Alkylimidazolium-Based Ionic Liquids: Measurements and Perturbed-Chain Statistical Associating Fluid Theory Modeling. *Ind. Eng. Chem. Res.* **2014**, *53* (9), 3737–3748.
- (275) Huang, S. H.; Radosz, M. Equation of State for Small, Large, Polydisperse and Associating Molecules. *Ind. Eng. Chem. Res.* **1990**, *29*, 2284–2294.

- (276) Lindenbaum, S.; Boyd, G. E. Osmotic and Activity Coefficients for the Symmetrical Tetraalkyl Ammonium Halides in Aqueous Solution at 25°. *J. Phys. Chem.* **1964**, *68* (5), 911–917.
- (277) Kleiner, M. Thermodynamic Modeling of Complex Systems: Polar and Associating Fluids and Mixtures, Department of Biological and Chemical Engineering- Technische Universität Dortmund- PhD Thesis, 2008.
- (278) Albers, K.; Heilig, M.; Sadowski, G. Reducing the Amount of PCP–SAFT Fitting Parameters. 2. Associating Components. *Fluid Phase Equilib.* **2012**, *326*, 31–44.
- (279) Daubert, T. E.; Sibul, H. M.; Stebbins, C. C.; Danner, R. P.; Rowley, R. L.; Adams, M. E.; Wilding, W. V.; Marshall, T. L. *Physical and Thermodynamic Properties of Pure Chemicals: DIPPR: Data Compilation: Core + Supplements 1-10*; Taylor & Francis, 2000.
- (280) Prausnitz, J. M.; Lichtenthaler, R. N.; Azevedo, E. G. *Molecular Thermodynamics of Fluid-Phase Equilibria*, 3rd ed.; Prentice Hall: New Jersey, 1999.
- (281) Journal, B.; Maximo, G. J.; Costa, M. C.; Meirelles, A. J. A. Solid-Liquid Equilibrium of Triolein with Fatty Alcohols. *Brazilian J. Chem. Eng.* **2013**, *30* (1), 33–43.
- (282) Maximo, G. J.; Carareto, N. D. D.; Costa, M. C.; dos Santos, A. O.; Cardoso, L. P.; Krähenbühl, M. A.; Meirelles, A. J. A. On the Solid-Liquid Equilibrium of Binary Mixtures of Fatty Alcohols and Fatty Acids. *Fluid Phase Equilib.* **2014**, *366*, 88–98.
- (283) Costa, M. C.; Sardo, M.; Rolemberg, M. P.; Ribeiro-Claro, P.; Meirelles, A. J. A.; Coutinho, J. A. P.; Krähenbühl, M. A. The Solid-Liquid Phase Diagrams of Binary Mixtures of Consecutive, Even Saturated Fatty Acids: Differing by Four Carbon Atoms. *Chem. Phys. Lipids* **2009**, *157* (1), 40–50.
- (284) Gardas, R. L.; Coutinho, J. A. P. A Group Contribution Method for Viscosity Estimation of Ionic Liquids. *Fluid Phase Equilib.* **2008**, *266* (1–2), 195–201.
- (285) Diedrichs, A.; Gmehling, J. Measurement of Heat Capacities of Ionic Liquids by Differential Scanning Calorimetry. *Fluid Phase Equilib.* **2006**, *244*, 68–77.
- (286) Niedermeyer, H.; Hallett, J. P.; Villar-Garcia, I. J.; Hunt, P. A.; Welton, T. Mixtures of Ionic Liquids. *Chem. Soc. Rev.* **2012**, *41* (41), 7780–7802.
- (287) Fernandez, L. Personal Communication.
- (288) *Handbook of Chemistry and Physics*, 63 rd.; Weast, R. C., Ed.; CRC Press: Boca Raton, 1982.
- (289) Nakayama, H. Solid-Liquid and Liquid-Liquid Phase Equilibria in the Symmetrical Tetraalkylammonium Halide–Water Systems. *Bull. Chem. Soc. Jpn.* **1981**, *54* (12), 3717–3722.
- (290) Carareto, N. D. D.; Castagnaro, T.; Costa, M. C.; Meirelles, A. J. A. The Binary (Solid+liquid) Phase Diagrams of (Caprylic or Capric acid)+(1-Octanol or 1-Decanol). *J. Chem. Thermodyn.* **2014**, *78*, 99–108.
- (291) Moreno, E.; Cordobilla, R.; Calvet, T.; Cuevas-Diarte, M. A.; Gbabode, G.; Negrier, P.; Mondieig, D.; Oonk, H. A. J. Polymorphism of Even Saturated Carboxylic Acids from N-Decanoic to N-Eicosanoic Acid. *New J. Chem.* **2007**, *31* (6), 947–957.
- (292) Inoue, T.; Hisatsugu, Y.; Suzuki, M.; Wang, Z.; Zheng, L. Solid-Liquid Phase Behavior of Binary Fatty Acid Mixtures: 3. Mixtures of Oleic Acid with Capric Acid (Decanoic Acid) and Caprylic Acid (Octanoic Acid). *Chem. Phys. Lipids* **2004**, *132* (2), 225–234.
- (293) Misra, A. K.; Misra, M.; Panpalia, G. M.; Dorle, A. K. Thermoanalytical and Microscopic Investigation of Interaction between Paracetamol and Fatty Acid Crystals. *J. Macromol. Sci. Part A* **2007**, *44* (7),

685–690.

- (294) Inoue, T.; Hisatsugu, Y.; Ishikawa, R.; Suzuki, M. Solid – Liquid Phase Behavior of Binary Fatty Acid Mixtures 2 . Mixtures of Oleic Acid with Lauric Acid , Myristic Acid , and Palmitic Acid. *Chem. Phys. Lipids* **2004**, *127* (2), 161–173.
- (295) Hong, J.; Hua, D.; Wang, X.; Wang, H.; Li, J. Solid-Liquid-Gas Equilibrium of the Ternaries Ibuprofen + Myristic Acid + CO<sub>2</sub> and Ibuprofen + Tripalmitin + CO<sub>2</sub>. *J. Chem. Eng. Data* **2010**, *55* (1), 297–302.
- (296) Zeng, J. L.; Cao, Z.; Yang, D. W.; Xu, F.; Sun, L. X.; Zhang, L.; Zhang, X. F. Phase Diagram of Palmitic Acid-Tetradecanol Mixtures Obtained by DSC Experiments. *J. Therm. Anal. Calorim.* **2009**, *95* (2), 501–505.
- (297) Costa, M. C.; Rolemberg, M. P.; Meirelles, A. J. A.; Coutinho, J. A. P.; Krähenbühl, M. A. The Solid–liquid Phase Diagrams of Binary Mixtures of Even Saturated Fatty Acids Differing by Six Carbon Atoms. *Thermochim. Acta* **2009**, *496* (1–2), 30–37.
- (298) Gbabode, G.; Negrier, P.; Mondieig, D.; Moreno, E.; Calvet, T.; Cuevas-Diarte, M. A. Fatty Acids Polymorphism and Solid-State Miscibility. Pentadecanoic Acid-Hexadecanoic Acid Binary System. *J. Alloys Compd.* **2009**, *469* (1–2), 539–551.
- (299) Gandolfo, F. G.; Bot, A.; Flöter, E. Phase Diagram of Mixtures of Stearic Acid and Stearyl Alcohol. *Thermochim. Acta* **2003**, *404* (1–2), 9–17.
- (300) Cedeño, F. O.; Prieto, M. M.; Espina, A.; García, J. R. Measurements of Temperature and Melting Heat of Some Pure Fatty Acids and Their Binary and Ternary Mixtures by Differential Scanning Calorimetry. *Thermochim. Acta* **2001**, *369* (1–2), 39–50.
- (301) Sato, K.; Yoshimoto, N.; Suzuki, M.; Kobayashi, M.; Kaneko, F. Structure and Transformation in Polymorphism of Petroselinic Acid. *J. Phys. Chem.* **1990**, *94* (18), 3180–3185.
- (302) Maximo, G. J.; Santos, R. J. B. N.; Brandao, P.; Esperanca, J. M. S. S.; Costa, M. C.; Meirelles, A. J. A.; Freire, M. G.; Coutinho, J. A. P. Generating Ionic Liquids from Ionic Solids: An Investigation of the Melting Behavior of Binary Mixtures of Ionic Liquids. *Cryst. Growth Des.* **2014**, *14* (9), 4270–4277.
- (303) Abbott, A. P.; Boothby, D.; Capper, G.; Davies, D. L.; Rasheed, R. K. Deep Eutectic Solvents Formed between Choline Chloride and Carboxylic Acids: Versatile Alternatives to Ionic Liquids. *J. Am. Chem. Soc.* **2004**, *126* (29), 9142–9147.
- (304) Paiva, A.; Craveiro, R.; Aroso, I.; Martins, M.; Reis, R. L.; Duarte, A. R. C. Natural Deep Eutectic Solvents – Solvents for the 21st Century. *ACS Sustain. Chem. Eng.* **2014**, *2* (5), 1063–1071.
- (305) Radošević, K.; Cvjetko Bubalo, M.; Gaurina Srček, V.; Grgas, D.; Landeka Dragičević, T.; Radojčić Redovniković, I. Evaluation of Toxicity and Biodegradability of Choline Chloride Based Deep Eutectic Solvents. *Ecotoxicol. Environ. Saf.* **2015**, *112*, 46–53.
- (306) Chemat, F.; Anjum, H.; Shariff, A. M.; Kumar, P.; Murugesan, T. Thermal and Physical Properties of (Choline Chloride+urea+l-Arginine) Deep Eutectic Solvents. *J. Mol. Liq.* **2016**, *218*, 301–308.
- (307) Stolarska, O.; Soto, A.; Rodríguez, H.; Smiglak, M. Properties Modification by Eutectic Formation in Mixtures of Ionic Liquids. *RSC Adv.* **2015**, *5* (28), 22178–22187.
- (308) Stolarska, O.; Rodríguez, H.; Smiglak, M. Eutectic Mixtures of Pyrrolidinium-Based Ionic Liquids. *Fluid Phase Equilib.* **2016**, *408*, 1–9.
- (309) Fukaya, Y.; Iizuka, Y.; Sekikawa, K.; Ohno, H. Bio Ionic Liquids: Room Temperature Ionic Liquids Composed Wholly of Biomaterials. *Green Chem.* **2007**, *9* (11), 1155–1157.

- (310) Muhammad, N.; Hossain, M. I.; Man, Z.; El-Harbawi, M.; Bustam, M. A.; Noaman, Y. A.; Mohamed Alitheen, N. B.; Ng, M. K.; Hefter, G.; Yin, C.-Y. Synthesis and Physical Properties of Choline Carboxylate Ionic Liquids. *J. Chem. Eng. Data* **2012**, *57* (8), 2191–2196.
- (311) Petkovic, M.; Ferguson, J. L.; Gunaratne, H. Q. N.; Ferreira, R.; Leitão, M. C.; Seddon, K. R.; Rebelo, L. P. N.; Pereira, C. S. Novel Biocompatible Cholinium-Based Ionic Liquids—toxicity and Biodegradability. *Green Chem.* **2010**, *12* (4), 643–649.
- (312) Janz, G. J.; Tomkins, R. P. T. *Nonaqueous Electrolytes Handbook*; Academic Press: New York-London, 1972; Vol. 1.
- (313) Jenck, J. Palladium Catalyzed Carbonylation of Conjugated Dienes with Catalyst Recycle. US 4454333 A, 1984.
- (314) Hiroshi Ogawa, Tatsuhiro Suwa, C. H. S. Adhesive Composition and Optical Member. US 20090014123 A1, 2009.
- (315) Nockemann, P.; Binnemans, K.; Thijs, B.; Parac-Vogt, T. N.; Merz, K.; Mudring, A.-V.; Menon, P. C.; Rajesh, R. N.; Cordoyiannis, G.; Thoen, J.; Leys, J.; Glorieux, C. Temperature-Driven Mixing-Demixing Behavior of Binary Mixtures of the Ionic Liquid Choline Bis(trifluoromethylsulfonyl)imide and Water. *J. Phys. Chem. B* **2009**, *113* (5), 1429–1437.
- (316) Skarmoutsos, I.; Dellis, D.; Matthews, R. P.; Welton, T.; Hunt, P. A. Hydrogen Bonding in 1-Butyl- and 1-Ethyl-3-Methylimidazolium Chloride Ionic Liquids. *J. Phys. Chem. B* **2012**, *116* (16), 4921–4933.
- (317) Ruiz, E.; Ferro, V. R.; Palomar, J.; Ortega, J.; Rodriguez, J. J. Interactions of Ionic Liquids and Acetone: Thermodynamic Properties, Quantum-Chemical Calculations, and NMR Analysis. *J. Phys. Chem. B* **2013**, *117* (24), 7388–7398.
- (318) Kang, J. W.; Diky, V.; Chirico, R. D.; Magee, J. W.; Muzny, C. D.; Kazakov, A. F.; Kroenlein, K.; Frenkel, M. Algorithmic Framework for Quality Assessment of Phase Equilibrium Data. *J. Chem. Eng. Data* **2014**, *59* (7), 2283–2293.
- (319) Cunico, L. P.; Ceriani, R.; Sarup, B.; O’Connell, J. P.; Gani, R. Data, Analysis and Modeling of Physical Properties for Process Design of Systems Involving Lipids. *Fluid Phase Equilib.* **2014**, *362*, 318–327.
- (320) Renon, H.; Prausnitz, J. M. Local Compositions in Thermodynamic Excess Functions for Liquid Mixtures. *AIChE J.* **1968**, *14* (1), 135–144.
- (321) Fernandez, L.; Silva, L. P.; Martins, M. A. R.; Ferreira, O.; Pinho, S. P.; Coutinho, J. A. P.; Ortega, J. Indirect Assessment of the Fusion Properties of Choline Chloride from Solid Liquid Equilibria Data. Submitted.
- (322) Yan, X.; Dong, Q.; Hong, X. Reliability Analysis of Group-Contribution Methods in Predicting Critical Temperatures of Organic Compounds. *J. Chem. Eng. Data* **2003**, *48* (2), 374–380.
- (323) Joback, S. M. A Unified Approach to Physical Property Estimation Using Multivariate Statistical Techniques (Doctoral Dissertation), Cambridge, MA, 1984.
- (324) Ambrose, D. Correlation and Estimation of Vapor-Liquid Critical Properties. I. Critical Temperatures of Organic Compounds. *Natl. Phys. Lab. NPL Rep. Chem* **1978**, *92*.
- (325) Constantinou, L.; Gani, R. New Group Contribution Method for Estimating Properties of Pure Compounds. *AIChE J.* **1994**, *40* (10), 1697–1710.
- (326) Smith, J. R. L.; Negishi, E.; Arai, K.; Saito, S. Measurement of Critical Temperatures of Terpenes. *J. Chem. Eng. Japan* **1990**, *23* (1), 99–102.

- (327) Tsonopoulos, C.; Ambrose, D. Vapor–Liquid Critical Properties of Elements and Compounds. 6. Unsaturated Aliphatic Hydrocarbons. *J. Chem. Eng. Data* **1996**, *41* (4), 645–656.
- (328) Martins, M. A. R.; Domańska, U.; Schröder, B.; Coutinho, J. A. P.; Pinho, S. P. Selection of Ionic Liquids to Be Used as Separation Agents for Terpenes and Terpenoids. *ACS Sustain. Chem. Eng.* **2016**, *4* (2), 548–556.
- (329) Sanchez-Vicente, Y.; Cabanas, A.; Renuncio, J. A. R.; Pando, C. Supercritical CO<sub>2</sub> as a Green Solvent for Eucalyptus and Citrus Essential Oils Processing: Role of Thermal Effects upon Mixing. *RSC Adv.* **2013**, *3* (17), 6065–6075.
- (330) García-Abarrio, S. M.; Torcal, M.; Haya, M. L.; Urieta, J. S.; Mainar, A. M. Thermophysical Properties of {(±)-Linalool + Propan-1-Ol}: A First Stage towards the Development of a Green Process. *J. Chem. Thermodyn.* **2011**, *43* (4), 527–536.
- (331) Riedel, L. Estimation of Unknown Critical Pressures of Organic Compounds. *Zeitschrift fur Elektrochemie* **1949**, *53*, 222–228.
- (332) Lyderren, A. L. *Estimation of Critical Properties of Organic Compounds by the Method of Group Contributions. Engineering Experiment Station Report 3.*; College of Engineering, University of Wisconsin: Madison, Wisconsin, 1955.
- (333) Wilson, M.; Jasperson, L. V. Cited by Poling Et. Al. (2000). Paper Presented at the AIChE Meeting, New Orleans, LA.
- (334) Marrero-Morejón, J.; Pardillo-Fontdevila, E. Estimation of Pure Compound Properties Using Group-Interaction Contributions. *AIChE J.* **1999**, *45* (3), 615–621.
- (335) Ambrose, D. Correlation and Estimation of Vapor-Liquid Critical Properties. II. Critical Pressures and Volumes of Organic Compounds. *Natl. Phys. Lab. NPL Rep. Chem* **1979**, *98*.
- (336) Daubert, T. E. State-of-the-Art-Property Predictions. *Hydrocarb. Process.* **1980**, 107–112.
- (337) Fedors, R. F. A Relationship between Chemical Structure and the Critical Temperature. *Chem. Eng. Commun.* **1982**, *16* (1–6), 149–151.
- (338) Klincewicz, K. M.; Reid, R. C. Estimation of Critical Properties with Group Contribution Methods. *AIChE J.* **1984**, *30* (1), 137–142.
- (339) Joback, K. G.; Reid, R. C. Estimation of Pure-Component Properties from Group-Contributions. *Chem. Eng. Commun.* **1987**, *57* (1–6), 233–243.
- (340) Somayajulu, G. R. Estimation Procedures for Critical Constants. *J. Chem. Eng. Data* **1989**, *34* (1), 106–120.
- (341) Chein-Hsiun, T. Group-Contribution Estimation of Critical Temperature with Only Chemical Structure. *Chem. Eng. Sci.* **1995**, *50* (22), 3515–3520.
- (342) Marrero, J.; Gani, R. Group-Contribution Based Estimation of Pure Component Properties. *Fluid Phase Equilib.* **2001**, *183–184*, 183–208.
- (343) Wen, X.; Qiang, Y. A New Group Contribution Method for Estimating Critical Properties of Organic Compounds. *Ind. Eng. Chem. Res.* **2001**, *40* (26), 6245–6250.
- (344) Poling, B. E.; Prausnitz, J. M.; O'Connell, J. P. *The Properties of Gases and Liquids*, Fifth.; McGraw-Hill: New York, 2000.
- (345) Spencer, C. F.; Daubert, T. E.; Danner, R. P. A Critical Review of Correlations for the Critical

- Properties of Defined Mixtures. *AIChE J.* **1973**, *19* (3), 522–527.
- (346) Lee, B. I.; Kesler, M. G. A Generalized Thermodynamic Correlation Based on Three-Parameter Corresponding States. *AIChE J.* **1975**, *21* (3), 510–527.
- (347) van der Waals, J. D. On the Continuity of the Gaseous and Liquid States (Doctoral Dissertation), Universiteit Leiden, 1873.
- (348) Redlich, O.; Kwong, J. N. S. On the Thermodynamics of Solutions. V. An Equation of State. Fugacities of Gaseous Solutions. *Chem. Rev.* **1949**, *44* (1), 233–244.
- (349) Soave, G. Equilibrium Constants from a Modified Redlich-Kwong Equation of State. *Chem. Eng. Sci.* **1972**, *27* (6), 1197–1203.
- (350) Peng, D.-Y.; Robinson, D. B. A New Two-Constant Equation of State. *Ind. Eng. Chem. Fundam.* **1976**, *15* (1), 59–64.
- (351) Chaves, I. D. G.; López, J. R. G.; Zapata, J. L. G.; Robayo, A. L.; Niño, G. R. Process Simulation in Chemical Engineering. In *Process Analysis and Simulation in Chemical Engineering*; Springer International Publishing: Cham, 2016; pp 1–51.
- (352) Domańska, U.; Papis, P.; Szydłowski, J.; Królikowska, M.; Królikowski, M. Excess Enthalpies of Mixing, Effect of Temperature and Composition on the Density, and Viscosity and Thermodynamic Properties of Binary Systems of {Ammonium-Based Ionic Liquid + Alkanediol}. *J. Phys. Chem. B* **2014**, *118* (44), 12692–12705.
- (353) Yaws, C. L. *Thermophysical Properties of Chemicals and Hydrocarbons*; William Andrew, 2008.
- (354) Kenyon, J.; Pickard, R. H. VII.-Investigations on the Dependence of Rotatory Power on Chemical Constitution. Part XI. The Co-Ordination of the Rotatory Powers (a) of Menthyl Compounds, (B) of the Menthones, and (c) of the Borneols. *J. Chem. Soc. Trans.* **1915**, *107*, 35–62.
- (355) Müller, A. Die Parachore, Viskositäten Und Chelatringbildung Der Alkohole. *Eur. J. Lipid Sci. Technol.* **1942**, *49* (8), 572–578.
- (356) Martínez-López, J. F.; Mainar, A. M.; Urieta, J. S.; Pardo, J. I. Thermophysical Properties of {R-Fenchone + Ethanol} at Several Temperatures and Pressures. *J. Chem. Thermodyn.* **2014**, *69*, 48–55.
- (357) Atik, Z.; Ewing, M. B.; McGlashan, M. L. Chiral Discrimination in Liquids. Excess Molar Volumes of (1 - x)A<sup>+</sup> + xA<sup>-</sup>, Where A Denotes Limonene, Fenchone, and .alpha.-Methylbenzylamine. *J. Phys. Chem.* **1981**, *85* (22), 3300–3303.
- (358) Liu, H.; Kido, S.; Kamiyama, T.; Fujisawa, M.; Kimura, T. Thermodynamic Properties of Chiral Fenches in Some Solutions at T = 298.15 K. *J. Chem. Thermodyn.* **2011**, *43* (4), 627–634.
- (359) Florido, P. M.; Andrade, I. M. G.; Capellini, M. C.; Carvalho, F. H.; Aracava, K. K.; Koshima, C. C.; Rodrigues, C. E. C.; Gonçalves, C. B. Viscosities and Densities of Systems Involved in the Deterpenation of Essential Oils by Liquid-Liquid Extraction: New UNIFAC-VISCO Parameters. *J. Chem. Thermodyn.* **2014**, *72*, 152–160.
- (360) Comelli, F.; Francesconi, R.; Castellari, C. Densities, Viscosities, and Excess Molar Enthalpies of Binary Mixtures Containing Essential Oils at (298.15 and 313.15) K. The (S)-(-)-Limonene + Cineole, (S)-(-)-Limonene + Linalool, and Cineole + Linalool Systems. *J. Chem. Eng. Data* **2001**, *46* (4), 868–872.
- (361) Clará, R. A.; Marigliano, A. C. G. G.; Sólamo, H. N.; Clará, R. A.; Marigliano, A. C. G. G.; Sólamo, H. N. Density, Viscosity, and Refractive Index in the Range (283.15 to 353.15) K and Vapor Pressure of  $\alpha$ -

- Pinene, D-Limonene, ( $\pm$ )-Linalool, and Citral Over the Pressure Range 1.0 kPa Atmospheric Pressure. *J. Chem. Eng. Data* **2009**, *54* (3), 1087–1090.
- (362) Torcal, M.; Teruel, M. I.; García, J.; Urieta, J. S.; Mainar, A. M. PpT Measurements of the (Ethanol + Linalool), (Propan-1-Ol + Linalool), and (Propan-2-Ol + Linalool) Mixtures: Cubic and Statistical Associating Fluid Theory-Based Equation of State Analyses. *J. Chem. Eng. Data* **2010**, *55* (11), 5332–5339.
- (363) Lepori, L.; Mengheri, M.; Mollica, V. Discriminating Interactions between Chiral Molecules in the Liquid Phase: Effect on Volumetric Properties. *J. Phys. Chem.* **1983**, *87* (18), 3520–3525.
- (364) Barata, P. A.; Serrano, M. L. Densities and Viscosities of Thymol + 1,8-Cineole. *J. Chem. Eng. Data* **1994**, *39* (2), 298–301.
- (365) Alfaro, P.; Langa, E.; Martínez-López, J. F.; Urieta, J. S.; Mainar, A. M. Thermophysical Properties of the Binary Mixtures (1,8-Cineole + 1-Alkanol) at T = (298.15 and 313.15) K and at Atmospheric Pressure. *J. Chem. Thermodyn.* **2010**, *42* (2), 291–303.
- (366) Torcal, M.; García-Abarrio, S.; Pardo, J. I.; Mainar, A. M.; Urieta, J. S. P, T Measurements and Isobaric Vapor–Liquid–Equilibria of the 1,3,3-Trimethyl-2-oxabicyclo[2,2,2]octane + Propan-1-Ol Mixture: Cubic and Statistical Associating Fluid Theory-Based Equation of State Analysis. *J. Chem. Eng. Data* **2010**, *55* (12), 5932–5940.
- (367) Lasarte, J. M.; Martín, L.; Langa, E.; Urieta, J. S.; Mainar, A. M. Setup and Validation of a PpT Measuring Device. Volumetric Behavior of the Mixture 1,8-Cineole + Ethanol. *J. Chem. Eng. Data* **2008**, *53* (6), 1393–1400.
- (368) Comelli, F.; Ottani, S.; Francesconi, R.; Castellari, C. Densities, Viscosities, and Refractive Indices of Binary Mixtures Containing N-Hexane + Components of Pine Resins and Essential Oils at 298.15 K. *J. Chem. Eng. Data* **2002**, *47* (1), 93–97.
- (369) Tavares Sousa, A.; Nieto de Castro, C. A. Density of  $\alpha$ -Pinene, B-Pinene, Limonene, and Essence of Turpentine. *Int. J. Thermophys.* **1992**, *13* (2), 295–301.
- (370) Ribeiro, A.; Bernardo-Gil, G. Densities and Refractive Indices of Components of Pine Resin. *J. Chem. Eng. Data* **1990**, *35* (2), 204–206.
- (371) Cunha, D. L.; Coutinho, J. A. P.; Daridon, J. L.; Reis, R. A.; Paredes, M. L. L. Experimental Densities and Speeds of Sound of Substituted Phenols and Their Modeling with the Prigogine–Flory–Patterson Model. *J. Chem. Eng. Data* **2013**, *58* (11), 2925–2931.
- (372) Cheng, K.-W.; Kuo, S.-J.; Tang, M.; Chen, Y.-P. Vapor–liquid Equilibria at Elevated Pressures of Binary Mixtures of Carbon Dioxide with Methyl Salicylate, Eugenol, and Diethyl Phthalate. *J. Supercrit. Fluids* **2000**, *18* (2), 87–99.
- (373) do Carmo, F. R.; Evangelista, N. S.; Fernandes, F. A. N.; de Sant’Ana, H. B. Evaluation of Optimal Methods for Critical Properties and Acentric Factor of Biodiesel Compounds with Their Application on Soave–Redlich–Kwong and Peng–Robinson Equations of State. *J. Chem. Eng. Data* **2015**, *60* (11), 3358–3381.
- (374) Neves, C. M. S. S.; Batista, M. L. S.; Claudio, A. F. M.; Santos, L. M. N. B. F.; Marrucho, I. M.; Freire, M. G.; Coutinho, J. A. P. Thermophysical Properties and Water Saturation of [PF6]-Based Ionic Liquids. *J. Chem. Eng. Data* **2010**, *55* (11), 5065–5073.
- (375) Neves, C. M. S. S.; Carvalho, P. J.; Freire, M. G.; Coutinho, J. A. P. Thermophysical Properties of Pure and Water-Saturated Tetradecyltrihexylphosphonium-Based Ionic Liquids. *J. Chem. Thermodyn.* **2011**, *43* (6), 948–957.

- (376) Ohno, H.; Yoshizawa, M. Ion Conductive Characteristics of Ionic Liquids Prepared by Neutralization of Alkylimidazoles. *Solid State Ionics* **2002**, *154–155*, 303–309.
- (377) Neves, C. M. S. S.; Rodrigues, A. R.; Kurnia, K. A.; Esperança, J. M. S. S.; Freire, M. G.; Coutinho, J. A. P. Solubility of Non-Aromatic Hexafluorophosphate-Based Salts and Ionic Liquids in Water Determined by Electrical Conductivity. *Fluid Phase Equilib.* **2013**, *358*, 50–55.
- (378) Freire, M. G.; Carvalho, P. J.; Gardas, R. L.; Marrucho, I. M.; Santos, L. M. N. B. F.; Coutinho, J. A. P. Mutual Solubilities of Water and the [Cnmim][Tf2N] Hydrophobic Ionic Liquids. *J. Phys. Chem. B* **2008**, *112* (6), 1604–1610.
- (379) Freire, M. G.; Carvalho, P. J.; Gardas, R. L.; Santos, L. M. N. B. F.; Marrucho, I. M.; Coutinho, J. A. P. Solubility of Water in Tetradecyltriethylphosphonium-Based Ionic Liquids. *J. Chem. Eng. Data* **2008**, *53* (10), 2378–2382.
- (380) Freire, M. G.; Neves, C. M. S. S.; Carvalho, P. J.; Gardas, R. L.; Fernandes, A. M.; Marrucho, I. M.; Santos, L. M. N. B. F.; Coutinho, J. A. P. Mutual Solubilities of Water and Hydrophobic Ionic Liquids. *J. Phys. Chem. B* **2007**, *111* (45), 13082–13089.
- (381) Freire, M. G.; Neves, C. M. S. S.; Shimizu, K.; Bernardes, C. E. S.; Marrucho, I. M.; Coutinho, J. A. P.; Lopes, J. N. C.; Rebelo, L. P. N. Mutual Solubility of Water and Structural/Positional Isomers of N-Alkylpyridinium-Based Ionic Liquids. *J. Phys. Chem. B* **2010**, *114* (48), 15925–15934.
- (382) Freire, M. G.; Neves, C. M. S. S.; Ventura, S. P. M.; Pratas, M. J.; Marrucho, I. M.; Oliveira, J.; Coutinho, J. A. P.; Fernandes, A. M. Solubility of Non-Aromatic Ionic Liquids in Water and Correlation Using a QSPR Approach. *Fluid Phase Equilib.* **2010**, *294* (1–2), 234–240.
- (383) Freire, M. G.; Santos, L. M. N. B. F.; Fernandes, A. M.; Coutinho, J. A. P.; Marrucho, I. M. An Overview of the Mutual Solubilities of Water-Imidazolium-Based Ionic Liquids Systems. *Fluid Phase Equilib.* **2007**, *261* (1–2), 449–454.
- (384) Maia, F. M.; Rodríguez, O.; Macedo, E. A. LLE for (Water + Ionic Liquid) Binary Systems Using [Cxmim][BF4] (X = 6, 8) Ionic Liquids. *Fluid Phase Equilib.* **2010**, *296* (2), 184–191.
- (385) Maia, F. M.; Rodríguez, O.; Macedo, E. A. Relative Hydrophobicity of Equilibrium Phases in Biphasic Systems (Ionic Liquid + Water). *J. Chem. Thermodyn.* **2012**, *48*, 221–228.
- (386) Maia, F. M.; Rodríguez, O.; MacEdo, E. A. Free Energy of Transfer of a Methylene Group in Biphasic Systems of Water and Ionic Liquids [C3mpip][NTf2], [C3mpyrr] [NTf2], and [C4mpyrr][NTf2]. *Ind. Eng. Chem. Res.* **2012**, *51* (23), 8061–8068.
- (387) Maia, F. M.; Tsvintzelis, I.; Rodriguez, O.; Macedo, E. A.; Kontogeorgis, G. M. Equation of State Modelling of Systems with Ionic Liquids: Literature Review and Application with the Cubic Plus Association (CPA) Model. *Fluid Phase Equilib.* **2012**, *332*, 128–143.
- (388) Bhattacharjee, A.; Carvalho, P. J.; Coutinho, J. A. P. The Effect of the Cation Aromaticity upon the Thermophysical Properties of Piperidinium- and Pyridinium-Based Ionic Liquids. *Fluid Phase Equilib.* **2014**, *375*, 80–88.
- (389) Carvalho, P. J.; Ventura, S. P. M. S. P. M.; Batista, M. L. S.; Schroeder, B.; Goncalves, F.; Esperanca, J.; Mutelet, F.; Coutinho, J. A. P. J. A. P.; Schröder, B.; Gonçalves, F.; Esperança, J.; Mutelet, F.; Coutinho, J. A. P. J. A. P. Understanding the Impact of the Central Atom on the Ionic Liquid Behavior: Phosphonium vs Ammonium Cations. *J. Chem. Phys.* **2014**, *140* (6), 64505.
- (390) Batista, M. L. S.; Neves, C. M. S. S.; Carvalho, P. J.; Gani, R.; Coutinho, J. A. P. Chameleonic Behavior of Ionic Liquids and Its Impact on the Estimation of Solubility Parameters. *J. Phys. Chem. B* **2011**, *115* (44), 12879–12888.



- (391) Bhattacharjee, A.; Luís, A.; Lopes-da-Silva, J. A.; Freire, M. G.; Carvalho, P. J.; Coutinho, J. A. P. Thermophysical Properties of Sulfonium- and Ammonium-Based Ionic Liquids. *Fluid Phase Equilib.* **2014**, *381*, 36–45.
- (392) Ge, M.-L.; Ren, X.-G.; Song, Y.-J.; Wang, L.-S. Densities and Viscosities of 1-Propyl-2,3-Dimethylimidazolium Tetrafluoroborate + H<sub>2</sub>O at T = (298.15 to 343.15) K. *J. Chem. Eng. Data* **2009**, *54* (4), 1400–1402.
- (393) Rodríguez, H.; Brennecke, J. F. Temperature and Composition Dependence of the Density and Viscosity of Binary Mixtures of Water + Ionic Liquid. *J. Chem. Eng. Data* **2006**, *51* (6), 2145–2155.
- (394) Gardas, R. L.; Dagade, D. H.; Coutinho, J. A. P.; Patil, K. J. Thermodynamic Studies of Ionic Interactions in Aqueous Solutions of Imidazolium-Based Ionic Liquids [Emim][Br] and [Bmim][Cl]. *J. Phys. Chem. B* **2008**, *112* (11), 3380–3389.
- (395) Gómez-Díaz, D.; Navaza, J. M.; Sanjurjo, B. Density, Kinematic Viscosity, Speed of Sound, and Surface Tension of Hexyl, Octyl, and Decyl Trimethyl Ammonium Bromide Aqueous Solutions. *J. Chem. Eng. Data* **2007**, *52* (3), 889–891.
- (396) Jacquemin, J.; Husson, P.; Padua, A. A. H.; Majer, V. Density and Viscosity of Several Pure and Water-Saturated Ionic Liquids. *Green Chem.* **2006**, *8* (2), 172–180.
- (397) Oliveira, F. S.; Freire, M. G.; Carvalho, P. J.; Coutinho, J. A. P.; Lopes, J. N. C.; Rebelo, L. P. N.; Marrucho, I. M. Structural and Positional Isomerism Influence in the Physical Properties of Pyridinium NTF<sub>2</sub>-Based Ionic Liquids: Pure and Water-Saturated Mixtures. *J. Chem. Eng. Data* **2010**, *55* (10), 4514–4520.
- (398) Ferreira, A. R.; Freire, M. G.; Ribeiro, J. C.; Lopes, F. M.; Crespo, J. G.; Coutinho, J. A. P. Overview of the Liquid–Liquid Equilibria of Ternary Systems Composed of Ionic Liquid and Aromatic and Aliphatic Hydrocarbons, and Their Modeling by COSMO-RS. *Ind. Eng. Chem. Res.* **2012**, *51* (8), 3483–3507.
- (399) F. Eckert, A. Klamt, COSMOtherm Version C2.1 Release 01.08, COSMOlogic GmbH & Co. KG, Leverkusen, Germany, 2006.
- (400) Kurnia, K. A.; Coutinho, J. A. P. Overview of the Excess Enthalpies of the Binary Mixtures Composed of Molecular Solvents and Ionic Liquids and Their Modeling Using COSMO-RS. *Ind. Eng. Chem. Res.* **2013**, *52* (38), 13862–13874.
- (401) Freire, M. G.; Ventura, S. P. M.; Santos, L. M. N. B. F.; Marrucho, I. M.; Coutinho, J. A. P. Evaluation of COSMO-RS for the Prediction of LLE and VLE of Water and Ionic Liquids Binary Systems. *Fluid Phase Equilib.* **2008**, *268* (1–2), 74–84.
- (402) Tsionopoulos, C. Thermodynamic Analysis of the Mutual Solubilities of Normal Alkanes and Water. *Fluid Phase Equilib.* **1999**, *156* (1–2), 21–33.
- (403) Martins, M. A. R.; Neves, C. M. S. S.; Kurnia, K. A.; Santos, L. M. N. B. F.; Freire, M. G.; Pinho, S. P.; Coutinho, J. A. P. Analysis of the Isomerism Effect on the Mutual Solubilities of Bis(trifluoromethylsulfonyl)imide-Based Ionic Liquids with Water. *Fluid Phase Equilib.* **2014**, *381*, 28–35.
- (404) Machanová, K.; Jacquemin, J.; Wagner, Z.; Bendová, M. Mutual Solubilities of Ammonium-Based Ionic Liquids with Water and with Water/Methanol Mixture. *Procedia Eng.* **2012**, *42*, 1229–1241.
- (405) Gardas, R. L.; Ge, R.; Ab Manan, N.; Rooney, D. W.; Hardacre, C. Interfacial Tensions of Imidazolium-Based Ionic Liquids with Water and N-Alkanes. *Fluid Phase Equilib.* **2010**, *294* (1–2), 139–147.
- (406) Domańska, U.; Rękawek, A.; Marciniak, A. Solubility of 1-Alkyl-3-Ethylimidazolium-Based Ionic

- Liquids in Water and 1-Octanol. *J. Chem. Eng. Data* **2008**, *53* (5), 1126–1132.
- (407) Kurnia, K. A.; Neves, C. M. S. S.; Freire, M. G.; Santos, L. M. N. B. F.; Coutinho, J. A. P. Comprehensive Study on the Impact of the Cation Alkyl Side Chain Length on the Solubility of Water in Ionic Liquids. *J. Mol. Liq.* **2015**, *210*, 264–271.
- (408) Rocha, M. A. A.; Ribeiro, F. M. S.; Schröder, B.; Coutinho, J. A. P.; Santos, L. M. N. B. F. Volatility Study of [C1C1im][NTf2] and [C2C3im][NTf2] Ionic Liquids. *J. Chem. Thermodyn.* **2014**, *68*, 317–321.
- (409) Rocha, M. A.; Coutinho, J. A.; Santos, L. M. Evidence of Nanostructuration from the Heat Capacities of the 1,3-Dialkylimidazolium Bis(trifluoromethylsulfonyl)imide Ionic Liquid Series. *J. Chem. Phys.* **2013**, *139* (10), 104502.
- (410) Rocha, M. A. A.; Bastos, M.; Coutinho, J. A. P.; Santos, L. M. N. B. F. Heat Capacities at 298.15 K of the Extended [CnC1im][Ntf2] Ionic Liquid Series. *J. Chem. Thermodyn.* **2012**, *53*, 140–143.
- (411) Tariq, M.; Freire, M. G.; Saramago, B.; Coutinho, J. A. P.; Lopes, J. N. C.; Rebelo, L. P. N. Surface Tension of Ionic Liquids and Ionic Liquid Solutions. *Chem. Soc. Rev.* **2012**, *41* (2), 829–868.
- (412) Carvalho, P. J.; Freire, M. G.; Marrucho, I. M.; Queimada, A. J.; Coutinho, J. A. P. Surface Tensions for the 1-Alkyl-3-Methylimidazolium Bis(trifluoromethylsulfonyl)imide Ionic Liquids. *J. Chem. Eng. Data* **2008**, *53* (6), 1346–1350.
- (413) Tariq, M.; Forte, P. A. S.; Gomes, M. F. C.; Lopes, J. N. C.; Rebelo, L. P. N. Densities and Refractive Indices of Imidazolium- and Phosphonium-Based Ionic Liquids: Effect of Temperature, Alkyl Chain Length, and Anion. *J. Chem. Thermodyn.* **2009**, *41* (6), 790–798.
- (414) C. Pais, A. A. C.; Sousa, A.; Eusebio, M. E.; Redinha, J. S. Solvation of Alkane and Alcohol Molecules. Energy Contributions. *Phys. Chem. Chem. Phys.* **2001**, *3* (18), 4001–4009.
- (415) Cabani, S.; Gianni, P.; Mollica, V.; Lepori, L. Group Contributions to the Thermodynamic Properties of Non-Ionic Organic Solutes in Dilute Aqueous Solution. *J. Solution Chem.* **1981**, *10* (8), 563–595.
- (416) Rocha, M. A. A.; Coutinho, J. A. P.; Santos, L. M. N. B. F. Cation Symmetry Effect on the Volatility of Ionic Liquids. *J. Phys. Chem. B* **2012**, *116* (35), 10922–10927.
- (417) Watanabe, Y.; Katsuta, S. Distribution of a Monovalent Anion in Various Ionic Liquid/Water Biphasic Systems: Relationship of the Distribution Ratio of Picrate Ions with the Aqueous Solubility of Ionic Liquids. *J. Chem. Eng. Data* **2014**, *59* (3), 696–701.
- (418) Gardas, R. L.; Costa, H. F.; Freire, M. G.; Carvalho, P. J.; Marrucho, I. M.; Fonseca, I. M. A.; Ferreira, A. G. M.; Coutinho, J. A. P. Densities and Derived Thermodynamic Properties of Imidazolium-, Pyridinium-, Pyrrolidinium-, and Piperidinium-Based Ionic Liquids. *J. Chem. Eng. Data* **2008**, *53* (3), 805–811.
- (419) Esperança, J. M. S. S.; Guedes, H. J. R.; Blesic, M.; Rebelo, L. P. N. Densities and Derived Thermodynamic Properties of Ionic Liquids. 3. Phosphonium-Based Ionic Liquids over an Extended Pressure Range. *J. Chem. Eng. Data* **2005**, *51* (1), 237–242.
- (420) Blesic, M.; Swadzba-Kwasny, M.; Belhocine, T.; Gunaratne, H. Q. N.; Lopes, J. N. C.; Gomes, M. F. C.; Padua, A. A. H.; Seddon, K. R.; Rebelo, L. P. N. 1-Alkyl-3-Methylimidazolium Alkanesulfonate Ionic Liquids, [CH2+1mim][CH2+1SO3]: Synthesis and Physicochemical Properties. *Phys. Chem. Chem. Phys.* **2009**, *11* (39), 8939–8948.
- (421) Tariq, M.; Carvalho, P. J.; Coutinho, J. A. P.; Marrucho, I. M.; Lopes, J. N. C.; Rebelo, L. P. N. Viscosity of (C2 - C14) 1-Alkyl-3-Methylimidazolium Bis(trifluoromethylsulfonyl)amide Ionic Liquids in an Extended Temperature Range. *Fluid Phase Equilib.* **2011**, *301* (1), 22–32.

- (422) Rocha, M. A. A.; Lima, C. F. R. A. C.; Gomes, L. R.; Schröder, B.; Coutinho, J. A. P.; Marrucho, I. M.; Esperança, J. M. S. S.; Rebelo, L. P. N.; Shimizu, K.; Lopes, J. N. C.; Santos, L. M. N. B. F. High-Accuracy Vapor Pressure Data of the Extended [CnC1im][Ntf2] Ionic Liquid Series: Trend Changes and Structural Shifts. *J. Phys. Chem. B* **2011**, *115* (37), 10919–10926.
- (423) Almeida, H. F. D.; Freire, M. G.; Fernandes, A. M.; Lopes-da-Silva, J. A. J. A.; Morgado, P.; Shimizu, K.; Filipe, E. J. M.; Canongia Lopes, J. N. J. N.; Santos, L. M. N. B. F. L. M. N. B. F.; Coutinho, J. A. P. J. A. P. Cation Alkyl Side Chain Length and Symmetry Effects on the Surface Tension of Ionic Liquids. *Langmuir* **2014**, *30* (22), 6408–6418.
- (424) Shimizu, K.; Bernardes, C. E. S.; Canongia Lopes, J. N. Structure and Aggregation in the 1-Alkyl-3-Methylimidazolium Bis(trifluoromethylsulfonyl)imide Ionic Liquid Homologous Series. *J. Phys. Chem. B* **2013**, *118* (2), 567–576.
- (425) Beyer, L.; Hartung, J.; Widera, R. Reaktionen an nickel(II)koordinierten N-Acylthioharnstoffen Mit Säurechloriden: Ein Einfacher Zugang Für Neue Thioharnstoff-Derivate. *Tetrahedron* **1984**, *40* (2), 405–412.
- (426) Hartung, J.; Weber, G.; Beyer, L.; Szargan, R. Zur Komplexbildung von N-(Thiocarbamoyl)benzamidinen. *Zeitschrift für Anorg. und Allg. Chemie* **1985**, *523* (4), 153–160.
- (427) Abram, U.; Muenze, R.; Hartung, J.; Beyer, L.; Kirmse, R.; Koehler, K.; Stach, J.; Behm, H.; Beurskens, P. T. Synthesis and Characterization of technetium(V) Complexes with N-(Thiocarbamoyl)benzamidinen. X-Ray Crystal Structure of bis[N-(N,N-diethylthiocarbamoyl)benzamidinato]oxotechnetium(V) Chloride, [TcO(et2tcb)2]Cl. *Inorg. Chem.* **1989**, *28* (5), 834–839.
- (428) Henkel, H. J.; Labes, D.; Hagen, V. Quantum Chemical Studies on Substituted Benzamidines as Inhibitors of the Serine Proteinases Trypsin and Thrombin. *Pharmazie* **1983**, *38* (5), 342–346.
- (429) Ensink, J. W.; Shepard, C.; Dudl, R. J.; Williams, R. H. Use of Benzamidine as a Proteolytic Inhibitor in the Radioimmunoassay of Glucagon in Plasma. *J. Clin. Endocrinol. Metab.* **1972**, *35* (3), 463–467.
- (430) Jeffcoate, S. L.; White, N. Use of Benzamidine to Prevent the Destruction of Thyrotropin-Releasing Hormone (TRH) by Blood. *J. Clin. Endocrinol. Metab.* **1974**, *38* (1), 155–157.
- (431) Ribeiro da Silva, M. A. V.; Santos, L. M. N. B. F.; Schröder, B.; Beyer, L. Thermochemical Studies of Three N-Thiocarbamoylbenzamidines. *J. Chem. Thermodyn.* **2004**, *36* (7), 555–559.
- (432) Ribeiro da Silva, M. A. V.; Santos, L. M. N. B. F.; Schröder, B. Thermochemical Studies of Two N-(Diethylaminothiocarbonyl)benzimidido Derivatives. *J. Chem. Thermodyn.* **2006**, *38* (11), 1455–1460.
- (433) Ribeiro da Silva, M. A. V.; Santos, L. M. N. B. F.; Schröder, B. Standard Molar Enthalpies of Formation of Two Crystalline bis[N-(diethylaminothiocarbonyl)benzamidinato]nickel(II) Complexes. *J. Chem. Thermodyn.* **2004**, *36* (9), 753–757.
- (434) Schröder, B.; Gomes, L. R.; Santos, L. M. N. B. F.; Brandão, P.; Low, J. N. A Second Monoclinic Polymorph of N-(Diethyl-Amino-Thio-Carbon-Yl)-N'-phenyl-Benzamidine. *Acta Crystallogr. Sect. E. Struct. Rep. Online* **2011**, *E67* (Pt 4), o962–o963.
- (435) Schröder, B.; Gomes, L. R.; Low, J. N.; Santos, L. M. N. B. F.; Rodrigues, A. S. M. C. Structure and Solid-liquid Phase Transition Thermodynamics of N-(Diethylaminothiocarbonyl)benzimidido Derivatives. *J. Mol. Struct.* **2011**, *1004* (1–3), 257–264.
- (436) Stempel, S.; Scherlinger, M.; Ng, C. A.; Hungerbühler, K. Screening for PBT Chemicals among The “existing” and “new” chemicals of the EU. *Environ. Sci. Technol.* **2012**, *46* (11), 5680–5687.

- (437) Gouin, T.; Mackay, D.; Webster, E.; Wania, F. Screening Chemicals for Persistence in the Environment. *Environ. Sci. Technol.* **2000**, *34* (5), 881–884.
- (438) Oleszek-Kudlak, S.; Grabda, M.; Shibata, E.; Eckert, F.; Nakamura, T. Application of the Conductor-like Screening Model for Real Solvents for Prediction of the Aqueous Solubility of Chlorobenzenes Depending on Temperature and Salinity. *Environ. Toxicol. Chem.* **2005**, *24* (6), 1368–1375.
- (439) Arp, H. P. H.; Niederer, C.; Goss, K.-U. Predicting the Partitioning Behavior of Various Highly Fluorinated Compounds. *Environ. Sci. Technol.* **2006**, *40* (23), 7298–7304.
- (440) Niederer, C.; Goss, K.-U. Effect of Ortho-Chlorine Substitution on the Partition Behavior of Chlorophenols. *Chemosphere* **2008**, *71* (4), 697–702.
- (441) Wittekindt, C.; Goss, K.-U. Screening the Partition Behavior of a Large Number of Chemicals with a Quantum-Chemical Software. *Chemosphere* **2009**, *76* (4), 460–464.
- (442) Nakajoh, K.; Grabda, M.; Oleszek-Kudlak, S.; Shibata, E.; Eckert, F.; Nakamura, T. Prediction of Vapour Pressures of Chlorobenzenes and Selected Polychlorinated Biphenyls Using the COSMO-RS Model. *J. Mol. Struct. Theochem* **2009**, *895* (1–3), 9–17.
- (443) Zhang, X.; Brown, T. N.; Wania, F.; Heimstad, E. S.; Goss, K.-U. Assessment of Chemical Screening Outcomes Based on Different Partitioning Property Estimation Methods. *Environ. Int.* **2010**, *36* (6), 514–520.
- (444) Schröder, B.; Santos, L. M. N. B. F.; Marrucho, I. M.; Coutinho, J. A. P. Prediction of Aqueous Solubilities of Solid Carboxylic Acids with COSMO-RS. *Fluid Phase Equilib.* **2010**, *289* (2), 140–147.
- (445) Schröder, B.; Santos, L. M. N. B. F.; Rocha, M. A. A.; Oliveira, M. B.; Marrucho, I. M.; Coutinho, J. A. P.; Schröder, B.; Santos, L. M. N. B. F.; Rocha, M. A. A.; Oliveira, M. B.; Marrucho, I. M.; Coutinho, J. A. P. Prediction of Environmental Parameters of Polycyclic Aromatic Hydrocarbons with COSMO-RS. *Chemosphere* **2010**, *79* (8), 821–829.
- (446) Schröder, B.; Freire, M. G.; Varanda, F. R.; Marrucho, I. M.; Santos, L. M. N. B. F.; Coutinho, J. A. P. Aqueous Solubility, Effects of Salts on Aqueous Solubility, and Partitioning Behavior of Hexafluorobenzene: Experimental Results and COSMO-RS Predictions. *Chemosphere* **2011**, *84* (4), 415–422.
- (447) Wang, Z.; MacLeod, M.; Cousins, I. T.; Scheringer, M.; Hungerbühler, K. Using COSMOtherm to Predict Physicochemical Properties of Poly- and Perfluorinated Alkyl Substances (PFASs). *Environ. Chem.* **2013**, *8* (4), 389–398.
- (448) Klamt, A.; Eckert, F.; Hornig, M.; Beck, M. E.; Bürger, T. Prediction of Aqueous Solubility of Drugs and Pesticides with COSMO-RS. *J. Comput. Chem.* **2002**, *23* (2), 275–281.
- (449) Etzweiler, F.; Senn, E.; Schmidt, H. W. H. Method for Measuring Aqueous Solubilities of Organic Compounds. *Anal. Chem.* **1995**, *67* (3), 655–658.
- (450) Andersson, J. T.; Schröder, W. A Method for Measuring 1-Octanol–water Partition Coefficients. *Anal. Chem.* **1999**, *71* (16), 3610–3614.
- (451) Schröder, W.; Andersson, J. T. Fast and Direct Method for Measuring 1-Octanol-Water Partition Coefficients Exemplified for Six Local Anesthetics. *J. Pharm. Sci.* **2001**, *90* (12), 1948–1954.
- (452) TURBOMOLE, a Development of University of Karlsruhe and Forschungszentrum Karlsruhe GmbH, 1989-2013, TURBOMOLE GmbH, since 2007; [Http://www.turbomole.com/](http://www.turbomole.com/).
- (453) Steffen, C.; Thomas, K.; Huniar, U.; Hellweg, A.; Rubner, O.; Schroer, A. TmoleX--a Graphical User

- Interface for TURBOMOLE. *J. Comput. Chem.* **2010**, *31* (16), 2967–2970.
- (454) COSMOconfX v3.0, COSMOlogic. GmbH & Co. Leverkusen; 2013.
- (455) Braun, U.; Richter, R.; Sieler, J.; Beyer, L.; Leban, I.; Golič, L. Structure of N-(Diethylaminothiocarbonyl)benzamidine. *Acta Crystallogr. Sect. C Cryst. Struct. Commun.* **1988**, *44* (2), 355–357.
- (456) Braun, U.; Sieler, J.; Richter, R.; Leban, I.; Golič, L. Crystal and Molecular Structure of N-(Diethylaminothiocarbonyl)-N'-Phenyl-Benzamidine. *Cryst. Res. Technol.* **1988**, *23* (1), 35–39.
- (457) Dreyfus, M.; Bensaude, O.; Dodin, G.; Dubois, J. E. Tautomerism in Cytosine and 3-Methylcytosine. A Thermodynamic and Kinetic Study. *J. Am. Chem. Soc.* **1976**, *98* (20), 6338–6349.
- (458) Dreyfus, M.; Dodin, G.; Bensaude, O.; Dubois, J. E. Tautomerism of Purines. 2. Amino-Imino Tautomerism in 1-Alkyladenines. *J. Am. Chem. Soc.* **1977**, *99* (21), 7027–7037.
- (459) Mühl, P.; Gloe, K.; Hoyer, E.; Dietze, F.; Beyer, L. N-Acylthioharnstoffe- Effektive Extraktionsmittel in Der Flüssig-Flüssig-Extraktion von Metallionen. *Zeitschrift für Chemie* **1986**, *26*, 81–94.
- (460) Eckert, F.; Klamt, A. COSMOtherm. Version C3.0 Release 14.01. COSMOlogic. GmbH & Co. Kg, Leverkusen. 2014.
- (461) Eckert, F. COSMOtherm User's Manual Version C3.0 Release 14.01, COSMOlogic GmbH & Co. Kg, Leverkusen, Germany. 2013.
- (462) Dallos, A.; Liszi, J. (Liquid + Liquid) Equilibria of (Octan-1-ol + Water) at Temperatures from 288.15 K to 323.15 K. *J. Chem. Thermodyn.* **1995**, *27* (4), 447–448.
- (463) Yalkowsky, S. H.; He, Y.; Jain, P. *Handbook of Aqueous Solubility Data*, 2nd ed.; CRC Press, 2010.
- (464) US EPA EPISuite 4.1, US EPA. (2012). Estimation Programs Interface Suite™ for Microsoft® Windows, v 4.11. United States Environmental Protection Agency, Washington, DC, USA.
- (465) Schröder, B.; Coutinho, J. A. P.; Santos, L. M. N. B. F. Predicting Physico-Chemical Properties of Alkylated Naphthalenes with COSMO-RS. *Polycycl. Aromat. Compd.* **2013**, *33* (1), 1–19.
- (466) Mackay, D.; Shiu, W. Y.; Ma, K.-C.; Lee, S. C. *Handbook of Physical-Chemical Properties and Environmental Fate for Organic Chemicals, Volume 1, 2°*; Taylor & Francis Group, 2006.
- (467) Theodoridis, G. Chapter 4 Fluorine-Containing Agrochemicals: An Overview of Recent Developments. *Adv. Fluor. Sci.* **2006**, *2*, 121–175.
- (468) Luteijn, J. M.; Tipker, J. A Note on the Effects of Fluorine Substituents on the Biological Activity and Environmental Chemistry of Benzoylphenylureas. *Pestic. Sci.* **1986**, *17* (4), 456–458.
- (469) Jeschke, P. The Unique Role of Fluorine in the Design of Active Ingredients for Modern Crop Protection. *Chembiochem* **2004**, *5* (5), 571–589.
- (470) PBT Profiler, [Http://www.pbtprofiler.net](http://www.pbtprofiler.net), as Accessed 29/07/2015.
- (471) Arnot, J. A.; Mackay, D. Policies for Chemical Hazard and Risk Priority Setting: Can Persistence, Bioaccumulation, Toxicity, and Quantity Information Be Combined? *Environ. Sci. Technol.* **2008**, *42* (13), 4648–4654.
- (472) Rogers, I. H. Environmental Effects of Terpenoid Chemicals: A Review. *J. Am. Oil Chem. Soc.* **1978**, *55* (2), A113–A118.

- (473) Svendby, T. M.; Lazaridis, M.; Tørseth, K. Temperature Dependent Secondary Organic Aerosol Formation from Terpenes and Aromatics. *J. Atmos. Chem.* **2008**, *59* (1), 25–46.
- (474) Steinbrecher, R.; Koppmann, R. Biosphäre Und Atmosphäre: Bedeutung Biogener Kohlenwasserstoffe. *Chemie unserer Zeit* **2007**, *41* (3), 286–292.
- (475) Miller, D. J.; Hawthorne, S. B. Solubility of Liquid Organic Flavor and Fragrance Compounds in Subcritical (Hot/Liquid) Water from 298 K to 473 K. *J. Chem. Eng. Data* **2000**, *45* (2), 315–318.
- (476) Tamura, K.; Li, H. Mutual Solubilities of Terpene in Methanol and Water and Their Multicomponent Liquid–liquid Equilibria. *J. Chem. Eng. Data* **2005**, *50* (6), 2013–2018.
- (477) Surburg, H.; Panten, J. *Common Fragrance and Flavor Materials: Preparation, Properties and Uses*, 5th ed.; Wiley-VCH, 2006.
- (478) Schröder, B.; Martins, M. A. R. R.; Coutinho, J. A. P. P.; Pinho, S. P. Aqueous Solubilities of Five N-(Diethylaminothiocarbonyl)benzimidazole Derivatives at T = 298.15 K. *Chemosphere* **2016**, *160*, 45–53.
- (479) Góral, M. Recommended Liquid–liquid Equilibrium Data. Part 3. Alkylbenzene–water Systems. *J. Phys. Chem. Ref. Data* **2004**, *33* (4), 1159–1188.
- (480) Neely, B. J.; Wagner, J.; Robinson, R. L.; Gasem, K. A. M. Mutual Solubility Measurements of Hydrocarbon–water Systems Containing Benzene, Toluene, and 3-Methylpentane. *J. Chem. Eng. Data* **2008**, *53* (1), 165–174.
- (481) SPARC on-Line Calculator, October 2011 Release w4.6.1691-s4.6.1687. Accessed May 2013.
- (482) Gmehling, J.; Li, J.; Schiller, M. A Modified UNIFAC Model. 2. Present Parameter Matrix and Results for Different Thermodynamic Properties. *Ind. Eng. Chem. Res.* **1993**, *32* (1), 178–193.
- (483) US EPA EPISuite 4.1, US EPA. (2012). Estimation Programs Interface Suite™ for Microsoft® Windows, WSKowwin v 1.42. United States Environmental Protection Agency, Washington, DC, USA.
- (484) Knobloch, K.; Pauli, A.; Iberl, B.; Weigand, H.; Weis, N. Antibacterial and Antifungal Properties of Essential Oil Components. *J. Essent. Oil Res.* **1989**, *1* (3), 119–128.
- (485) Maczynski, A.; Wisniewska-Gocłowska, B.; Goral, M. Recommended Liquid–liquid Equilibrium Data. Part 1. Binary Alkane–water Systems. *J. Phys. Chem. Ref. Data* **2004**, *35* (43), 549–577.
- (486) Krug, R. R.; Hunter, W. G.; Grieger, R. A. Enthalpy-Entropy Compensation. 2. Separation of the Chemical from the Statistical Effect. *J. Phys. Chem.* **1976**, *80* (21), 2341–2351.
- (487) Ferreira, O.; Pinho, S. P. Solubility of Flavonoids in Pure Solvents. *Ind. Eng. Chem. Res.* **2012**, *51* (18), 6586–6590.
- (488) Gill, S. J.; Nichols, N. F.; Wadsö, I. Calorimetric Determination of Enthalpies of Solution of Slightly Soluble Liquids II. Enthalpy of Solution of Some Hydrocarbons in Water and Their Use in Establishing the Temperature Dependence of Their Solubilities. *J. Chem. Thermodyn.* **1976**, *8* (5), 445–452.
- (489) Hefter, G. T. Critical Evaluation of Toluene + Water Solubility. In *IUPAC solubility data series*; Kertes, A. S., Shaw, D. G., Eds.; Pergamon Press: Oxford, 1989; pp 369–375.
- (490) Zaitsau, D. H.; Verevkin, S. P.; Sazonova, A. Y. Vapor Pressures and Vaporization Enthalpies of 5-Nonanone, Linalool and 6-Methyl-5-Hepten-2-One. Data Evaluation. *Fluid Phase Equilib.* **2015**, *386*, 140–148.
- (491) Verevkin, S. P. Determination of the Ortho -, Para -, and Meta -Interactions in Secondary -

- Alkylphenols from Thermochemical Measurements. *Berichte der Bunsengesellschaft für Phys. Chemie* **1998**, *102* (10), 1467–1473.
- (492) Serpinskii, V. V.; Voitkevich, S. A.; Lyuboshits, N. Y. Determination of Saturated Vapour Pressures of Fragrances. *Zhurnal Fiz. Khimii* **1953**, *27*, 1032–1038.
- (493) Wypych, George. (2008; 2012). *Knovel Solvents - A Properties Database*. ChemTec Publishing. Online Version Available at: <http://app.knovel.com/hotlink/toc/id:kpKSAPD005/knovel-Solvents-Properties/knovel-Solvents-Properties>.
- (494) Harini, M.; Adhikari, J.; Rani, K. Y. Prediction of Vapor–liquid Coexistence Data for P-Cymene Using Equation of State Methods and Monte Carlo Simulations. *J. Chem. Eng. Data* **2014**, *59* (10), 2987–2994.
- (495) Griffin, S.; Wyllie, S. G.; Markham, J. Determination of Octanol–water Partition Coefficient for Terpenoids Using Reversed-Phase High-Performance Liquid Chromatography. *J. Chromatogr. A* **1999**, *864* (2), 221–228.

Estes anexos só estão disponíveis para consulta através do CD-ROM.  
Queira por favor dirigir-se ao balcão de atendimento da Biblioteca.

Serviços de Biblioteca, Informação Documental e Museologia  
Universidade de Aveiro